FDTD modelling, Measurements and Analyses of Post Reception Synthetic Focusing Techniques in Ground Penetrating Radars

Rajagopal Nilavalan

September 2000

A thesis submitted to the University of Bristol in accordance with the requirements for the degree of Doctor of Philosophy in the Faculty of Engineering, Department of Electrical and Electronic Engineering.

Abstract

Subsurface probing has applications in areas such as civil engineering, geophysics, military, forensic and archaeology. Various techniques are being employed for these explorations ranging from small hand held systems to vehicle mounted systems.

The Ground Penetrating Radar (GPR) is a promising technique for subsurface probing. Most conventional GPRs employ a transmitter-receiver pair and have limitations in terms of resolution, operation in clutter environments, penetrable depths and operating speeds.

However, the Post Reception Synthetic Focussing (PRSF) approach, which makes use of an antenna array, is an effective technique to enhance the operations of GPRs. In this method, one element transmits at a time and the subsequent reflected signals are recorded at all the elements that have the resolution cell in their 'field of view'. Focusing onto particular volume in the subsurface is achieved by applying appropriate two way timing corrections to align the signals.

In this thesis, the PRSF technique is analysed through theoretical and practical means to estimate its properties and investigate possible methods that will enhance the detection process with the view of implementing a full practical system. The theoretical analysis of a GPR system is complex due to various components of the system and the nature of electromagnetic interactions associated with these elements. In order to analyse these coupled elements and get a better understanding of their operation, a general full wave field solving method is employed. In this thesis, the Finite Difference Time Domain (FDTD) method is applied to investigate the PRSF method in GPR problems. The properties and problems analysed with this method include antenna modelling and design, GPR system modelling, system resolutions, processing gain, near surface detection, detection in clutter environments, de-focussing features and signal power estimations. Hardware designs and processing techniques that will enhance the detection process are also investigated with the FDTD calculations. Finally comparisons of theoretical estimations and practical measurements are carried out for the detection of buried objects in soil, using a line array of bowtie elements in the GPR measuring facility at University of Bristol.

To my parents

Acknowledgement

First, I should like to express my gratitude to Prof. Joe McGeehan for kindly giving me the opportunity to study for a PhD within the Centre for Communications Research (CCR) at the University of Bristol and for his continued encouragement and support. I would also like to thank him for the financial support received during my study.

I gratefully thank Prof. Ralph Benjamin and Dr. Geoff Hilton for their advice, enthusiasm and support for this research and the preparation of the thesis. Their profound understanding and experience have been invaluable. I am extremely grateful to Geoff for reading this entire thesis and I also would like to thank Dr.Nishan Canagarajah and Dr. Ian Craddock for their helpful suggestions.

The Finite-Difference Time-Domain (FDTD) analysis of the GPR could not have been achieved without Dr.Chris Railton and the other members of the mathematical modelling group. Particularly, I am appreciative to Dr.Ian Craddock and Dr.Chris Railton for the support and advise with the FDTD Package.

Thanks to my colleagues Ewan McCutcheon and Stuart Litobarski in the Ground Penetrating Radar (GPR) research group in CCR for their useful suggestions, support and friendship. Practical measurements were made possible by their efforts in building the GPR measuring facility at University of Bristol.

Other thanks must go to my colleagues (and ex-colleagues) at the CCR, for their humour and support. Special thanks to Ross, Tony, Dave, Li Ma, Dominique, Kaya, James, Mohan and Pageman. I am grateful to Nishan and Thabithaal for their advices and the friendship I enjoyed during my stay in Bristol. I would also like to thank Priyantha, Anil, Renuka, Palitha, Rohan and my friends at Hodgkin house who made my stay a memorable one.

Finally, I would like to thank my family specially my mother, for their love and support during my study.

Author's Declaration

Unless otherwise acknowledged, the content of this thesis is the original and sole work of the author. No portion of the work in this thesis has been submitted by the author in support of an application for any other degree or qualification, at this or any other University or institution of learning. The views expressed in this thesis are those of the author, and not necessarily of the University of Bristol.

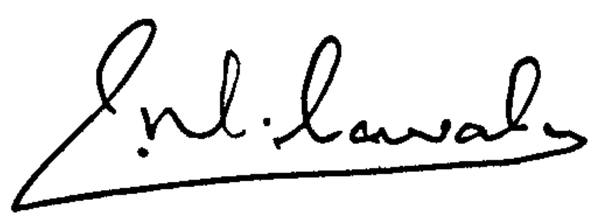

Rajagopal Nilavalan

Copyright

Contents

List of Figures

List of Tables

List of Principal Symbols

E_x, E_y, E_z	Electric field intensity
H_x, H_y, H_z	Magnetic field intensity
ε_r	Relative permitivity (dielectric constant)
ε_{rr}	Loss factor
tan δ	Loss tangent
μ	Permeability
σ	Conductivity
ω	Angular frequency
λ	Wavelength
Δx, Δy, Δz	Cell sizes
Δt	Time step
π	Pi
σ_{rcs}	Target radar cross section
f	Frequency
Z: Z_1, Z_2	Characteristic impedance
k	Boltsman's constant
T_0	Ambient temperature in Kelvin

List of Abbreviations

ABC	Absorbing Boundary Conditions
CM	Connection Machines
CNR	Complex Natural Resonance
CW	Continuous Waves
FDTD	Finite Difference Time Domain Method
FM-CW	Frequency Modulated Continuous Waves
GPR	Ground Penetrating Radar
MDS	Minimum Detectable Signal level
MDD	Maximum Detectable Depths
MOM	Method of Moments
NF	Noise Figure
PRSF	Post Reception Synthetic Focusing
RAM	Radar Absorbing Material
RCS	Radar Cross Section
SNR	Signal to Noise Ratio
TLM	Transmission Line Matrix

List of Publications

R.Benjamin, G.Hilton, R.Nilavalan, S.Litobarski and E.McCutcheon, Synthetically-Focused Surface-Penetrating Radar for Operation from a Moving Vehicle, *Proceedings of the Second International Conference on Detection of Abandoned Land Mines*, IEE, pp.60-3, Edinburgh, UK, 1998.

R.Nilavalan, G.S.Hilton and R.Benjamin, A FDTD Model for the Post-Reception Synthetic Focusing Surface Penetrating Radar with Mine Detecting Applications, *Proceedings of the IEE National Conference on Antennas and Propagation*, IEE, pp.69-72, York, UK, 1999.

R.Benjamin, G.Hilton, S.Litobarski, E.McCutcheon and R.Nilavalan, Post-Detection Synthetic Near Field Focusing in Radar or Sonar, *Electronics Letters*, vol.35, no.8, pp.664-6, IEE, UK, 1999.

R.Nilavalan, G.S.Hilton and R.Benjamin, Wideband Printed Bowtie Antenna Element Development for Post Reception Synthetic Focusing Surface Penetrating Radar, *Electronics Letters*, vol.35, no.20, pp.1771-2, IEE, UK, 1999.

R.Nilavalan, G.S.Hilton, R.Benjamin and I.Craddock, FDTD Analysis of a Post-Reception Synthetic Focusing Surface Penetrating Radar Performance in Various Ground Conditions, *Proceedings of the Millennium Conference on Antennas and Propagation*, Davos, Switzerland, April 2000.

1. Introduction

1.1. Introduction

The primary object of the work described in this thesis is to analyse an efficient technique for subsurface probing and the investigations of possible methods that will enhance the detection process with the view of implementing a full practical system. The need to probe the subsurface arises from a variety of diverse fields which include civil engineering, geophysics, archaeology, forensic investigations, military and de-mining. The search for suitable tools to accomplish this task has given birth to new techniques and ideas. The non-destructive evaluation of buried objects is of interest for variety of engineering and environmental applications. Hence, the knowledge of precise location and the object properties is the primary concern. A wide range of probing techniques are available for subsurface investigations and these depend upon the type of surface being considered. The use of radio frequencies for subsurface probing is an attractive solution since radio waves can penetrate the soil and by processing the signal returns subsurface images can be visualised. Although it is difficult to obtain high precision images, target identification is possible.

Probing techniques require good hardware designs and processing methods. The design procedure is complex due to the operational environment and the interaction between various elements in such systems. A realistic investigation and design need analysis tools that can incorporate all system components and yield accurate information. Furthermore investigation of appropriate processing techniques are also necessary to enhance detection.

This chapter discusses the subsurface probing techniques in general and appropriate analysis tools that can be used to analyse such probing methods. Finally it describes the authors work and gives an overview of this thesis.

1.2. Subsurface Probing and Ground Penetrating Radars

Currently, several techniques are being used to map the subsurface. They vary in size from hand held systems to complex vehicle mounted systems. Most techniques discussed in this section are merely able to establish the presence of a target and its very approximate location, but most applications require the exact location of subsurface objects in a very complex environment.

1.2.1. Resistivity Method

The resistivity method [1] of subsurface exploration is a simple method involving pairs of electrodes. A pair of electrodes is used to introduce current into the ground. The current flow pattern in soil depends on the conductivity, obstacles and any other irregularities in soil. A second pair of electrodes (or multiple pairs) are then used to measure the voltage pattern due to the current flow pattern of the first electrodes. This resistivity information is used to map the subsurface through suitable processing.

This method is slow in operation and provides only the resistive profile of the subsurface.

1.2.2. Gravity Method

The earth gravitational fields are altered by the subsurface features and objects such as voids etc [2]. The change in Earth's gravity fields can be measured using microgravimeters. Gravity anomalies are extremely small relative to the total field and are usually measured in micro-Gals (one micro-Gal is about 1 billionth of the Earth's total gravitational field). This method is of little use because of the ultra sensitive nature of the measurements.

1.2.3. Magnetic Methods

Buried ferrous objects and other similar subsurface anomalies disturb the Earth's magnetic fields [2]. These variations in the magnetic fields can be measured using magnetometers. The detection depends on the amount of magnetic materials present and the distance to the sensors. But the magnetic field measurements can only be useful in isolation as they can be obscured by power lines and other environmental features such as solar magnetic storms etc.

1.2.4. Thermal Methods

Thermal infrared methods measure the Earth's surface temperature and its variations due to the underlying objects. New techniques, such as heating the soil with microwave sources and subsequent observations of the surface temperature [3] have been put forward as methods for the detection of abandoned land mines.

1.2.5. Nuclear Methods

Nuclear methods are being tested for buried land mine detection [4]. The high nitrogen concentration of the explosives is detected by the characteristics of the γ rays emitted in the thermal neutron capture reaction. This method is an expensive technique, and obviously has damaging effects on the environment

1.2.6. Seismic Methods

Acoustic waves couple into soil at very low frequencies (1- 30KHz) [2]. The sound waves, which reflect directly from underground surfaces with density contrasts, are used to map soil and bed rock stratigraphy. The reflections are precisely measured using detectors called the Geophones. This information is used with the in soil sound velocity to map the subsurface. A *shallow ground water table* of the site is necessary for velocity estimations. Seismic methods are useful in deep ground explorations of 50 feet to several hundred feet. Although seismic methods are time consuming and have poor imaging capabilities, these are useful in high radar attenuating mediums.

1.2.7. Electromagnetic Methods

Electromagnetic explorations operate by inducing currents in soil from a transmitting coil and measurement of induced fields with a similar coil [2]. The induced fields vary depending on the subsurface objects. Metal detectors make use of this principle to detect buried metallic objects, but has limited applications since it is mostly suitable for the detection of metallic and conductive objects.

The Ground Penetrating Radar (GPR) [5] utilises high frequency electromagnetic fields in the detection process. A transmitting antenna radiates a signal into the soil and a receiving antenna is used to observe the scattered signals. The travel time taken for the back-scattered energy is used to calculate the target locations. Since the GPRs can employ remote, non-contacting transducers and give better accuracy of target locations, this method is preferred over resistivity and seismic methods. Because of the high frequency of operation, the GPRs are capable of mapping the subsurface with better resolution compared to other techniques discussed in this section. For example, the human visual system employs very high visible frequencies for target discrimination (or imaging). But very high frequencies are not possible to employ because of the very small penetrable depths (skin depths) hence the choice is radio frequencies.

The operation and the properties of GPR systems for detection and mapping of the subsurface are to be considered in this thesis. The present GPR techniques have limitations in terms of resolution, operation in clutter environments, penetrable depths and operating speeds [5]. It has been proposed [6] that the Post Reception Synthetic Focusing (PRSF) technique in GPR problems is an attractive solution to improve performance. A detailed description of GPR methods and the PRSF technique is given in chapter 2.

The complex calculations associated with the GPR need rigorous consideration. A realistic analysis of the system will help to:

- estimate the system properties in practical environments
- understand the nature of problems encountered in these types of GPR problems
- identify limitations of the system
- develop possible solutions to problems encountered by these systems

- verify possible solutions before implementing expensive systems
- aid system design
- analyse possible imaging methods that will aid detection

1.3. System Analysis

In order to analyse the performance of GPR type problems a number of techniques have been put forward and are briefly described here.

Generally electromagnetic problems can be analysed by solving the wave equations analytically or numerically. Analytical techniques make simplifying assumptions about the geometry of the problem to apply closed-form solutions. On the other hand, numerical techniques try to solve the fundamental field equations directly. In most cases, the analytical solutions for all but very simple cases are not possible and numerical techniques are used. Numerical methods can be broadly classified as differential methods and integral methods [7]. In differential methods, Maxwell's differential equations are solved with appropriate boundary conditions while in integral methods, an integral equation is derived from Maxwell's difference equations (generally expressed, using Green's functions) and these integral equations are subsequently solved with suitable boundary conditions [7]. For subsurface analyses, the integral solutions are more complex, as the analytical derivation of the half space dyadic Green's function is considerably more difficult compared to the free space function.

1.3.1. Ray Tracing

Ray tracing techniques, which do not incorporate rigorous electromagnetic analyses, are considered for the analysis of GPR systems. Ray tracing is used to determine the propagation paths and integration along these paths to determine travel times and amplitudes. The amplitudes include contributions from source-receiver directional properties, spreading, reflection and transmission coefficients and attenuation. Ray tracing methods are fast compared to other general analysing techniques. Zeng and McMechan [8] employed ray tracing methods to analyse monostatic and bistatic GPR responses from several tank and pipe configurations. Ewen *et al* [9] used this technique

to analyse defocusing mechanisms in a PRSF-GPR. However, the main limitation of this technique is that all the components associated with GPR are de-coupled, giving no scope to analyse the inter related effects.

1.3.2. Analytical Techniques

Scattering from objects can be calculated using analytical techniques. This is based on the Fresnel-Kirchhof diffraction formula [10, 11], which is derived from an integral representation of wave equations. These analyses were further extended to calculate scattering from buried objects [12] and incorporate the propagation characteristics of spherical waves in lossy dielectrics, but the effects of air space were ignored and therefore assume only the operation in the lossy dielectric media. These authors derived a microwave holographic imaging technique for subsurface radar based on these scattering estimations.

A similar approach was taken by Deming and Devaney [13] in which they incorporated the antenna characteristics for the scattering estimations, but the air-soil interface effects were again neglected.

Junkin and Anderson [14] employed a spectral diffraction algorithm to investigate the antenna properties near a dielectric half space. This algorithm was developed using the solution of the Maxwell's difference equation in the spectral domain (Fourier transform of space variables). Minimisation of the computations was achieved by assuming a one dimensional GPR problem.

1.3.3. Method of Moments

The Method of Moments (MOM) is a technique for solving complex integral equations by reducing them to a system of simpler linear equations. The solution process consists of employing basis and weighting functions to find a suitable current distribution that best fits the known conditions (boundary and/or incident field conditions). In GPR problems, the MOM methods are used to calculate the scattered fields and the natural resonance of buried targets [15, 16]. This problem is more complicated because of the difficulties in estimating the half space dyadic Green function, which is important in the integral representation of the wave fields. This important limitation in GPR

analysis was overcome for problems involving bodies of revolution [15, 16], but for more generalised targets further analysis is required.

The MOM methods are preferred in the ultra wide band GPR systems since the analysis in the frequency domain will help to incorporate the dispersive properties of soil easily. Furthermore the complex natural frequencies are easy to calculate (that is without employing any incident fields) compared to other numerical techniques such as the FDTD where the excitation field is important.

A similar integral equation approach was taken by Xiong and Tripp [17], where they examined some approximate solutions to overcome the difficulties encountered in the estimation of the Green's function. They compared their results with Finite Difference Time Domain (FDTD) simulations to validate their analysis for frequencies less than 200MHz.

1.3.4. Transmission Line Matrix Method

The Transmission Line Matrix (TLM) method is performed in the time domain and the entire region of the analysis is grided. Appropriate fields are assigned for each node in this grid and these nodes are connected by transmission lines. Hence an excitation at the source node will propagate to the adjacent nodes through these transmission lines. The characteristic impedance of the transmission lines are calculated based on the dielectric properties and the dimensions of the grid. GPR problems were analysed using this technique for a two dimensional case [18], to theoretically simulate a pulsed radar. The boundary conditions to simulate the free space can be easily modelled with the TLM method using matched terminations to terminate the transmission lines. General TLM methods require more memory compared to similar techniques such as FDTD for computations per node [19].

1.3.5. FDTD Methods

FDTD method was first proposed by Yee in 1966 for a simple Cartesian co-ordinate system [20]. Although this method is a useful technique to handle electromagnetic problems it did not gain considerable attention until the computing costs became low. This method makes use of the direct full wave numerical solution of Maxwell's time

dependent curl equations. It employs second order accurate central difference approximations for the space and time derivatives in the Maxwell's curl equations [20] to iteratively calculate field values in a discretised problem space. The time and space discretisation are performed to limit the errors in the sampling process and to ensure stability of the algorithm. The problem space is limited with special boundary conditions, which are used to simulate free space or any other relevant conditions. The FDTD methods are widely employed to solve many diverse electromagnetic problems because of its generality and efficient solution process.

1.3.5.1. Applications

Since FDTD is a time domain technique, it is very useful in analysing radiating structures over a wide range of frequencies. It has been used to analyse radiating structures like horn antennas, microstrip patch antennas [21], monopoles [22], dipoles, printed bowties [23], guiding structures such as wave-guides and feeds [24], as well as microstrip circuits [25] including cross talk in digital circuits [26].

Currently, FDTD is the most common time domain numerical technique that is being used in Radar Cross Section (RCS) computation of complex targets because of its simplicity in discretising such targets [27].

The analysis of radio wave scattering from geophysical surfaces is a complicated task due to lack of detailed information on the signatures of discrete objects that appear in the surface. Although the scattering estimation doesn't need to be precise for far-field radars, it is quite significant for near-field operated ground penetrating radars. Hastings et al [28] and Wong et al [29] performed detailed analyses of surface scattering using FDTD methods. They provided general method to calculate scattered fields from arbitrary inhomogeneities on the surface.

The use of FDTD techniques in the analysis of Ground Penetrating Radars (GPR) has gained considerable attention in the past. The calculations associated with the GPRs are highly complex due to antenna response, operation in the near field of the antenna and the dielectric properties of the soil. The FDTD method is capable of addressing most of these parameters in a single computer run without much extra computational effort. Bourgeoie et al [30, 31] used a three dimensional FDTD model to analyse a

conventional ground penetrating radar. They used a scale model to compare their studies with practical measurements. Robert et al [32] used a similar model to analyse reflected fields from submerged pipes in water. The dispersive nature of soils has also been incorporated in some FDTD analyses [33].

Considering the electromagnetic analysing techniques, which have been used with complex GPR problems, it is obvious that the FDTD methods and the TLM methods are more flexible in incorporating all the components of the GPR system. Because of the close proximity of the components (such as the feeds, antennas, soil and the buried targets in a GPR configuration), the system cannot be realistically analysed by considering these elements separately. If the antennas are analysed individually the effects due to mutual coupling and the multiple reflections associated with the system are ignored in the analysis. Hence a realistic investigation should incorporate all the elements of the system with less complexities. In this thesis, FDTD methods are employed in analysing the GPR problems because,

- Of the complexities involved in the PRSF-GPR system
- The simplicity of the FDTD methods
- The ease of modelling the components of the GPR system
- A very good knowledge of FDTD modelling at University of Bristol.

1.4. Summary of Author's Work

Having given a general introduction to the intended work in this thesis, it is appropriate to elaborate on the author's contributions. The author's main area of study in this thesis is the analysis of the PRSF technique in ground probing radars. Analyses have been performed to investigate the PRSF-GPR system using FDTD methods and the subsequent verification of the analyses through practical measurements. The authors main contributions in this study includes,

- Development of a PRSF-GPR FDTD model that can be used to analyse a wide range of problems [34].
- Analysis of the PRSF-GPR technique in various practical soil conditions [35]

- Evaluation of the nature of clutter returns that can be expected in a PRSF-GPR system [35]
- Investigation of possible techniques that will enhance the system detection capabilities.
- Formulation of an analytical method to investigate the return signal strengths that can be used to estimate the noise limits of the system [36].
- Development of a wide band printed bowtie element for the practical analysis of the system [23]

1.5. Thesis Overview

Chapter 1 has discussed the importance of subsurface probing and the currently available techniques for subsurface detection. Investigation of the existing techniques suggested that the Ground Penetrating Radar method is a suitable technique that can meet the present day requirements. However, the conventional GPR methods [5] need further refinements to improve their capabilities. Hence, it is important to analyse techniques that can enhance the detection capabilities of the conventional GPRs. Furthermore, various analytical and numerical techniques that can be used to analyse such complex electromagnetic problems have been presented.

Chapter 2 considers the GPR methods in more detail and provides some background information on the existing methods. The applications of the GPR in various fields, basic methodology, signal types and identification methods are outlined. It describes the PRSF technique and its features in detail. The PRSF technique is the main concern of this thesis, and it is theoretically and practically analysed in the subsequent chapters.

Chapter 3 gives a brief introduction to the numerical FDTD method, which is employed to analyse most of the complex problems associated with the PRSF-GPR method. This chapter further proceeds to develop a numerical model for the PRSF-GPR with an 8 element printed dipole array. This PRSF-GPR model is used to demonstrate the basic properties such as synthetic focusing, target detection, horizontal and vertical resolutions and the processing gain of the model. Furthermore, a method to overcome limitations due to reverberating signals caused by the metallic back plane of the antenna is also discussed.

In Chapter 4, the PRSF-GPR model developed in chapter 3 is further modified to analyse the PRSF operation in various soil conditions. Analyses include target detection in near surface, clutter, non-flat ground and stratified media. In this section, the nature of clutter returns from pebble-like targets are also estimated and compared with FDTD calculations. Furthermore, techniques that can enhance the detection process in practical environments are described and investigated with the FDTD calculations.

Chapter 5 investigates noise limits and system parameters of the GPR in order to estimate the system performance in practical soil conditions and to aid a full practical system design. Since a full FDTD model for the complete PRSF-GPR is not possible, an analytical model is formulated to compute the return signal strengths from individual paths, and it is verified against an 8-element array FDTD model described in chapter 3. The noise limited maximum detectable depths under various practical conditions are also investigated.

Chapter 6 is devoted to the development of a wide band antenna element that can be employed in a practical PRSF-GPR system and to compare theoretical investigations presented in the previous chapters with practical measurements. This chapter includes a summary of existing GPR antennas and proceeds to develop a bowtie antenna element through FDTD methods. The antenna element characteristics, such as input response and radiation patterns, are verified against practical measurements. Furthermore, a 4-element array is also investigated through practical measurements.

In Chapter 7, the analyses presented in this thesis are validated where possible against practical measurements using a bowtie element array. All measurements are conducted at 1 GHz due to the maximum frequency of the digitising oscilloscope of 1.5GHz. Furthermore, an adaptive technique to enhance detection is also described and tested. The GPR measuring facility at University of Bristol that is used in these measurements is described in Appendix D.

Finally chapter 8 summarises the work presented in this thesis and draws some broad conclusions with future considerations.

References

[1] M.H.Loke, Electrical Imaging Surveys for Environmental and Engineering Studies, *A practical Guide to 2-D and 3-D surveys*, Technical note for Advanced Geoscience, Inc. USA

[2] Methods & Applications manual, Northeast Geophysical Services, USA

[3] L.J.Carter, M.J.Sullivan, Y.J.Hung and J.C.C.Teng, Thermal imaging for land mine detection, *Proceedings of EUREL/IEE International Conference on the Detection of Abandoned Land Mines*, IEE, Edinburgh, pp. 110-111, 1998.

[4] G.Nebbia et al, Advanced Nuclear technique for humanitarian de-mining, *Proceedings of EUREL/IEE International Conference on the Detection of Abandoned Landmines*, IEE, Edinburgh, pp. 157-159, 1998.

[5] D.J.Daniels, *Surface Penetrating Radar*, Electronics and Communications Engineering Journal, pp. 165-182, Aug. 1996.

[6] R.Benjamin, Post Detection Synthetic Focusing in Near-field Radar, *Proceedings of EUREL/IEE International conference on the detection of abandoned land mines*, IEE, Edinburgh, pp. 133-137, Oct 1996

[7] I.J.Craddock, *Enhanced Numerical Techniques for Time Domain Electromagnetic Analysis*, PhD thesis, 1995.

[8] X.Zeng and G.A.McMechan, GPR Characterisation of Buried Tanks and Pipes, *Geophysics*, vol. 62, pp. 797-806, 1997.

[9] R.Benjamin, G.S.Hilton, S.Litobarsski, E.McCutcheon and R.Nilavalan, Microwave Detection of Subsurface Objects, *6th Report to DERA*, University of Bristol, UK.

[10] J.W.Goodman, *Introduction to Fourier Optics*, McGraw Hill, 1968.

[11] N.Osumi and K.Ueno, Microwave Holographic Imaging with Improved Resolution, *IEEE Transaction on Antenna and Propagation*, vol. AP-32, pp. 1018-1026, 1984.

[12] N.Osumi and K.Ueno, Microwave Holographic Imaging of Underground Objects, *IEEE Transaction on Antenna and Propagation*, vol. AP-33, pp. 152-159, 1985.

[13] R.W.Deming and A.J.Devaney, Diffraction Tomography for Multi-monostatic Ground Penetrating Radar, *Inverse Problems*, Vol.13, No.1, pp.29-45, 1997

[14] G.Junkin and A.P.Anderson, Limitations in Microwave Holographic Synthetic Aperture Imaging Over a Lossy Half Space, *IEE Proceedings*, vol. 135, Pt.F, pp. 321-329, 1988

[15] S.Vitebskiy, L.Carin, M.A.Ressler and F.H.Le, Ultra wideband Short Pulse Ground Penetrating Radar: Simulation and Measurement, *IEEE Transactions on Geoscience and Remote Sensing*, vol. 35, pp.762-772, 1997.

[16] L.Carin, N. Geng, M.McClure, J. Sichina and L.Nguyen, Ultra-Wide-Band Synthetic Aperture Radar for Mine Field Detection, *IEEE Antennas and Propagation Magazine*, vol. 41, pp. 18-33, 1999

[17] Z.Xiong and A.C.Tipp, 3-D Electromagnetic Modelling for Near-Surface Targets Using Integral Equations, *Geophysics*, vol. 62, pp. 1097-1106, 1997.

[18] C.Liu and L.C.Shen, Numerical Simulation of Subsurface Radar for Detecting Buried Pipes, *IEEE Transactions on Geoscience and Remote Sensing*, vol. 29, pp. 795-797, 1991

[19] Y.Hao, Development and Characterisation of a Conformal FDTD Method for Oblique Electromagnetic Structures, PhD thesis, University of Bristol, 1998.

[20] K.S.Yee, Numerical Solution of Initial Boundary Value Problems Involving Maxwell's Equations in Isotropic Media, *IEEE transaction on Antenna and Propagation*, vol. AP-14, pp. 302-307, 1966.

[21] G.S.Hilton, C.J.Railton and M.A.Beach, Modelling Parasitically-Coupled Patch Antennas using the Finite Difference Time Domain Technique, *8th International conference on Antennas and Propagation Conference Proceedings*, vol. 1, pp. 186-189, 1993.

[22] J.G.Maloney and G.S.Smith, A study of Transient Radiation from the Wu-King Resistive Monopole – FDTD analysis and Experimental Measurements, *IEEE Transactions on Antennas and Propagation*, vol. AP-41, no.5, pp.668-675, 1993.

[23] R.Nilavalan, G.S.Hilton and R.Benjamin, Wide Band Printed Bowtie Antenna Element Development for Post Reception Synthetic Focusing Surface Penetrating Radar, *Electronics Letters*, vol. 35, pp. 1771-1772, 1999

[24] M.DePourcq, Field and Power-Density Calculations in Closed Microwave Systems by Three Dimensional Finite Difference, *Proceedings of the IEE*, vol. 132 H, no. 6, pp. 360-368, 1985.

[25] D.M.Sheen, M.D.Abouzahra and J.A.Kong, Application of the Three Dimensional Time Domain Method to the Analysis of Planar Microstrip Circuits, *IEEE Transactions on Microwave Theory and Techniques*, vol. MTT-38, no 7, pp. 849-857, 1990.

[26] N.M.Pothecary and C.J.Railton, Analysis of Cross-Talk on High-Speed Digital Circuits Using the Finite Difference Time-Domain Method, *International Journal of Numerical Modelling*, vol. 4, pp. 225-240, 1991.

[27] A.Taflove and K.R.Umashankar, Review of FD-TD Numerical Modelling of Electromagnetic Wave Scattering and Radar Cross Section, *Proceedings of the IEEE*, vol. 77, no 5, pp. 682-699, 1989.

[28] F.D.Hastings, J.B.Schneider and S.L.Broschat, A Monte-Carlo FDTD Technique for Rough Surface Scattering, *IEEE Transactions on Antennas and Propagation*, vol. AP-43, no.11, pp.1183-1191, 1995.

[29] P.B.Wong, G.L.Tyler, J.E.Baron, E.M.Gurrola and R.A.Simpson, A three-wave FDTD Approach to Surface Scattering with Applications to Remote Sensing of Geophysical Surfaces, *IEEE Transactions on Antennas and Propagation,* vol. AP-44, no.4, pp.504-514, 1996.

[30] J.M.Bourgeois and G.S.Smith, A Fully Three Dimensional Simulation of a Ground-Penetrating Radar: FDTD Theory Compared with Experiment, *IEEE*

Transactions on Geoscience and remote sensing, vol. GE-34, no.1, pp.36-44, 1996.

[31] J.M.Bourgeois and G.S.Smith, A Complete Electromagnetic Simulation of the Separated Aperture Sensor for Detecting Buried Land Mines, *IEEE Transactions on Antennas and Propagation*, vol. AP-46, no 10, 1998.

[32] R.L.Roberts and J.J.Daniels, Modelling Near-field GPR in Three Dimensions Using the FDTD Method, *Geophysics,* vol. 62, no. 4, pp. 1114-1126, 1997.

[33] F.L.Teixeira, W.C.Chow, M.Strake, M.L.Gristaligo and T.Wang, Finite-Difference Time -Domain Simulation of Ground Penetrating Radar on Dispersive, Inhomogeneous, and Conductive Soils, *IEEE Transactions on Geoscience and Remote Sensing*, vol. GE-36, no.6, pp.1928-441937, 1998.

[34] R.Nilavalan, G.S.Hilton and R.Benjamin, A FDTD Model for the Post-Reception Synthetic Focusing Surface Penetrating Radar, *Proceedings of the IEE Conference on Antennas and Propagation*, York, pp. 69-72, 1999.

[35] R.Nilavalan, G.S.Hilton and R.Benjamin, FDTD Analysis of a Post-Reception Synthetic Focusing Surface Penetrating Radar Performance in Various Ground Conditions, *Proceedings of the Millennium Conference on Antennas and Propagation*, Davos, 2000.

[36] R.Nilavalan, R.Benjamin, G.S.Hilton, S.Litobarsski and E.McCutcheon, Microwave Detection of Subsurface Objects, *Report on Noise Limits for DERA*, University of Bristol, UK

2. Ground Penetrating Radars & Post Reception Synthetic Focusing

2.1. Introduction

An overview of Ground Penetrating Radar (GPR) techniques for subsurface probing was given in chapter 1, a detailed account is described here. The GPR method is a realistic solution to the present day requirements for subsurface probing. Present day requirements generally demand target detection and classification. The target echoes observed by receiving antennas in GPR systems can be used to locate the target accurately and also for subsurface imaging in some advanced systems. Section 2.2 looks into the background, different signal types and the processing techniques that are being used with the GPRs. However, current GPR techniques suffer from limited penetration depths due to attenuation in soil, poor operation in clutter, limited resolution achievable and search rate. A method to enhance GPR is Post Reception Synthetic Focusing (PRSF) [1] and this will be discussed in section 2.3 together with its implementation in Subsurface probing methods.

2.2. Ground Penetrating Radars

2.2.1. Background

The history of the GPRs dates back to 1910 with very simple Continuous Wave (CW) radars to pulsed techniques in 1926 [2]. Initial investigations included dipoles operating from vertical boreholes. These GPRs were primarily concerned with applications in the detection of various mineral deposits and rock formations. In 1970s

the GPR was investigated for military applications such as underground tunnel and mine detection [3]. From 1970 to the present day the GPR technique has been applied in various military and civil investigations.

2.2.2. Applications

As in all engineering innovations, the GPR is being further developed based on its applications. It is being used in various challenging applications such as [4, 5, 6, 7],

- Archaeological Investigations
- Pipe and cable detection
- Bridge deck inspection
- Detection of buried ordinances and tunnels
- Geophysical explorations of mineral deposits and rocks
- Forensic investigations
- Polar explorations (Ice layer thickness measurements)
- Planetary explorations (i.e. Mars)
- Medical applications (tumor detection)

2.2.3. Methodology

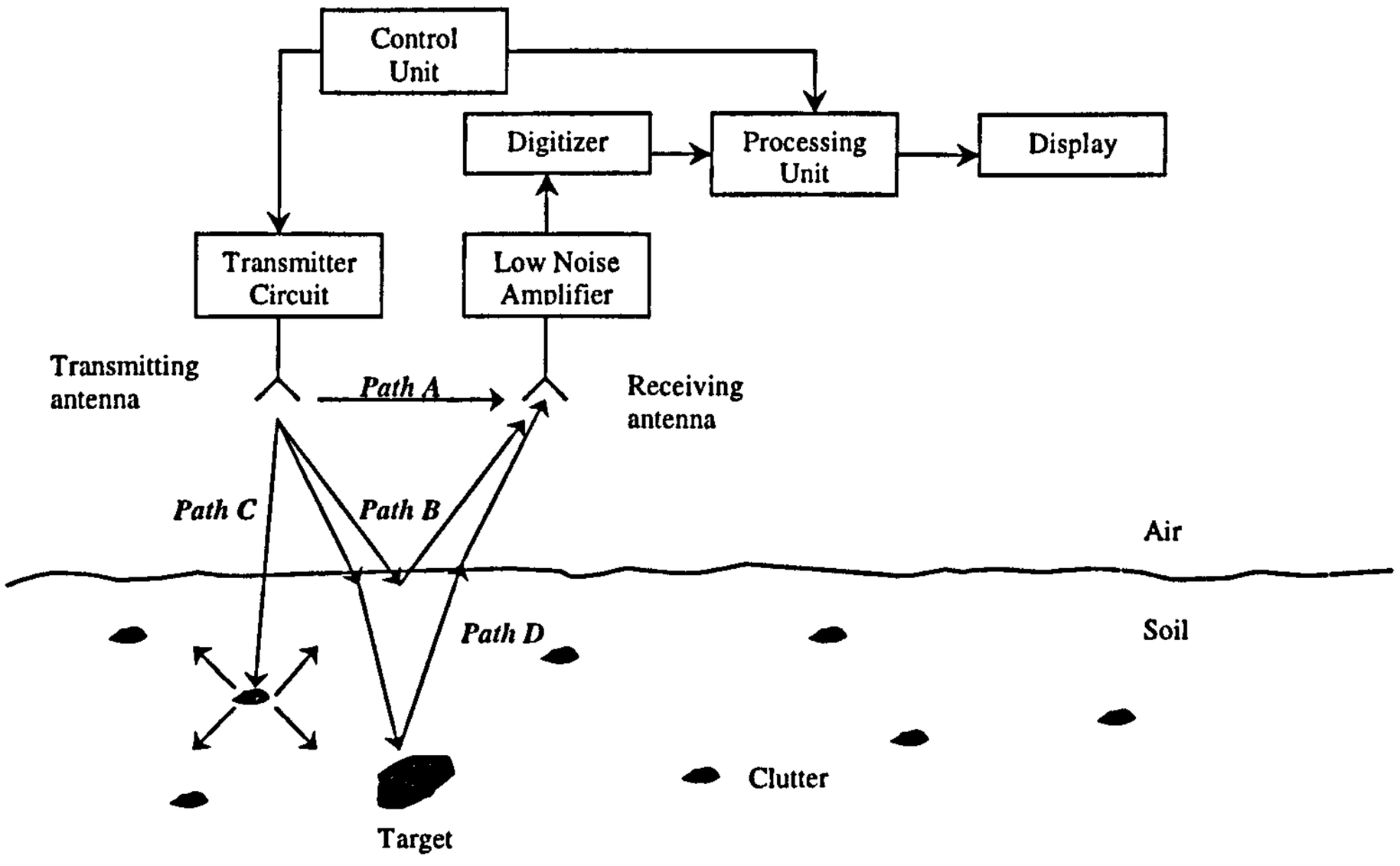

Figure 2.1 Ground penetrating radar

The GPR makes use of general radar concepts to detect objects in the subsurface. In a GPR, an electromagnetic signal is transmitted into the soil as shown in figure 2.1. The reflected signals from the object buried in soil are received using a receiver antenna. Antennas are placed near, or in-contact with, the soil-air interface to probe the subsurface. The GPRs, when operating in non-contact mode, have to deal with direct coupling between elements (path A in figure 2.1), reflections caused at the air-ground interface (path B) and the reflections from various dielectric discontinuities such as cavities, voids, transitions between soil and rock, filled areas or buried objects encountered in the soil (path C). The reflected signal from a specific target (path D) will be contaminated by reflected signals from various dielectric discontinuities which have the same path delays, and this unwanted clutter makes the target identification a difficult task. Clutter encountered by GPRs is quite significant and provides a great challenge for target identification. The successful detection of subsurface objects primarily depends on the following requirements,

- The efficient transmission of signals in to the soil.
- Adequate resolution to identify the buried objects.
- Sufficient signal to noise ratio.
- Acceptable clutter levels.

2.2.4. Modes of Operation

Generally the bi-static mode of operation (where separate transmitter and receiver elements are used) is preferred, as very high switching is necessary for mono-static mode operations (single element for transmission and reception) where reflections occur from very short ranges compared to the free-space radar. Wide band directional couplers are another consideration with mono-static mode operations.

2.2.5. Signal Types

Most conventional GPR systems operate at frequencies less than 1.5GHz. In long range investigations of, for example, geological strata or deep ice, frequencies as low as few tens of MHz are used [8]. Different types of waveforms and modulation techniques are

being used with the GPR systems. The choice of waveform type is primarily governed by the type of application and the nature of signal processing techniques.

2.2.5.1. Pulse Modulated Carrier.

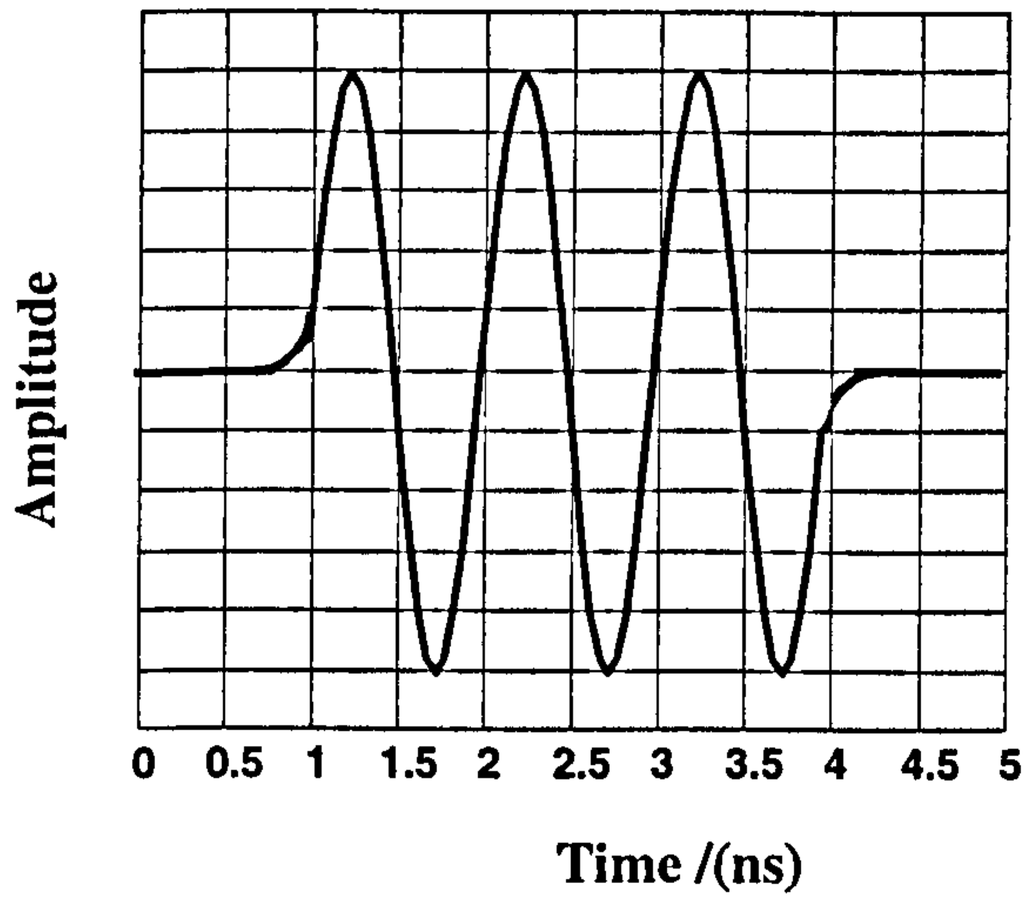

Figure 2.2 Pulse modulated carrier

Pulse modulated carrier signals (figure 2.2) can be used to detect deeply buried targets [9]. These signals are easy to transmit from antennas, which have limited bandwidths. Narrow band pulses would suffer from the strong reflections at the air-soil interface, which significantly mask the return signals from the shallowly buried targets. The use of signal processing techniques would overcome some of these limitations, and these are reported in chapter 4.

2.2.5.2. Impulse or Base Band Pulses.

Impulse or base band pulses are very useful in detecting shallowly buried targets. Since soil exhibits high attenuating characteristics with increasing frequency, base band pulses can be employed to overcome some of these limitations. However higher frequency contents of ultra wide band pulses also suffer attenuation and dispersion due to the soil characteristics. Chan *et al* employed these types of pulses to characterise subsurface targets [10]. Challenging wide bandwidth antenna designs are also required to transmit such pulses.

2.2.5.3. Frequency Modulated Continuous Waves (FM-CW)

High-resolution images are possible with frequency modulated signals. The transmitted signal is linearly swept over a frequency range and the resulting reflected signals are mixed with the transmitted signal to find the beat signal, which provides the target location [11]. The strong surface reflections from the air-soil interface can be reduced, through band limiting the beat signals. A typical system is shown in figure 2.3.

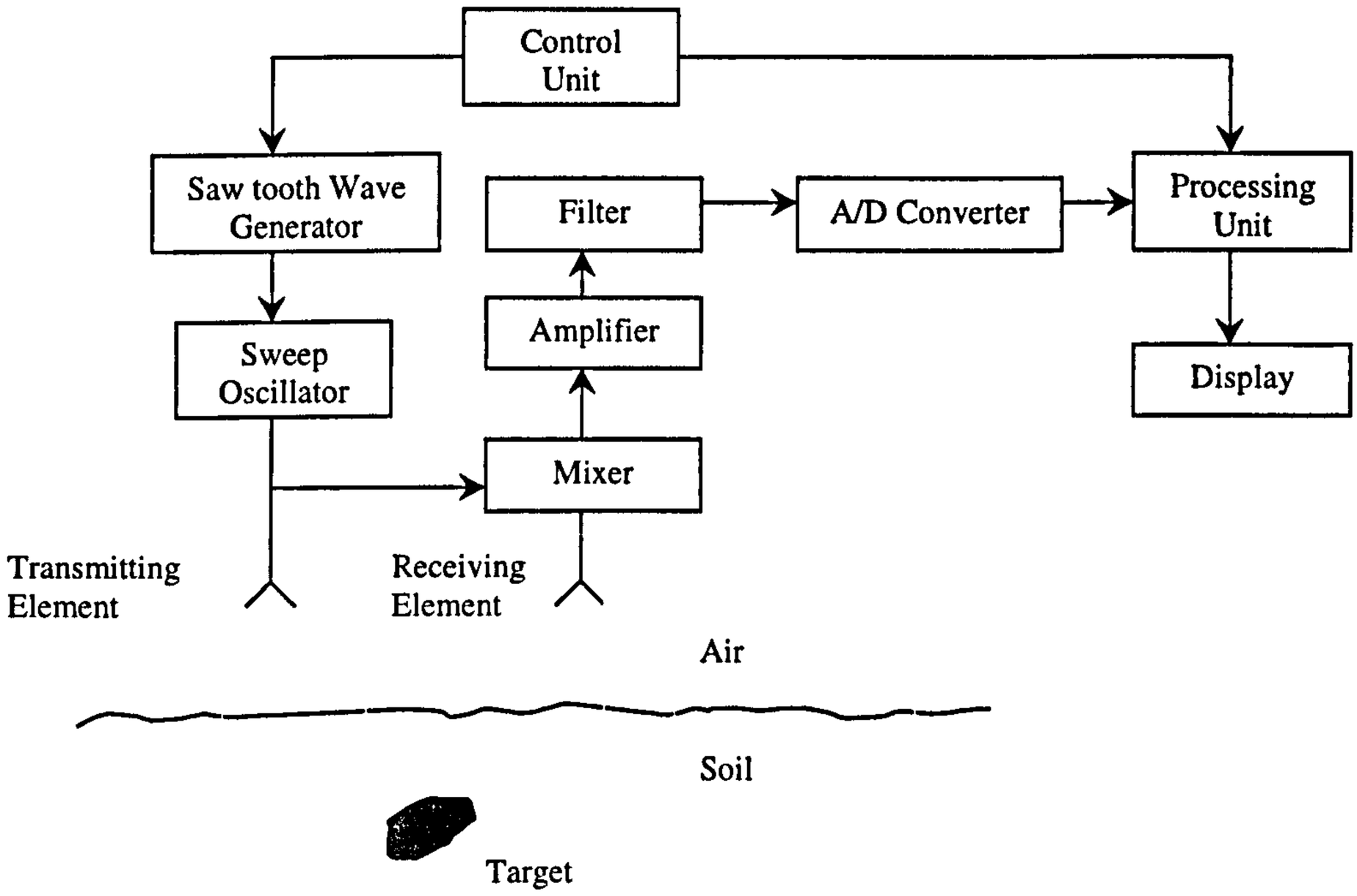

Figure 2.3 Frequency modulated continuous wave system

In principle the FM-CW signal is an alternative to a wide band video pulse. The biggest advantage of this system is the better control of the transmitted spectral shape compared to the video pulse, which would be distorted by the antenna response. The complexity involved in this method and the extra processing requirements for imaging restricts the use of the FM-CW systems in many simple applications.

2.2.5.4. Synthetic Signals.

Synthetic spectral signals are similar to the FM-CW technique. In these types of system, a range of discrete frequencies of controlled amplitude and phase corresponding to a time domain pulse is transmitted. The received signals are processed using a network analyser, which provides the magnitude and phase

information of the received pulse. Inverse Fourier transforms of the analyser output gives the time domain pulse, which provides the necessary range information [12]. Synthetic signals are useful with the band-limited components, which generally create ringing in the system response. These types of signals also eliminate the need for high power pulses since the power is spread among its frequency components.

2.2.5.5. Continuous Waves

Single frequency signals are being used with systems employing microwave holography, which is discussed in section 2.2.6.4. Frequencies in the range of hundreds of MHz are employed considering the high attenuation in Soil. Continuous waves are of limited use because of their poor performance in high clutter that are usually eliminated by time gating techniques.

Although several waveforms are being used with the GPR systems, more emphasis is being shown towards the modulated pulses and base band pulses because of the simplicity involved and the lower signal processing requirements.

2.2.6. Target Detection and Identification.

Target detection and identification is generally achieved by basic time domain analyses which leads to image processing. Although the resolution achievable in most GPR systems limits the image quality, knowledge-based interpretations will enhance the target identification.

2.2.6.1. General Processing Techniques

General processing techniques involve basic time domain calculations and pulse compression techniques. Filters such as the matched filter [13] are being utilised to pick out the target echo and modify its shape to give a single peak, which increases the detection probability. FM-CW GPR uses the beat frequency for target location calculation and time domain analyses for the imaging process.

2.2.6.2. Polarisation Discrimination Methods

Polarisation signatures are another useful property to discriminate buried targets. Signals scattered from targets, which are longer in one dimension such as pipes and cables, have a larger component parallel or perpendicular to the longer axis depending on the target type and environment [8]. The relationship between the incident and reflected (scattered) polarisation for a generic target can be represented by, [14]

$$\begin{bmatrix} E_x^s \\ E_y^s \end{bmatrix} = \begin{bmatrix} s_{11}\, s_{12} \\ s_{21}\, s_{22} \end{bmatrix} \begin{bmatrix} E_x^i \\ E_y^i \end{bmatrix} \tag{2.1}$$

Where,

E_x^s, E_y^s : Scattered field conponents

E_x^i, E_y^i : Incident field conponents

s : Matrix representing the multiplying factors

This property could be used to discriminate between the objects which have a single longer dimension. Orthogonal antenna measurements at rotated positions are being used with this type of target identification technique [10]. The disadvantage of this method is it is insensitive to flat surfaces. Although the air-soil interface reflections can be minimised, there are possibilities where symmetric or isotropic targets producing very low level of signals, which are difficult to identify.

2.2.6.3. Target Resonance Methods

Another target classification technique is to use Complex Natural Resonance (CNR) frequencies of buried targets [15]. The late time response of the back-scattered signals from buried targets can be expanded using the singularity expansion technique [15] in which each singularity corresponds to a CNR. A back-scattered waveform from a subsurface target can be represented by a few exponentially damped sinusoids as [15],

$$r(t) = \sum_{i}^{N} a_i . \exp(s_i t) \tag{2.2}$$

where,

$r(t)$: received waveform

s_i : complex natural resonance

N : number of resonances within the frequency band of the radar

a_i : multiplying coefficient

In the complex frequency domain it can be represented by,

$$L[r(t)]=\sum_{i=1}^{N}\frac{a_i}{(s-s_i)} \tag{2.3}$$

Where,

L : Laplace Transform operator.

These natural frequencies (singularities) can be extracted using various mathematical techniques. It has been observed that the CNR frequencies are almost independent of the orientation and location of the antenna, but their strengths are affected by these parameters [15]. Although this technique is an alternative to the imaging technique, it is only useful for the identification of known targets as the CNR frequencies depends on the physical dimensions and characteristics of the buried targets.

2.2.6.4. Microwave Holography

Microwave holography is useful in imaging concealed objects, which are optically opaque but are transparent to microwaves. Generally the microwave holographic technique makes use of a probe to sample the reflected signals by scanning over an aperture [16]. The sampled microwave returns are compared with a reference signal and employed to make the hologram [17]. High-resolution techniques involving fixed transmitter /receiver pair scanning also appeared in the literature [18]. The general set-up of the microwave holographic method is shown schematically in figure 2.4.

The holograms (or a reduced size photographic transparency of the hologram), when illuminated with an appropriate beam, produces the details of the concealed objects. This method of imaging is an extension of optical holography, with the image reconstruction being done using digital processing techniques [19]. Holographic methods are also being used with cross-polar techniques to reject the air-soil reflections, which severely limits the target identification. Anderson and Richards demonstrated this principle in detecting buried pipes [20].

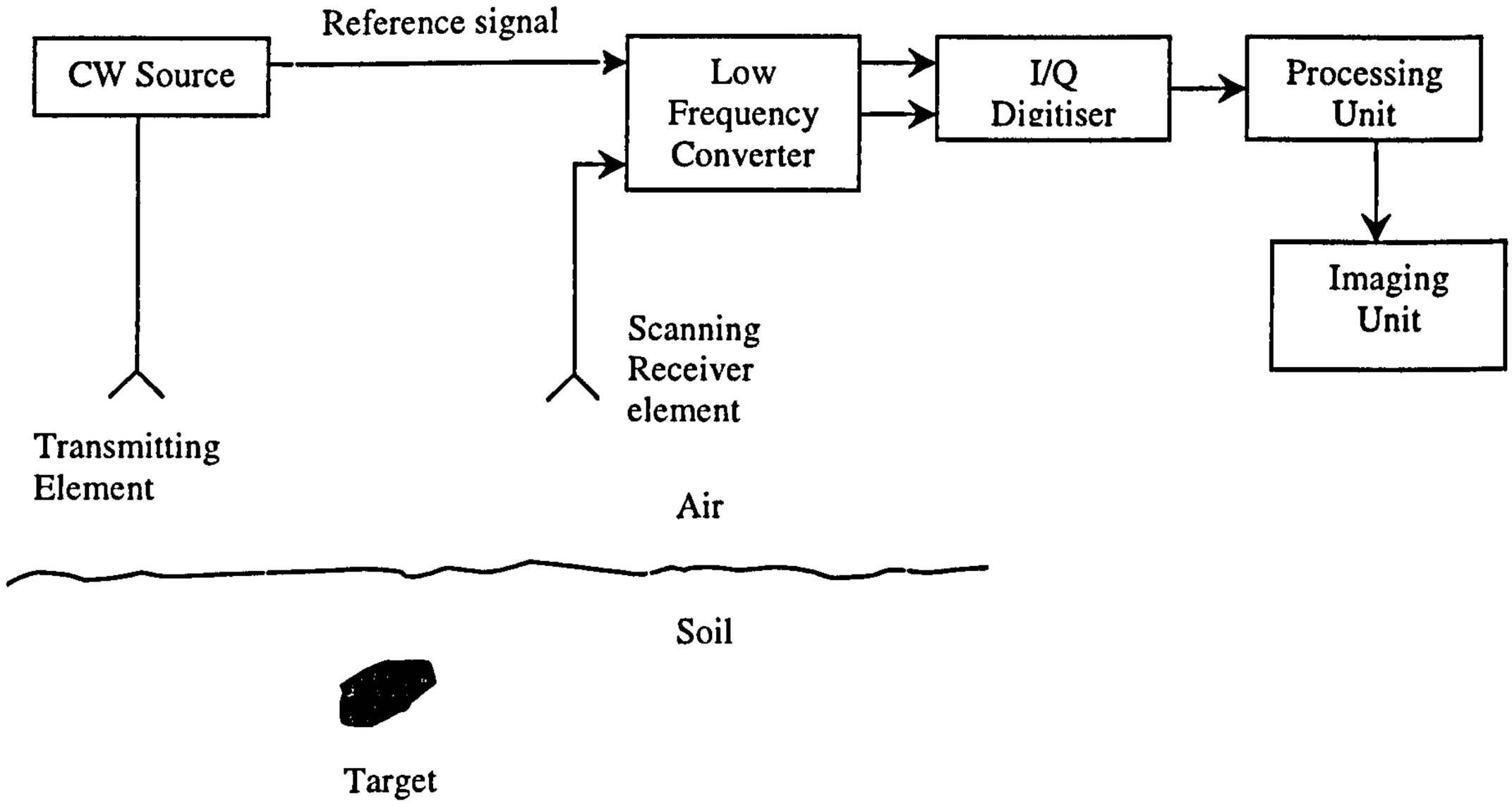

Figure 2. 4 Schematic representation of microwave holographic scanning system

Optical holographic techniques are attractive and useful for the three dimensional imaging of free space objects because of very high resolution achievable, however microwave holography has limitations due to one way-focusing, and hence poor resolution compared to other advanced techniques. Microwave holographic techniques are slow in mapping the subsurface and have limitations in high clutter environments since there is no time gating employed in processing.

2.2.6.5. Synthetic Aperture Techniques

The highly successful synthetic aperture techniques of remote sensing in free space radar systems are also employed to investigate the subsurface. In synthetic aperture radars, the irradiation and the subsequent reception of the reflected signals from the targets are performed from a mobile platform that synthesises a wider aperture antenna [21]. The resulting signals are properly aligned considering the timing, phase and antenna location to generate the information that would have been generated by a simple wide aperture antenna, hence giving a finer resolution.

In subsurface applications, figure 2.5, a transmitter-receiver pair (together or individually) is scanned over a 2D area to simulate a wider aperture for subsequent image reconstruction. Osumi and Ueno [22] used similar techniques to map the

subsurface. Magg *et al* [23] used a single transmitting horn and a receiving dipole element array on a moving platform to theoretically analyse their synthetic aperture technique. Generally the image reconstruction is performed in two stages comprising pulse compression for optimisation against noise and aperture synthesis for the finer resolution.

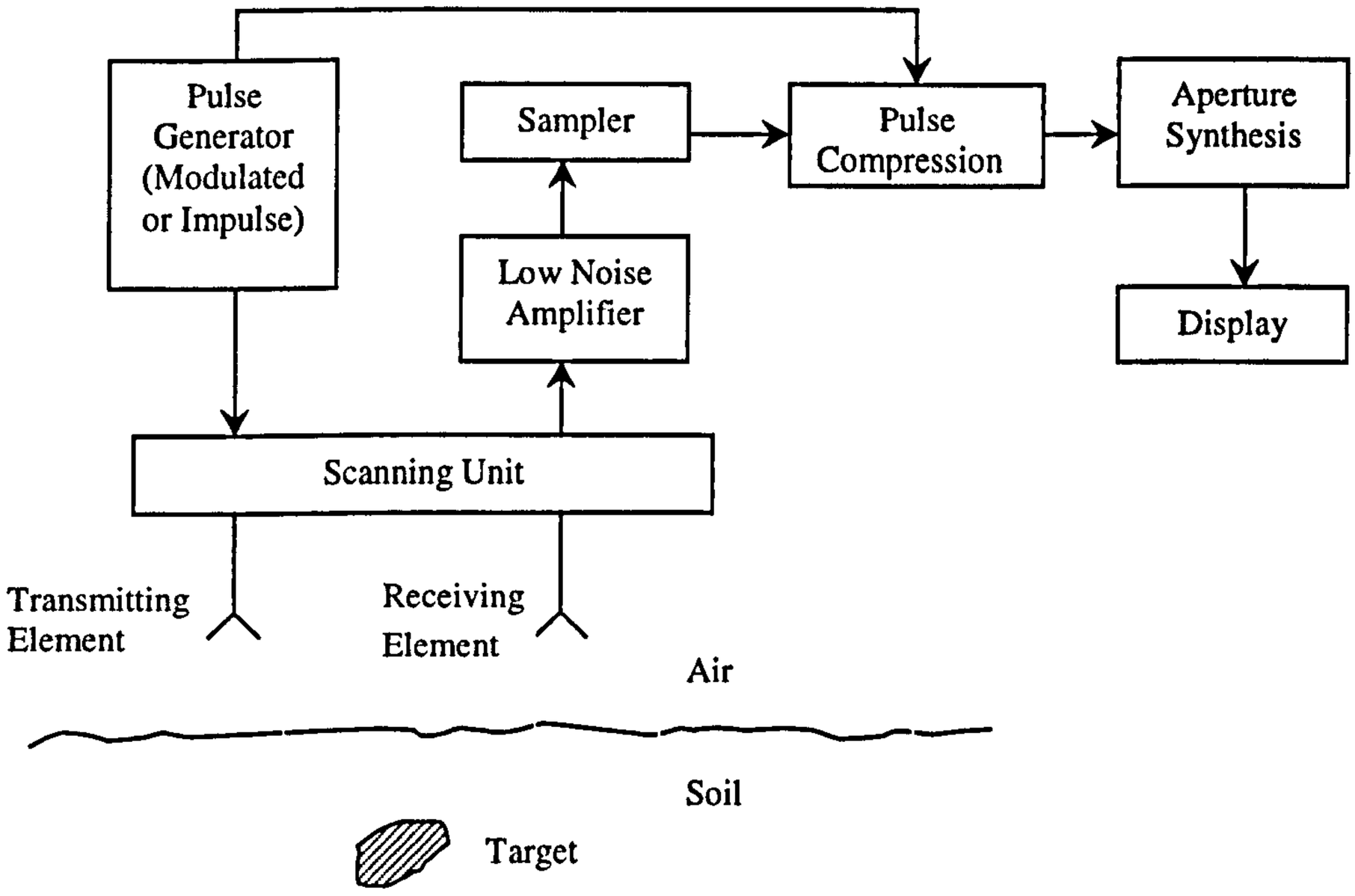

Figure 2.5 Synthetic aperture method

The use of broadband pulses in this technique enhances the vertical resolution and provides significant advantage over the microwave holographic method. But this type of subsurface mapping will take a long time to scan the subsurface and will have a relatively poor processing gain compared to the methods discussed in the following sections.

2.2.6.6. Spot Focusing Techniques

Near-field spot focusing in subsurface applications was first proposed by Benjamin [24,25] for the detection buried land mines. This method involves spot focusing in transmit and receive radiation to enhance detection process. The general set-up of this system is schematically represented in figure 2.6.

The relative timing and phase is adjusted in the network feeding the elements to focus the transmitted signals onto the desired location. Focusing is implemented considering

the path delays associated with each element to the desired resolution cell. Subsequent return signals are also focused to the same location using a similar arrangement, producing two way focusing on to the desired resolution cell.

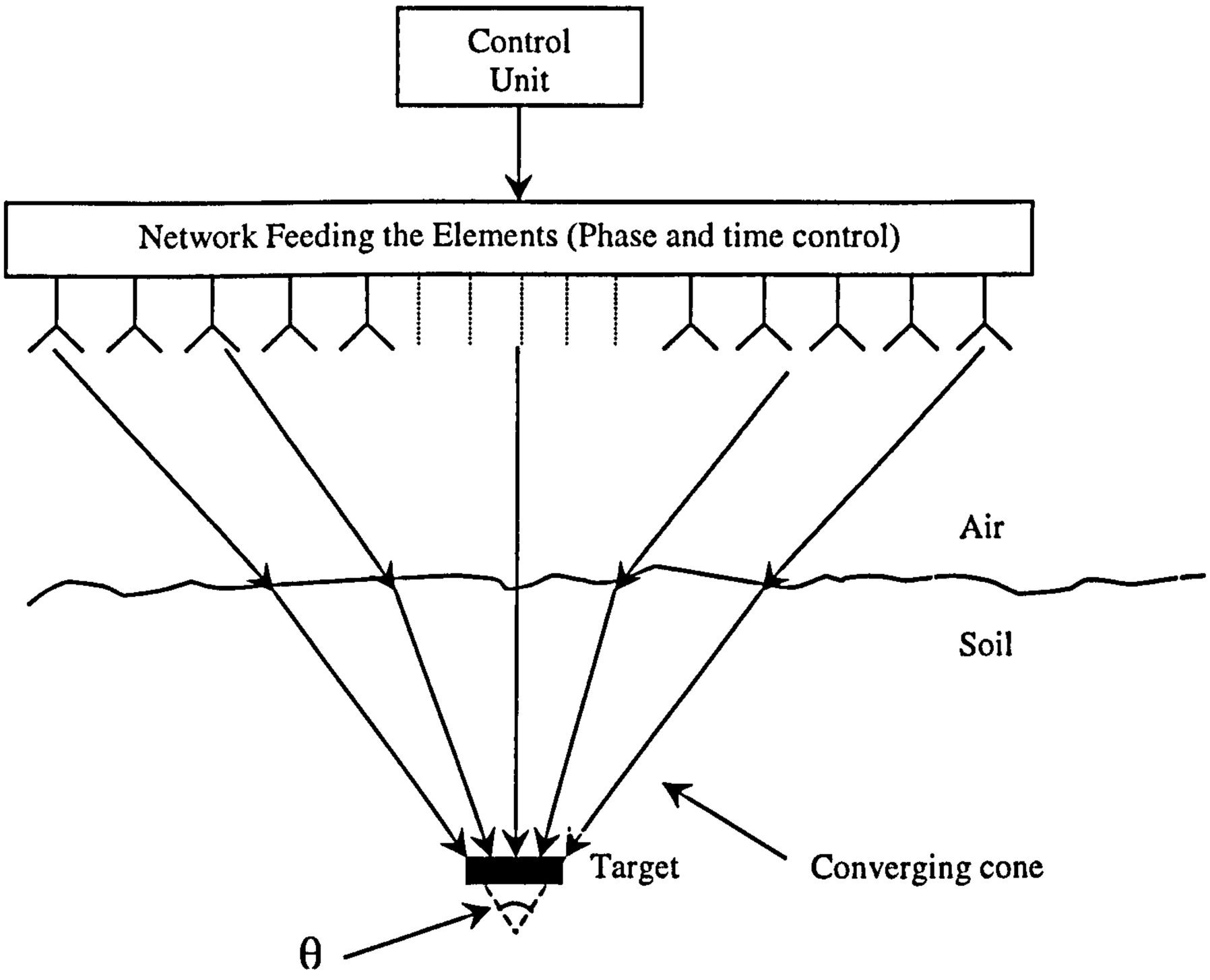

Figure 2.6 Near field spot focusing

It has been shown, in [25], that the spot focusing technique would achieve a lateral resolution of $\lambda/2\theta$ and a vertical resolution of $2\lambda/\theta^2$ (i.e. if not limited by the pulse length). Where, λ is the wavelength (in soil) corresponding to the operating frequency and θ is the convergence angle as in figure 2.6. The focusing gain associated with the spot focusing technique further improves the detection process in high attenuating soils. The processing gain achievable in this kind of technique is much more significant compared to other subsurface investigations methods, hence permitting operation at higher frequencies and improving the resolutions. Since spot focusing is involved, it is capable of discriminating the clutter arising from other subsurface anomalies that obscure the detection process and the imaging of the subsurface objects.

The promising features of the spot focusing technique gave birth to an effective practical implementation concept using post reception methods [1]. The post reception

synthetic focusing technique is outlined in the next section and considerable attention is given to this concept in this thesis.

2.3. Post Reception Synthetic Focusing

2.3.1. Overview

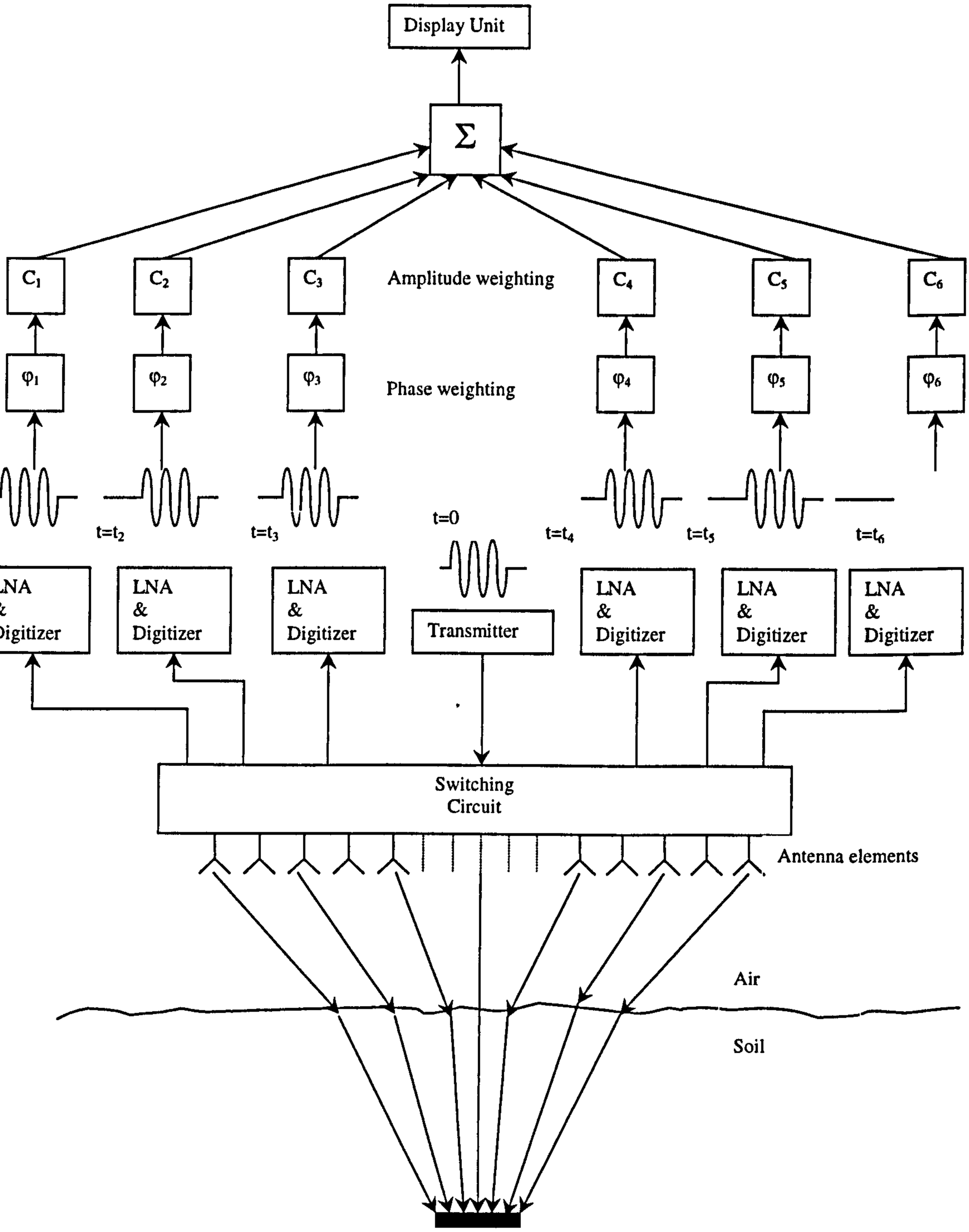

Figure 2.7 Post-Reception Synthetic focusing GPR

The post reception synthetic focusing method [26] is a time domain technique which shares some properties with the synthetic aperture radar [21]. The PRSF technique is realised using an N element array as considered in figure 2.7. Contrary to the conventional focusing techniques (section 2.2.6.6), focusing is done off-line using the collected data. One element transmits at a time and the subsequent reflected signals are recorded at all the elements, which have the resolution cell in their 'field of view'. This field of view, for instance, may be regarded as the antenna element's half power beam width. This procedure is repeated with other transmitting elements, which have the resolution cell within their field of view. For the subsequent off-line near-field focusing, appropriate two way timing corrections (φ in figure 2.7) are applied and coherently added to focus the signals to the relevant resolution cells. This procedure is illustrated in figure 2.7 and figure 2.8.

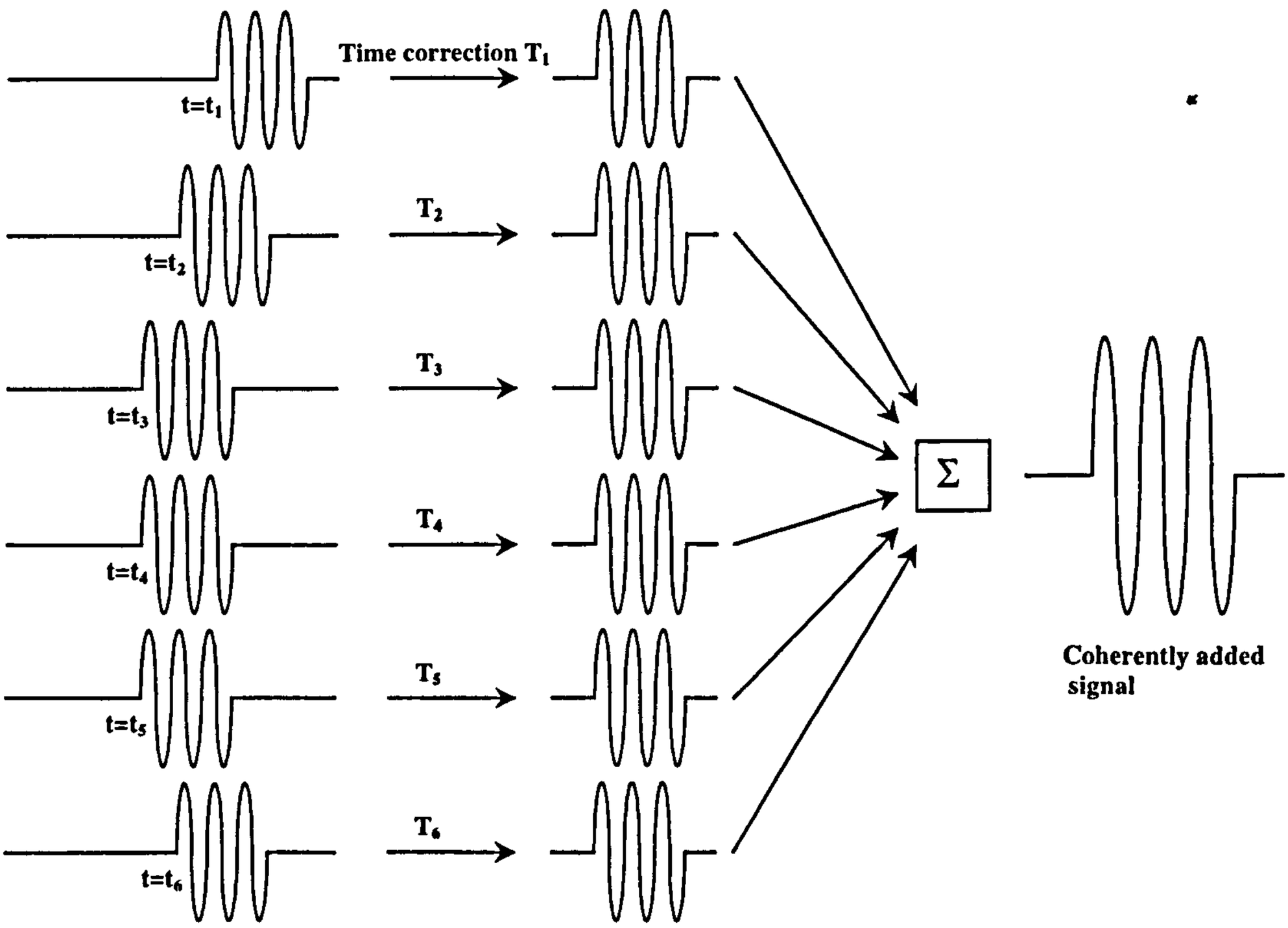

Figure 2.8 Time domain coherent addition of target signals at the target location

Furthermore, appropriate amplitude scaling (C1-C_6 in figure 2.7) for path losses to each transmitter-receiver path via the resolution cell, would further enhance the detection process.

Hence, if n paths are associated with a resolution cell, the PRSF technique could be analytically represented by,

$$V = \sum_{i=1}^{n} C_i U(t - T_i) \tag{2.4}$$

where,

V : Synthetically focused signal.

$U(t)$: Signal received from path i.

n : Number of paths which are associated with the resolution cell.

C_i : Scaling factor for path i.

T_i : Path delay from the transmitting element to the receiving element via the resolution cell.

Unlike the conventional focusing techniques where all elements transmit at the same time to focuss on to a single resolution cell, this method uses a single element to transmit at a time for the subsequent near-field focusing of all distinguishable three dimensional resolution cells. Hence a reduction in mean power transmission is possible with the PRSF technique.

2.3.2. Processing Gain

The processing gain of a PRSF system is determined by the number of elements that have the resolution cell in their field of view. Hence, the deeply buried target will benefit from a higher processing gain, partially equalising the extra path losses. If each of N elements transmit in turn, reception in (N-1)/2 elements would provide the necessary information. (i.e. element A transmits and element B receives is same as element B transmits and element A receives). Hence the system processing gain is given by [25],

$$G = \frac{N(N-1)}{2} \tag{2.5}$$

Where,

G : Gain of the system

N : Number of elements that see the resolution cell.

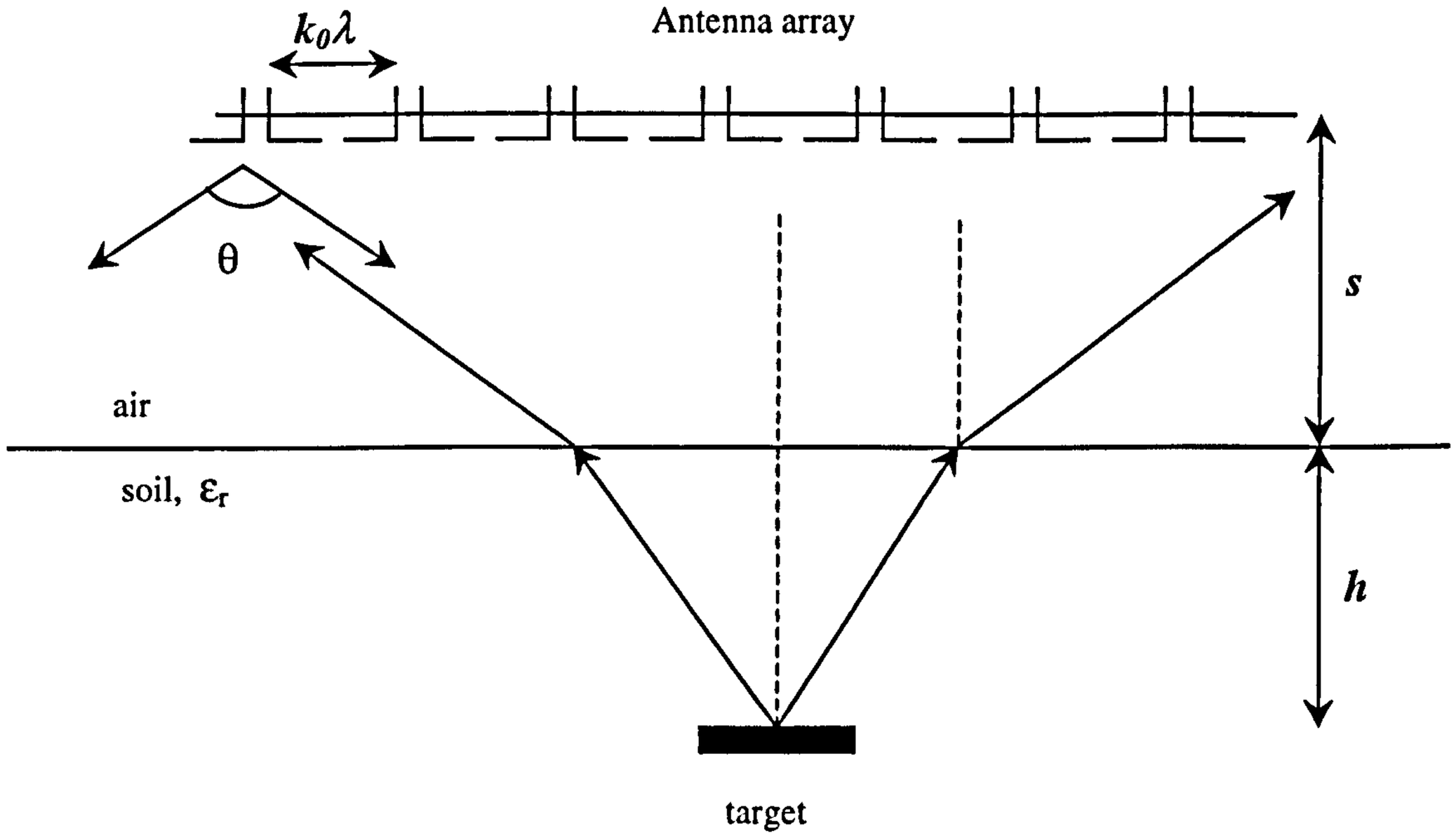

Figure 2.9 Number of elements that see the target

As shown in figure 2.9, the number of elements that see the resolution cell in a subsurface system depend on the following factors:-

- The separation between the antenna array and the air-soil interface, *s*.
- Depth of the focusing resolution cell, *h*.
- The inter element spacing in the antenna array, $k_0\lambda$.
- Useful radiation pattern of the transmitting and receiving antenna elements, θ. (i.e., a broad beam towards the soil over the bandwidth of the antenna)
- Dielectric constant of the soil, ε_r.

The processing gain achievable with the PRSF technique is higher than the other probing techniques that employ a pair of transmitting and receiving elements because of the different number of paths and provides a significant advantage in the detection process.

2.3.3. Resolving Power

The spatial resolving capabilities of a system are usually described in terms of the resolution. More precisely, it is the ability of the system to discriminate whether one or more targets are being observed. The resolving power of a PRSF technique can be

illustrated through the vertical and lateral resolutions. The lateral resolution achievable depends on the following factors,

- Useful radiation pattern of the antenna elements
- Operating wavelength of the system
- Loss characteristics of the soil.

It has been shown [21,25] that the in-air lateral resolution achievable in this kind of system is $\lambda/2\theta$, as in the spot focusing technique (i.e. assuming a loss-less medium and full usable aperture length), and a brief description is given in Appendix A. The convergent angle depends on the exploitable aperture length of the array. Wider beam patterns of the antenna elements in the array would increase the effective aperture length, and hence the resolution. Furthermore, an interesting phenomenon in the subsurface applications is that both λ and θ are reduced approximately inversely proportional to the square root of dielectric constant of the medium ($\approx 1/\sqrt{\varepsilon_r}$). Hence the lateral resolution is almost independent of the subsurface dielectric constant.

The loss characteristics of the soil would also affect the resolution, as the longer paths in soil would undergo more attenuation compared to the shorter paths. This effect is less significant since, in general, the high attenuating medium will exhibit a higher permittivity [27], hence a narrow in-soil convergent angle which makes the path length variation insignificant.

The depth resolution of the PRSF technique is given by $2\lambda/\theta^2$ [25]. The depth resolution will increase as $\sqrt{\varepsilon_r}$, though it will be degraded up to a limit, which is set by the pulse length in soil $n\lambda_a/(2\sqrt{\varepsilon_r})$. Where n is the number of cycles in the transmitted pulse. Hence a shorter pulse length will give a better resolution and will improve the detectability of the shallowly buried objects. Sections 3.5- 3.7 further consider the lateral and vertical resolutions and verify these findings.

2.3.4. Operation in High Clutter Environments

Surface penetrating radar operates in a high clutter environment which makes the target detection and identification a challenging task. Clutter can be classified into volume and surface clutter. The volume clutter arises mainly due to the dielectric

discontinuities in soil and various other embedded pebble-like objects. The surface clutter is caused by air-soil interface reflections.

In the PRSF system, volume clutter, arises from a small area common to all the possible paths defined by the distinct element pairs. Clutter associated with each unique path is generated from the discontinuities and pebble-like objects within the common-delay common-view clutter volume as shown in figure 2.10 defined by [28],

- The locus-surface of path delay equal to that from the transmit element via the centre of the given resolution cell to the receive element. (An ellipsoid of revolution, flattened in the soil due to refraction, with transmitter and receiver as foci and passes through the wanted resolution cell)
- A thickness, orthogonal to that locus surface, varying by ± half the pulse length. (This thickness is inversely proportional to square root of ε_r).
- The beam cross section of both transmitter and receiver at the resolution cell (both reduced due to refraction in soil).

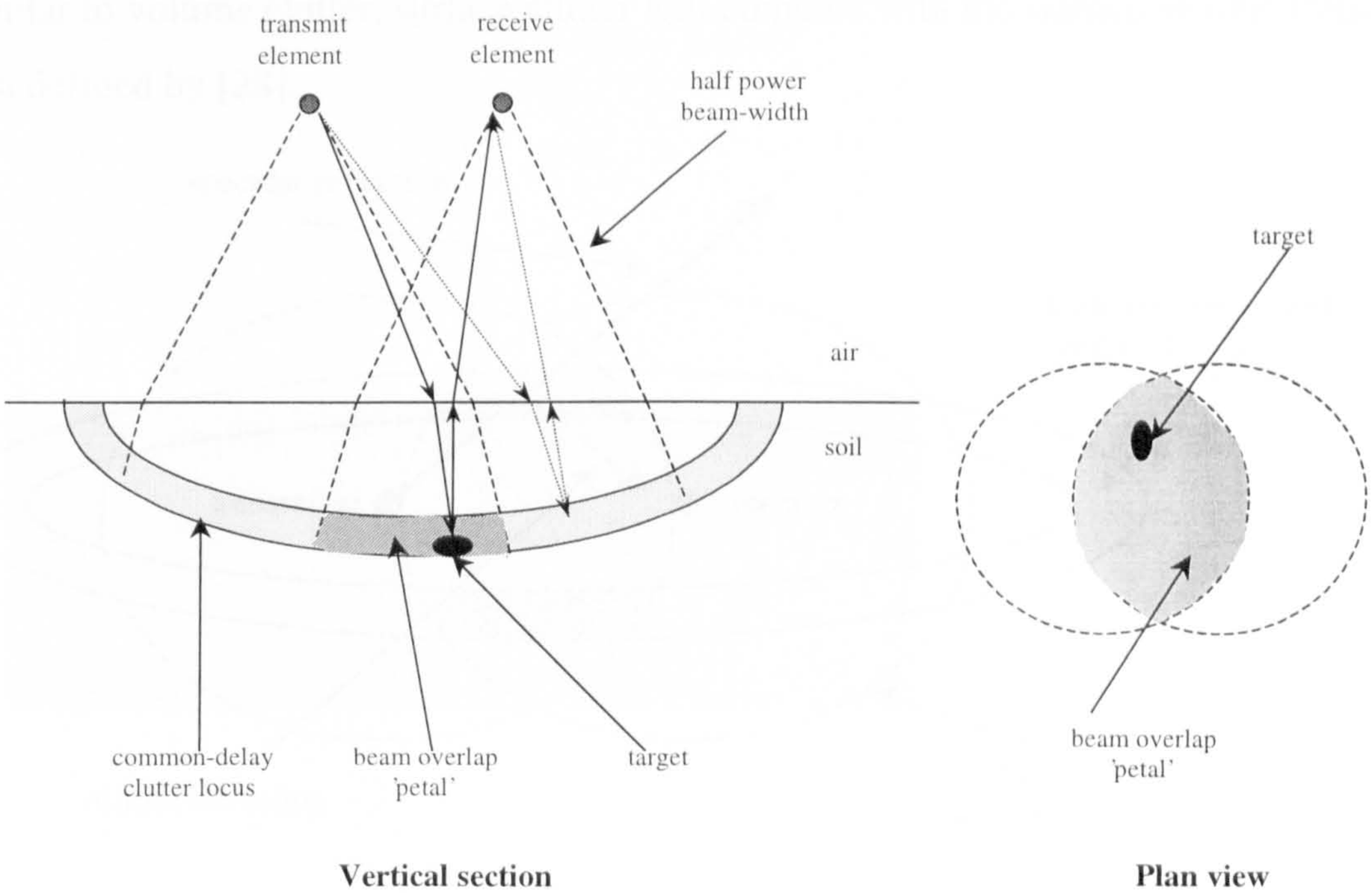

Figure 2.10 Common delay clutter volume

In the PRSF technique, the coherent summation of these clutter signals from various paths will only arise from the focused resolution cell as shown figure 2.11. Moreover,

the unique capability of the PRSF concept is that each path can be weighted to reduce the clutter contributions before the summation process, giving an advantage over the other subsurface systems. This clutter reduction technique is described by Benjamin [28] and a brief description is given in Appendix C. The capabilities of the PRSF technique when operating in clutter environments are demonstrated using FDTD method in chapter 4.

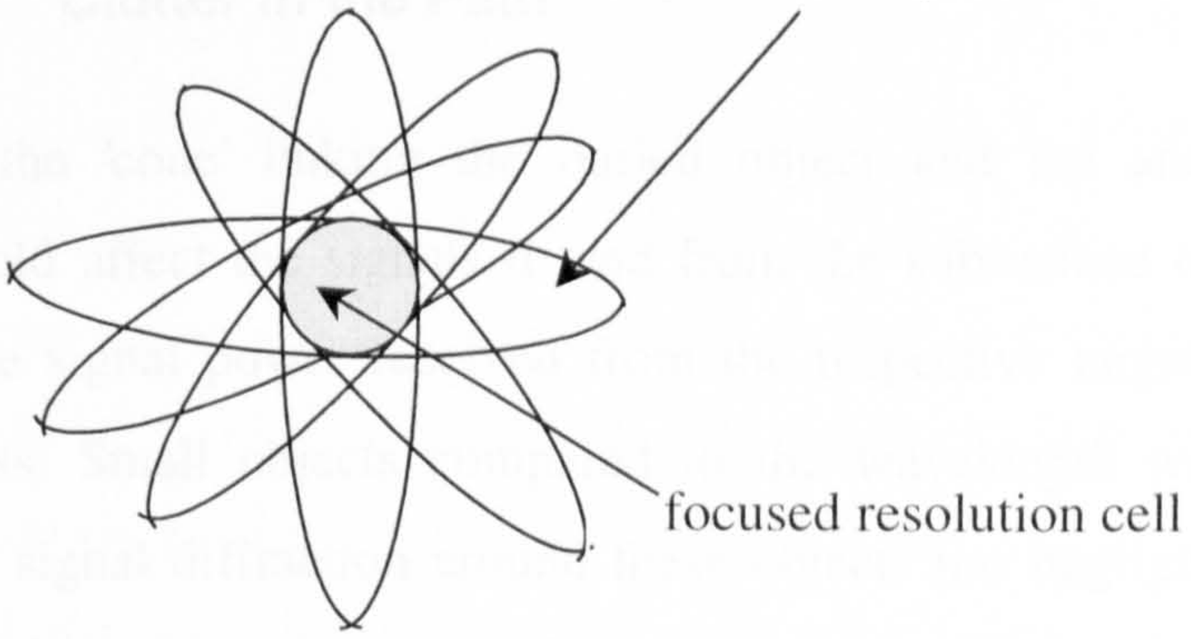

Figure 2.11 Clutter in PRSF system

Similar to volume clutter, surface clutter will compete with the wanted signals from the area defined by [28],

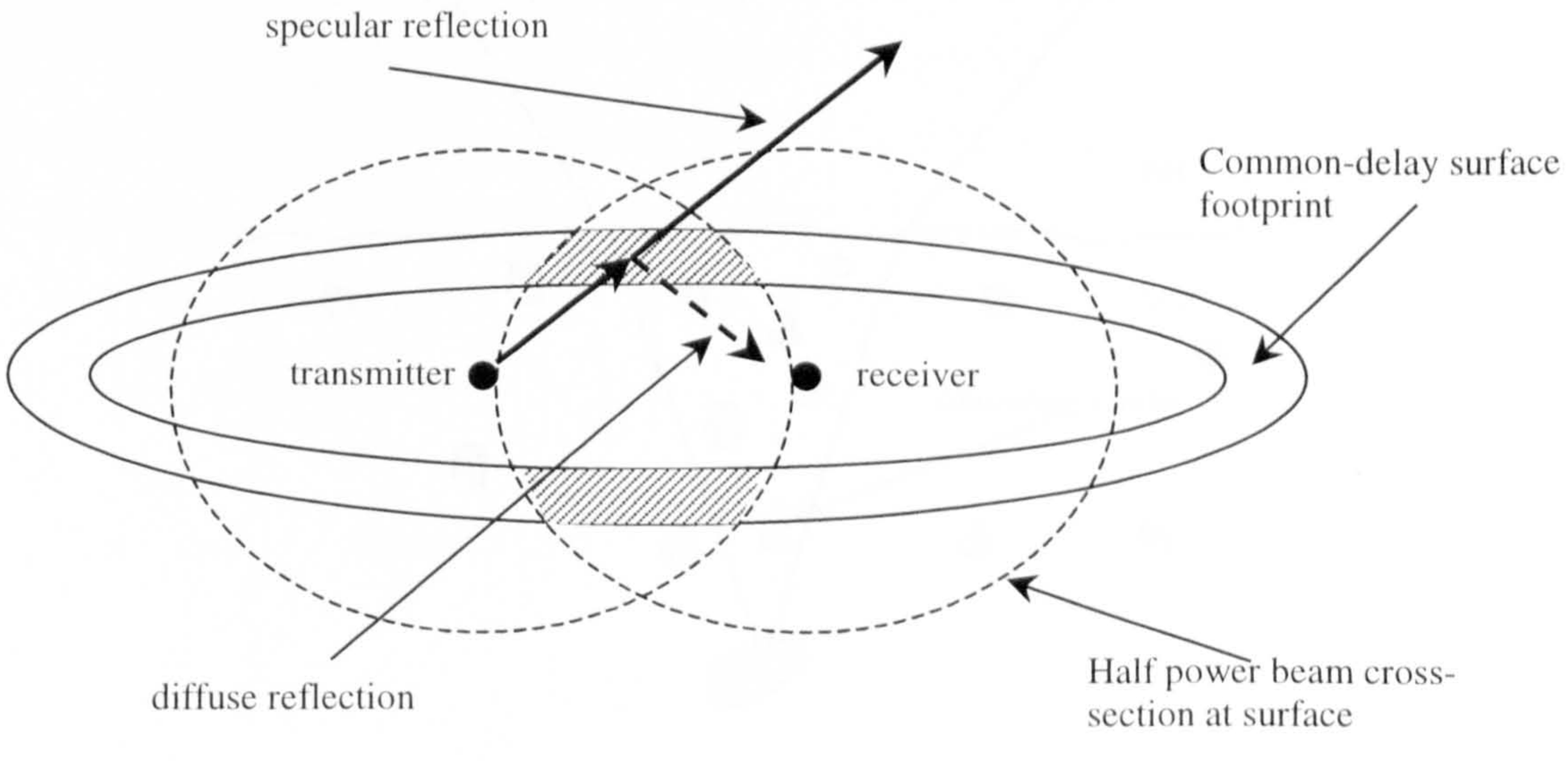

Figure 2.12 Surface clutter

- Common-delay surface footprint defined by the locus, whose outer and inner perimeters corresponds to path delays equal to that from the transmit element via the centre of the given resolution cell to the receive element ± half the pulse length.

- The in air beam widths of both transmit and receive elements.

Furthermore, for smooth ground conditions, the specular reflection from such footprints will point well away from the receiver and only the diffuse scatter will interfere with the wanted signals as shown figure 2.12. The effects of such reflections are further reduced for deeply buried objects as the overlaps between different paths in the PRSF technique is minimal.

2.3.5. Clutter in the Path

Clutter within the 'cone' linking the buried object and the antenna array, as in figure 2.13, would affect the signals to and from the subsurface objects. This effect could reduce the signal power received from the respective targets and degrade the detection process. Small objects compared to the wavelength would not limit the detection as the signal diffraction around these objects has negligible absorption and scattering. But objects large compared to the wavelength would cause significant degradation of the signal.

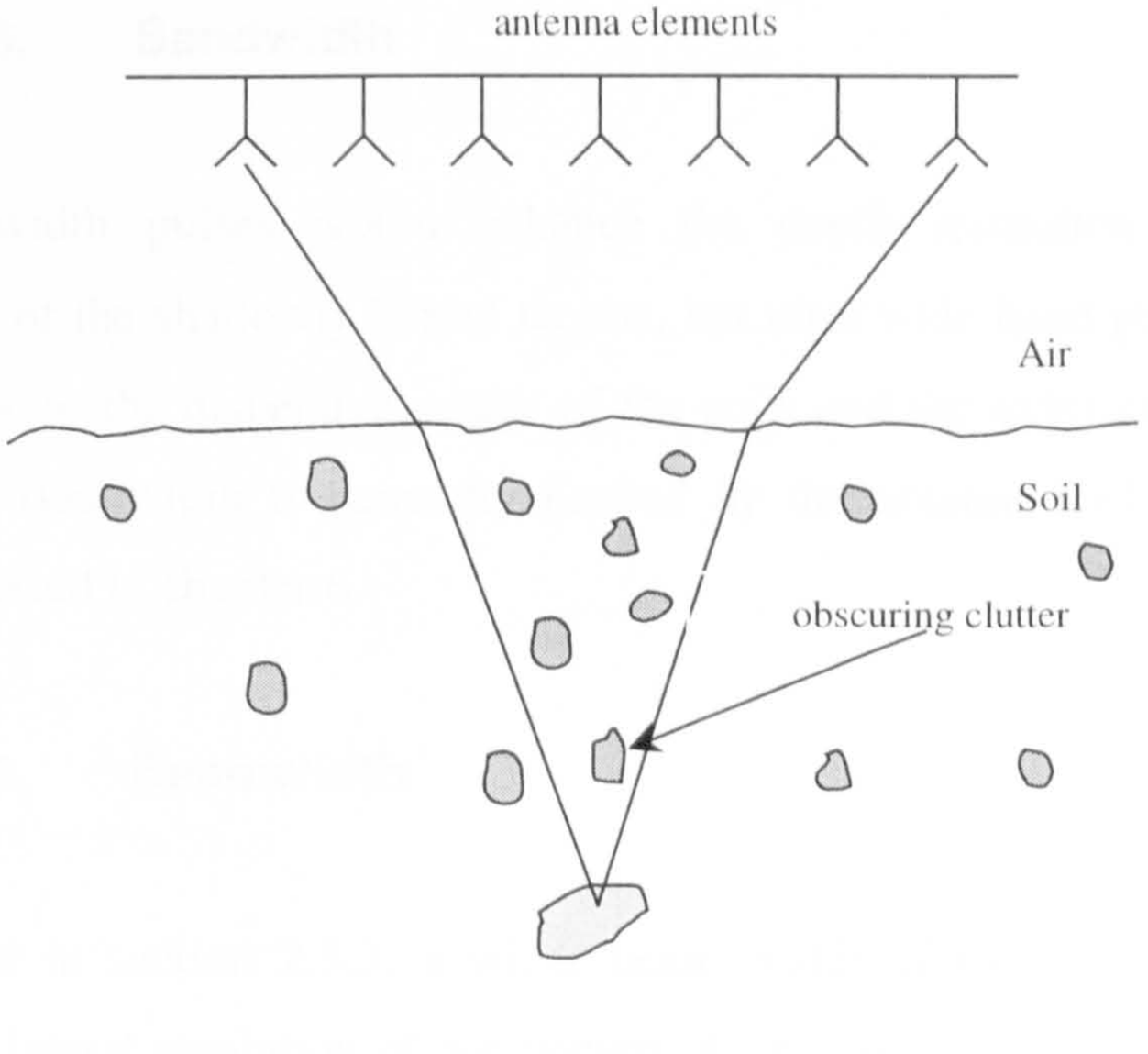

Figure 2.13 Clutter in the path

2.3.6. Search Rate

The PRSF technique, when applied from a moving array, is fast compared to most conventional GPRs that employ only a transmitter-receiver antenna pair. The close

range propagation delays associated with the GPRs and the fast signal processing place the limit only on the mechanical movement of the array. This kind of fast mapping technique is well suited for mine clearance operation that is rather slow with the conventional GPR techniques.

2.3.7. Choice of Frequency

The main benefits of using a high frequency are fine resolution, accurate object location, good distinction of shallowly buried objects and high processing gain for a given size of antenna array. On the other hand, a lower frequency would provide a better ground penetration, minimal effects from small pebble like objects, less hardware (number of elements) and signal processing requirements. The extra gain achievable and the better performance in a clutter environment of the PRSF technique can compensate the soil attenuation and the extra clutter degradations at high frequencies would give a better target identification scheme.

2.3.8. Bandwidth

Wide bandwidth pulses would enhance the depth resolution and increase the detectability of the shallowly buried targets, but ultra wide band pulses would also be degraded due to the dispersive nature of the soils and the extra attenuation at higher frequencies. Bandwidth is generally limited by the antenna-feed match and this is further discussed in chapter 6.

2.3.9. Beamwidth

As discussed in section 2.3.3, a wider beam width of the individual element will enhance the lateral resolution of the system. As the number of elements that 'see' the target would also increase, it will further increase the processing gain of the system. Hence a simple antenna element with wide bandwidth and beamwidth properties is appropriate for a practical system.

2.3.10. Data Collection and Recording

The receiving elements would record the time domain signals emerging from all resolution cells within the field of view of both receive and active-transmit elements. Data collection time depends on the path delays, number of paths (elements) and the speed and dynamic range of digitisation. Signals from deeply buried targets will influence the required quantisation [28].

2.3.11. Ground Characteristics

The time alignment of the received signals in focusing requires some knowledge of the dielectric constant of the soil. The attenuation coefficient also would help in scaling the signal amplitude for path losses. An adaptive technique, which is described in chapter 7, also enhances the alignment process with only an approximate knowledge of the permitivity of the soil. The soil permitivity could also be estimated from the first air-soil interface return of the transmitted signal or using the method described in chapter 7.

2.3.12. Surface Features

Micro and Macro scale features of the air-soil interface can interfere with the detection process. Surface roughness large compared to the wavelength would give rise to a strong diffuse scatter and destroy the phase coherence of the signals penetrating the ground. Hence this effect would interfere with the coherent focusing considered in the PRSF technique. However, a lower frequency of operation would significantly reduce such limitations.

Macro scale features like

- Two dimensional gradients
- Concave or convex surface features
- Combination of the above

can also degrade the focusing as these features may introduce unwanted lens-like effects in the focusing procedure[28].

2.3.13. Variations in Soil Dielectric Constant

A smoothly varying ground permitivity or a stratified media would decorrelate the signals received and misguide the systems target locating capability. In addition to this effect, a stratified media would give unnecessary signal reflections at the interfaces, which would reduce the signal power received and degrade the depth resolving capability of the system.

2.4. Summary

Subsurface sensing is becoming increasingly important because of its wide range of applications. A search for a viable tool to map the subsurface has brought considerable engineering innovations in this field. Presently, Ground Penetrating Radar techniques are gaining attention for subsurface sensing. The general GPR techniques have been discussed in this chapter. The applications of the GPR in various fields and the basic methodology have been outlined with signal types and identification methods. The signal types discussed include pulse modulated carrier, impulse or base band pulses, frequency modulated continuos waves and synthetic signals. Although these waveforms are being used with the GPR systems, modulated pulses and base band pulses are preferred in most systems because of the simplicity involved and the lower signal processing requirements.

Identification and processing techniques such as polarisation discrimination methods, target resonance methods, microwave holography, synthetic aperture techniques, spot focusing techniques and the PRSF technique have also been described. In order to explain the relatively new PRSF technique, resolutions, operation in clutter environment, choice of frequency, antenna bandwidth and beamwidth requirements, ground characteristics and surface features that limit the focusing process have been outlined. Among the techniques described in this section, the PRSF technique is a promising technique in overcoming the limitations suffered by most conventional ground penetrating radars. In theory, this technique is capable of producing high-resolution images, low power transmission, high-speed search and a better performance in a high clutter environment. These attractive features of the PRSF technique therefore require a more detailed theoretical and practical analysis, and thus are developed in the following chapters.

References.

[1] R.Benjamin, Post Detection Synthetic Focusing in Near-field Radar, *Proceedings of EUREL/IEE International Conference on the Detection of Abandoned Land Mines*, IEE, Edinburgh, pp. 133-137, Oct 1996

[2] D.J.Daniels, *Surface Penetrating Radars*, IEE, UK, 1996.

[3] R.M.Lerner, Ground Radar Systems, US Patent 3831173, 1974.

[4] D.Goodman and Y.Nishimura, 2-D Synthetic Radagrams for Archaeological Investigation, *Proceedings of the 4th International Conference on Ground Penetrating Radar*, Finland, pp. 339-343, 1992

[5] G.J.Weil, Non-destructive Testing of Bridge Highway and Airport Pavements, *Proceedings of the 4th International Conference on Ground Penetrating Radar*, Finland, pp. 259-266, 1992

[6] R.Benjamin, G.S.Hilton, R.Nilavalan, S.Litorbarsky and E.McCutcheon, Synthetically-focused Surface Penetrating Radar for Operation from a Moving Vehicle, *Proceedings of EUREL/IEE International Conference on the Detection of Abandoned Land Mines*, IEE, Edinburgh, pp. 110-111, 1998

[7] Y Barbin, F.Nicolin, W.Kofman, V.Zolotarev and V.Glotov, Mars 96 GPR Program, *Journal of applied Geophysics*, vol. 33, pp. 27-37, 1995.

[8] D.J.Daniels, D.J.Gunton and Scott, Introduction to Subsurface Radar, *IEE Proceedings*, vol. 135, Pt. F, no. 4, pp. 278-320, 1988.

[9] D.K.Hall, A Review of the utility of remote sensing in Alaskan permafrost studies, *IEEE Transactions on Geoscience and Remote Sensing*, vol. 20, pp. 390-394, 1982.

[10] L.C.Chan, L.Peters and D.L.Moffatt, Improved Performance of a Subsurface Radar Target Identification System Through Antenna Design, *IEEE Transactions on Antennas and Propagation*, Vol. 29, No. 2, pp 307-311, 1981.

[11] T.Moriyama, H.Kasahara, Y.Yamaguchi and H.Yamada, Advanced Polarimetric Subsurface FM-CW Radar, *IEEE Transactions on Geoscience and Remote Sensing*, Vol. 36, No. 3, pp. 725-731, 1998.

[12] L.A.Robinson, W.B.Weir and L.Young, Location and Recognition of Discontinuities in Dielectric Media Using Synthetic RF Pulses, *Proceedings of the IEEE* , vol. 62, no. 1, pp. 36-44, 1974

[13] J.L.Kurtz, J.W.Fisher, G.Skau, J.Armaghani, and J.G.Moxley, Advances in Ground-Penetrating Radar for Road Subsurface Measurements, *Proceedings of SPIE - the International Society for Optical Engineering*, vol. 3066, pp.11-21, 1997.

[14] M.J.B.Scanlan, *Modern Radar Techniques*, Collins, UK, 1987.

[15] L.C.Chan, D.L.Moffatt and L.Peters, Characterisation of Subsurface Radar Targets, *Proceedings of the IEEE*, vol. 67, no. 7, pp. 991-1000, 1979.

[16] R.P.Dooley, X-band Holography, *Proceedings of the IEEE*, vol. 53, pp. 1733-1735, 1965.

[17] D.N.Swingler and A.P.Anderson, Simple Microwave Holograms and Moire Fringes using the Spinning-Dipole Field-Perturbation Technique', *Electronic Letters*, vol. 5, no. 14, pp. 314-315, 1969

[18] R.D.Orme and A.P.Anderson, High Resolution Microwave Holographic Technique, *Proceedings of the IEE*, vol. 120, no. 4, pp. 401-406, 1973.

[19] A.P.Anderson and R.D.Orme, Multilevel Computer-processed Displays of Small Concealed Objects Remotely Imaged by Microwave Holography, *Proceedings of the IEE*, vol. 122, no. 1, pp. 22-24, 1975.

[20] A.P.Anderson and P.J.Richards, Microwave Imaging Of Subsurface Cylindrical Scatters from Cross-polar Back scatter, *Electronic Letters*, vol. 13, no. 20, pp. 617-619, 1977

[21] R.Benjamin, Synthetic Aperture Antennas, *Microwave Journal*, pp. 68-81, 1995.

[22] N.Osumi and K.Ueno, Microwave Holographic Imaging Method with Improved Resolution, *IEEE Transactions on Antennas and Propagation*, vol. 32, no. 10, pp. 1018-1026, 1984.

[23] M.Magg and J.Nitsch, Mine Detection with Microwaves, Advanced Pattern Recognition Techniques, *RTO Lecture Series 214*, Bristol, UK, 1998.

[24] R.Benjamin, Near-Field Spot-Focused Microwaves, European Patent GB 9611801.3; 6/6/1996.

[25] R.Benjamin, Near-field Spot Focused Microwave Sensing for the Detection of Buried Land-Mines, *Proceedings of EUREL/IEE International Conference on the Detection of Abandoned Land Mines*, IEE, Edinburgh, pp. 128-132, Oct 1996

[26] R.Benjamin, Synthetic Post-Reception Focusing, European Patent GB 9611800.5; 6/6/1996.

[27] F.T.Ulaby, R.K.Moore and A.K.Fung, *Microwave Remote Sensing*, vol. 111, Artech House, 1986.

[28] R.Benjamin, Clutter and Related Effects in Post-Reception Synthetically-Focused Ground-Penetrating Radar, *Report for DERA on Microwave Detection of Subsurface Objects*, UK, Nov 1998.

3. Finite Difference Time Domain Methods and the Modelling of a Post Reception Synthetic Focusing Ground Penetrating Radar

3.1. Introduction

Theoretical analyses of electromagnetic problems are important for a better understanding hence allowing improvements in design. Accurate analytical models and analysis have been used with simple problems such as cylindrical monopole/dipole, circular loops and open-ended wave guides [1]. However, most electromagnetic problems are complex in nature and hence have generally been solved with approximate equations with acceptable assumptions. A variety of full wave methods were described in chapter 1, though it is the FDTD approach that will be considered here as a numerical method for the analysis. As discussed in chapter 1, the FDTD method has been shown to provide accurate analysis for the solution of complex electromagnetic problems.

Ground Penetrating Radar (GPR) systems incorporate several features that need to be analysed simultaneously to accurately predict performance, namely:

- The antenna response.
- The presence of the soil in the near field of the antenna.
- Mutual coupling between antenna elements.
- Multiple reflections between the buried target and soil-air interface.

- The electrical irregularities in the soil.
- Multiple interactions of the scattering signals with other subsurface anomalies.

FDTD techniques are capable of addressing all these complexities in a realistic environment and have been used to analyse simple conventional GPRs in the past. Bourgeois *et al* used FDTD methods to calculate the signals reflected from buried cylindrical objects [2] and from buried land mines [3]. Similar theoretical modelling and verifications were conducted by Roberts and Daniels [4].

The Post Reception Synthetic Focusing (PRSF) technique [5,6] as described in chapter 2, is going to be considered here for GPR. This chapter describes the general FDTD method and its application to the analysis and development of a PRSF-GPR system. It is important to consider topics such as discretisation, stability, boundary conditions and excitation in FDTD methods in the context of GPR with considerations given for implementation of electrically large problems. While general principles of the PRSF technique can be handled analytically, detailed theoretical calculations of the PRSF technique in ground penetrating radar applications need further considerations.

A full FDTD model of the complete PRSF-GPR system would be prohibitively complex and slow in operation. On the other hand, since all the components of a PRSF-GPR system can be incorporated in the FDTD analysis, theoretical validation and evaluation of the PRSF-GPR concept is viable for a scaled down system. This will therefore be considered here. The basic properties such as resolution and target detection capabilities are analysed. As a result of the FDTD analysis, degradations due to reverberating energy between antenna back plane and air-soil interface are identified and a technique to suppress reverberating energy is investigated.

The FDTD algorithm used for this analysis was developed by the Numerical Modelling Group at University of Bristol [7]. Over the past years, the basic algorithm proposed by Yee (Yee Algorithm) [8] was improved with various novel techniques to handle complex and large problems.

3.2. Full-wave FDTD methods

3.2.1. The Yee Algorithm

Yee proposed that difference equations could be used to replace the partial differential equations representing Maxwell's equations. The differential forms of Maxwell's equations for a charge free environment are [9]

$$\nabla \times H = \sigma E + \varepsilon \frac{\partial E}{\partial t} \tag{3.1}$$

$$\nabla \times E = -\mu \frac{\partial H}{\partial t} \tag{3.2}$$

Where, H the magnetic field, E the electric field, ε the permitivity of the medium and σ conductivity.

In Cartesian co-ordinate system, equation 3.1 and equation 3.2 can be represented by,

$$\frac{\partial E_y}{\partial z} - \frac{\partial E_z}{\partial y} = \mu_x \frac{\partial H_x}{\partial t} \tag{3.3}$$

$$\frac{\partial E_z}{\partial x} - \frac{\partial E_x}{\partial z} = \mu_y \frac{H_y}{\partial t} \tag{3.4}$$

$$\frac{\partial E_x}{\partial y} - \frac{\partial E_y}{\partial x} = \mu_z \frac{\partial H_z}{\partial t} \tag{3.5}$$

$$\frac{\partial H_x}{\partial y} - \frac{\partial H_y}{\partial z} = \sigma_x E_x + \varepsilon_x \frac{\partial E_x}{\partial t} \tag{3.6}$$

$$\frac{\partial H_x}{\partial z} - \frac{\partial H_z}{\partial x} = \sigma_y E_y + \varepsilon_y \frac{\partial E_y}{\partial t} \tag{3.7}$$

$$\frac{\partial H_y}{\partial x} - \frac{\partial H_x}{\partial y} = \sigma_z E_z + \varepsilon_z \frac{\partial E_z}{\partial t} \tag{3.8}$$

In difference form,

$$\mu_x \frac{(H_x^{t+} - H_x^{t-})}{\Delta t} = \frac{(E_y^{z+} - E_y^{z-})}{\Delta z} - \frac{(E_z^{y+} - E_z^{y-})}{\Delta y} \tag{3.9}$$

$$\mu_y \frac{(H_y^{t+} - H_y^{t-})}{\Delta t} = \frac{(E_z^{xz+} - E_z^{x-})}{\Delta x} - \frac{(E_x^{z+} - E_x^{z-})}{\Delta z} \tag{3.10}$$

$$\mu_z \frac{(H_z^{t+}-H_z^{t-})}{\Delta t}=\frac{(E_x^{y+}-E_x^{y-})}{\Delta y}-\frac{(E_y^{x+}-E_y^{x-})}{\Delta x} \tag{3.11}$$

$$\varepsilon_x \frac{(E_x^{t+}-E_x^{t-})}{\Delta t}+\sigma_x E_x=\frac{(H_z^{y+}-H_z^{y-})}{\Delta y}-\frac{(H_y^{z+}-H_y^{z-})}{\Delta z} \tag{3.12}$$

$$\varepsilon_y \frac{(E_y^{t+}-E_y^{t-})}{\Delta t}+\sigma_y E_y=\frac{(H_x^{z+}-H_x^{z-})}{\Delta z}-\frac{(H_z^{x+}-H_z^{x-})}{\Delta x} \tag{3.13}$$

$$\varepsilon_z \frac{(E_z^{t+}-E_z^{t-})}{\Delta t}+\sigma_z E_z=\frac{(H_y^{x+}-H_y^{x-})}{\Delta x}-\frac{(H_x^{y+}-H_x^{y-})}{\Delta y} \tag{3.14}$$

Where Δx, Δy, Δz are the cell sizes and Δt is the time step.

The FDTD algorithm iteratively calculates the field values in the problem space that is discretised into unit cells. Each unit cell is assigned with three orthogonal electric and three orthogonal magnetic fields as shown in figure 3.1. In this kind of formulation, every electric field component will be surrounded by four circulating magnetic field components and the magnetic field component by four electric field components. These fields are updated at each time step in the discretised problem space whilst stepping through time.

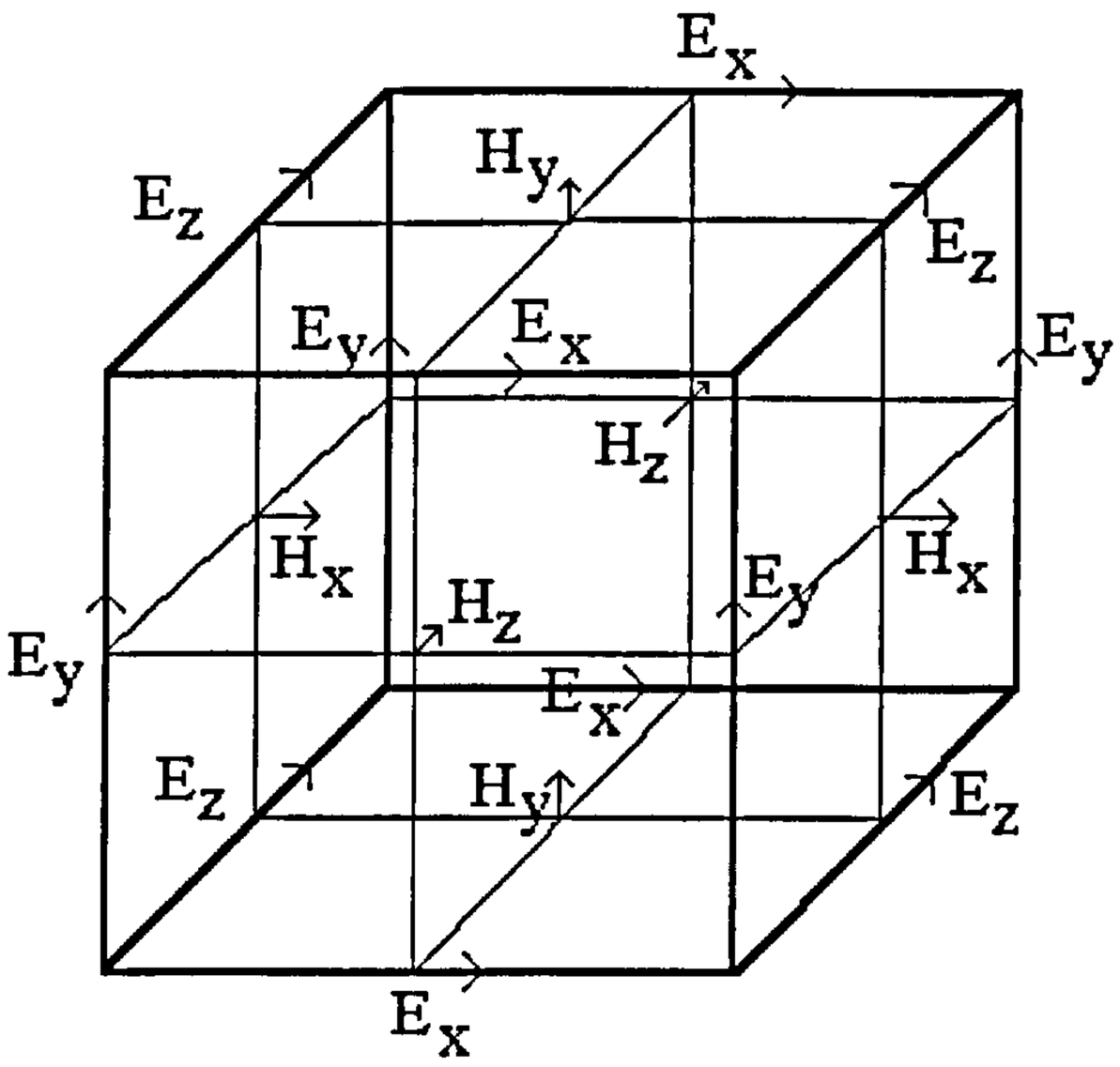

Figure 3.1 The unit cell

In the GPR model described in section 3.3.2, the ε, σ terms in soil types and antenna are assumed to be constant with frequency over the range of interest.

3.2.2. Discretisation

The FDTD problem space is divided into cells to calculate the fields iteratively. There are different methods for the formulation of the mesh. It varies from a uniform mesh in rectangular co-ordinate system [8,10] to grids in non-orthogonal or curvilinear co-ordinate systems [11]. The axis-graded grid in the rectangular co-ordinate system, in which a varying space step is used in each direction and successive nodes, is computationally efficient for complicated electromagnetic problems. It permits finer discretisation in areas of rapid field fluctuations and a coarser discretisation elsewhere. Recently there has been more emphasis shown towards sub-griding [12, 13], where a sub domain is defined with finer mesh within the coarse problem space. Even though this method is computationally very efficient, it has not yet been generalised for use in most complex electromagnetic problems.

For this particular application the GPR model employed a finer mesh for antenna structures and a coarser mesh for free space and soil.

The cell sizes in the discretised problem space depend on stability and accuracy requirements of the problem. Hence the cell sizes are chosen such that they satisfy some predetermined conditions.

3.2.3. Stability and Accuracy

The computation time and the memory requirements of a FDTD model are almost proportional to the number of cells in the problem space. The GPR model of the order of 2000,000 cells, and hence requires longer run time. Stability of the model and the accuracy of the simulated results are directly related to the cell sizes.

3.2.3.1. Stability Criterion

Stability conditions are necessary to avoid spurious increase in the computed filed values with time increment. These instabilities could generally occur when solving explicit differential equations using numerical methods [14].

It can be shown that the stability criterion for the general three dimensional FDTD algorithm is of the form [10],

$$\Delta t \leq \frac{1}{V_{\max}\sqrt{\frac{1}{\Delta x^2}+\frac{1}{\Delta y^2}+\frac{1}{\Delta z^2}}} \tag{3.15}$$

$V_{\max}$ is the maximum wave phase velocity within the model. Which in this case is the speed of light [10].

3.2.3.2. Cell Size and Numerical Dispersion

Propagation of electromagnetic waves in a discretised problem space (FDTD Domain) has limitations over the actual wave propagation. That is, the phase velocity of the numerical waves is equivalent to speed of light only at an ideal situation where the terms Δt, Δx, Δy and Δz in equations 3.9 – 3.14 approaches zero. Very small delta quantities will lead to a very high memory requirement and run time. Hence a trade off is necessary between accuracy and the computational constraints. Analysis shows that numerical wave velocities strongly depend on the wavelength [15]. Hence dispersion is caused by the grid itself. Since this error is cumulative, it can lead to significant errors with electrically large problems like the modelling of ground penetrating radars. A cell size of less than $\lambda/10$ will give reasonably good results [16], where λ corresponds to the shortest wavelength of interest. But a cell size of $\lambda/20$ will give more accurate results where the fields change more rapidly (e.g., near metal edges). Railton and McGeehan made use the priori knowledge of asymptotic behaviour of the fields at the strip edges to overcome the necessity for high node density in these regions [17].

Pseudo refraction [14] is another kind of error due to cell size dependent velocities where a sudden change of cell size may cause refraction exactly as in a dielectric boundary. Hence a gradual change of cell size helps to reduce these errors.

3.2.4. Boundary Conditions

In FDTD method, Maxwell's equations are solved by applying boundary conditions. Boundary conditions vary according to the nature of the problems. The boundaries can be free space, metal or dielectric interfaces. Each of these boundaries has their own response to the electromagnetic fields.

3.2.4.1. Absorbing Boundaries.

Absorbing Boundary Conditions (ABC) are employed to handle open electromagnetic problems like antennas, ground penetrating radars etc in order to truncate the problem space, which is unbound in nature. In other words they are being used to simulate the computational domain to infinity as accurate as possible [18]. Different techniques such as [14],

- Extrapolation methods.
- Averaging processes.
- Introduction of losses.
- Use of outgoing wave equations

are being used to achieve these conditions. The most common ABCs used are based on approximations of the outgoing wave equations by linear expressions- Mur's discretisation is a well-known example of this method [18]. All these ABCs are not perfect, but they are capable of providing simulations with engineering values. Railton et al [19] investigated the properties of various absorbing boundary conditions and provided a useful summary of their performance.

A recent development in this field is a perfectly matched layer, in which the electric and magnetic fields are split and absorbed separately by assigning losses. Very low reflections have been observed with this absorbing technique [20, 21].

3.2.4.2. Modelling Conductors

Perfect metal conductors are modelled in the FDTD simulation process by forcing the electrical fields within this volume to zero. Since the skin depth of metals are very small, this assumption would not create significant errors in the computation process. If, however, incorporation of very thin metal sheets will need a fine grid increment, which must be less than or equal to the sheet thickness, and this would increase the computer storage and execution time requirements. Several methods have been proposed to allow spatial grid increments to be much larger than the thickness of the sheets. A comparison of these methods can be found in [22].

For this particular model, zero tangential electric fields at the metallic boundaries (such as antenna surface) are used and thus small losses associated with the conductors are ignored.

3.2.4.3. Dielectric Interface

Analysis of multi layered structures involve computation of electric and magnetic fields over the dielectric interfaces. The continuity of the tangential electric and magnetic fields are maintained across the interface of different dielectric materials. Since the basic algorithms (Equations 3.9 – 3.14) are for a uniform media, computation on the interface needs further modifications. It has been shown that for a uniform mesh (i.e., a uniform space step between nodes) it is possible to use the average value of the dielectric constants at a dielectric boundary, but for a non uniform mesh more rigorous approach must be used [23, 24]. Railton and McGeehan [24] introduced a more efficient method to handle very thin materials. Losses in these dielectric media can also be incorporated in the simulation process.

3.2.5. Modelling Lossy Materials

Dielectric losses in materials arise from polarisation and ohmic losses. Polarisation losses, which are due to the molecular dipole alignments with time varying electromagnetic fields, are frequency dependent and vary significantly at higher frequencies. The dielectric constant of the materials is represented by a complex number and the imaginary part is used to model the ac losses (dipolar losses) as shown below,

For sinusoidal field variations equation 3.1 can be represented by,

$$\nabla \times H = \sigma E + j\omega\varepsilon E \tag{3.16}$$

Where, ω is the phase velocity, σ represents the conduction losses and ε (a real number) representing the stored energy. Rearranging equation 3.16,

$$\nabla \times H = j\omega E\left(\varepsilon - \frac{j\sigma}{\omega}\right) \tag{3.17}$$

$$\nabla \times H = j\omega\varepsilon_c^* E \tag{3.18}$$

where,

$$\varepsilon_c^* = \varepsilon - \frac{j\sigma}{\omega} \tag{3.19}$$

for free space, equation 3.18 becomes,

$$\nabla \times H = j\omega\varepsilon_o E \tag{3.20}$$

Where, ε_o is the permitivity of free space.

Comparing equation 3.20 and equation 3.18 it is evident that the losses can be represented by a complex permittivity, hence the ac losses are also included in equation 3.19 to become,

$$\varepsilon_c^{**} = \varepsilon - \frac{j\sigma}{\omega} - j\varepsilon_1^{"} \tag{3.21}$$

with $\varepsilon_1^{"}$ representing the ac losses. Hence the permittivity can be replaced by a real term $\varepsilon^{'}$ and an imaginary term $\varepsilon^{"}$ to become,

$$\varepsilon_c^{**} = \varepsilon^{'} - j\varepsilon^{"} \tag{3.22}$$

where,

$$\varepsilon^{"} = \varepsilon_1^{"} + \frac{\sigma}{\omega} \tag{3.23}$$

Conversely the single frequency losses can also be represented by a total conductivity term given by,

$$\sigma_t = \sigma + \varepsilon_1^{"}\omega \tag{3.24}$$

In FDTD modelling, the conductive losses and the polarisation losses can be modelled by a total conductivity term as in equation 3.24 or a frequency dependent permittivity. Lubbers et al [25] used the time domain Fourier transform of the frequency dependent dielectric properties (Real and Imaginary) to model dispersive materials. This technique is useful in analysing systems over a wider bandwidth.

Fixed dielectric properties (frequency independent) are assumed for the GPR model and the total conductivity term is used for the losses.

3.2.6. Excitation

Having defined the problem with necessary boundary conditions and material properties the simulation process is initiated by exciting the problem with a known field placed at appropriate location. Initially the field values over the defined discretised space are assumed zero and the iteration process is continued with the excited field values.

3.2.6.1. Excitation Method

The excitation used depends on the type of the problem. For instance, Thiel and Mitra demonstrated the use of current sheets in their earth surface impedance calculation model [26] while Hilton used a voltage source to excite a microstrip patch antenna [9]. These sources are sufficiently spaced from the simulating object to accommodate the secondary fields. More accurate results can be obtained using mode templates [27] in which the electric fields and the magnetic fields are excited depending on the problem.

3.2.6.2. Excitation Function

One of the important aspects of time domain analysis such as the FDTD is that any pulse shape can be used to excite a structure. The frequency spectrum of the pulse also has influence on the mesh size. Generally the excitation function is chosen depending on the analysis. For wide band analysis, Gaussian and raised cosine pulses are often employed [9]. In section 3.3, use of a modulated square pulse in time domain analysis of a post reception synthetic focusing ground penetrating radar will be demonstrated.

3.3. FDTD Modelling of a Post Reception Synthetic Focusing Ground Penetrating Radar

The PRSF-GPR system makes use of an antenna array to focus on to the subsurface. A non-contact mode of operation is considered here, as this mode is a general method and also preferred for applications such as detection of unexploded ordinances and mines. An operating frequency, around 2GHz was considered for this initial investigation as most conventional GPRs operate lower than 1.5GHz.

3.3.1. Single Element Antenna Model for the PRSF-GPR

A printed dipole meets most of the requirements for the analyses of a PRSF-GPR system. A more complex antenna configuration was not initially considered as it would increase the run time and the memory requirements.

3.3.1.1. A Simple Antenna Configuration for PRSF-GPR Model

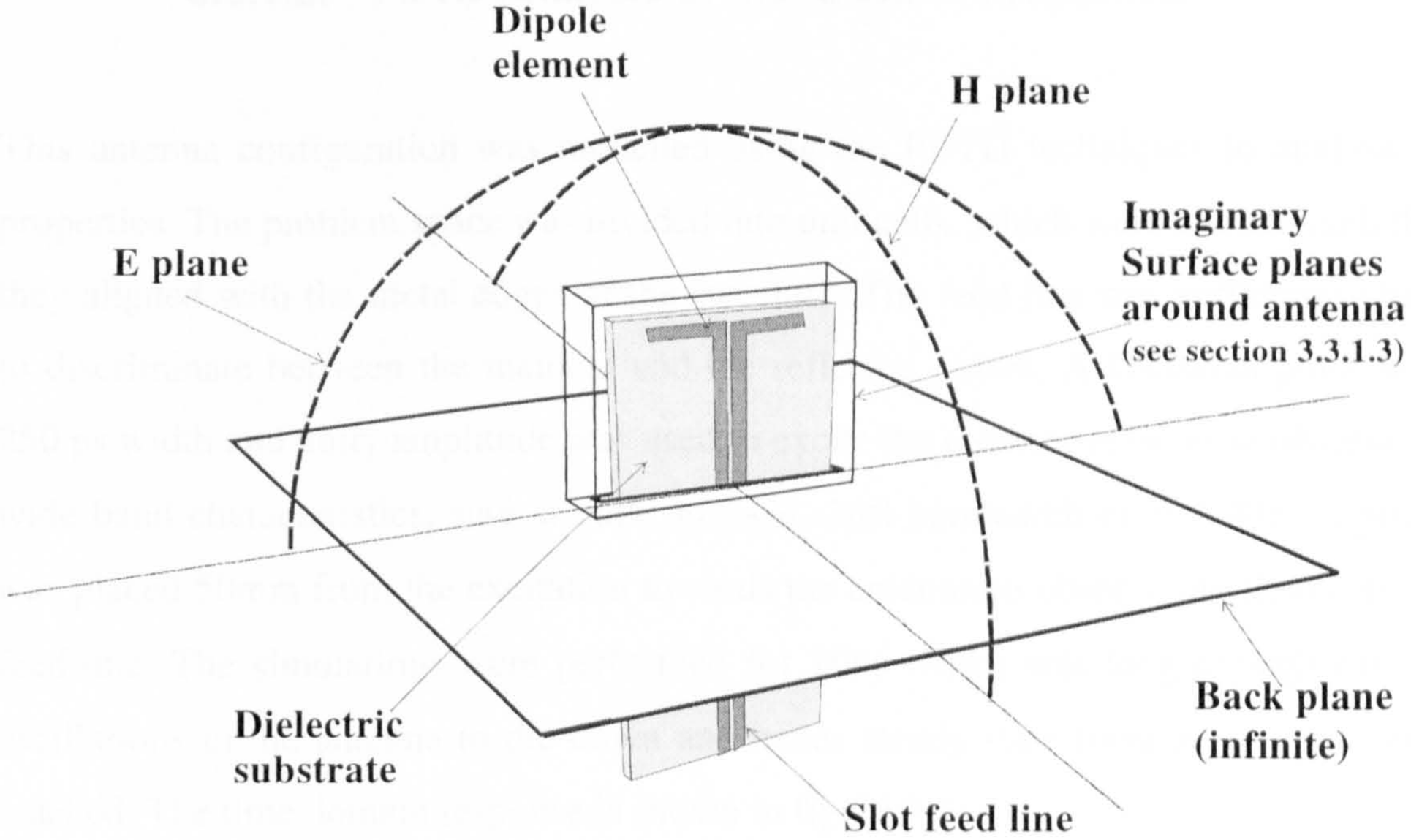

Figure 3.2 The antenna configuration.

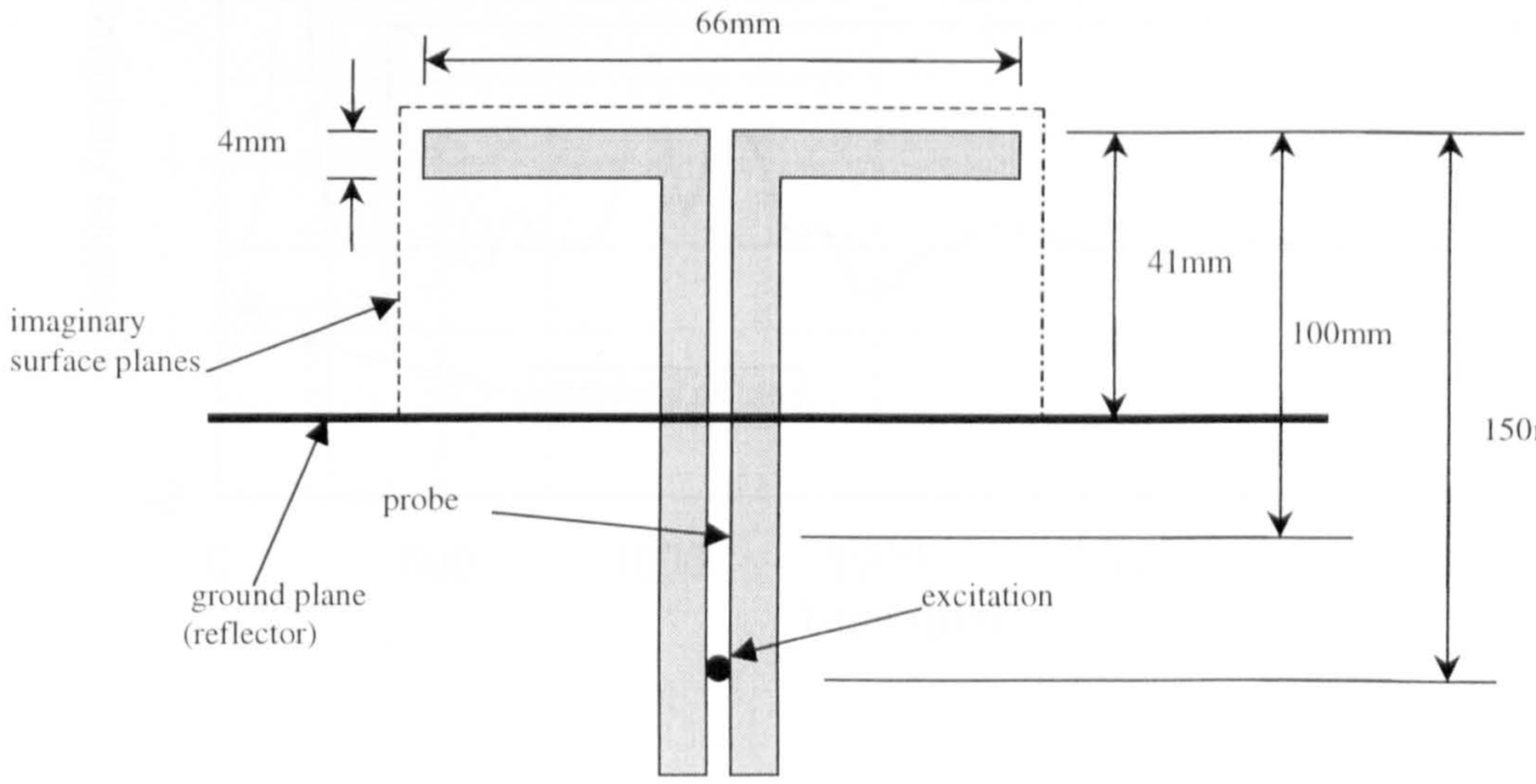

Figure 3.3 Printed dipole antenna

The antenna configuration used in this analysis is shown in figure 3.2 and 3.3 comprises a printed dipole fed by a balanced line that passed through a ground plane (reflector). The feed was a coplanar strip line that was printed on the same substrate (RTDUROID S880). The ground plane contains a rectangular hole to accommodate the feed line and the substrate as shown, and was extended to the absorbing boundary of the model.

3.3.1.2. FDTD Analysis of the Antenna Properties

This antenna configuration was modelled using the FDTD techniques to analyse its properties. The problem space was divided into unit cells, which were chosen such that they aligned with the metal edges of the structure. The feed line was sufficiently long to discriminate between the incident and the reflected pulses. A Gaussian pulse with 250 ps width and unity amplitude was used to excite the element in order to observe its wide band characteristics, such a pulse gives a -3dB bandwidth of ≈ 9GHz. A probe was placed 50mm from the excitation towards the antenna to observe the fields on the feed-line. The simulations were performed for 10ns which was long enough for the oscillations in the antenna to die down and hence steady state (near zero) conditions reached. The time domain response is shown in figure 3.4.

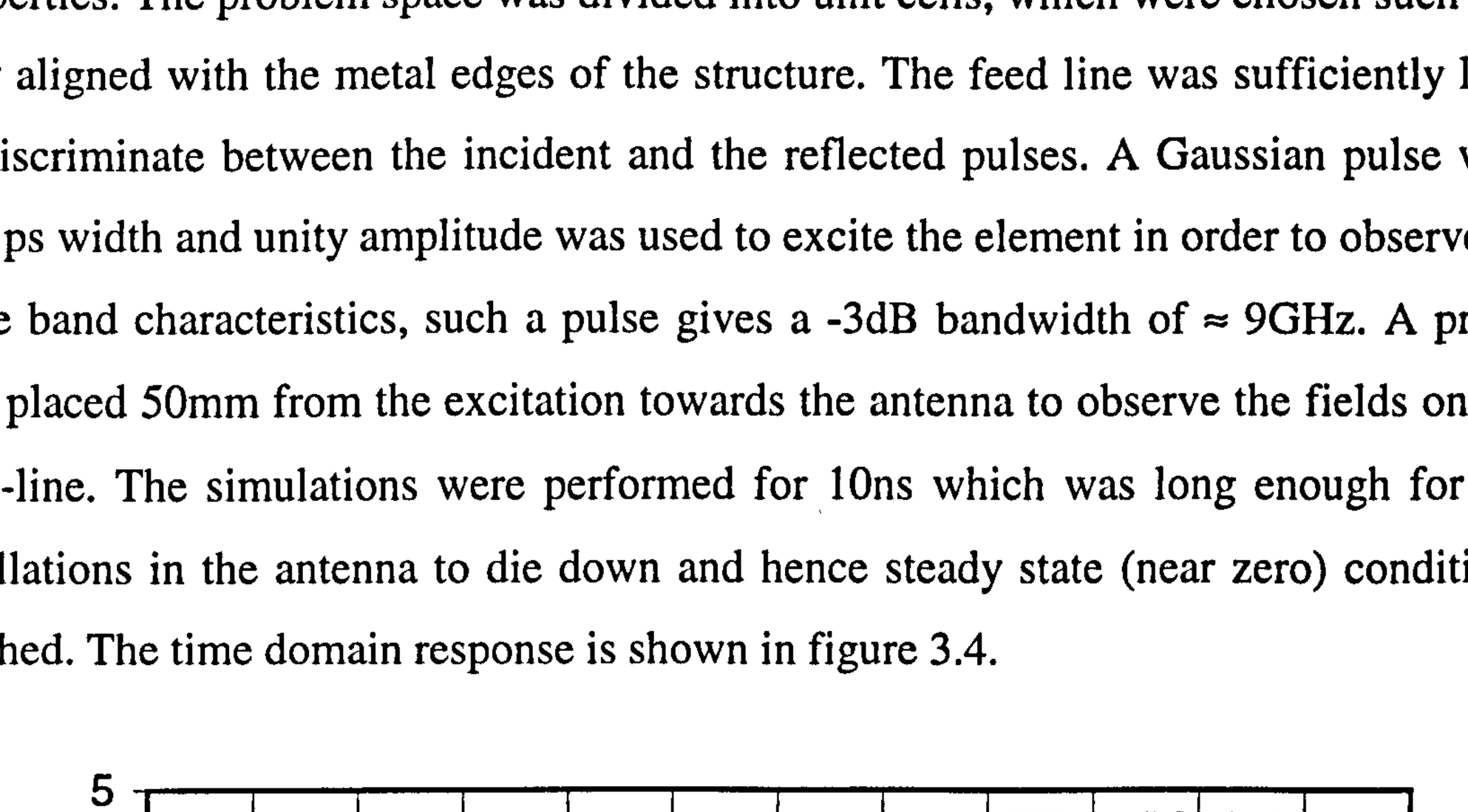

Figure 3.4 Time domain response

Figure 3.4 shows the incident and the reflected pulses observed at the probe location. Separating the incident (applied) pulse from the reflections monitored on the feed line, and transforming this data to the frequency domain allows the input frequency response of the antenna to be determined. The calculated return loss is shown in figure 3.5.

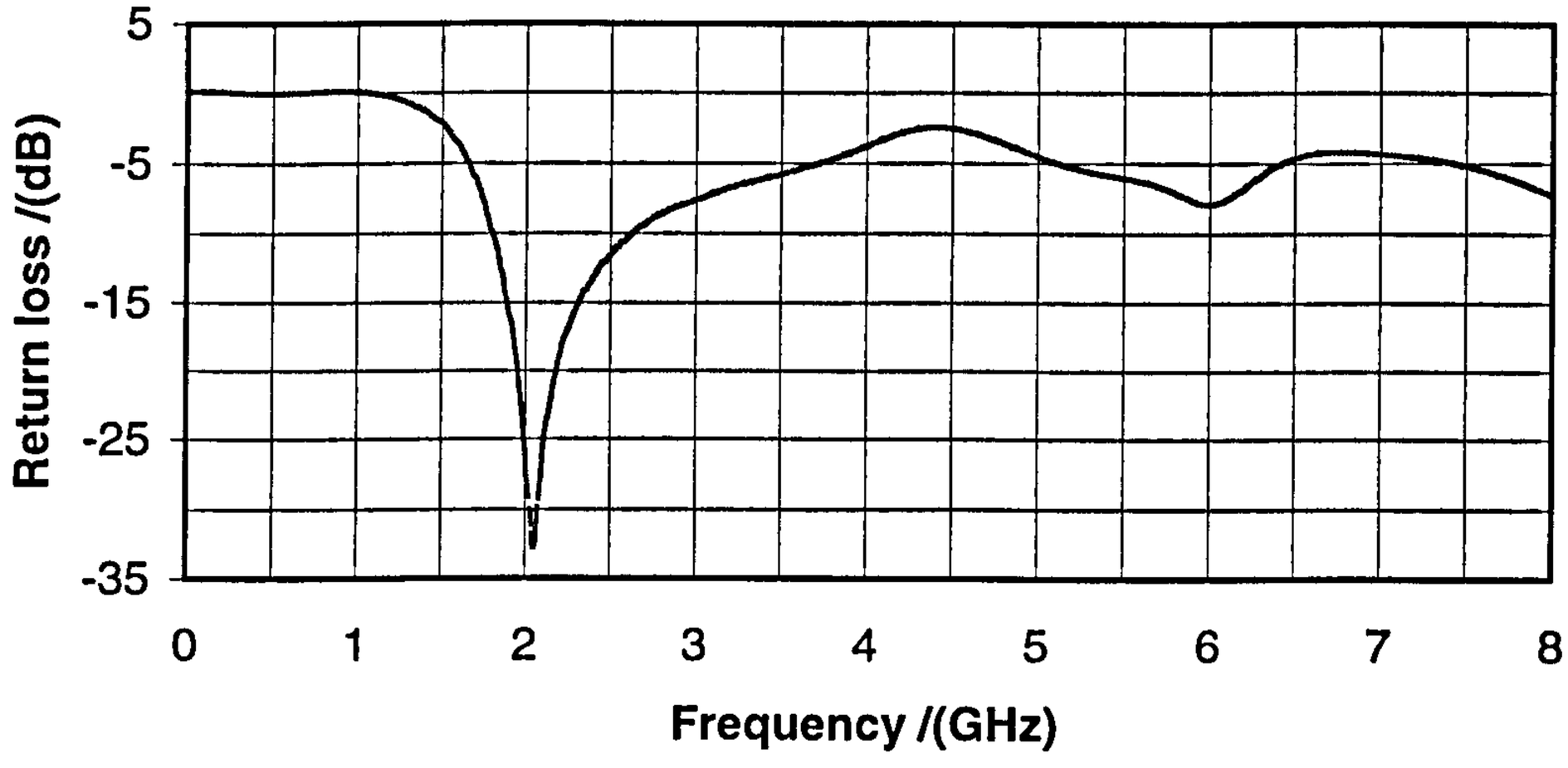

Figure 3.5 Return loss of the dipole antenna model

From figure 3.5 it can be seen that the antenna operates close to 2GHz and has a -10dB bandwidth of 800MHz (1.8-2.6GHz).

3.3.1.3. Radiation Pattern

Although the antenna is to be operated close to the ground, the far field patterns can be used to indicate whether the antenna is suitable for operation as a GPR antenna (i.e. broad beams, no nulls). The far field radiation pattern of the dipole antenna was found by post processing the near field frequency domain data calculated on the near field planes (shown in figure 3.2) at specific frequencies. The tangential electric and magnetic field components on these five planes surrounding the antenna element and the reflector aperture were recorded. The magnitudes and phases of the fields were calculated and, together with their images due to the (infinite) ground plane, were converted to equivalent electric and magnetic current sources on the surface. Transformation of these sources to the far-field region allowed the prediction of the

far-field radiation levels at any angular direction in space. The far field patterns were obtained for 1.8GHz and 2.6GHz, which corresponds to the limits of the operating bandwidth of the antenna. The corresponding far field patterns are shown in figures 3.6 and 3.7.

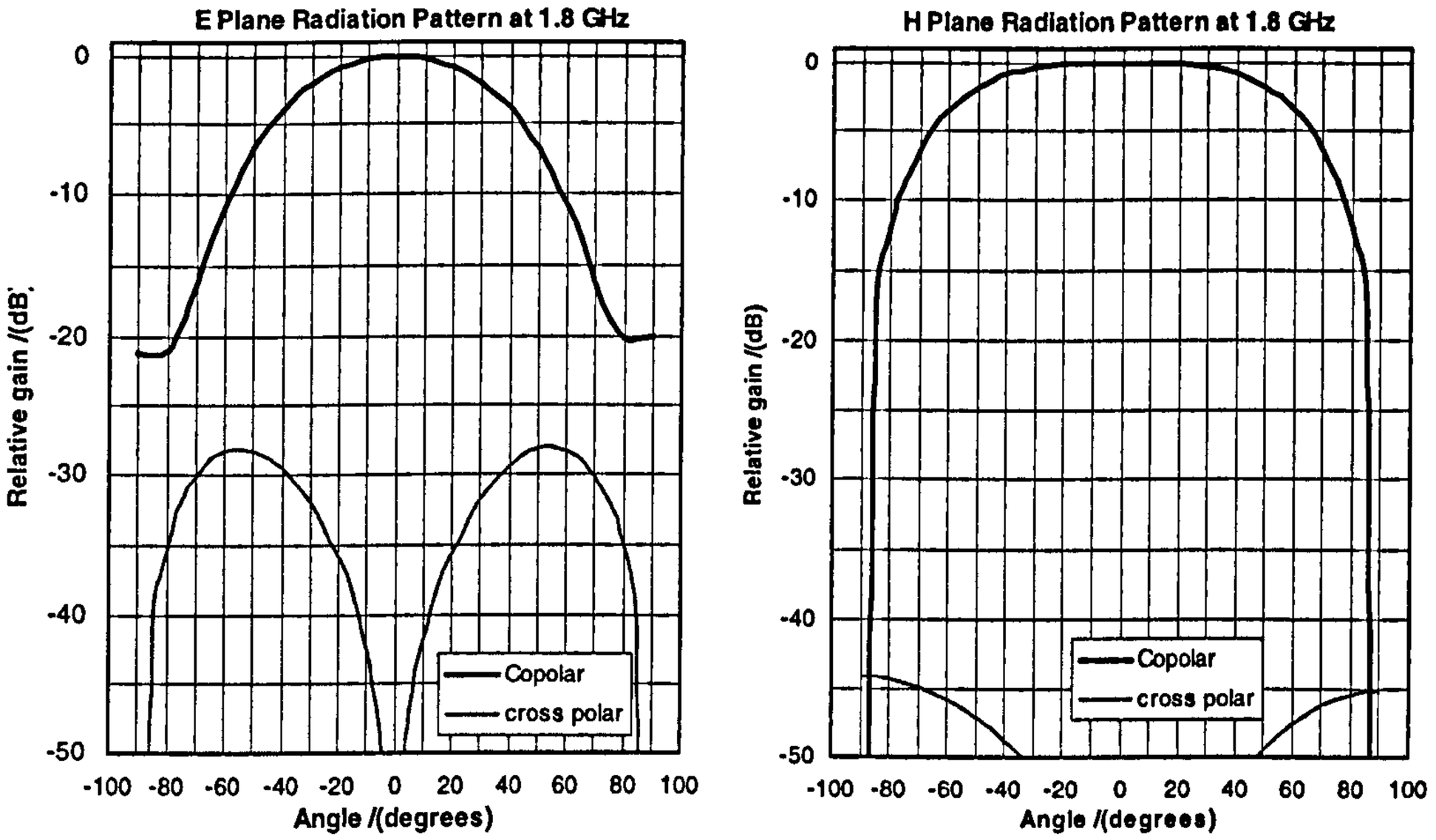

Figure 3.6 Radiation pattern at 1.8GHz

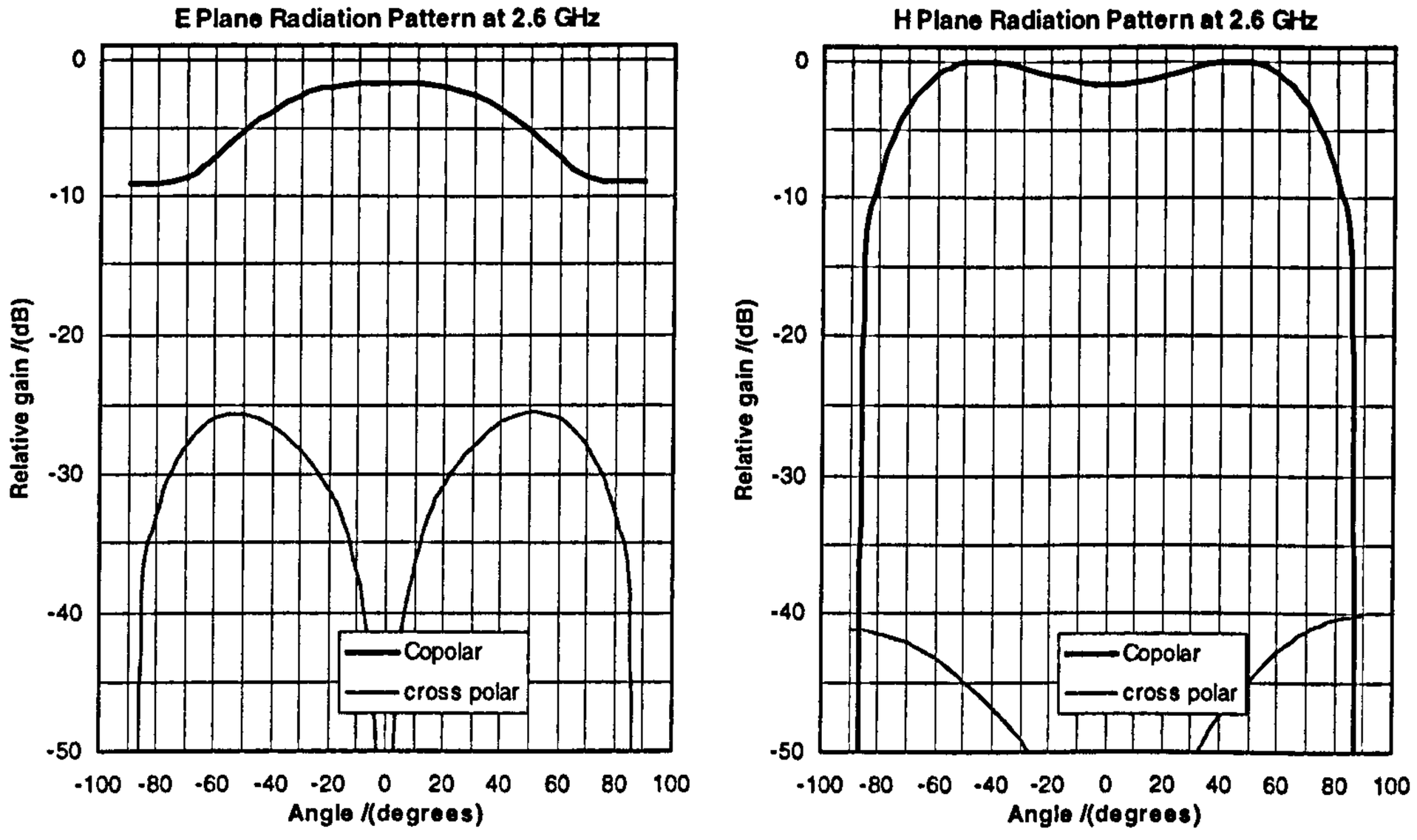

Figure 3.7 Radiation pattern at 2.6GHz

Figure 3.6 and 3.7 show that the dipole element has a half power beam width of $\pm 35^0$ in the E plane and $\pm 50^0$ in the H plane at 1.8GHz and $\pm 40^0$ and $\pm 65^0$ at 2.6 GHz with low cross-polar characteristics. A null appears at 0^0 in the H plane pattern of 2.6GHz.

The operating bandwidth and the wide beamwidth of the antenna is suitable for a PRSF-GPR. Such an antenna will support the transmission of a 4 cycle pulse at 2.1GHz (approximately 550 MHz bandwidth). The half power beamwidth of the element is assumed $\pm 45^0$ in the calculation to follow.

3.3.2. PRSF-GPR Array Model

The analysis of the single element showed that it has sufficient bandwidth and beamwidth. Therefore a line array antenna model was developed to analyse the PRSF-GPR.

3.3.2.1. PRSF-GPR Configuration

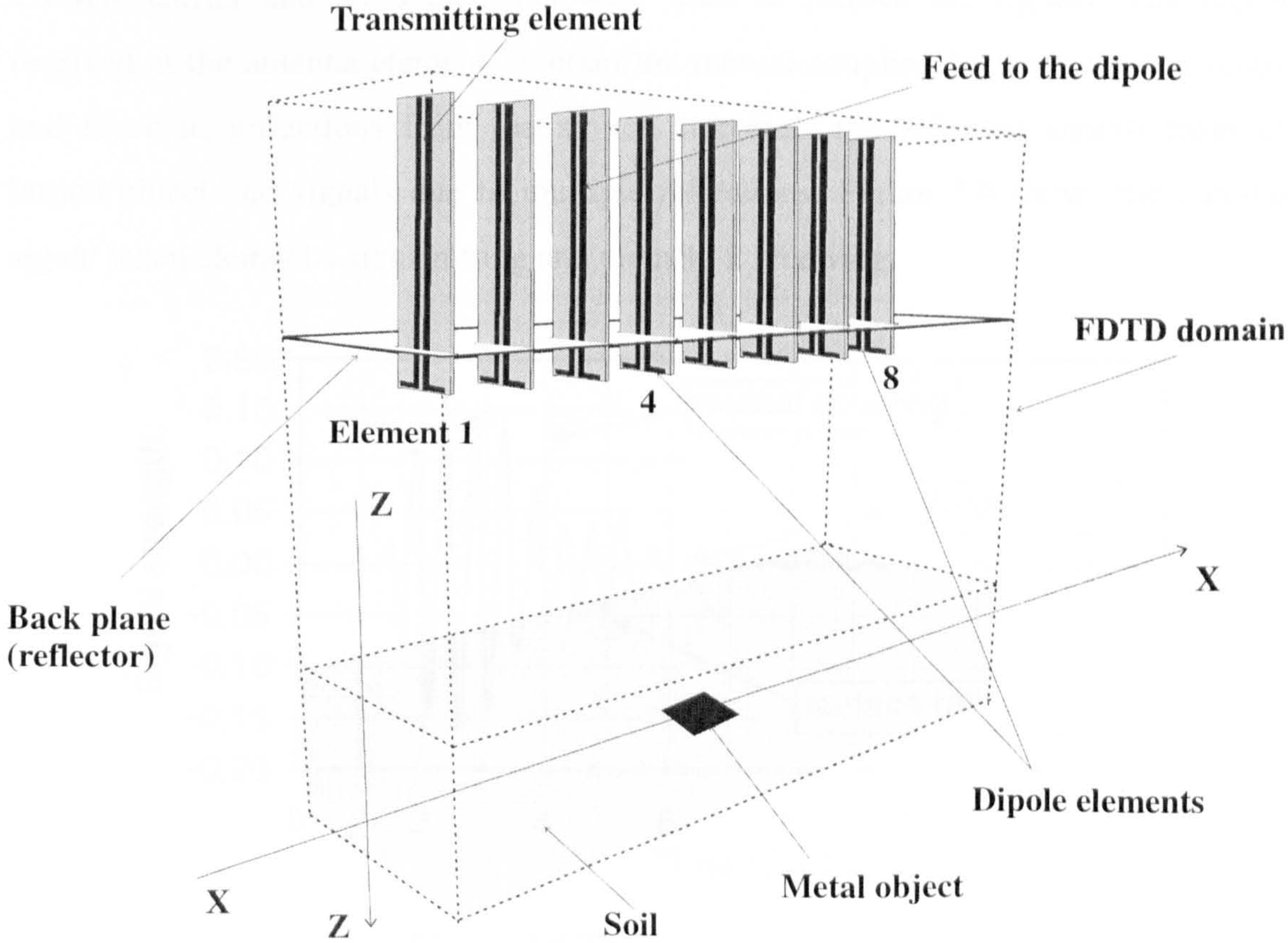

Figure 3.8 The PRSF-GPR model

The PRSF-GPR model, as shown in figure 3.8, comprises an antenna array of printed dipole elements together with specimen soil and test objects buried within the soil. Antenna elements are placed about two wavelengths (285mm) from the soil to give suitable ground clearance. The antenna array consists of eight-printed dipole elements with $0.65\lambda_{air}$ inter element spacing. The elements are mounted over a ground plane that is spaced one-quarter wavelength away from the dipoles.

3.3.2.2. FDTD Modelling

FDTD analysis was performed on the PRSF-GPR array model. The soil was modelled with a dielectric constant of 6, which corresponds to loamy sand (chapter 5). Since the transmitted signal has a bandwidth of approximately 500MHz at 2.1GHz the assumption of a constant dielectric constant will not significantly interfere with the analysis.

The first antenna element was excited with a modulated square pulse of 2ns width and 2.1GHz carrier and all 8 elements were used to receive the signals. The signals received at the antenna elements contain the mutual coupling between the transmitter and receiver, reflections from the air-soil interface, the reflected signals from the buried object and signals due to multiple reflections. Figure 3.9 shows the received signal when element 1 transmitting and element 2 receiving.

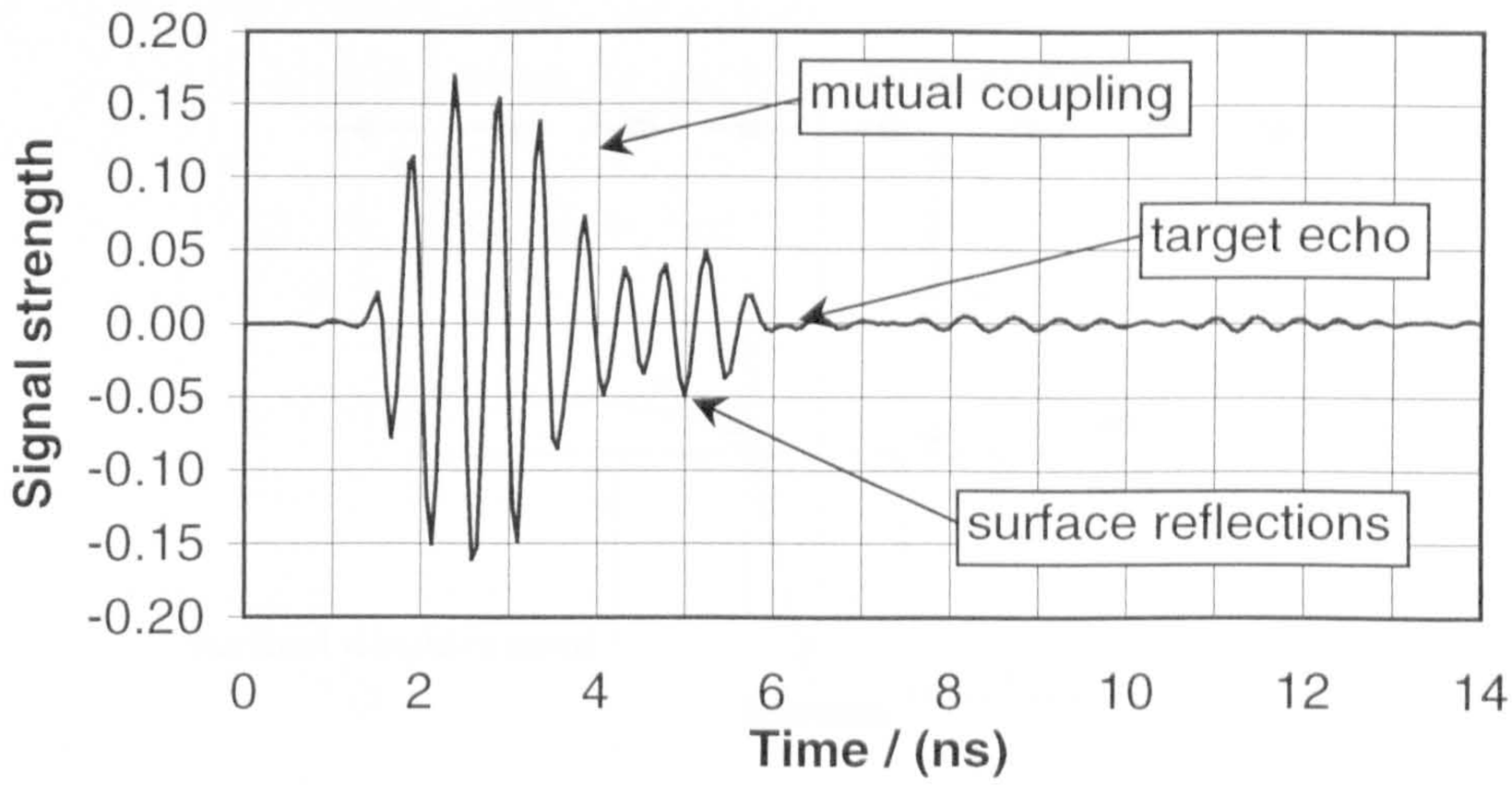

Figure 3.9 The received signals

It can be seen that the mutual coupling is by far the most dominant for this element pair. For elements further apart the surface reflections become significant. The

reflected signals from the buried target were calculated by running the same model without the buried metal plate and subtracting the received signals from the signals which were obtained with the object (known as background subtraction). One such calculated reflected signal for element 1 transmitting and element 4 receiving is shown in figure 3.10.

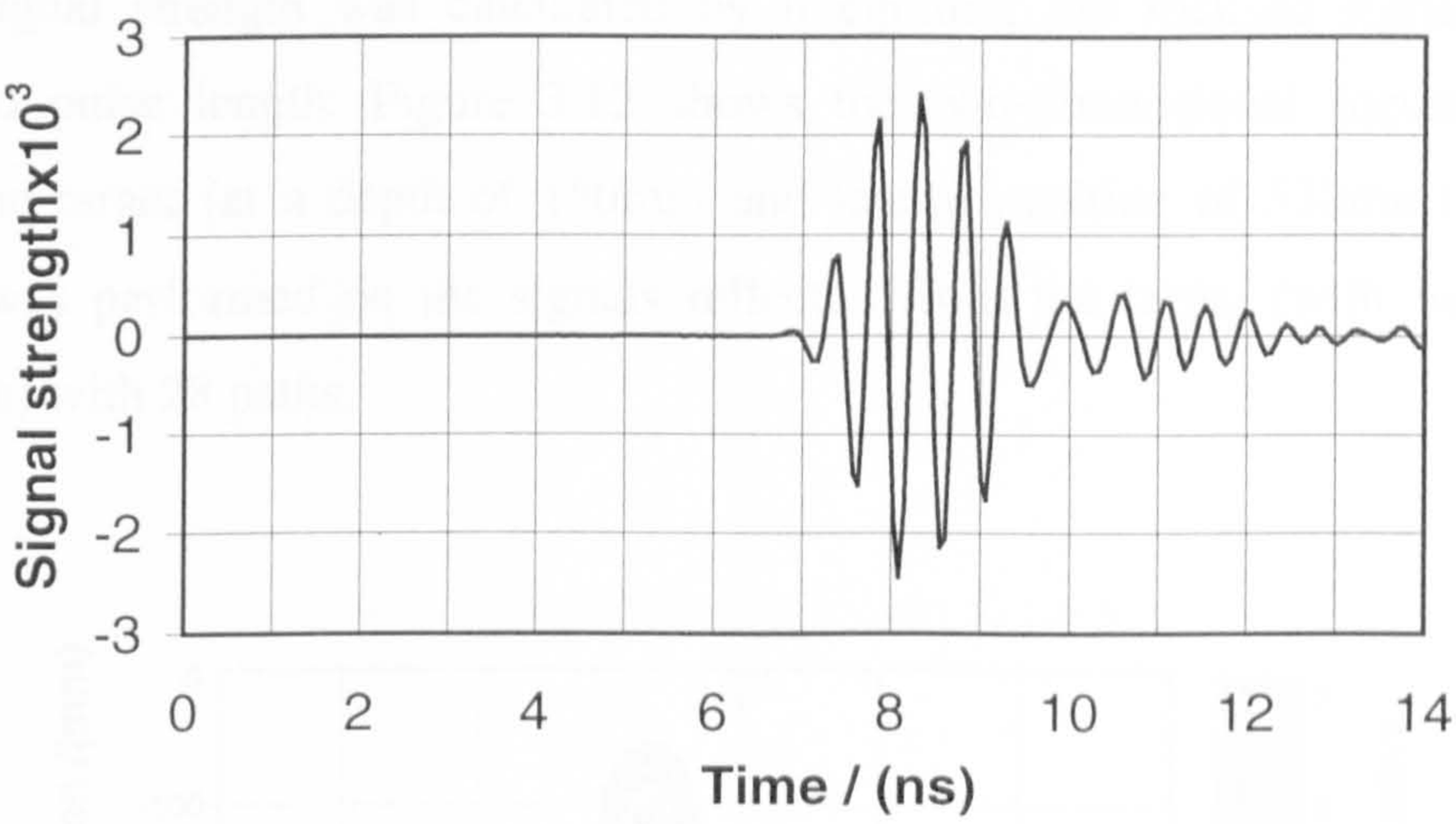

Figure 3.10 Calculated reflected signal

Figure 3.10 shows the signal reflected from the target and some late time signals, which are due to multiple reflections. (air-soil interface and antenna array, target and soil-air interface).

3.3.3. Post Reception Focusing with FDTD Results.

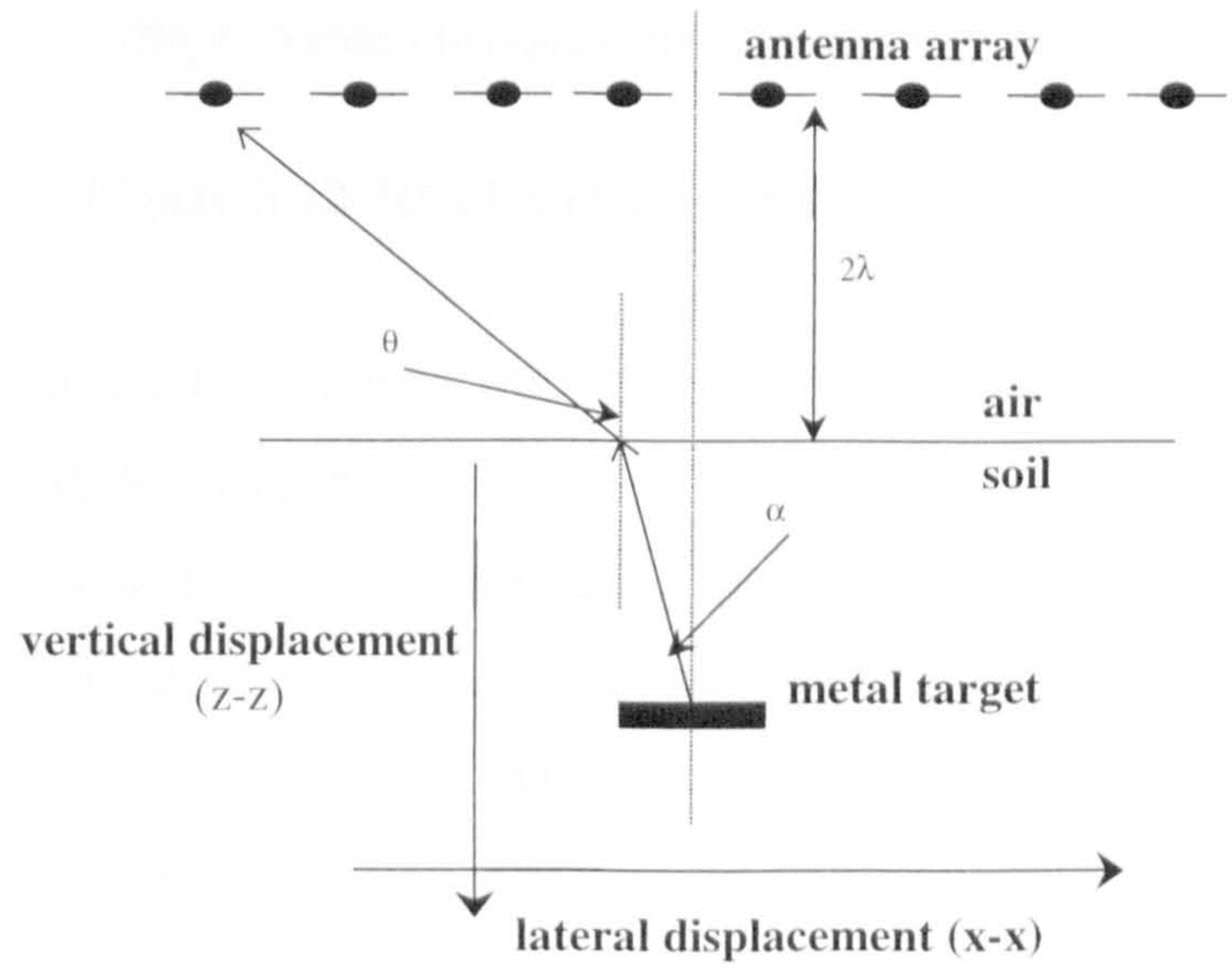

Figure 3.11 Target location

Post reception synthetic focusing is achieved by calculating the path delays associated with the different transmitting and receiving elements via the focusing point and adding the signals in phase coherence (section 2.3.1). The total path delay was calculated using a simple ray-tracing model. The point of inflection at the soil-air interface was approximated using a linear relationship (see Appendix B). Finally the focused signal strength was calculated by integrating the focused signal over the transmitted pulse length. Figure 3.12 shows the two-dimensional focussed results through the target (at a depth of 150mm and lateral position of 530mm). Synthetic focusing was performed on the signals reflected from the target (with back ground subtraction) with 28 paths.

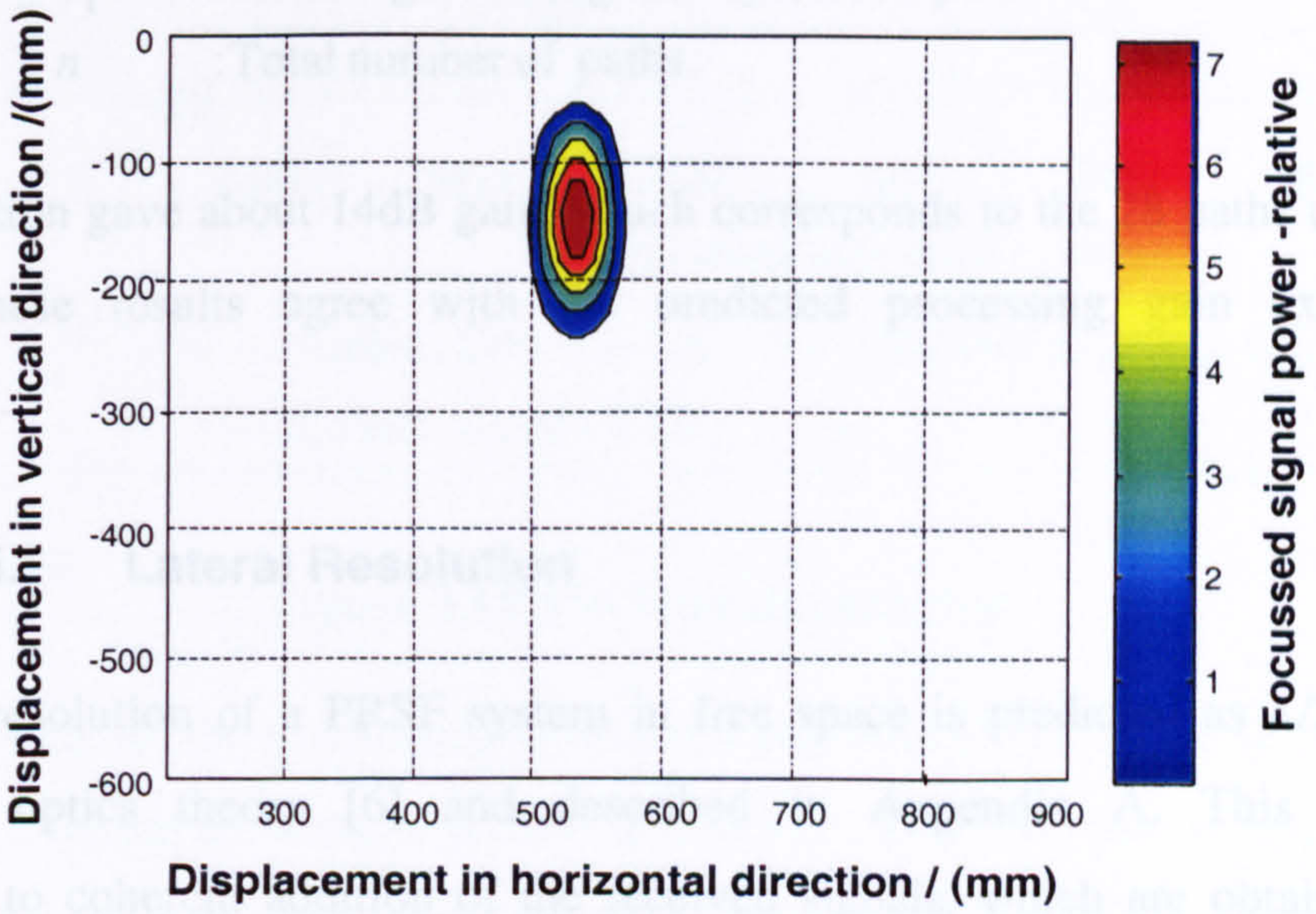

Figure 3.12 2D slice of through target location.

This result indicates a large return from the target location below the line array and demonstrates the PRSF concept. The analysis is limited to the 2 dimensional slice, as a detailed 3 dimensional imaging requires a planar array. Focusing with the total received signals (without background subtraction) for deeply buried targets also established the exact target location. Having established the correct target location it is useful to investigate the processing gain and the predicted resolutions associated with this technique.

3.3.4. Processing Gain of the System

The processing gain was calculated at the target location by comparing the focussed signal with the mean signal present as described below,

$$\text{Processing Gain} = \frac{V}{S} \tag{3.25}$$

Where,

V : Synthetically focussed signal

$$S = \frac{\sum_{i=1}^{n} \overline{S_i}}{n} \tag{3.26}$$

where,

$\overline{S_i}$: Mean signal strength (4 cycles) of path i

n : Total number of paths.

This calculation gave about 14dB gain, which corresponds to the 28 paths used in this analysis. These results agree with the predicted processing gain explained in section 2.3.2.

3.3.5. Lateral Resolution

The lateral resolution of a PRSF system in free space is predicted as $\lambda/2\theta$ through geometrical optics theory [6] and described in Appendix A. This estimation corresponds to coherent addition of the received signals, which are obtained by the maximum utilisation of the individual beam patterns of the antenna elements. Half power beamwidths are considered as the limiting case for each element. It was expected that a subsurface operation would yield the same resolution independent of the dielectric properties as the in-soil wavelength and convergent angle are scaled down by the same factor corresponding to the dielectric property of the soil.

The in-soil lateral resolution was determined through FDTD simulations. As shown in figure 3.11, a line array of 8 dipole elements with $0.65\lambda_{air}$ inter element spacing and $2\lambda_{air}$ antenna-soil separation will utilise the full half power antenna beamwidth for a centrally buried target at $0.95\lambda_{air}$ in soil with $\varepsilon_r = 6$. Hence the FDTD model described in section 3.3.2.2 was used to calculate the lateral resolution. Signals reflected from a

small buried target (30x30mm) of all possible 28 paths (with all 8 elements) were used in this calculations. Surface clutter (reflections) were eliminated in this analysis by back ground subtraction. Figure 3.13 shows the laterally focused signals (focusing along x-x in figure 3.8) at the target depth. These calculations were repeated for dielectric constants of ε_r= 1.8 and 30 to verify whether the lateral resolution is independent of the dielectric properties of soil.

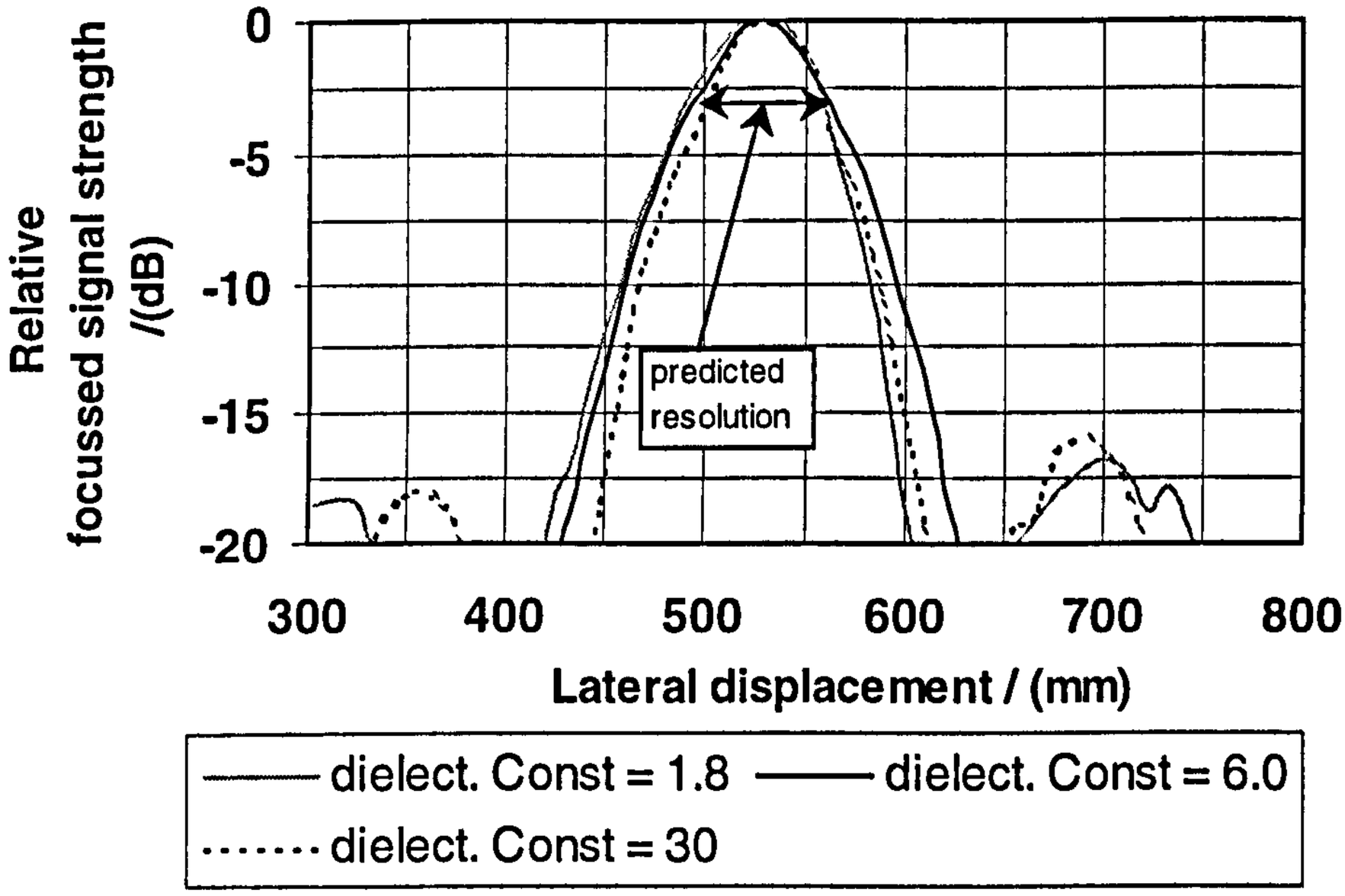

Figure 3.13 The lateral resolution

Half power points of the synthetically focused signals (i.e. 0.707 of the summed signal strength) for different dielectric constants of soil show a lateral width of approximately 65 mm against the predicted resolution of 50mm ($\lambda/2\theta$), figure 3.13. In geometrical optics predictions, the signal strength variation between different paths were neglected and the lateral resolution was derived for free space conditions, whereas in FDTD analysis all these features were incorporated in the calculation. Hence these factors would have contributed to the differences in these results.

3.3.6. Vertical Resolution.

The vertical resolution of a PRSF system was predicted as $2\lambda/\theta^2$ in free space [6]. Since λ and θ depends on the soil dielectric permitivity for subsurface applications the depth resolution often depends on the dielectric constant of the soil. Hence the resolution is either $2\lambda/\theta^2$, or defined by the pulse width of the transmitted signal as in

any pulsed systems. For a 4 cycle transmitted signal, the limit is set by the permitivity of the soil as shown below,

For $2\lambda/\theta^2$ to be less than the depth resolution set by the pulse width,

$$\frac{2\lambda_s}{\theta_s{}^2} < 2\lambda \tag{3.27}$$

where λ_s is the wavelength and θ_s is the convergent angle in soil. In terms of free space properties,

$$\frac{2\lambda_a/\sqrt{\varepsilon_r}}{\theta_a{}^2/\varepsilon_r} < \frac{2\lambda_a}{\sqrt{\varepsilon_r}} \tag{3.28}$$

$$\varepsilon_r < \theta_a{}^2 \tag{3.29}$$

with λ_a is the wavelength and θ_a is the convergent angle in free space. Hence for a system using dipole elements with half power beamwidths of $\pm 45^0$,

$$\varepsilon_r < 2.47 \tag{3.30}$$

Hence for most practical soil parameters the pulse length will define the vertical resolution. FDTD modelling was carried out in a soil dielectric constants of 6 and the reflections from the metal target were vertically focussed through the target location. The vertically focussed signal strengths are shown in figure 3.14.

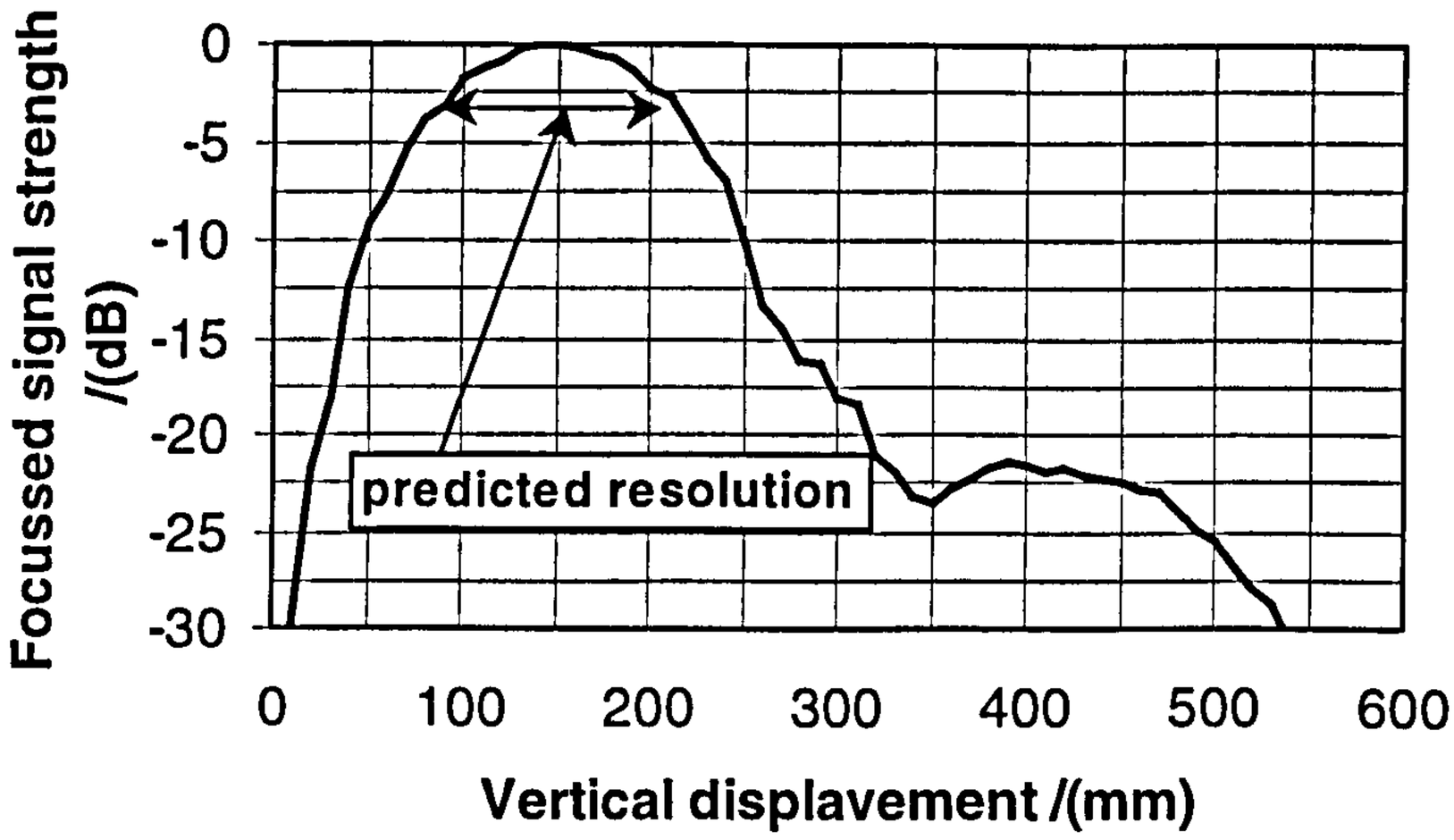

Figure 3.14 Vertical resolution with soil dielectric constant of 6

These results show a vertical resolution of 120mm and the predicted resolution is 117mm (2λ in soil ε_r= 6 at 2.1GHz). In order to have a better identification scheme, the vertical resolution would have to be improved further by using temporally short pulses.

3.3.7. Lateral Resolution in Lossy Media

The resolving power of the system in attenuating media was also analysed using the above techniques. A 30x30mm metal plate was buried in soil with ε_r= 6+j2 at a depth of $0.95\lambda_{air}$. Laterally focussed results are shown in figure 3.15.

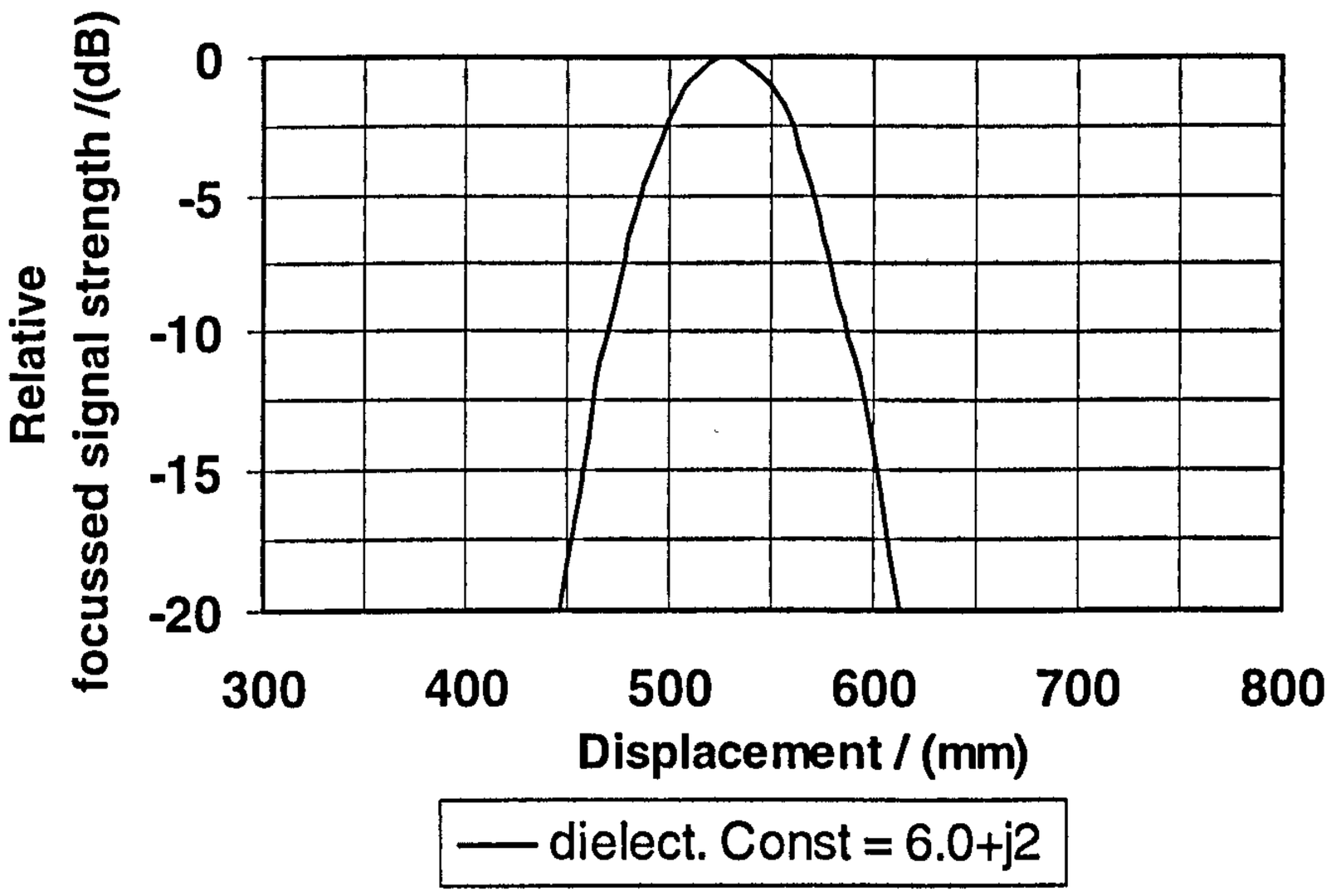

Figure 3.15 Lateral resolution with soil dielectric constant of 6+j2

The lateral resolution is consistent with the loss-less medium as the loss variations between various paths (in-soil path lengths) are minimal in the converging cone (see figure 2.6 in section 2.2.6.6). Although not shown, similar results were obtained for the vertical resolution. Generally high lossy soils exhibit a higher relative dielectric constant [28] which implies a narrower converging cone.

3.3.8. Reverberations

Further analysis with a larger metal plate (70x70mm) buried in soil with dielectric constant of 6 indicated the vertical resolution was larger than the expected resolution (Figure 3.16). Further time domain calculations showed a possible reason for this effect is that the signals from the target reverberate between the antenna back plane

(reflector) and the air-soil interface. Such signal reverberations in the PRSF-GPR system will mask the detection of the buried objects. In GPR systems, signals from shallowly buried targets are often lost in air-soil interface reflections (first bounce) which do not undergo attenuation as in the case of the buried targets. But the reverberating signals will interrupt the detection of deeply buried objects. The weak signals emerging from deep targets further contribute to this problem.

3.3.8.1. Improved System

One way of overcoming this problem is to use attenuating layers in front of the antenna array. Thus, the 2 way paths of the wanted signals will be attenuated twice and the reverberating energy more [29]. An alternative to this technique is to use an absorbing back plane, which will attenuate the reverberating energy with little overall loss of the transmitted signal. The system performance with an absorbing back plane has been analysed using FDTD, where an absorbing layer was added to the metallic reflector. The absorbing layer was 15mm thick with ε_r= 4+j3 (270 dB/m loss at 2.1GHz). Initially antenna input characteristics were analysed to make sure that the antenna input response was not significantly degraded by the absorber.

The reflected signals calculated from a metal plate of 70x70mm (with background subtraction) were vertically focussed and compared with the results from the previous model in figure 3.16.

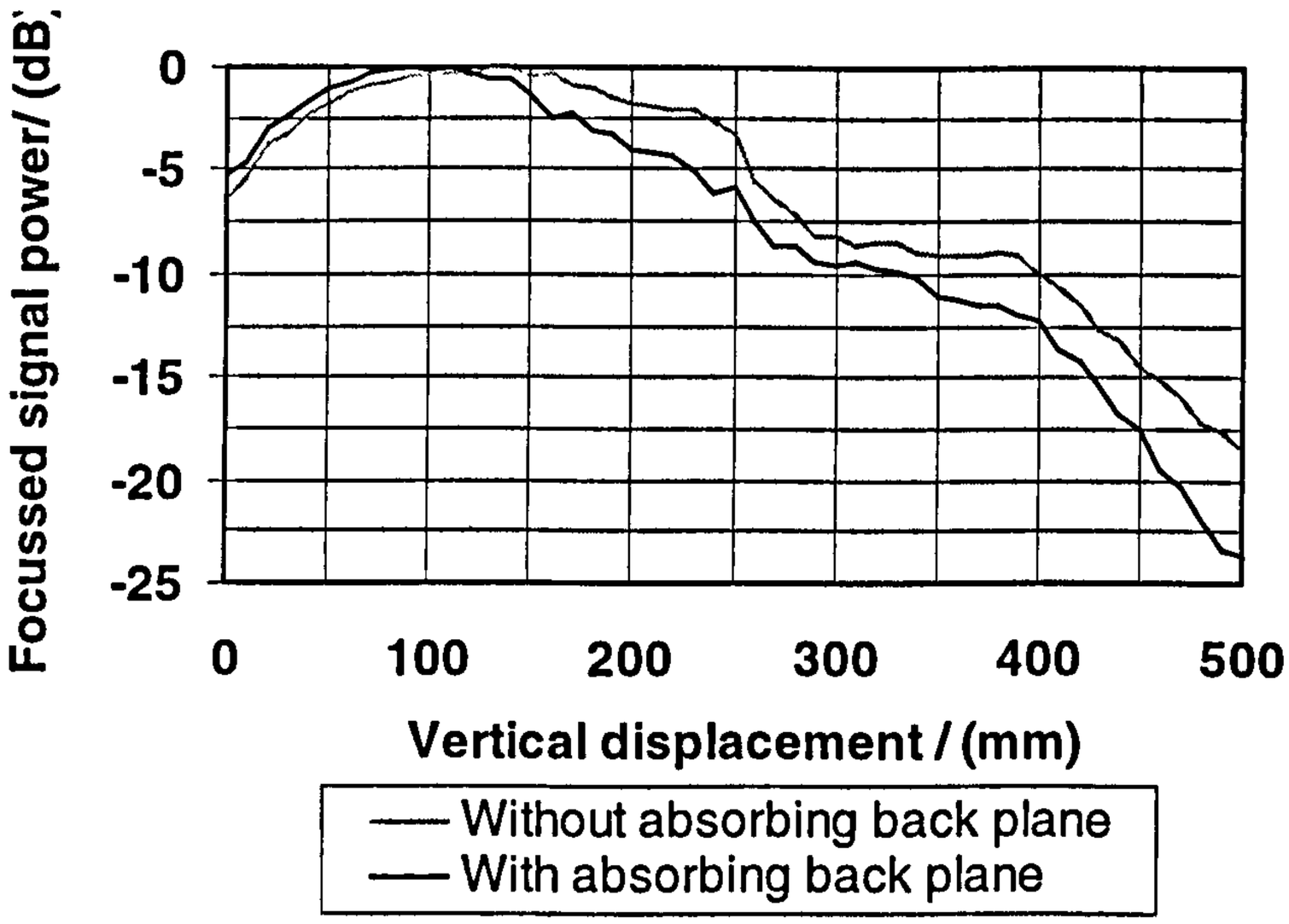

Figure 3.16 Vertical focusing with absorbing back plane

Figure 3.16 shows that this absorbing back plane reduces the width of half power points of the focussed signals by ≈75mm, thus reducing the effects of multiple bounces. The power losses due to the absorbing back plane is discussed in section 5.4.2

Further investigations were conducted with a small metal plate (30x30mm) buried at 150mm deep in soil to analyse the reverberations arising from surface clutter. The total signals that include such clutter (signals without back ground subtraction) were used to investigate the target location. Signals from the models with and without the absorbing back plane were compared with the surface clutter. Focussed signals with target returns that were calculated by background subtraction are also included in figure 3.17.

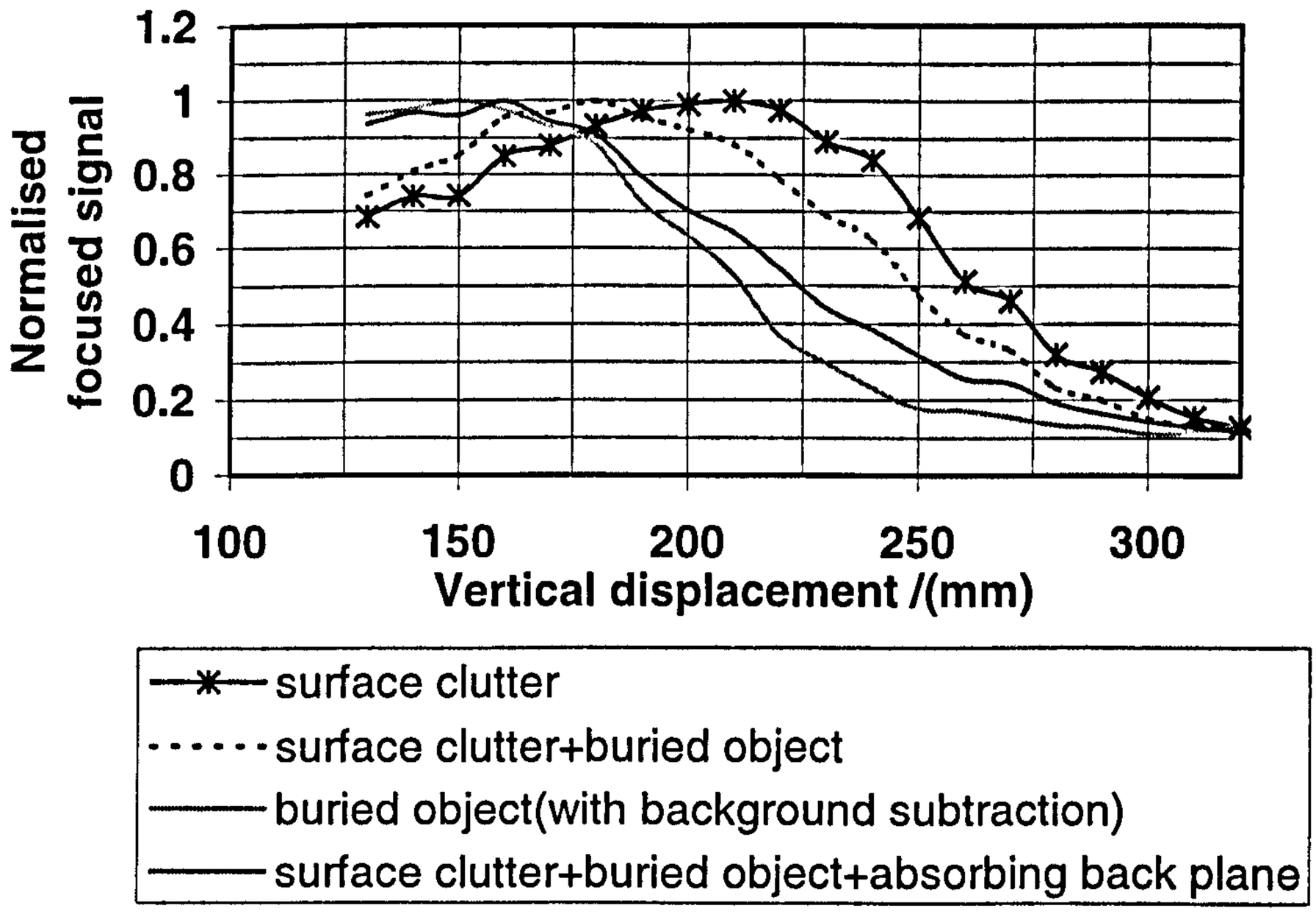

Figure 3.17 Vertical focusing through target location with reverberations

Figure 3.17 shows that the surface clutter (without the target) produces a peak at 200mm and the inclusion of the target moves the peak to 180mm. But with the absorbing back plane the correct target location is identified (150mm) and the normalised focussed signals are almost identical to that produced by back ground subtraction (where reverberations due to surface clutter are eliminated).

This analysis demonstrates that the absorbing layer helps to overcome the problems due to reverberations. The reverberating surface clutter masks the target signals, but the employment of the absorbing back plane helps to identify the target at its correct location. The absorbing layer also reduces the focussed signal power since it absorbs part of the transmitted signal power. Considering the gains that can be achieved with the employment of the absorbing back plane against the degraded transmitted power this technique is a possible solution to enhance detection.

3.4. Discussion

These analyses show that the FDTD is a powerful full wave technique to analyse the complex GPR problem. Although simple ray tracing techniques [30] can be used to calculate the resolutions of the PRSF-GPR system, it is difficult to incorporate the signals due to multiple bounces, mutual coupling and surface clutter. The estimation of signal strengths from various paths is also a challenging task when employing geometrical optics.

Although the FDTD method is a promising numerical simulation technique to investigate complex problems, it has its own drawbacks. These drawbacks are mainly due to its memory requirements, reflections from absorbing boundaries and the excessive time required for electrically large problems.

3.4.1. Memory Requirements

Memory requirement is a significant factor in modelling electrically large structures such as the ground penetrating radars and RCS calculation of aircrafts. The required memory is almost proportional to the size of the problem, as each cell has to store 6 field components for further updates of the fields. The type of algorithm used to implement the FDTD code and the different material properties also contributes to the memory requirements (parallel processing algorithm require much more memory). Approximately 100 Mbytes (1700,000 unit cells) were used in the post reception synthetic focusing ground penetrating radar model described in this chapter. Bourgeois et al [31] used 3.4 Gbytes for their GPR model on a multi processor machine for their two element conventional GPR model.

3.4.2. Run Times

The runtime of the problem depends on the problem size (number of elements) and the number of simulations performed. A higher number of iterations are needed for ground penetrating radar models since adequate time should be allowed for the reflected signal to reach the receiving antenna. Fast computers will reduce the time constraints significantly. Multi processor super computers such as Gray Y-MP (8 processors), Gray-3 (16 processors)[32] will dramatically reduce the computational time requirements. Another interesting prospect in overcoming the time constraints is the use of Connection Machines (CM) [32] or similar techniques. The connection machines have several thousand simple processors arranged in an optimum configuration for inter processor communications. These machines will also reduce the computational time significantly compared to HP workstations and Pentium processors. Bourgeois et al [31] reported that their GPR model required 17 minutes for 5000 iterations on a CM-5 machine (512 simple processors). The post reception synthetic focusing ground penetrating radar (which comprises 8 printed antenna elements) required approximately 10 hours on a 300 MHz Pentium II processor.

3.4.3. Possible Errors

Though the reflections from absorbing boundaries in FDTD modelling were kept low with the background subtraction for most cases, reflections associated with the target would have some effects in those analyses. Homogeneous soil conditions were assumed in all these models but practical soils will exhibit rather non-homogeneous properties. The PRSF-GPR system will perform well with temporally shorter pulses (for finer vertical resolution) but analysis of temporally short pulses in soil needs further considerations to incorporate dispersive soil conditions.

3.5. Summary

A general overview of the numerical finite difference time domain method and the modelling of a PRSF-GPR using FDTD methods has been presented in this chapter. Considerations have been given for the implementation of FDTD in electrically large complex electromagnetic problems and the new techniques in this field. The PRSF

concept has been analysed by simple geometric optic theory in the past [33] but application in complex surface penetrating radars require more rigorous analysis. Hence a three dimensional FDTD model of a ground penetrating radar which makes use of the post-reception synthetic-focusing techniques has been developed. The PRSF-GPR FDTD model consists of an antenna array with 8 dipole elements, feed lines, soil and the buried object. The concept of post reception synthetic focusing and its basic properties (resolutions, processing gain) have been demonstrated with the FDTD results. This analysis showed that the lateral resolution of the system is ≈ 65mm for 2.1GHz operating frequency with printed dipole elements and it is independent of the dielectric properties of the soil. A lateral resolution of 50mm was predicted with the geometrical optics theory(half power beamwidth of $\approx 45^0$). The vertical resolution of 120mm agreed well with the predicted 116mm, for soil dielectric constant of 6.

The theoretical analysis of this scheme also demonstrated some possible limitations due to reverberations. A possible solution to the reverberating energy in this type of system has also been analysed and found to be enhancing the system's detecting capabilities. This PRSF-GPR FDTD model is considered as the basic model for further analysis of the concept in some more challenging and realistic environments.

References

[1] C Balanis, *Antenna theory analysis and design*, John Willey & sons , New York , 1982

[2] J.M.Bourgoise and G.S.Smith, A Fully Three Dimensional Simulation of a Ground Penetrating Radar: FDTD Theory Compared with Experiment, *IEEE Transactions on Antennas and Propagation*, vol. AP-34, no.1, pp. 36-44, 1996.

[3] J.M.Bourgoise and G.S.Smith, A Complete Electromagnetic Simulation of the Separated Aperture Sensor for Detecting Buried Land Mines, *IEEE Transactions on Antennas and Propagation*, vol. AP-46, no. 10, pp. 1419-1426, 1998.

[4] R.L.Roberts and J.J.Daniels, Modelling Near-field GPR in Three Dimensions Using FDTD Methods, *Geophysics*, vol. 62, no. 4, pp. 1114-1126, 1997.

[5] R.Benjamin, Post Detection Synthetic Focusing in Near-field Radar, *Proceedings of EUREL/IEE International Conference on the Detection of Abandoned Land Mines*, IEE, Edinburgh, pp. 133-137, Oct 1996

[6] R.Benjamin, Near-field Spot Focused Microwave Sensing for the Detection of Buried Land-Mines, *Proceedings of EUREL/IEE International Conference on the Detection of Abandoned Land Mines*, IEE, Edinburgh, pp. 128-132, Oct 1996

[7] FDTD Electromagnetic Analysis Programs, *User Guide*, University of Bristol, 1993.

[8] K.S.Yee, Numerical solution of Initial Boundary Value Problems Involving Maxwell's Equations in Isotropic Media, *IEEE transaction on Antenna and Propagation*, vol. AP-14, pp. 302-307, 1966.

[9] G.S.Hilton, *An Investigation of Microstrip Patch Antennas and their Analysis by Finite Difference Time Domain Techniques*, PhD thesis, University of Bristol, UK, 1993.

[10] A Taflove and M.V.Brodwin, Numerical Solutions of Steady State Electromagnetic Scattering Problems Using the Time Dependent Maxwell's

Equations, *IEEE Transactions on Microwave theory and Techniques*, vol. MTT-23, no.8, pp. 623-630, 1975.

[11] M.Fusco, FDTD Algorith in Curvilinear Co-ordinates, *IEEE Transactions on Antennas and Propagation*, vol. AP-39, pp. 1463-14761, 1991.

[12] K.M.Krishnaiah and C.J.Railton, A stable subgridding Algorithm: An application to Eigenvalue Problems, *Telsiks–97 Conference Proceedings*, University of Nis, pp. 112-115, 1997.

[13] S.S.Zivanovic, K.S.Yee and K.K.Mei, A Subgridding Method for the Time-Domain Finite Difference Method to Solve Maxwell's Equations, *IEEE Transactions on Microwave theory and Techniques*, vol. MTT-39, no.3, pp. 471-479, 1991.

[14] A.Taflove, *Computational Electrodynamics: The Finite Difference Time Domain Method*, Artech House, USA, 1995.

[15] I.S.Kim and W.J.R.Hoefer, Numerical Dispersion Characteristics and Stability Factor for FDTD Method, *Electronic Letters*, vol. 26, pp 485-487, 1990.

[16] D.L.Paul, N.M.Pothecary and C.J.Railton, Calculation of the Dispersive Characteristics of Open Dielectric Structures by the Finite Difference Time Domain Method, *IEEE Transactions on Microwave Theory and Techniques*, vol. MTT-42, no.7, pp.1207-1212, 1994.

[17] C.J.Railton and J.P.McGeehan, Analysis of Micro-Strip Discontinuities Using the Finite Difference Time Domain Technique, *Proceedings of the IEEE Microwave Theory and Techniques Symposium Digest*, pp. 1009-1012, 1989.

[18] G.Mur, Absorbing Boundary Conditions for the Finite Difference Approximations of the Time Domain Electromagnetic Field Equation, *IEEE Transaction on Electromagnetic Compatibility*, vol. EMC-23, no.4, pp 377 - 382, 1981.

[19] C.J.Railton and E.M.Daniel, A Comparison of the Properties of Radiating Boundary-Conditions in the FDTD Method for Finite Discretisation and Non-

Planar Waves, *IEEE Transactions on Antennas and Propagation*, vol. AP-42, no.2, pp.276-281, 1994.

[20] J.P.Berenger, A Perfectly Matched Layer for the Absorption of Electromagnetic Waves, *Journal of Computational Physics*, vol. 114, pp 185- 200, 1994.

[21] J.P.Berenger, 3 Dimentional Perfectly Matched layer for the Absorption of Electromagnetic Waves, *Journal of Computational Physics*, vol. 127, pp 363-379, 1996.

[22] J.G.Maloney and G.S.Smith, A Comparison of Methods for Modelling Electrically Thin Dielectric and Conducting Sheets in the Finite Difference Time Domain Method, *IEEE Transactions on Antennas and Propagation*, vol. AP-41, no. 5, pp 690-694,1993.

[23] C.J.Railton and J.P.McGeehan, Characterisation of Microstrip Open-end with Rectangular and Trapezoidal Cross Section, *Electronics letters*, vol. 26, no.11, pp.685-686, 1990.

[24] C.J.Railton and J.P.McGeehan, An analysis of Microstrip with Rectangular and Trapezoidal Conductor Cross Sections, *IEEE Transactions on Microwave Theory and Techniques*, vol. MTT-38, no.8, pp.1017-1022, 1990.

[25] R.Luebbers, F.P.Hunsberger, K.S.Kunz, R.B.Standler and M.Schneider, A Frequency Dependent Finite Difference Time Domain Formulation for Dispersive Materials, *IEEE Transaction on Electromagnetic Compatibility*, vol. EMC-32, no.3, pp. 222 - 227, 1990.

[26] D.V.Thiel and R.Mittra, Surface Impedance Modelling Using the Finite Difference Time Domain Method, *IEEE Transactions on Geoscience and Remote Sensing*, vol. GE-35, No 5, 1997.

[27] C.J.Railton and J.P.McGeehan, The Use of Mode Templates to Improve the Accuracy of the Finite Difference Time Domain Method, *21st European Microwave Conference Proceedings*, vol. 21, pp. 1278-1283, 1991

[28] Ulaby et al, *Microwave Remote Sensing*, vol. 111, Artech House, 1986.

[29] R.Benjamin, Non-contact, Synthetically Near-Field Focused Operation without Index Matching, *Internal Report to DERA*, UK, 1998.

[30] R.Benjamin, G.S.Hilton, S.Litobarsski, E.McCutcheon and R.Nilavalan, Microwave Detection of Subsurface Objects, 6^{th} *Report to DERA*, University of Bristol, UK.

[31] J.M.Bourgeois and G.S.Smith, A Fully Three Dimensional Simulation of a Ground-Penetrating Radar: FDTD Theory Compared with Experiment, *IEEE Transactions on Geoscience and Remote Sensing*, vol. GE-34, no.1, pp.36-44, 1996.

[32] A.Taflove and K.R.Umashankar, Review of FD-TD Numerical Modelling of Electromagnetic Wave Scattering and Radar Cross Section, *Proceedings of the IEEE*, vol. 77, no. 5, pp. 682-699, 1989.

[33] R.Benjamin, Near-field Spot Focused Microwave Sensing for the Detection of Buried Land-Mines, *Proceedings of EUREL/IEE International Conference on the Detection of Abandoned Land Mines*, IEE, Edinburgh, pp. 128-132, Oct 1996

4. Analysis of PRSF-GPR in Various Soil Conditions

4.1. Introduction

Ground penetrating radars have to operate in a variety of soils, which have various electrical discontinuities. The most significant challenge in detection is the clutter arising from discontinuities such as from air-soil interface (known as surface clutter) or from subsurface features (volume clutter). Other significant features include non-flat ground and stratified ground conditions. These are particularly important to the PRSF technique as the coherent combination would be degraded by the assumption of flat and uniform dielectric properties of soil. The merits and possible limitations of the PRSF-GPR technique in clutter environments have been outlined in Chapter 2. A more detail theoretical analysis of the PRSF-GPR system in various soil conditions will help understand the nature of the problem and lead to possible solutions.

Analysis of clutter arising from subsurface features is complex due to various parameters related to the GPR and the complex nature of interactions between the subsurface objects. Practical experimental analyses are very difficult to perform in a controlled manner since inhomogeneous soil properties, setting up experiments, stability of electronic equipment and external interference will introduce errors. On the other hand, theoretical investigation considers these problems separately and helps to improve the understanding.

Chapter 3 introduced a simple FDTD model for the PRSF-GPR technique. This chapter analyses the PRSF-GPR system in different environments such as clutter, non-flat and stratified media. The simple FDTD model was further modified to include

these ground conditions. Simple analytical techniques are also employed as part of system verification. Furthermore, a new processing technique for longer modulated pulses is investigated with FDTD and results are presented showing the detection of targets buried near surface (air-soil interface) and stratified media.

4.2. Near Surface Detection

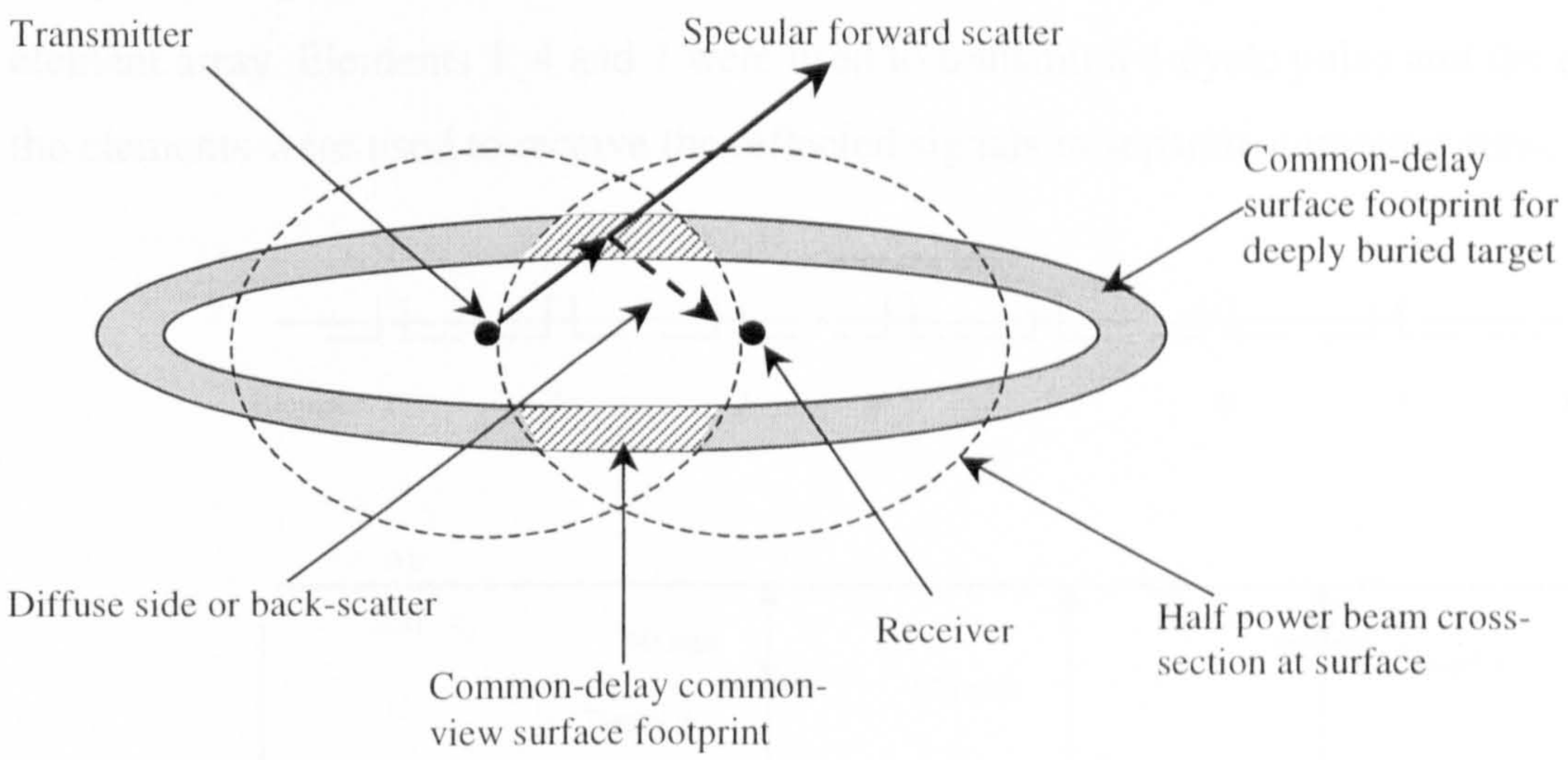

Figure 4.1 Plan view of the surface clutter locus for deeply buried targets

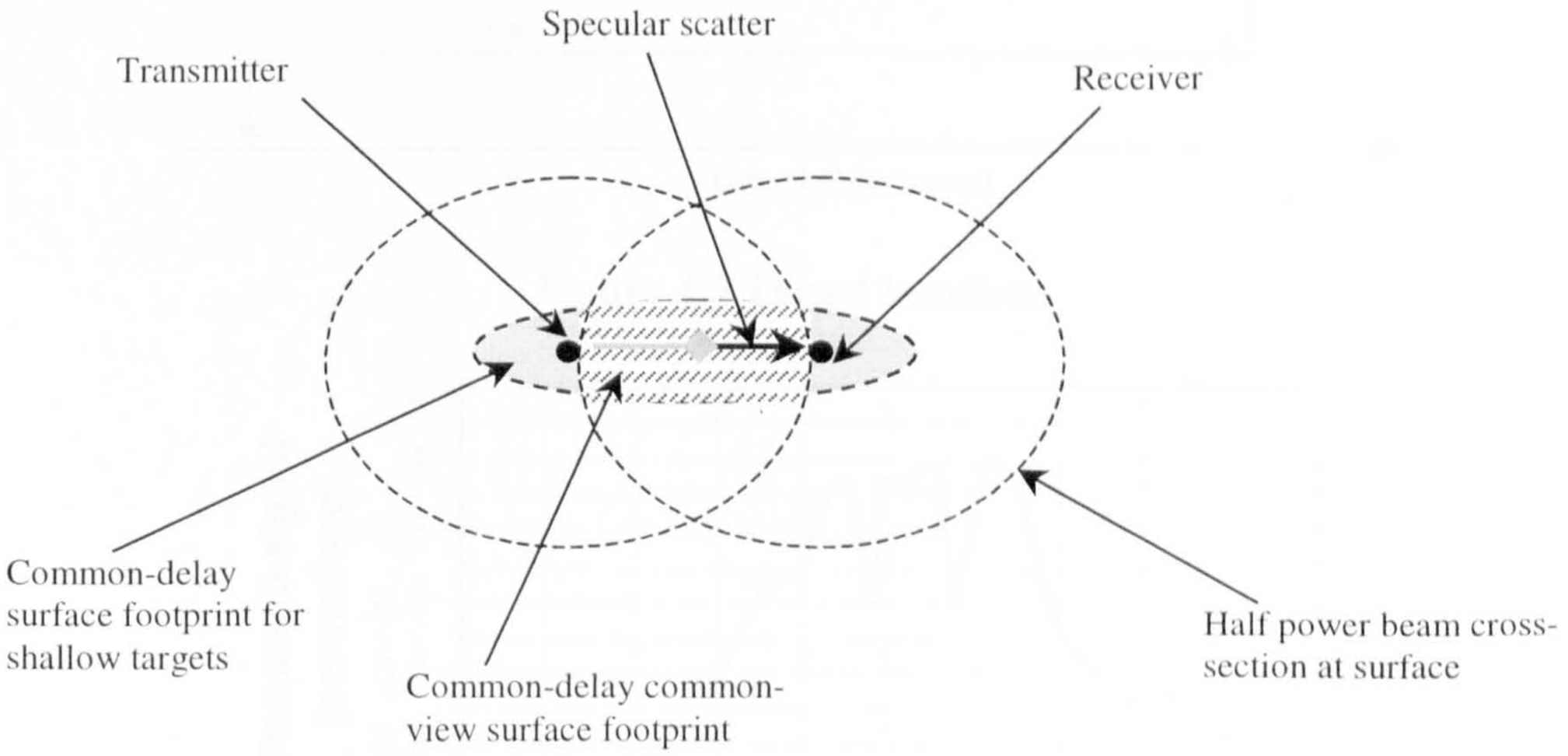

Figure 4.2 Plan view of the surface clutter locus for shallowly buried targets

Surface clutter in GPRs arise from the common-range common-view footprint as discussed in section 2.3.4. For deeply buried targets, only the diffused scatter from the common range footprint will compete with the target signals as shown in figure 4.1.

But for shallowly buried targets, the specular returns will also interfere with the detection (Figure 4.2). Longer modulated pulses have a wider footprint and hence high degradation is possible for relatively deeper targets. This effect can be easily seen in figure 4.4, where the FDTD results from a model with shallow targets are laterally focussed at 50mm depth. The locations of the metal targets (30x30mm) are shown in figure 4.3 and the soil was modelled with a dielectric constant of 6. This model comprised targets a, b and c at 80mm, 175 mm, and 50mm depths directly below the 8 element array. Elements 1, 4 and 7 were used to transmit a 4-cycle pulse and the rest of the elements were used to receive the reflected signals in separate computer runs.

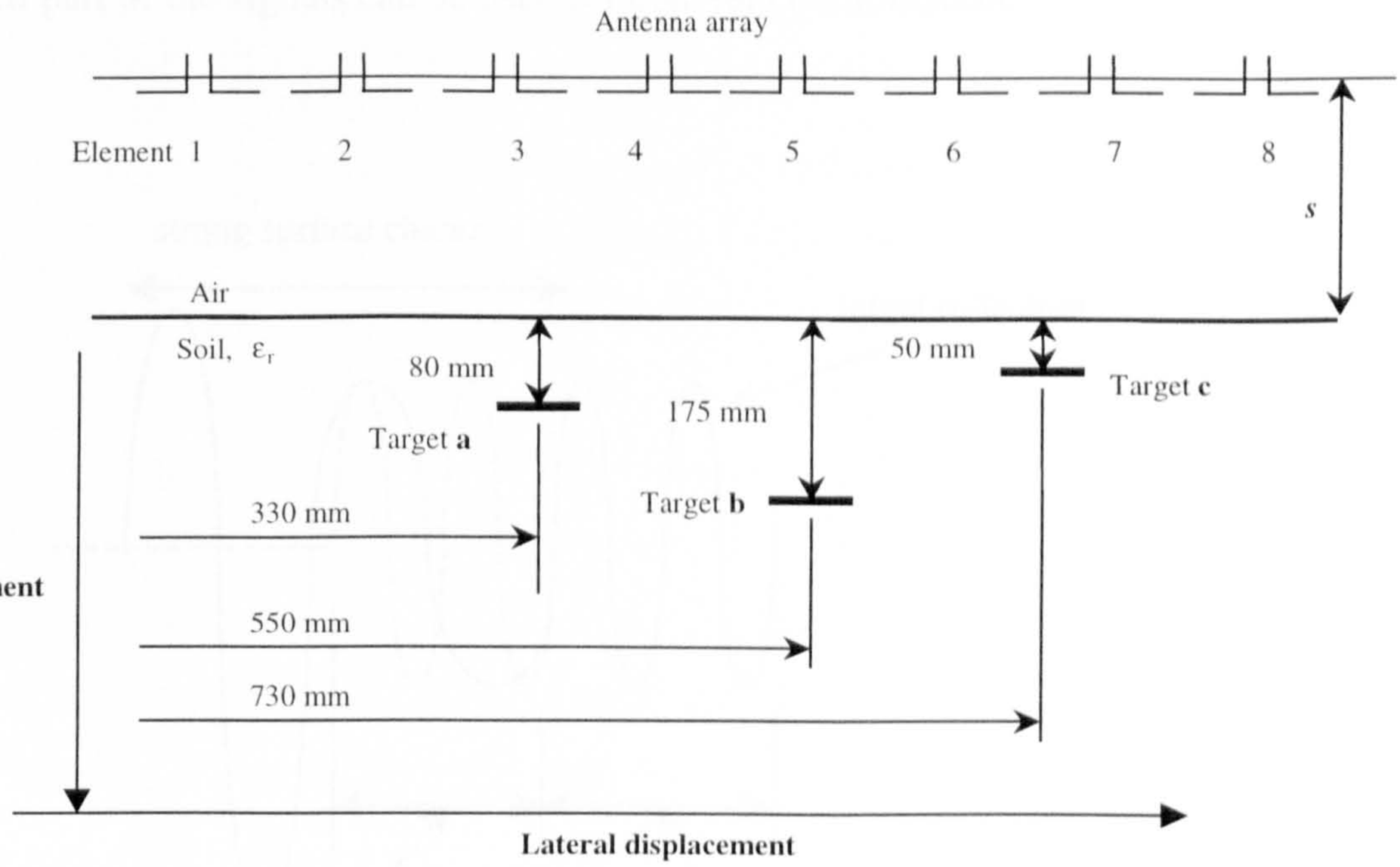

Figure 4.3 Target locations

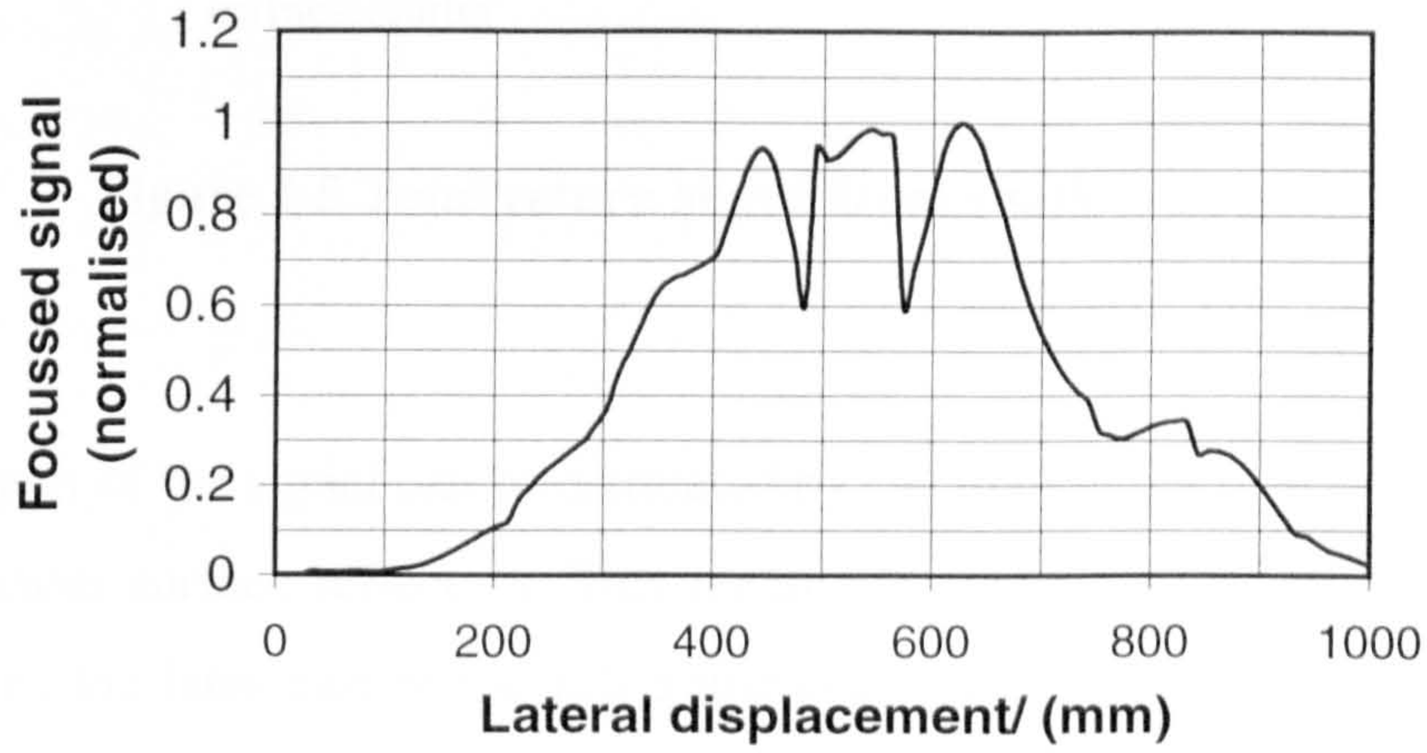

Figure 4.4 Lateral focusing at shallow target depth (50 mm)

Figure 4.4 shows that the signals from the targets being masked by the strong surface reflections (targets are at 330mm, 550mm and 730mm lateral displacements). Analysis of the individual signals from each path indicated that only a part of the signal is masked by the strong surface reflections. In post reception synthetic focusing, the relevant path delays are calculated with the assumed dielectric constant of soil and the corresponding signals are coherently added together. In this scenario, each path is assumed to contain the scaled down replica of the transmitted pulse and the full pulse length is considered for focusing. But the same coherence can be maintained even if a part of the signal is added with appropriate time offset. Figure 4.5 shows how the unmasked part of the signals can be used for coherent combination.

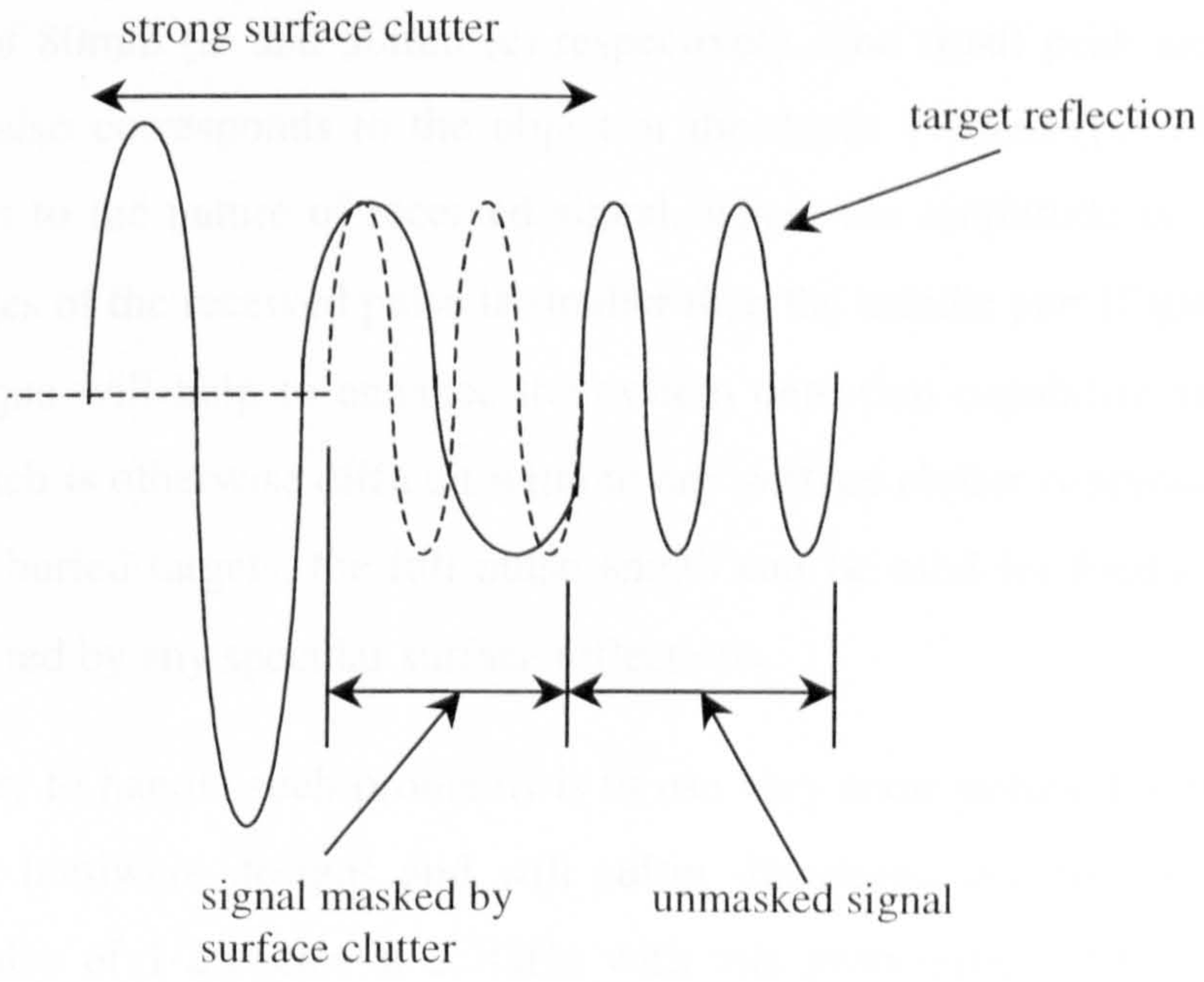

Figure 4.5 Total return signal from shallow target

The masked part of the signal can be estimated by calculating the path delay associated with the specular surface reflection. This technique was employed to coherently add the signals i.e., the later part of the full transmitted signal (0.75 cycles) was used for focusing. Figure 4.6 shows the laterally focussed signals at 50mm depth.

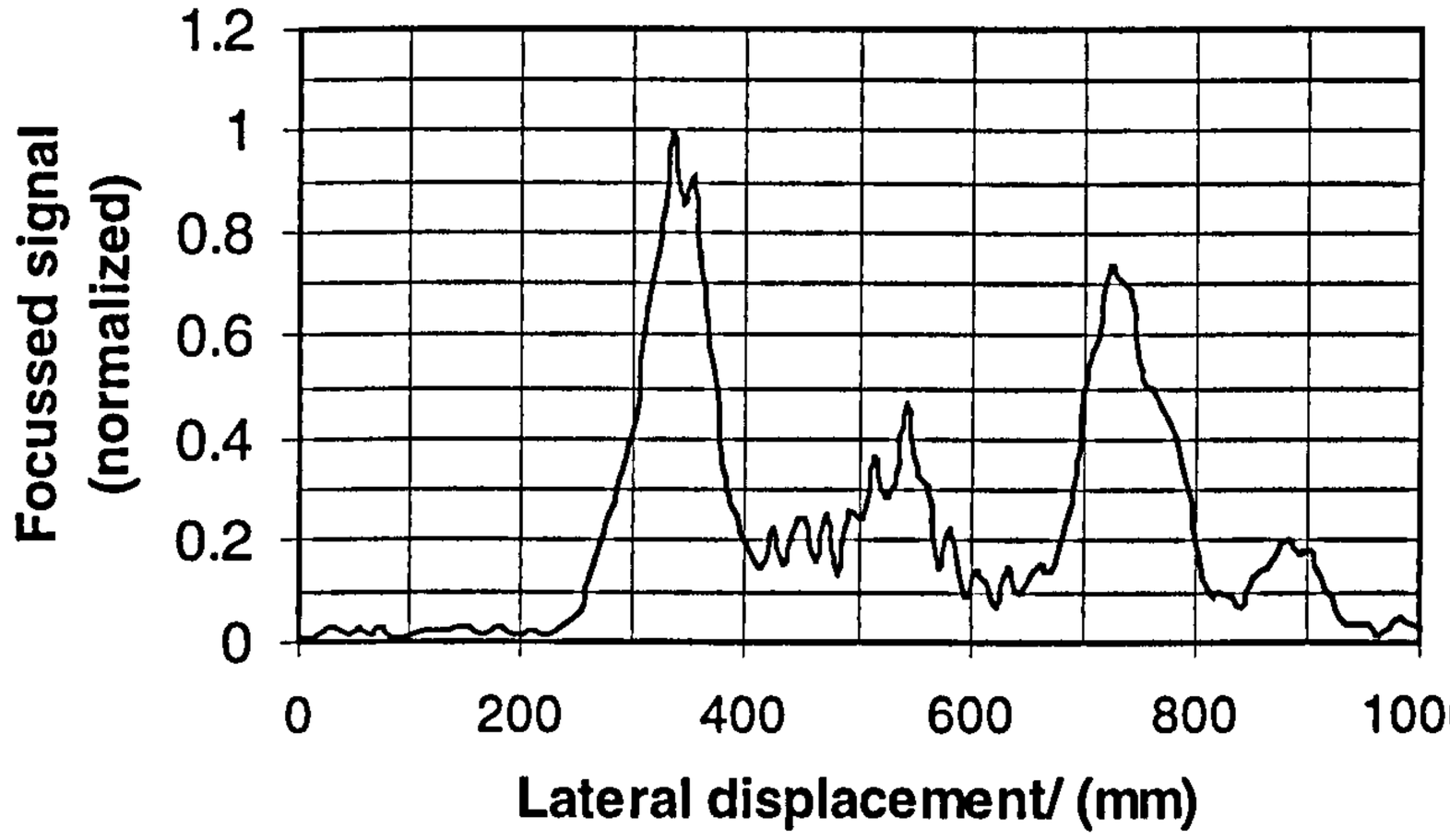

Figure 4.6 Focusing with part of the signal at 50mm depth

Figure 4.6 clearly shows two peaks, which exactly corresponds to the objects buried at the depth of 80mm (a) and 50mm (c) respectively. The small peak around 550mm in figure 4.6 also corresponds to the object at the depth 175mm (b). The signal levels corresponds to the nature of received signal, where the amplitude of the leading and trailing edges of the received pulse is smaller than the middle part (Figure 3.10). Hence this technique will help to enhance the system detection capability at shallow target depths, which is otherwise difficult without any surface clutter suppression techniques. For deeply buried targets, the full pulse length can be used for focusing, as they will not be affected by any specular surface reflections.

Another way to handle such problems is to use very short pulses, but this will require challenging hardware designs and will suffer dispersion due to soil characteristics. Hence a pulse of 1-2 cycles at 2.1GHz with this processing technique will enhance detection near air-soil interface. To transmit temporally short pulses the PRSF-GPR system would have to have elements with wider bandwidth capabilities to the dipole considered in this analysis.

4.3. Analysis in Volume Clutter Environment

The volume clutter arises mainly from embedded pebble-like objects and various other dielectric discontinuities in soil. The effects of volume clutter in detection of buried objects were briefly discussed in section 2.3.4, and a more detail theoretical analysis of

clutter due to pebble like objects is presented in this section. The basic FDTD model described in section 3.3.2 was used in the analysis with randomly positioned small metal blocks (5x5x5mm) to represent volume clutter. Absorbing back planes were also employed in this model to limit the multiple bouncing energy as discussed in section 3.3.7.

4.3.1. FDTD Model

The FDTD model used in this simulation is shown in figure 4.7 comprising 8 linear array elements. The method discussed in section 3.3.2.2 was followed to obtain the reflected signals from soil with all possible transmitting elements in order to maximise the processing gain, this required 7 computer runs. Reflections from soil-air interface were eliminated by background subtraction in order to analyse the clutter effects on their own.

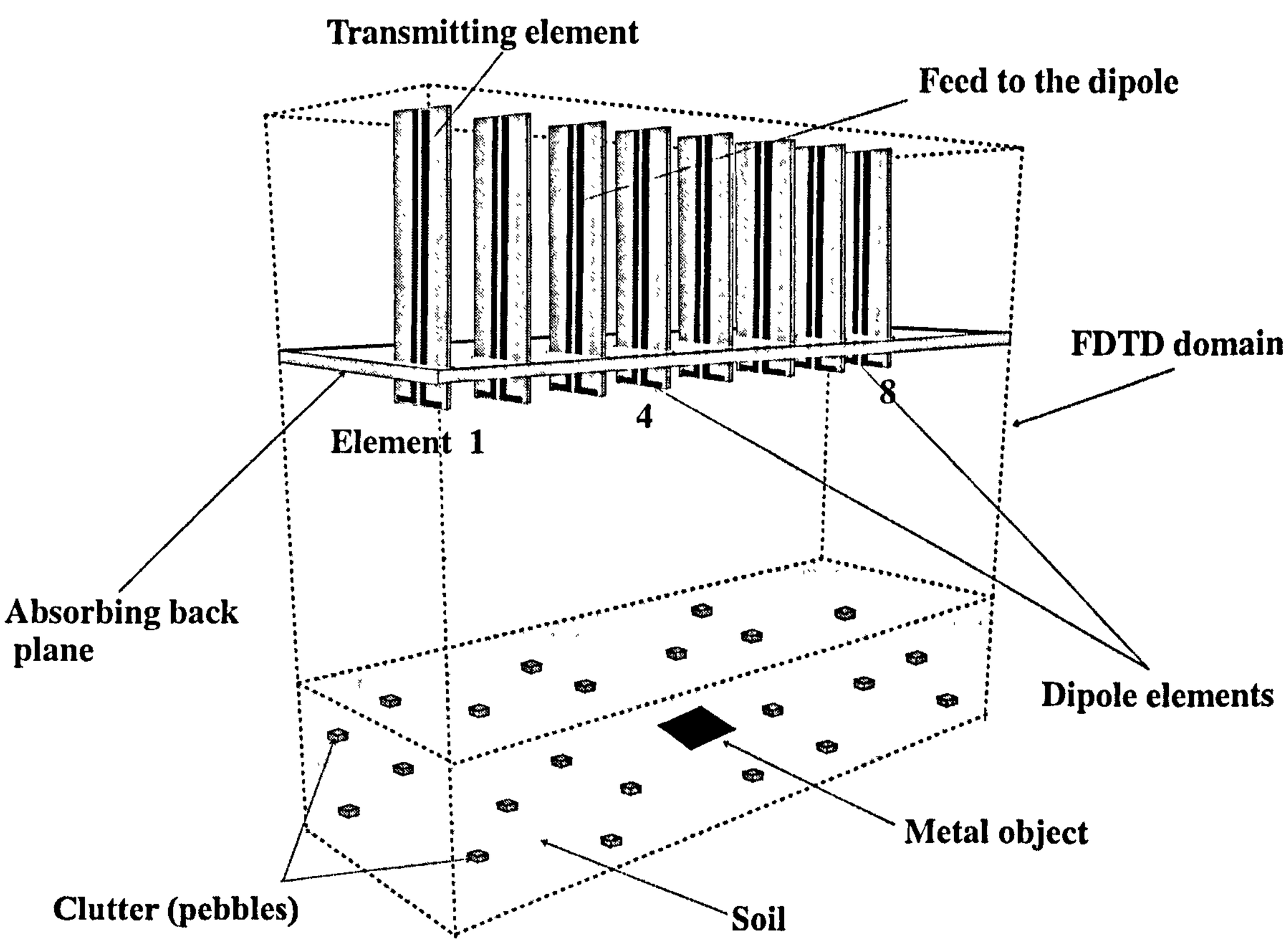

Figure 4.7 PRSF-GPR clutter model

4.3.2. Target Detection

The target detecting capabilities of the PRSF system were analysed with a metal plate of 50x50mm buried at 100mm depth and 400mm lateral displacement. Figure 4.8 shows the laterally focussed results using 7 and 28 paths. The 7 paths were with elements 1 and 4 transmitting and the rest receiving and the 28 paths were using all possible transmitting elements as shown in figure 4.7. All results were normalised with the maximum signal strength obtained with 28 paths.

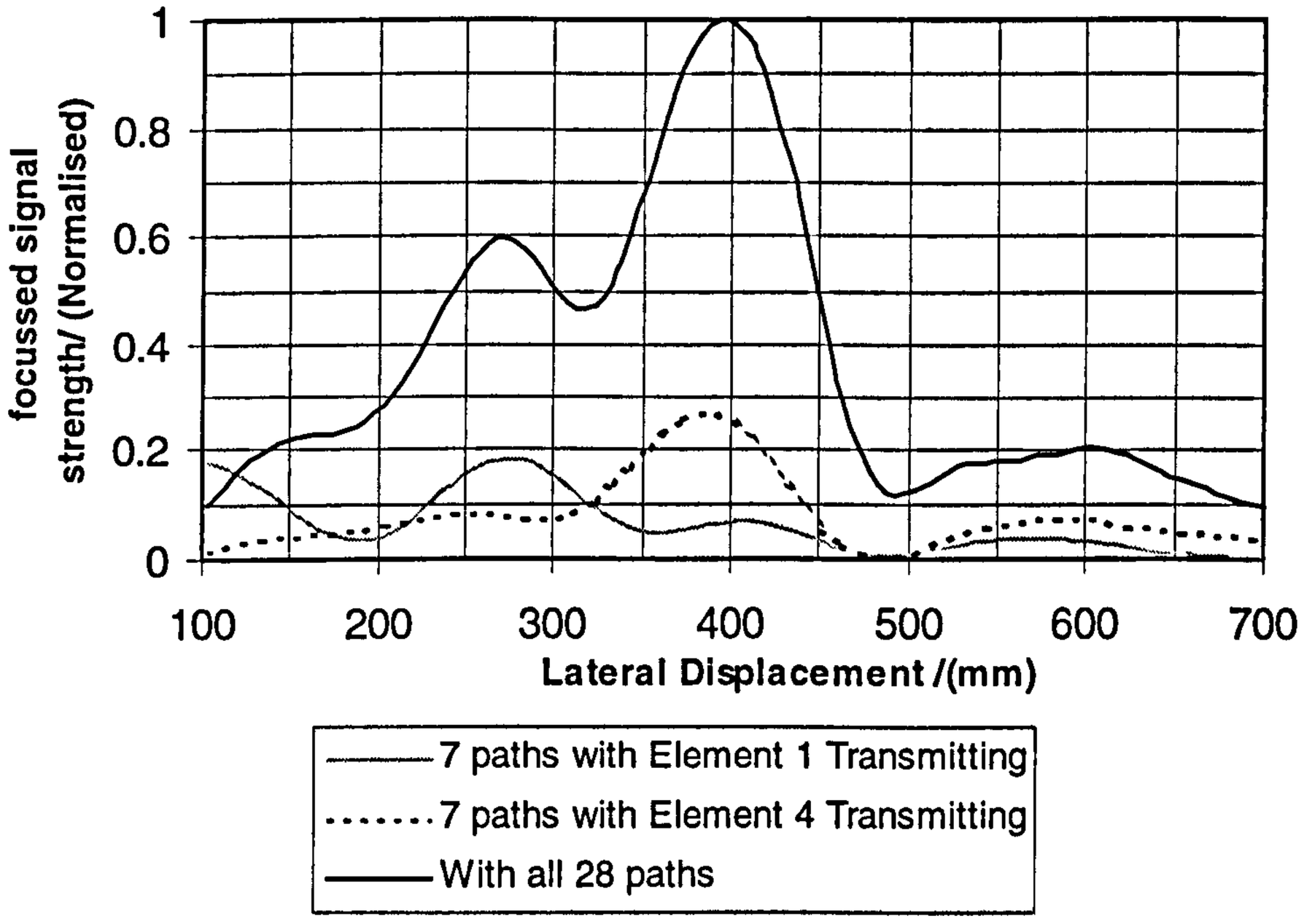

Figure 4.8 Synthetic focusing in a clutter environment

Figure 4.8 demonstrates the system capability in detecting subsurface object in clutter environments by use of multiple paths. Focusing with 7 paths with element 1 transmitting failed to identify the target and with element 4 transmitting, the target location is identified with a lateral error of ≈40mm. But with full processing gain of the system the target becomes visible with an error of ≈7 mm. As discussed in section 2.3.4, volume clutter in PRSF system arises from a small volume common to all the possible paths defined by the distinct element pairs. Hence the use of more paths will also reduce the common clutter volume and enhanced detection is made possible. Most conventional GPRs operate with a transmitter-receiver pair and the processing depends

only on a single path and this limits the detection of objects buried in clutter environments.

4.3.3. Nature of Clutter Returns

Analysis in section 4.3.2 shows that the clutter arising from pebble like objects degrade the target detecting capability of the system. Therefore, the strength of the target echo is also important, and this will depend upon the size of the object and its electrical properties. Echoes from plastic mine like targets are very weak because of the dielectric contrast between soil and such targets. Here the detection needs clutter reduction techniques, which can be easily implemented in synthetic post reception focusing techniques [1] to further enhances the detection process. To implement clutter reduction techniques it is important to analyse the nature of clutter returns. This section investigates the clutter returns in detail and provides some insight into this complex problem.

4.3.3.1. FDTD Numerical Analysis

FDTD simulations were performed on a model with random clutter distribution of 350 pebbles/m^3. This model consisted of soil and clutter objects with 8 element linear antenna array without the target. Surface reflections were eliminated from this analysis by performing a background subtraction with results from a model without the clutter objects. This was done to analyse the clutter arising only due to pebble like objects. An absorbing antenna back plane was also included in the FDTD models to eliminate the reverberating energy.

The reflected signals were used to obtain the mean clutter returns at each depth. The mean return was calculated by averaging the signal strengths obtained when focusing at different lateral displacements at these depths as shown in equation 4.1. The focusing points in the lateral direction were spaced 20mm which is less than the lateral resolution of the system at 2.1GHz (≈ 65mm).

Figure 4.9 shows the normalised mean clutter strengths along the vertical displacement given by,

$$m_{h=h_i} = \frac{\sum_{i=1}^{n} S_{x=x_i}}{n} \tag{4.1}$$

where,

$m_{h=h_i}$: mean clutter return at depth h_i

$S_{x=x_i}$:Synthetically focussed signal at a lateral displacement of x_i

n :number of points considered along the lateral axis

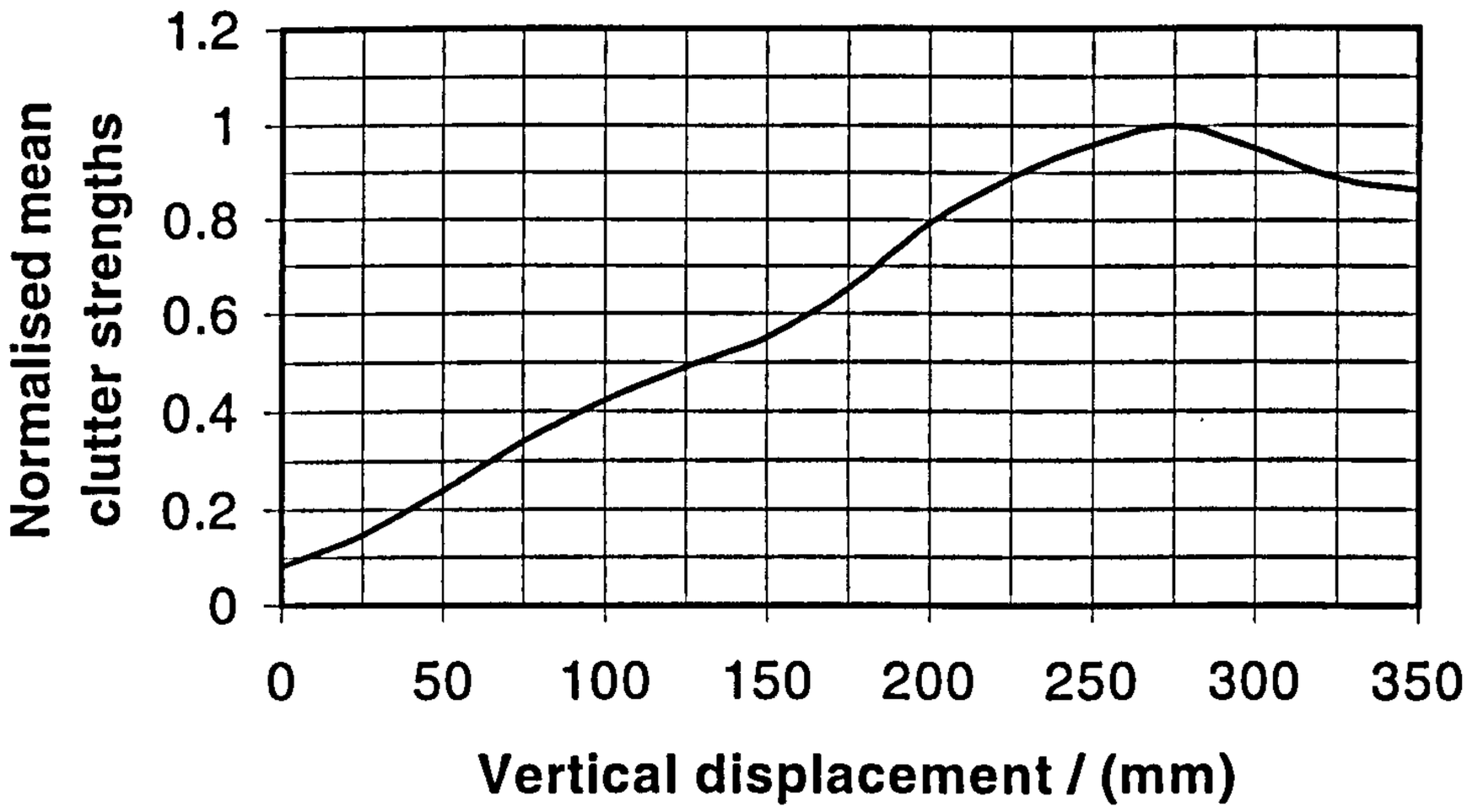

Figure 4.9 Mean clutter strengths along vertical axis

It can be seen from figure 4.9 the mean clutter returns increase with the depth and reduces after 275mm in soil. This behaviour is due to the increase in number of pebbles within the common delay clutter volume with depth, and decrease to the limited FDTD space. The FDTD absorbing boundary was placed at 450mm depth.

4.3.3.2. Non-Coherent Combination of Clutter

Having analysed the nature of clutter returns using FDTD methods, it is important to investigate this analytically in order to employ this in clutter reduction techniques. Clutter in PRSF-GPR system arises from the *common delay-common view volume* in

the clutter volume as described in section 2.3.4. As shown in figure 4.10, signals from the set of reflectors whose effective reflecting points are exactly on the same common-range surface would combine coherently, as would any separated by exactly 2π (i.e., for a 4 cycle pulse). Similarly signals from shells separated by exactly π (or 3π) would give rise to coherent cancellation. However the probability of either occurring depends on the random distribution of the pebbles in the common range clutter volume. Hence the non-coherent summation of signals from pebble like targets would give the mean clutter expected, while its variance will indicate the possibilities of coherent addition or coherent cancellation depending on the phase of the returned signal. With a large number of pebbles within each common range clutter shell and a large number of element pairs, the mean power would be a very good estimation of the clutter return.

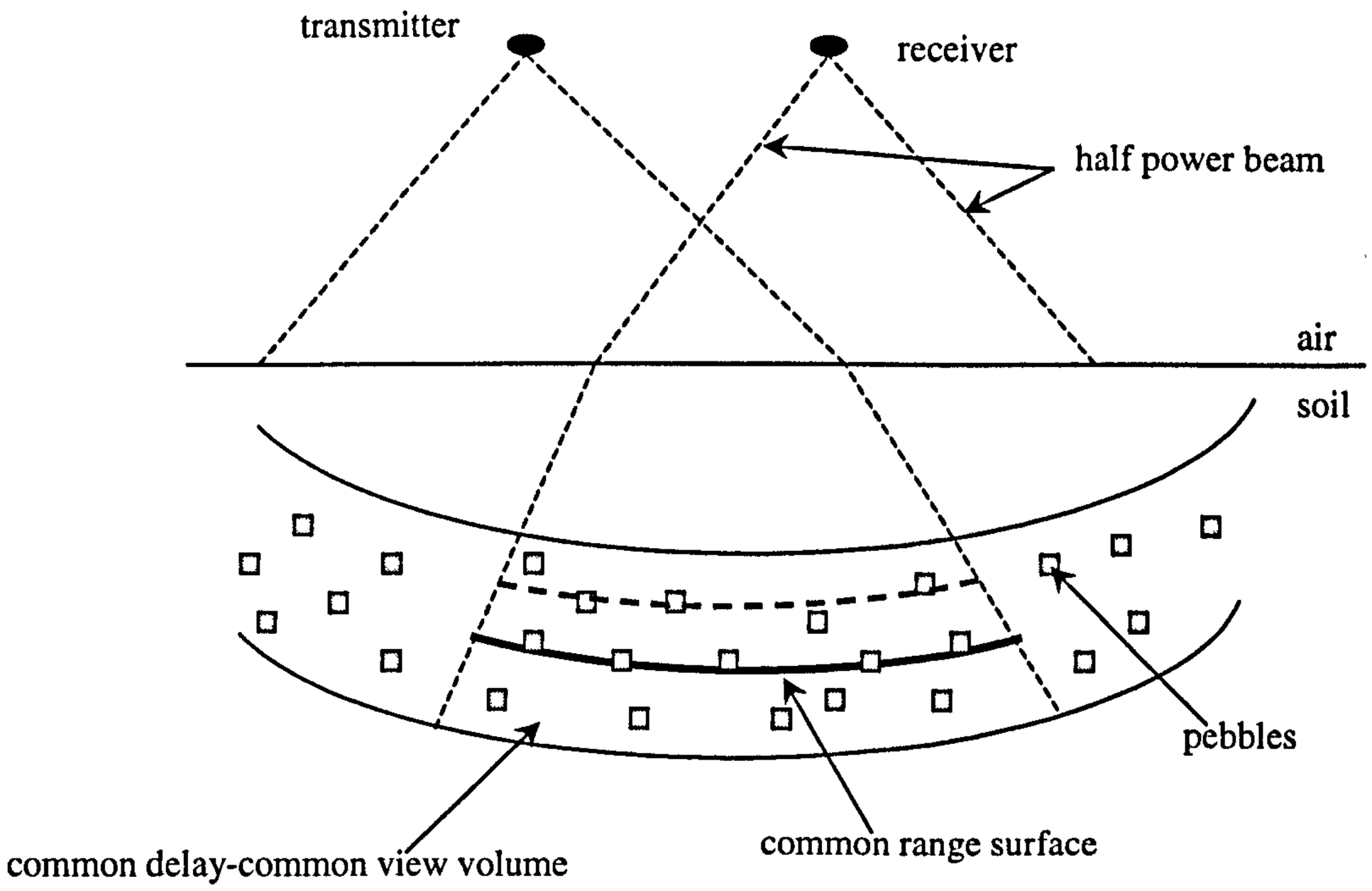

Figure 4.10 Common delay-common view volume

The non-coherent summation of clutter signals can be estimated by the calculation of the number of pebbles within the *common-range common-view clutter volume*. For an even clutter distribution, this will be proportional to the *common-range common-view clutter volume*. Soil attenuation properties can also be included in this analysis by appropriately scaling these non-coherently added signals by the estimated attenuating factors.

Figure 4.11 shows the comparison between the FDTD focussed signals and the estimated clutter returns by the non-coherent combination of the signals (using equation 4.1 for focusing) and shows that the clutter returns calculated analytically closely follows the results from FDTD.

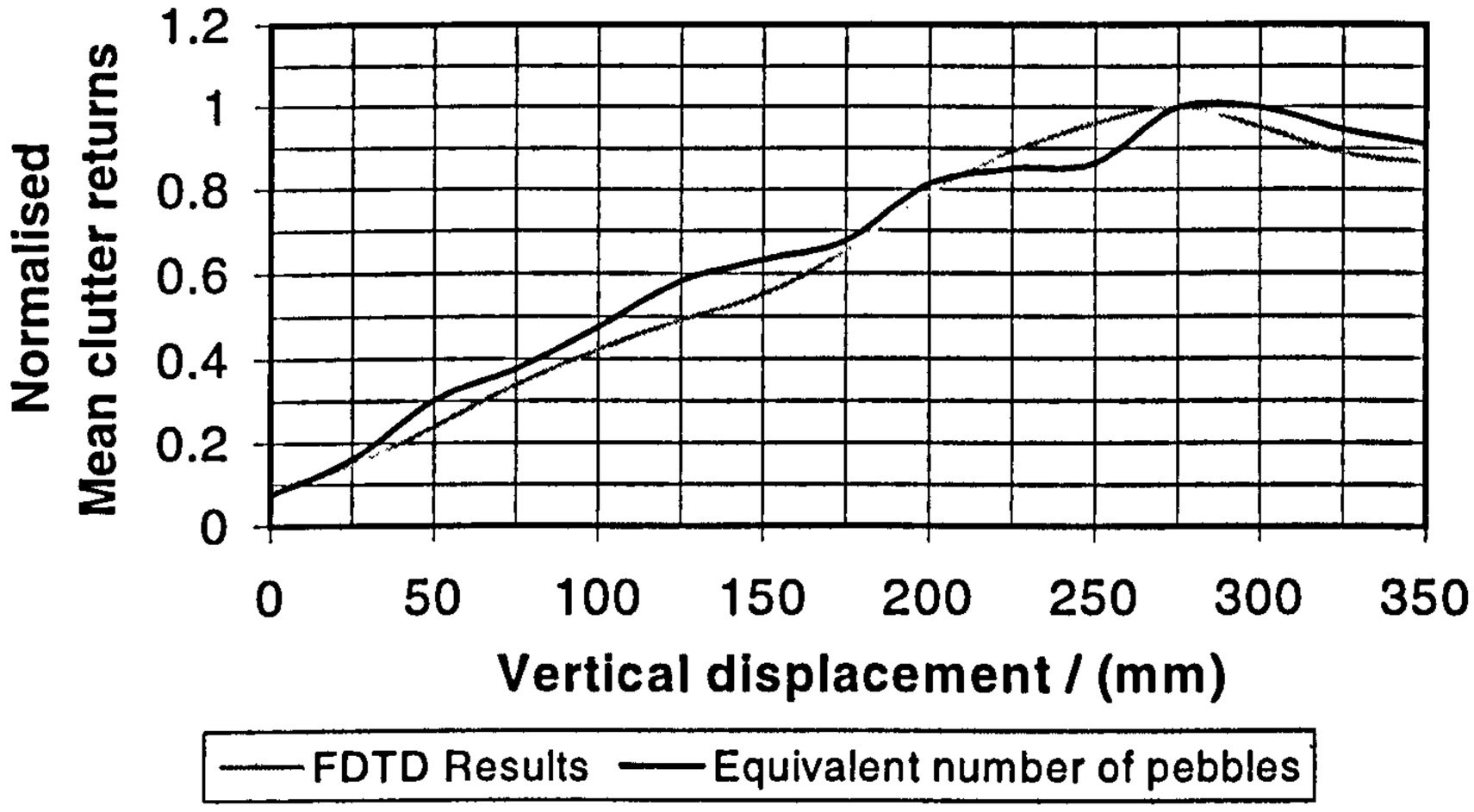

Figure 4.11 Comparison of FDTD clutter echoes with the estimated clutter

Having found a good matching between the predicted non-coherent summation of clutter signals with the FDTD clutter returns, this estimation was applied to detect objects masked by clutter signals.

4.3.3.3. Clutter Weighting

FDTD methods were employed to model the signals from a small metal plate (20x20mm) that was buried in a clutter environment at lateral and vertical locations of 550mm and 160mm, respectively. The calculated signals comprised of the returns from the metal object and the signals due to the pebble-like objects buried in the media with all elements transmitting. Pebbles were distributed in soil as shown in figure 4.7. Focusing these results indicated the target at its correct lateral location but failed to identify it at its correct vertical location as shown in figure 4.12 and figure 4.13. This behaviour is expected since the number of pebbles within the common range clutter volume of the FDTD model increases with the vertical displacement as discussed in section 4.3.3.2. Hence to detect the object at its correct location, clutter weightings were applied to each individual paths [1]. Each path was scaled down by the estimated non-coherent combination discussed in section 4.3.3.2.

Hence the PRSF can be represented by,

$$V = \sum_{i=1}^{n} a_i U(t - T_i) \tag{4.2}$$

where,

V : Synthetically focused signal.

$U(t)$: Signal received from path i at time t.

n : Number of paths which are associated with the resolution cell.

a_i **: Clutter scaling factor for path i derived as in section 4.3.3.2**

T_i : Path delay from the transmitting element to the receiving element via the resolution cell.

Laterally and vertically focussed results with clutter weightings are shown in figure 4.12 and figure 4.13.

These results show improvements on both lateral and vertical focusing. Figure 4.12 shows the target at its correct lateral location without clutter weighting and improvements at other horizontal displacements with clutter weighting. Figure 4.13 identifies the object with a vertical error of ≈10mm with clutter weighting. Hence this capability of the PRSF technique which has scope for weighting each path, further enhances the detection capability of the system.

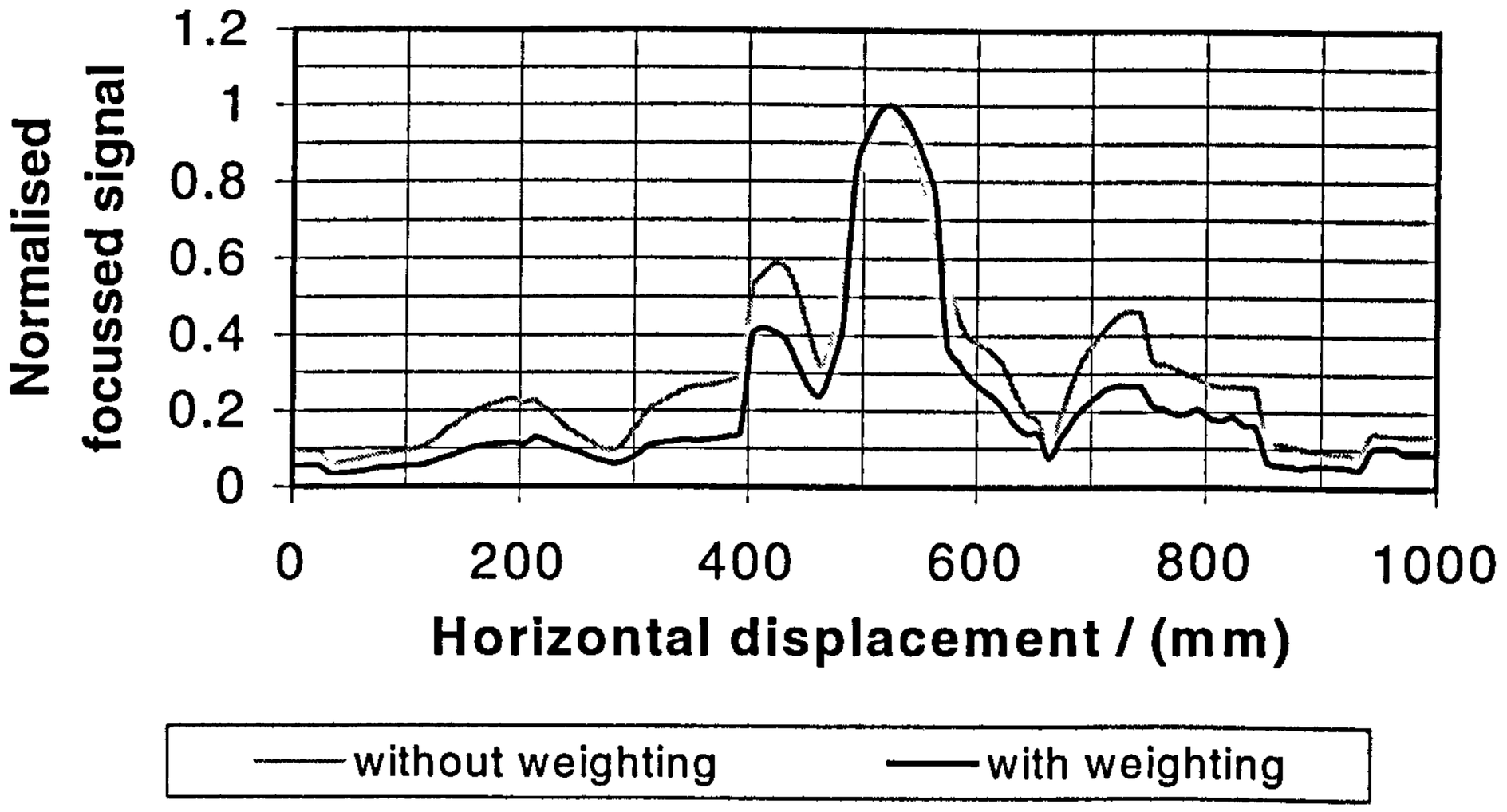

Figure 4.12 Lateral focusing at the target location.

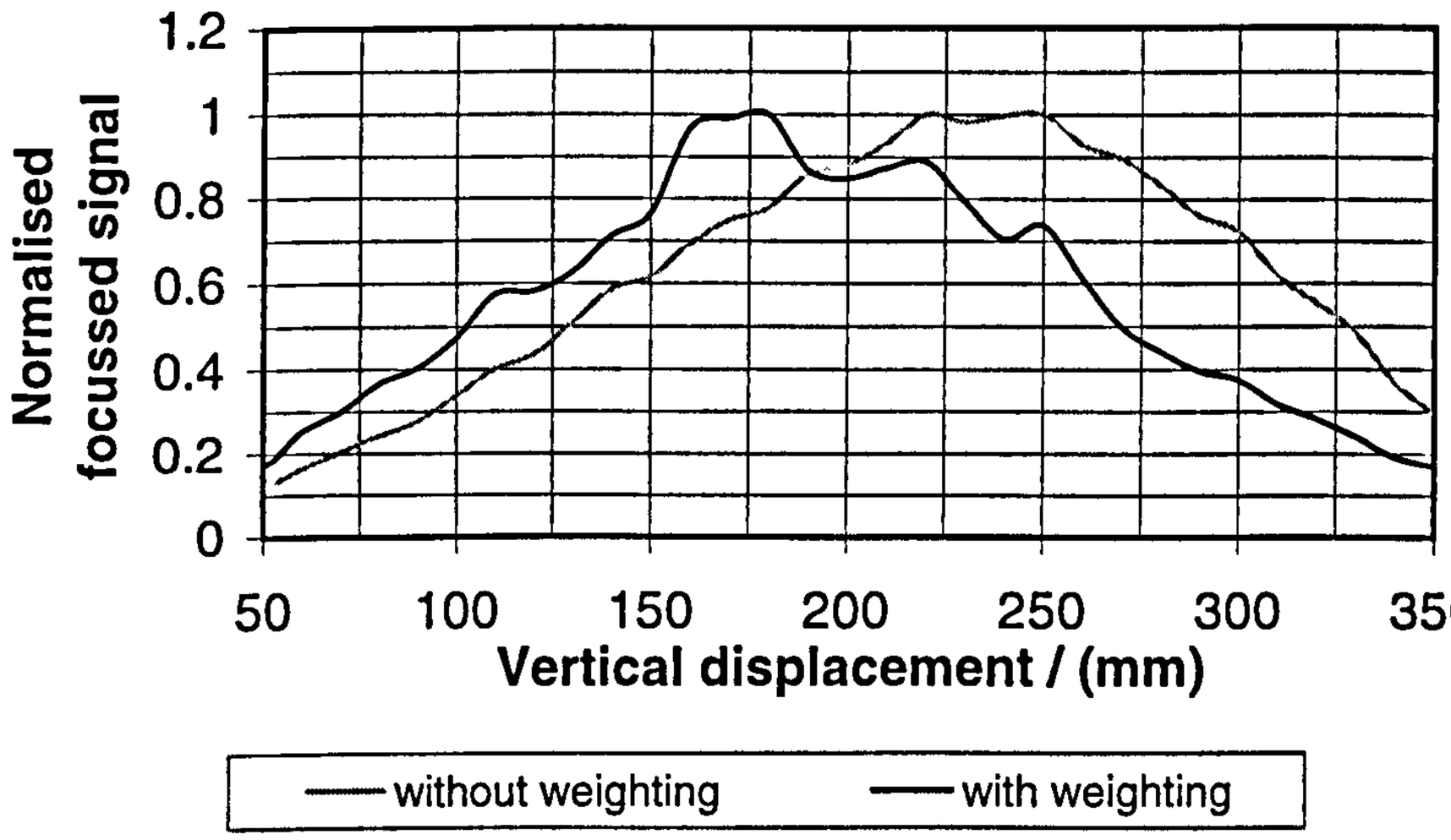

Figure 4.13 Vertical focusing at the target location

In practical clutter environments where the density of volume clutter is substantially uniform, the quantity of that clutter will be proportional to the *common-range common-view* volume and this will be a good estimation of the clutter returns [1]. Hence the clutter weighting can be performed based on this estimation.

Most subsurface radars discussed in chapter 2 operate with a transmitter-receiver pair and have little scope for clutter reduction processing. Some of these systems make use of general clutter reduction filters [2], which optimise the signals under known clutter and noise conditions [3], but design of these filters is difficult because of the complex nature of the clutter signals emerging from subsurface.

As discussed in chapter 2, further significant conditions that degrade the focusing scheme include macro scale ground features and stratified soil conditions. Due to these features the PRSF-GPR system is expected to have some effects on location of the target and the processing gain [4].

4.4. Analysis in De-Focusing Ground Conditions

The focusing process in a PRSF-GPR system depends on path delays from transmitter to receiver via resolution cells. Hence macro-scale surface features such as sloping, concave, convex ground will alter the path delays of assumed flat surface values. This

will result in misalignment of signals in the focusing process and lead to false target location and loss of processing gain.

Stratified media will also interfere with the detection of buried objects. Stratification has a more pronounced effect, as signals from wanted targets will be corrupted by signals reflecting at media interfaces. The FDTD technique is a very useful method in analysing such complex scenarios [5].

4.4.1. Non-Flat Ground

The PRSF-GPR FDTD model developed in section 4.3 was further used to analyse the system capabilities in non-flat ground conditions. A sloping air-soil interface with a slope of 10^0 was modelled, with a target located below the antenna array, as shown in figure 4.14, and the computed reflected signals were focused to investigate the target detection capabilities. The total reflected signals that included the surface clutter were used in this analysis. Figure 4.15 shows the focused signals in a 2D vertical slice for a soil dielectric constant of 8.

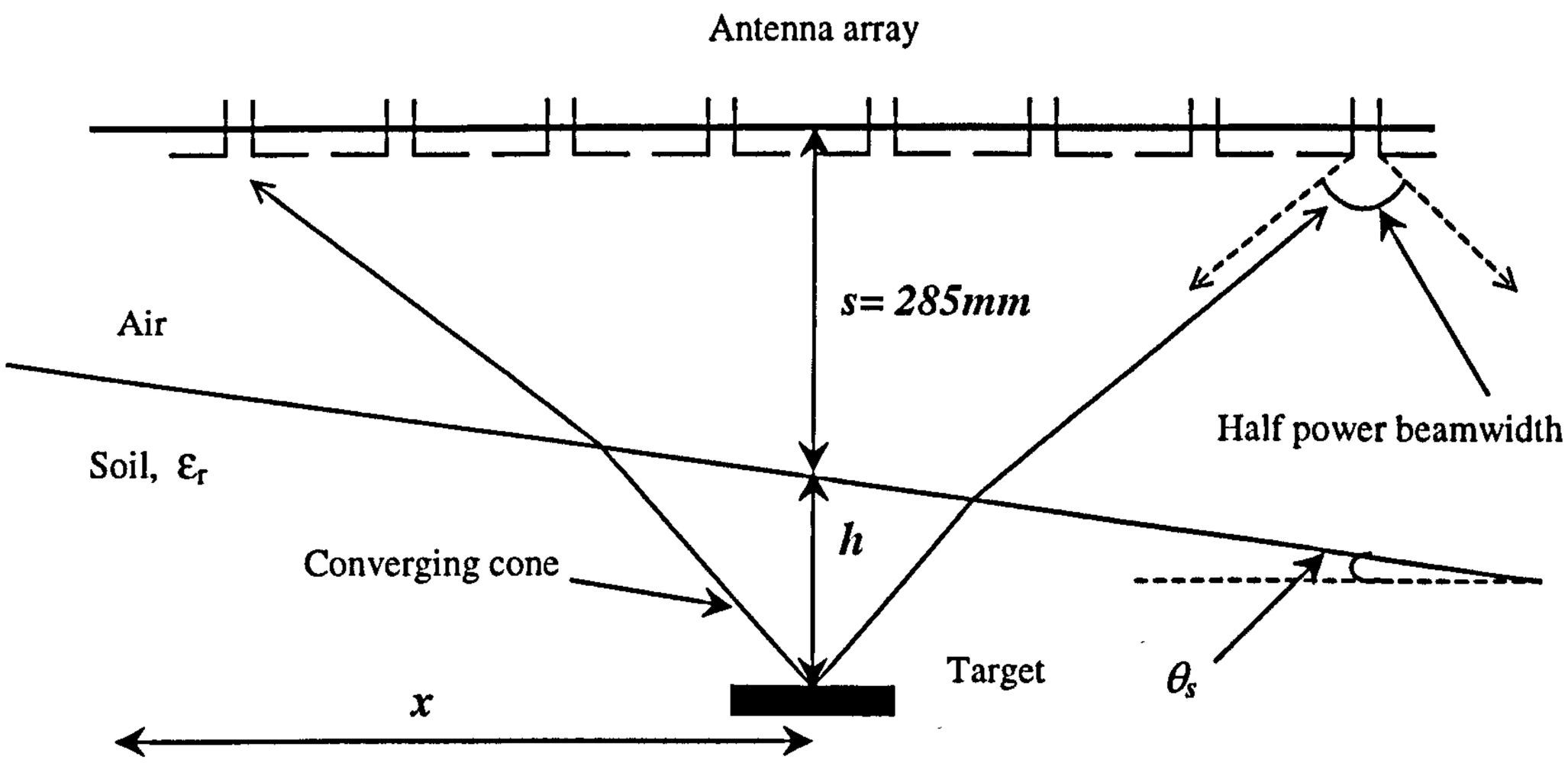

Figure 4.14 Sloping surface

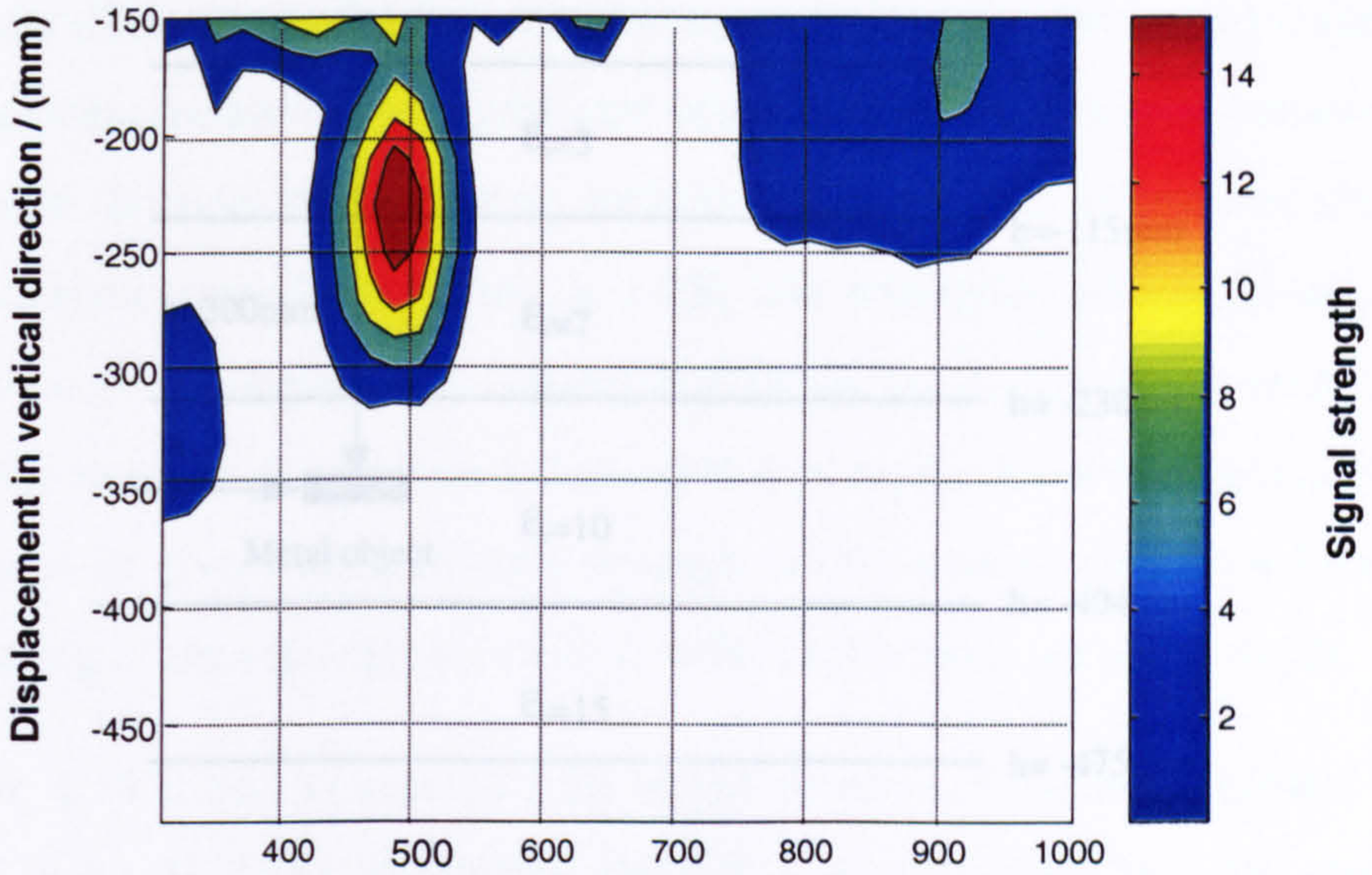

Figure 4.15 2D slice in non-flat ground

Figure 4.15 shows the target at x=490mm and h=225mm with lateral error of ≈25mm and vertical error of ≈10mm due to the defocusing mechanism. Further simulations were carried out with soil dielectric constant of 3 (dry soil) and 16 (wet soil). These analyses indicated,

- Target location is slightly offset by the slope with less dependence on the dielectric constant: This is expected as the converging cone (Figure 4.14) becomes narrower with high dielectric constants and hence not much significant variation in path lengths. For $\theta_s=10^0$,

  Lateral error ≈ 20-35mm

  Vertical error ≈ 5-10mm

- Reduction in processing gain is not very significant if the path length variations are minimal. For $\theta_s=10^0$, approximately 0.4 dB gain reduction was observed.

4.4.2. Stratified Soil Conditions

Stratified soil conditions have also been analysed using similar FDTD techniques. Signals reflected from a buried metallic target and the media interfaces (shown in figure 4.16) were used to investigate the effects of a realistic stratified media.

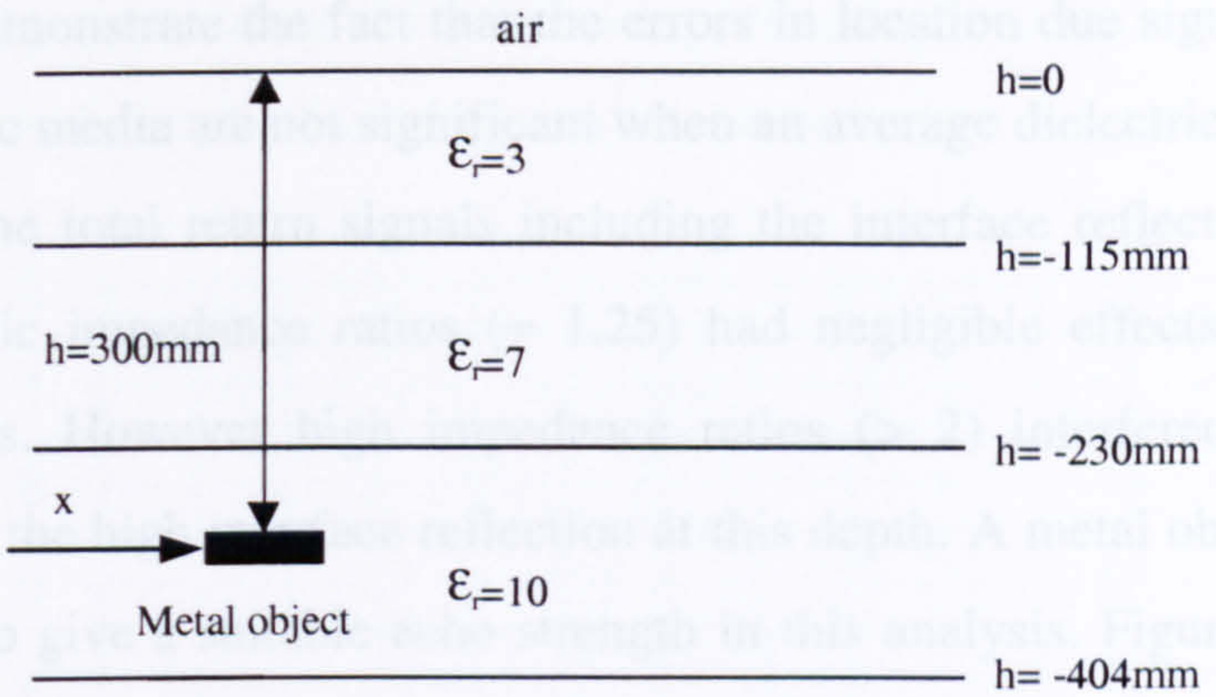

Figure 4.16 Stratified media model

Errors in location can be analysed with reflections from the metallic target that can be obtained by subtracting the signals from a similar model without the object. The detection process, as in the actual scenario, can be investigated with the total reflected signals (i.e., with all interface reflections). Figure 4.17 shows focusing with the subtracted signals and the target location at h=320mm and x= 515mm, just offset from its exact location of h=300mm and x=515mm. A dielectric constant of 5, which is the average of the first two media was used for focusing the signals. The error in target location is within the vertical resolution of the system. (130mm, i.e. 2λ at ε_r =5 and 2.1GHz)

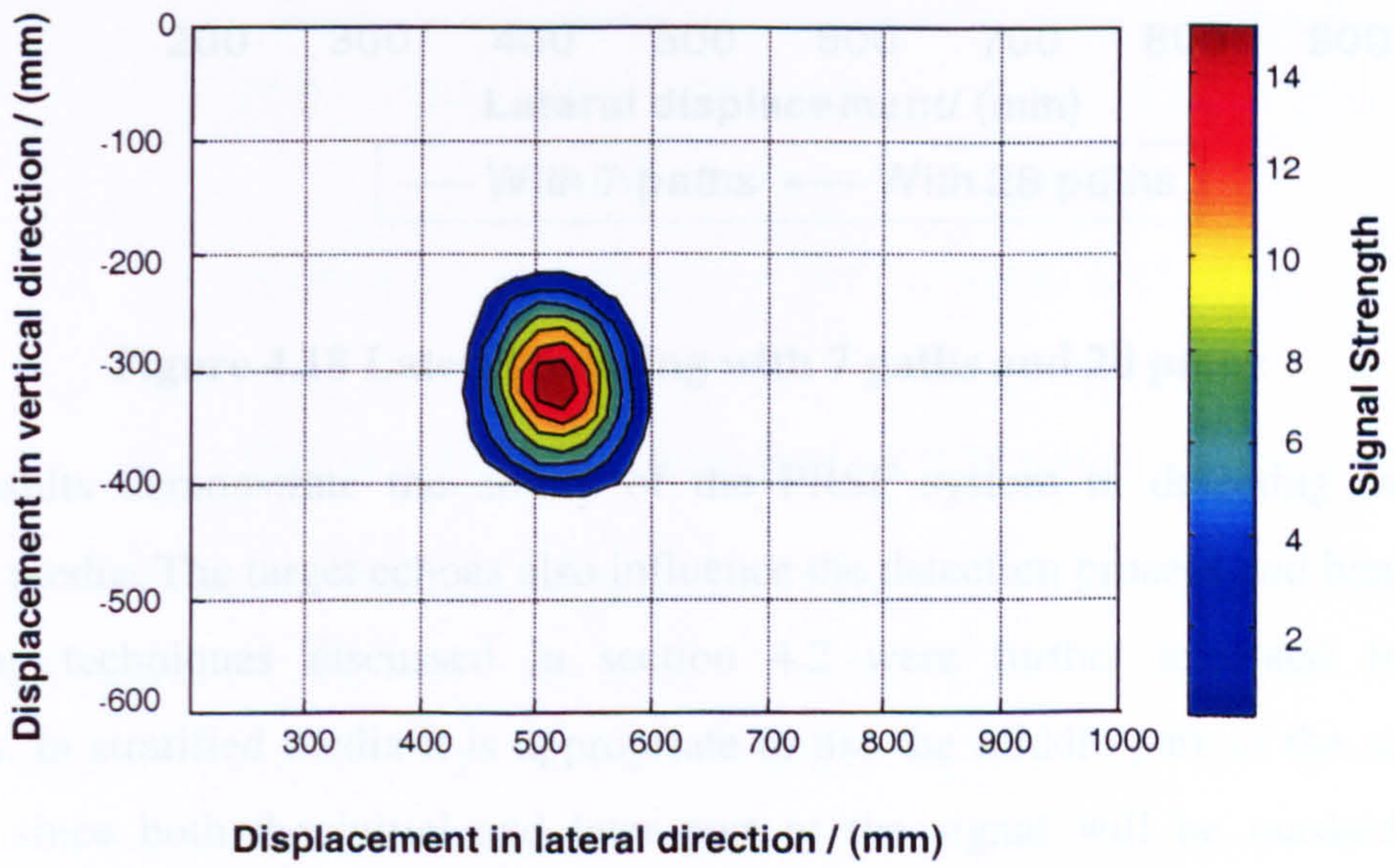

Figure 4.17 Focusing with the subtracted signals

These results demonstrate the fact that the errors in location due signal travel through various dielectric media are not significant when an average dielectric constant is used. Analysis with the total return signals including the interface reflections showed that low characteristic impedance ratios (≈ 1.25) had negligible effects in the synthetic focusing process. However high impedance ratios (> 2) interfered with the target detection due to the high interface reflection at this depth. A metal object of 50x50mm was employed to give a suitable echo strength in this analysis. Figure 4.18 shows the lateral focusing of the total signals (with interface reflections) at target depth.

From figure 4.18 it can be seen that the target detection is severely limited with less number of paths. However employing the full line array with 28 paths detected the target at its exact lateral location of 515mm. This is due to the fact that the reflections from the interfaces in the stratified media add non-coherently while the signals from the target add coherently.

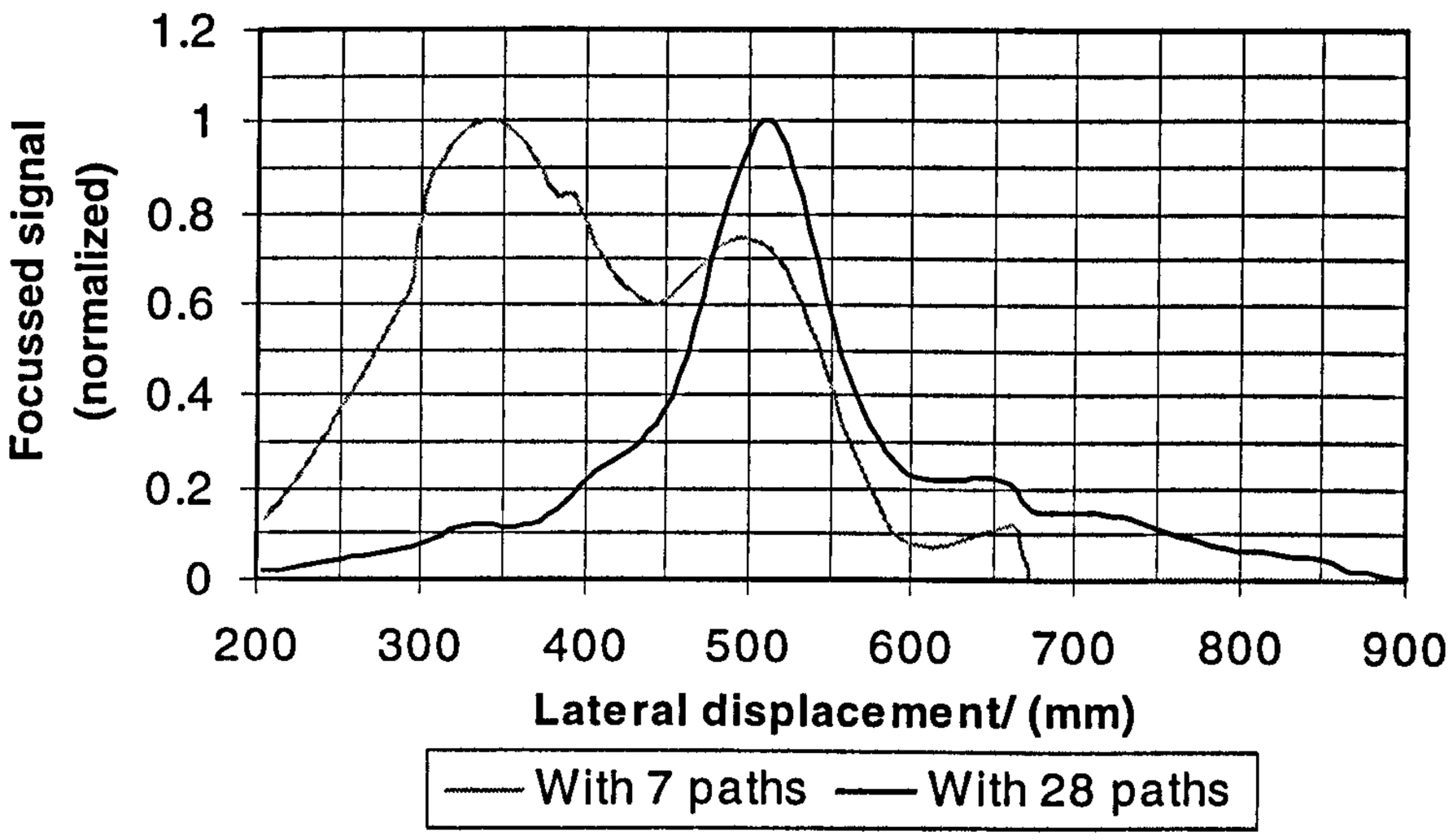

Figure 4.18 Lateral focusing with 7 paths and 28 paths

These results demonstrate the ability of the PRSF system in detecting targets in stratified media. The target echoes also influence the detection process and hence some processing techniques discussed in section 4.2 were further analysed for these scenarios. In stratified media it is appropriate to use the middle part of the signal for focusing since both the initial and later part of the signal will be masked by the interface reflections. Hence 1.25 cycles from the 4 cycles pulse was employed in this

analysis. Laterally focussed results with such processing technique for 7 paths and 28 paths are shown in figure 4.19 and figure 4.10 respectively.

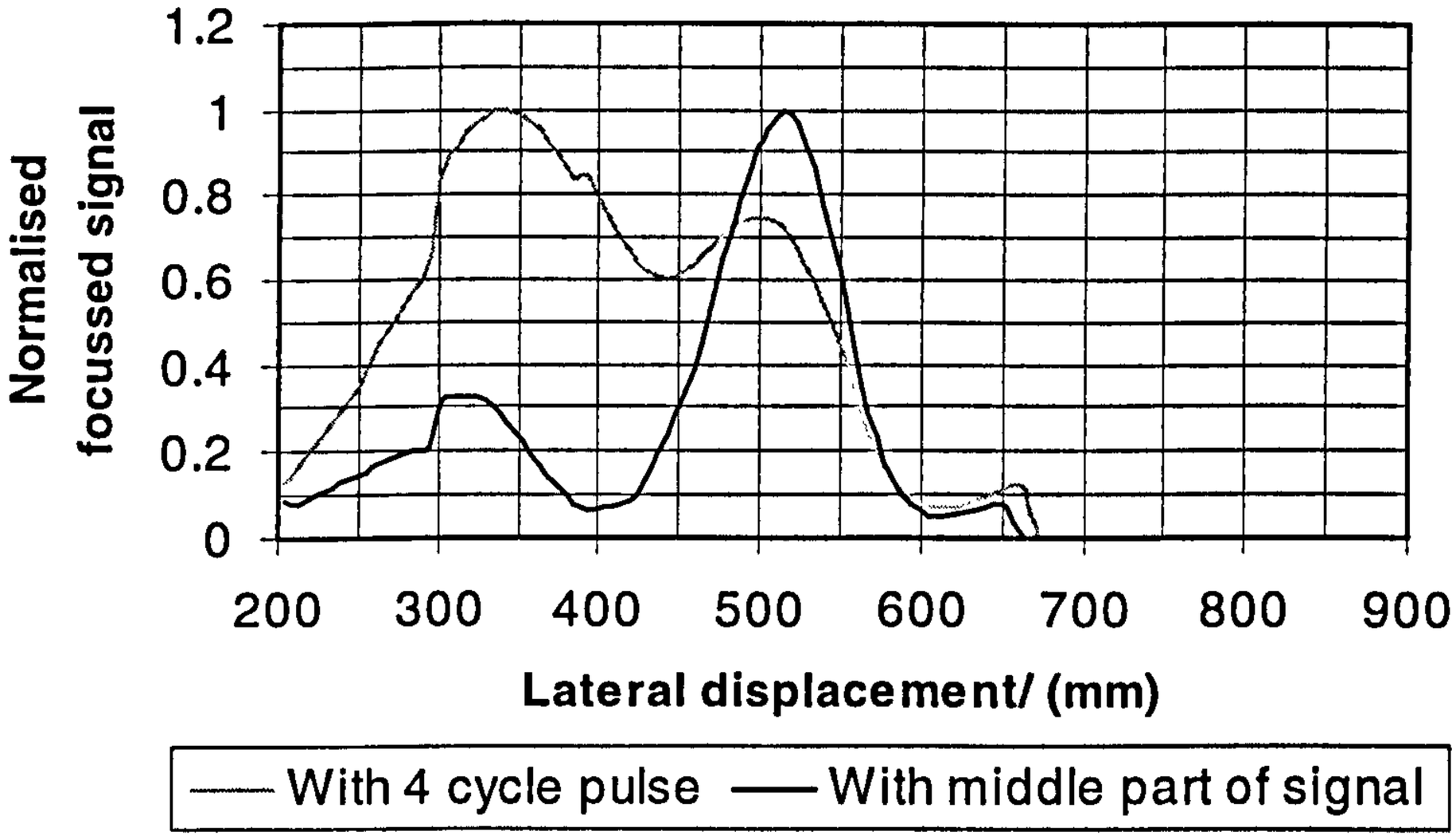

Figure 4.19 Target detection with 7 paths

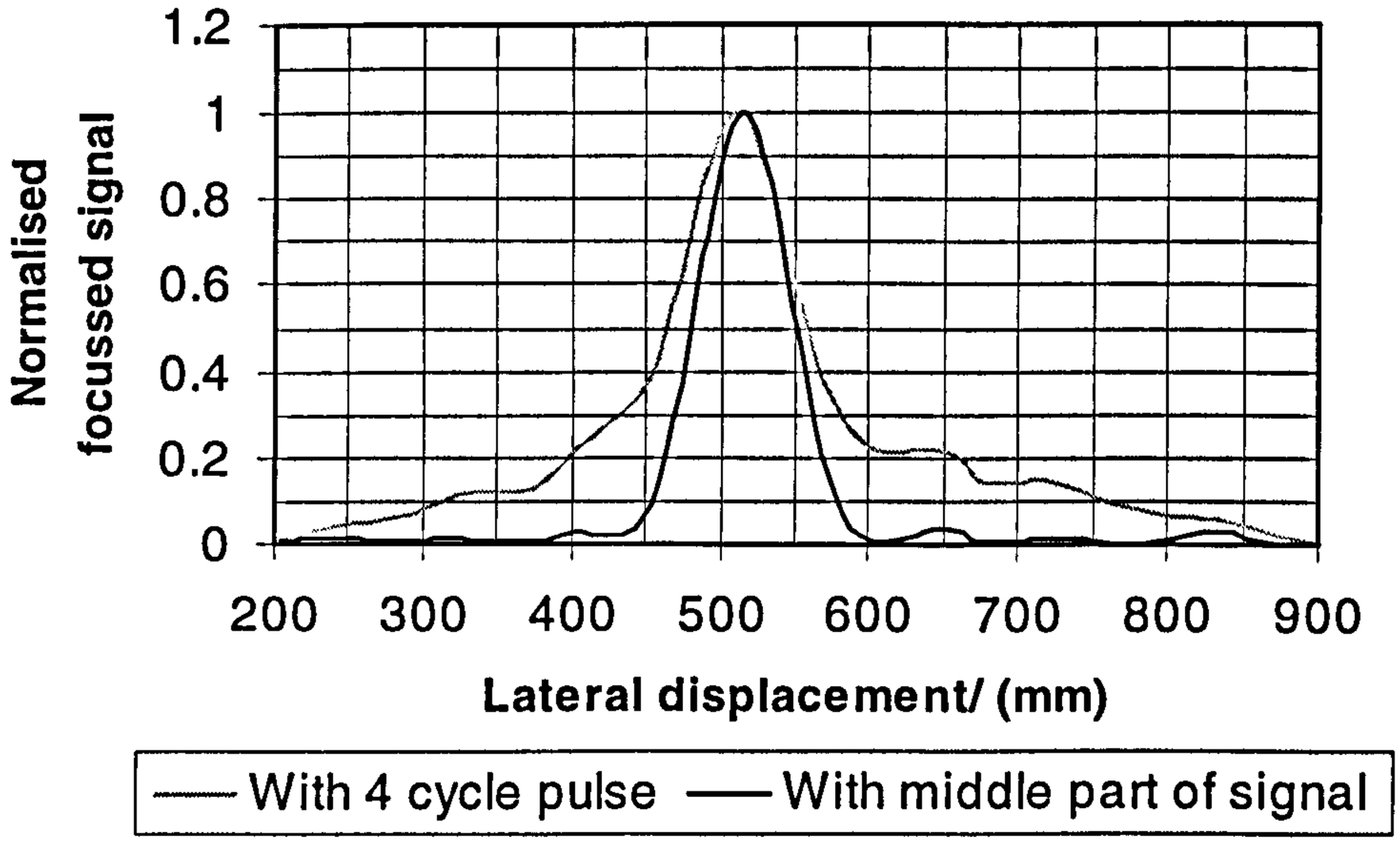

Figure 4.20 Target detection with 28 paths

Figure 4.19 demonstrates that by employing part of the signal, the target is identified at its exact location of 515mm with only 7 paths. Figure 4.20 indicates minor improvements with the full 28 paths as the synthetic focusing is sufficient to identify the target in this case. From figure 4.19 it is evident that the effects of interface reflections are minimised by employing part of the signal, hence this technique is useful in detecting targets which will be otherwise masked by non-coherent addition of

interface reflections. However detection of very low echo targets in media with high impedance ratios need further processing. For successful detection the interface reflections should be cancelled by subtracting it for each pair of antenna elements. The equivalent signal in the absence of any target can be derived by computation or by averaging from near-by equivalent paths. Furthermore analyses presented in this section considered the use of a four-cycle pulse, but in actual scenarios shorter pulses can be employed with wide band antennas which will further enhance detection in such difficult situations.

4.5. Summary

This chapter theoretically analysed the PRSF-GPR in some practical soil conditions. The signals required to investigate the system under these practical conditions have been calculated using FDTD method. The FDTD model developed in chapter 3 has been modified to incorporate various soil conditions. Analysis included detection in clutter environments (surface and volume), sloping-surface and stratified media. Investigation of the PRSF-GPR technique presented in this chapter indicated that this scheme on its own has a good detecting capability in clutter and stratified media. Analysis in volume clutter environment looked into the nature of clutter returns from pebble like objects and an analytical technique was employed to estimate these effects. The analytical estimations closely followed the FDTD numerical calculations. These estimates were further used to demonstrate a clutter reduction technique [1] in the detection process. Detection in sloping ground condition has been analysed with soil dielectric constants of 3,8 and 16 for a 10^0 sloping ground and showed that target detection is possible with a lateral error of ≈ 20-35mm and a vertical error of ≈5-10mm. Numerical investigations in stratified media indicated the system performs well with more number of paths employed. However detection in stratified media of high impedance ratios (>2) needs further processing such as background subtraction of signals without the target.

Furthermore, a processing technique that will enhance detection with longer pulses has also been suggested and tested with the calculated signals. This technique seems to

enhance detection closer to air-soil interface, which suffers from surface clutter, and in stratified media where interface reflections mask the wanted signals.

As a result of these analysis with FDTD simulations the system's capabilities have been demonstrated and some new suggestions were successfully tested. Analysis in clutter environment, detection near air-soil interfaces and detection in stratified soil conditions also stresses the need for a wide band antenna for the PRSF-GPR system. This chapter looked into various challenging soil conditions with a 8 element line array, but the full PRSF-GPR system will employ a planar array. Hence the system limitations in different soil types and practical system designs needs further considerations to accommodate the full planar array and will be considered in the next chapter.

References

[1] R.Benjamin, G.Hilton, S.Litobarski, E.McCutcheon and R.Nilavalan, Post-Detection Synthetic Near Field Focusing in Radar and Sonar, *Electronics Letters*, vol. 35, no. 8, pp. 664-666,1999.

[2] D.J.Daniels, D.J.Gunton and H.F.Scott, Introduction to Subsurface Radar, *IEE Proceedings*, vol. 135, pt. F, no. 4, pp. 278-320,1988

[3] N.Osumi and K.Ueno, Microwave Holographic Imaging Method with Improved Resolution, *IEEE Transactions on Antennas and Propagation*, vol. AP-32, no. 10, pp. 1018-1026, 1984.

[4] R.Benjamin, G.S.Hilton, R.Nilavalan, S.Litorbarsky and E.McCutcheon, Synthetically-Focussed Surface Penetrating Radar for Operation from a Moving Vehicle, *Proceedings of EUREL/IEE International Conference on the Detection of Abandoned Land Mines*, IEE, Edinburgh, pp. 60-63, 1998

[5] K.Demarest, R.Plumb, Z.Huang, FDTD Modelling of Scatterers in Stratified Media, *IEEE Transactions on Antennas and Propagation*, vol. AP-43, no.10, pp.1164-1168, 1995

5. Noise Limits of a PRSF-GPR System

5.1. Introduction

The thermal noise and clutter levels at the receiver limit the detection of the signal via a target. As the operating frequency is increased (and hence wavelength decreased), clutter and noise effects become more problematic. Since soil attenuation exponentially increases with depth [1] and signals from clutter also undergo attenuation, noise will also have significant effects on the operating range. Analysis in chapter 2 suggested that the PRSF-GPR system is less clutter limited compared to other conventional GPR systems and clutter estimation of the PRSF-GPR was considered in chapter 4. The clutter levels that will limit the system capabilities and operating range need a great deal of further analysis and it is outside the scope of this work.

The noise limited range (assuming zero clutter levels) that GPR can operate is primarily governed by the total path losses. The main factors that govern these path losses, are the soil attenuation loss, spreading loss (or path loss) and the target scattering losses. Thus the estimation of total power losses from a transmitter to receiver via a buried target is an important aspect for the estimation of the Maximum Detectable Depths (MDD).

Path losses vary with different kinds of soils. Since the major deciding factor of the path loss is the material attenuation loss, a survey of realistic soil parameters is critical in the process of loss estimation. The moisture content of the soil, operating frequency and their particle size mainly govern the soil's electrical properties, generally they exhibit an increasing attenuation with the moisture contents and frequency. An extensive survey of the soil's electrical properties have been done by *Ullaby et al* [2]

for remote sensing applications. Electrical properties of some soil types are given in section 5.3.

In the PRSF-GPR system, the processing gain and the operating frequency are two major factors in the detection process [3]. The processing gain mainly depends on the operating frequency, the array-soil spacing and number of elements. The array-soil separation will increase the processing gain since more elements can see the target but the spreading losses will also increase. On the other hand, a higher operating frequency gives finer resolution in the expense of extra material attenuation losses. Hence these inter linked parameters need careful consideration.

The total path losses associated with the PRSF-GPR can be calculated by FDTD simulations for a line array. However analytical techniques are more appropriate for the planar array and for analysis at deeper depths due to the size of FDTD model and the number of computer runs. Hence an analytical model is developed in this chapter. The analytical calculations were compared with FDTD simulations of a line array to verify the analysis and then used to investigate the system parameters. A survey of the dielectric properties of soil for a variety of conditions is also carried out to aid this analysis. Finally the maximum noise limited detectable depths for the PRSF-GPR are investigated for several soil conditions.

5.2. Power Losses Associated with the PRSF-GPR

The total losses associated with a GPR can be represented by [1],

- Cable losses
- Antenna Efficiency loss.
- Antenna mismatch loss.
- Transmission loss from air to soil and soil to air
- Antenna spreading loss.
- Attenuation loss of soil.
- Target scattering loss.

5.2.1. Cable Losses, L_c

Losses in the cables can be minimised by having the transmitter/receiver as close as possible to the antennas. Zero cable losses are assumed in following calculations.

5.2.2. Antenna Loss, L_e

Antenna losses are the power that is dissipated before radiation. These losses are high for antennas that are resistively loaded to improve bandwidth. However, generally antennas such as half wavelength dipoles can be designed with high efficiencies and hence losses are low.

E.g., (for both antennas)

$$L_e = 0.5 \text{ to } 1 \text{ dB} \tag{5.1}$$

5.2.3. Antenna Mismatch Loss, L_m

Antenna mismatch is the measure of how well the antenna is matched to the transmitter via the feed. Usually little power is lost for well-matched antennas and it is in the order of 1dB for both antennas.

5.2.4. Transmission Coupling loss, L_{t1} (air-soil) and L_{t2} (soil-air)

When electromagnetic energy is transmitted into soil, part of the energy is reflected and a part of it is transmitted into the soil. For the air-soil interface, where the angle of incidence is not normal, the losses on the forward path are given by [4],

$$L_{t1} = 10.\log_{10}\left(\left|1-\rho_1{}^2\right|\right) \text{dB} \tag{5.2}$$

where,

$$\rho_1 = \frac{k_1 \cos\theta_1 - \sqrt{1 - j\tan\delta}\sqrt{1 - k_1{}^2 \sin^2\theta_1}}{k_1 \cos\theta_1 + \sqrt{1 - j\tan\delta}\sqrt{1 - k_1{}^2 \sin^2\theta_1}} \tag{5.3}$$

$$k_1 = \sqrt{\frac{1}{\varepsilon_{soil}}} \tag{5.4}$$

θ_1 : Angle of incidence in air.

ε_{soil} : Dielectric constant of soil

$\tan\delta$: Loss tangent of soil.

On the return path the signal looses power at the soil-air interface. The loss at this interface is given by [4],

$$L_{t2} = 10.\log_{10}\left(\left|1-\rho_2{}^2\right|\right) \text{dB} \tag{5.5}$$

where,

$$\rho_2 = \frac{k_2\sqrt{1-j\tan\delta}\cos\theta_2 - \sqrt{1-k_2{}^2\sin^2\theta_2}}{k_2\sqrt{1-j\tan\delta}\cos\theta_2 + \sqrt{1-k_2{}^2\sin^2\theta_2}} \tag{5.6}$$

$$k_2 = \sqrt{\varepsilon_{soil}} \tag{5.7}$$

θ_2 : Angle of incidence in soil for the return path.

5.2.5. Spreading Loss, L_s

The spreading losses of an antenna element are related to its radiation pattern. In smooth surface conditions a radiator's spreading losses in the forward path can be given by (refer figure 5.1),

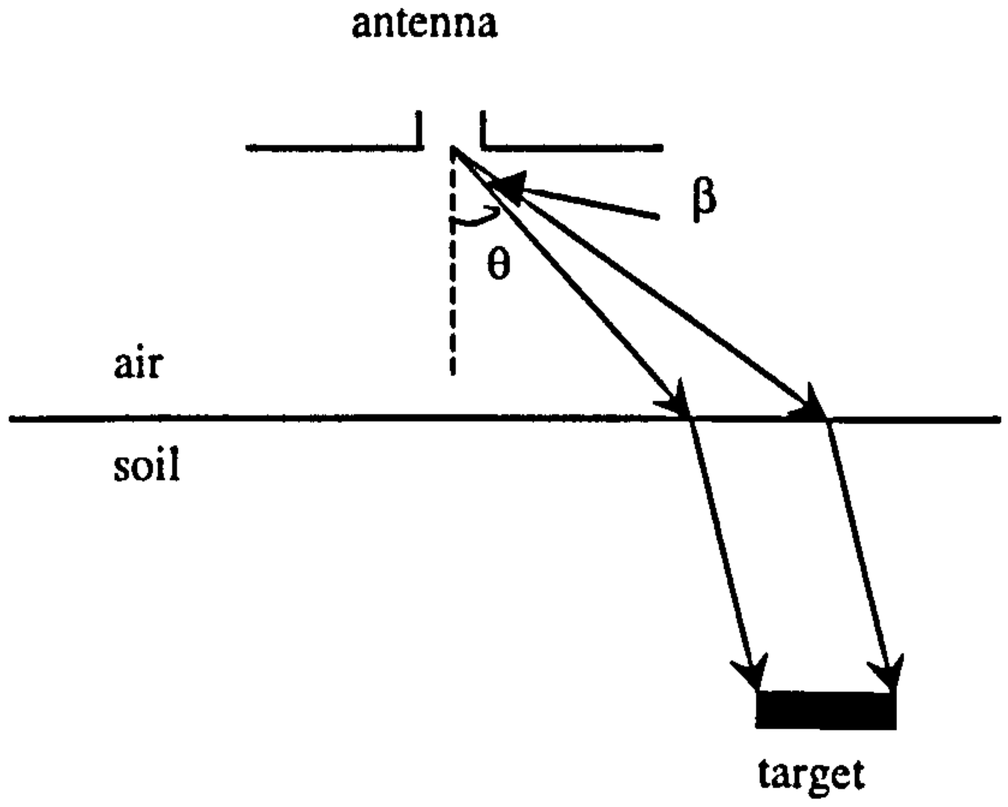

Figure 5.1 Spreading path for transmitted signal

$$L_{s(trans-target)} = 10.\log_{10}\left(\frac{G_{(\theta)}.\beta}{(4\pi)}\right) \text{dB} \tag{5.8}$$

where,

θ : Look angle.

$G_{(\theta)}$: Gain of transmitting antenna (for the specific look angle).

β : Solid angle in air, which after refraction, reaches the target.

The scattered signal power will be collected by the array elements that have the target in their half power beamwidths (for the co-polar patterns) as shown in figure 5.2. Considering the solid angle which will reach the array after refraction,

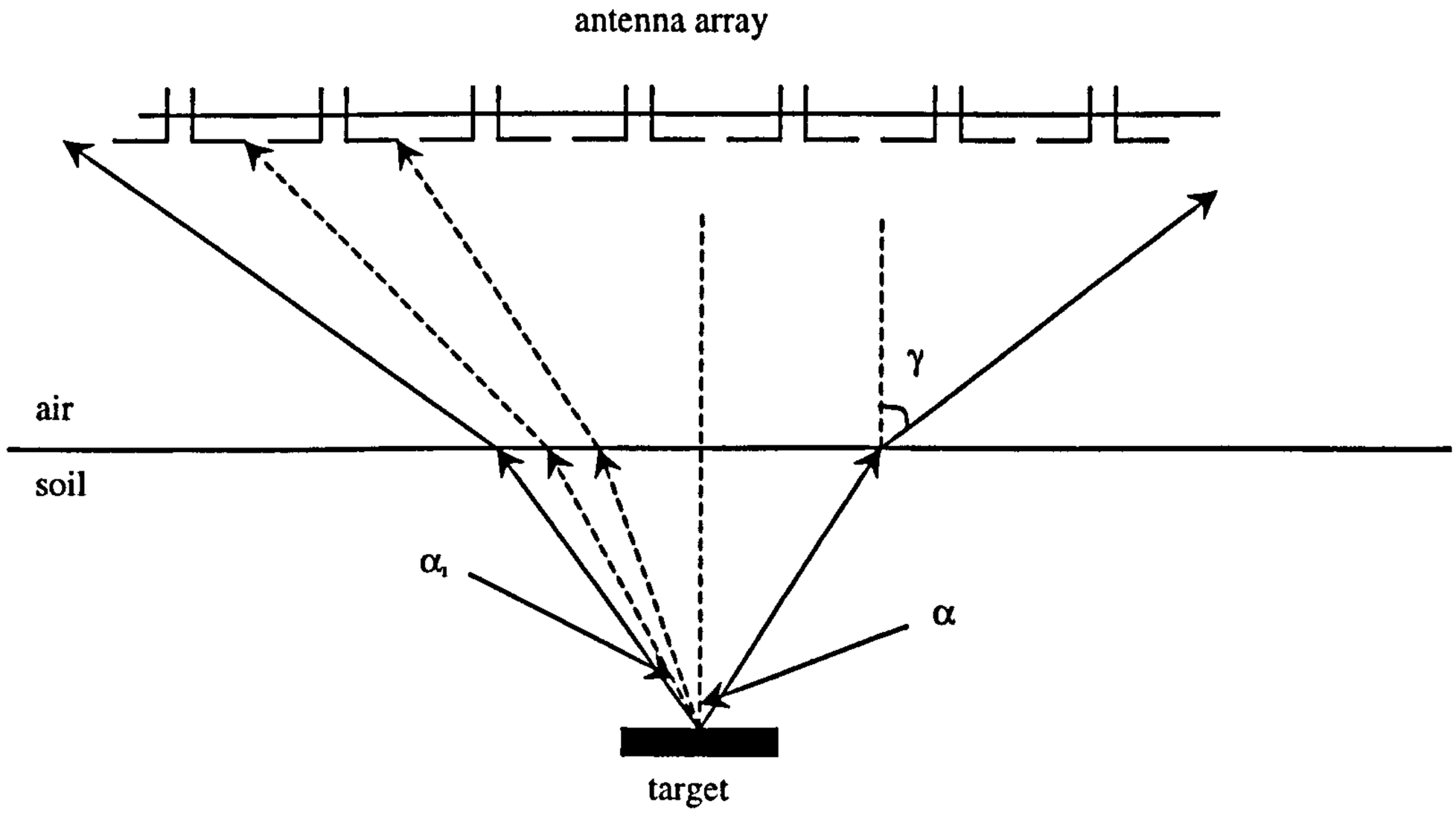

Figure 5.2 Spreading path for received signal

Solid angle in soil, which after refraction reaches the array which sees the target

$$= \alpha \quad (5.9)$$

total spreading for elements which see the target

$$= \frac{\alpha}{4\pi} \quad (5.10)$$

hence for the planar array,

$$L_{s-array(target-receiver)} = 10.\log\left[\frac{\alpha}{4\pi}\right] \text{ dB} \quad (5.11)$$

For "element i" in the line array,

Solid angle in soil, which after refraction reaches area A_i $= \alpha_i$

$$\text{Power density at the receiving element} = \frac{\alpha_i}{4\pi} \times \frac{1}{A_i} \quad (5.12)$$

$$L_{s-element,i(target-receiver)} = 10.\log\left[\frac{\alpha_i}{4\pi}\frac{A_{eff}}{A_i}\right] \quad (5.13)$$

where,

A_{eff} :Effective apperture area of element i $= \frac{4\pi G(\theta)}{\lambda^2}$ (5.14)

A_i :Physical area for element i = (inter element spacing)^2 (5.15)

γ : Antenna coplanar half power beam

λ : Wavelength in freespace

5.2.6. Target Scattering Loss, L_{sc}

When a radar illuminates a target, part of the energy is back scattered (or reflected back). This power is calculated in terms of Radar Cross Section (RCS). Since there is substantial variation of the reflected power about the target for any given illumination angle, an equivalent hypothetical target, which re-radiates isotropically, is used as the basis for this estimation. The equivalence is that the isotropic target be sized so that the power density back scattered is the same as that for the actual target [5]. Since most subsurface objects are non-metallic, the RCS depends on the dielectric properties of the soil.

Assuming a plane wave is incident on interface [1], the loss is given by,

$$L_{sc}=20\log\left(\frac{Z_1-Z_2}{Z_1+Z_2}\right)+10\log\frac{\sigma_{rcs}}{A} \qquad (5.16)$$

where,

Z_1 : Characteristic Impedance of the first layer of the material.

Z_2 : Characteristic Impedance of the second layer of material.

σ_{rcs} : Target radar cross section (as a proportion of intersection of both antenna beamwidths)

A : Target cross sectional area.

However for small targets, the back scattered signal strength depends on the physical dimensions and the dielectric properties of soil and the target. For metallic targets, RCS should be estimated considering the wavelength in the medium.

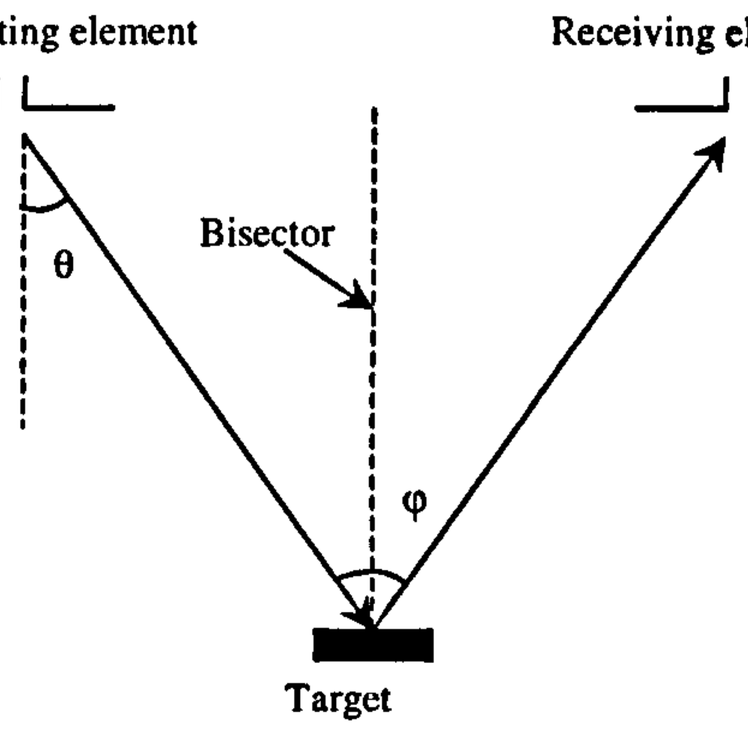

Figure 5.3 Bi-static RCS

Most GPRs operate in bi-static mode. The bi-static RCS can be estimated from the mono-static estimations for small bi-static angles ($\approx 10^0$). For simple targets such as spheres, this approximation can extend up to large angles ($\approx 100^0$) [6,7]. Assuming scattering beam width and the scattering efficiencies are independent of the look angles, the bi-static RCS can be approximated by the mono-static RCS measured on the bisector of the bi-static angle as shown in figure 5.3. Furthermore, Kell [7] showed that the bi-static RCS is very closely approximated by this estimation, when the mono-static RCS are measured at a frequency lower than the true frequency by the factor $\cos(\varphi/2)$, where, φ is the bi-static angle.

5.2.7. RCS of Some Simple Targets

RCS estimations can been performed using several techniques, for instance Geometrical Optics (GO), Physical Optics (PO), Geometrical theory of Diffraction, Method of moments and FDTD [8,5]. Some simple analytical estimations derived from GO theory is given below [5].

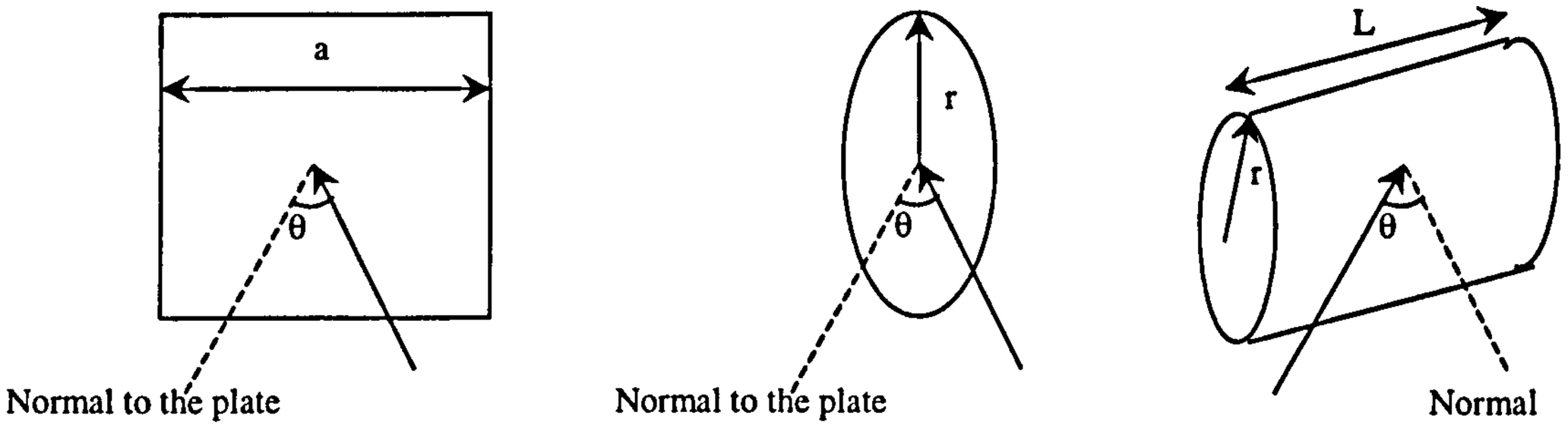

Figure 5.4 Basic shapes

5.2.7.1. For Square Flat Plate,

$$\sigma_{rcs} = \frac{4\pi a^4}{\lambda^2}\left[\frac{\sin\left(\frac{4\pi a \sin\theta}{\lambda}\right)}{\frac{4\pi a \sin\theta}{\lambda}}\right]^2 \cos^2\theta \qquad (5.17)$$

where,

a : Edge size

θ : Look angle

The RCS of flat plates have also been calculated using the geometrical theory of diffraction [9]. It was shown that this estimation provided a more accurate estimation compared to the GO or PO theory. The estimated RCS is given by,

$$\sigma_{rcs} = \frac{b^2}{\pi}\left|\left[\cos(ka\sin\theta)\frac{i\sin(ka\sin\theta)}{\sin\theta}\right] - \frac{e^{ika-i(\pi/4)}}{\sqrt{2\pi}(ka)^{3/2}} f_1 f_2\right|^2 \tag{5.18}$$

where

$$f_1 = \left[\frac{1}{\cos\theta} + \frac{e^{ika-i(\pi/4)}}{4\sqrt{2\pi}(ka)^{3/2}}\left(\frac{(1+\sin\theta)e^{-ika\sin\theta}}{(1-\sin\theta)^2} + \frac{(1-\sin\theta)e^{ika\sin\theta}}{(1+\sin\theta)^2}\right)\right] \tag{5.19}$$

$$f_2 = \left[1 - \frac{e^{i2ka-i(\pi/2)}}{8\pi(ka)^3}\right]^{-1} \tag{5.20}$$

a, b : Edge sizes

This estimation considers the multiple scattering from the edges of the metal plate. For smaller objects of approximately a wavelength size, the roundtrip travel of the signals is critical and the RCS falls in to the resonance region. Hence equation 5.18 is a better approximation compared to equation 5.17.

5.2.7.2. For Flat Disk

$$\sigma_{rcs} = \frac{16\pi r^4}{\lambda^2}\left[\frac{J_1\left(\frac{4\pi r\sin\theta}{\lambda}\right)}{\frac{4\pi r\sin\theta}{\lambda}}\right]^2 \cos^2\theta \tag{5.21}$$

where,

r : radius of the disk

5.2.7.3. For Circular Cylinder,

$$\sigma_{rcs} = \frac{2\pi r L^2}{\lambda}\left[\frac{\sin\left(\frac{2\pi L\sin\theta}{\lambda}\right)}{\frac{2\pi L\sin\theta}{\lambda}}\right]^2 \cos^2\theta \tag{5.22}$$

where,

L : length of the cylinder

The RCS estimations of flat plates (Equations 5.18) was employed for signal power comparisons in section 5.4

5.2.8. Material Attenuation Loss, La

Attenuation loss in soil is the dominant loss in practical conditions and it is a major factor in the choice of frequency. Attenuation can be due to conductive losses and dipolar losses (ac losses). These dipolar losses are due to a complex phenomenon known as the relaxation loss that depend on several factors, such as the water content and frequency of operation. These properties will be discussed in section 5.3.

A target echo undergoes two-way path attenuation in soil. The total soil attenuation losses are given by [1],

$$L_a = 8.686 R.2.\pi.f.\sqrt{\frac{\mu_o \mu_r \varepsilon_o \varepsilon_r \left(\sqrt{(1+\tan^2\delta)}-1\right)}{2}}\ \text{dB} \qquad (5.23)$$

where,

f : frequency in Hz.

$tan\ \delta$: loss tangent of soil

ε_r : relative permitivity of soil.

ε_o : absolute permitivity of free space.

μ_r : relative permeability of soil.

μ_o : absolute permeability of free space.

R : total path length in soil

$$\tan\delta = \frac{\varepsilon_e^{"}}{\varepsilon_o \varepsilon_r} \qquad (5.24)$$

$$\varepsilon_e^{"} = \varepsilon^{"} + \frac{\sigma}{\omega} \qquad (5.25)$$

$$\tan\delta = \frac{\sigma}{\omega \varepsilon_o \varepsilon_r} + \frac{\varepsilon^{"}}{\varepsilon_o \varepsilon_r} \qquad (5.26)$$

where,

σ : conductivity of the soil

ω : Angular velocity in rad/s

$\varepsilon^{"}$: Complex permitivity of soil

$\frac{\varepsilon^{"}}{\varepsilon_o \varepsilon_r}$: Dipolar losses

Equation 5.23 to 5.26 shows that the material losses are mostly governed by the dielectric properties of soil. At low frequencies the conductivity is significant but at higher frequencies the dipolar losses become significant.

5.3. Dielectric Properties of Soil

The dielectric properties of soil depend on the frequency, water content, particle size, temperature and salinity. In general, a soil medium is electrically a four-component dielectric mixture consisting of air, bulk soil, bound water and free water. Bound water refers to the water molecules held together by the soil particles and the free water is the water molecules that move with ease in the soil [2]. The amount of water contained in bound water and the free water depends on the total surface area of the solid soil particles. These solid soil particles are generally classified as sand, silt and clay according to size [2]. This is demonstrated in table 5.1 with figure 5.5 showing the textural classes of soils. For example, soil with 40%-60% silt, 0-20% sand and 40%-60% clay can be termed as silty clay

Particle Diameter (mm)	Soil type
0.000 - 0.002	Clay
0.002 - 0.020	Silt
0.020 - 0.200	Fine Sand
0.200 - 2.000	Coarse Sand

Table 5.1. Particle size classes (*from [2]*)

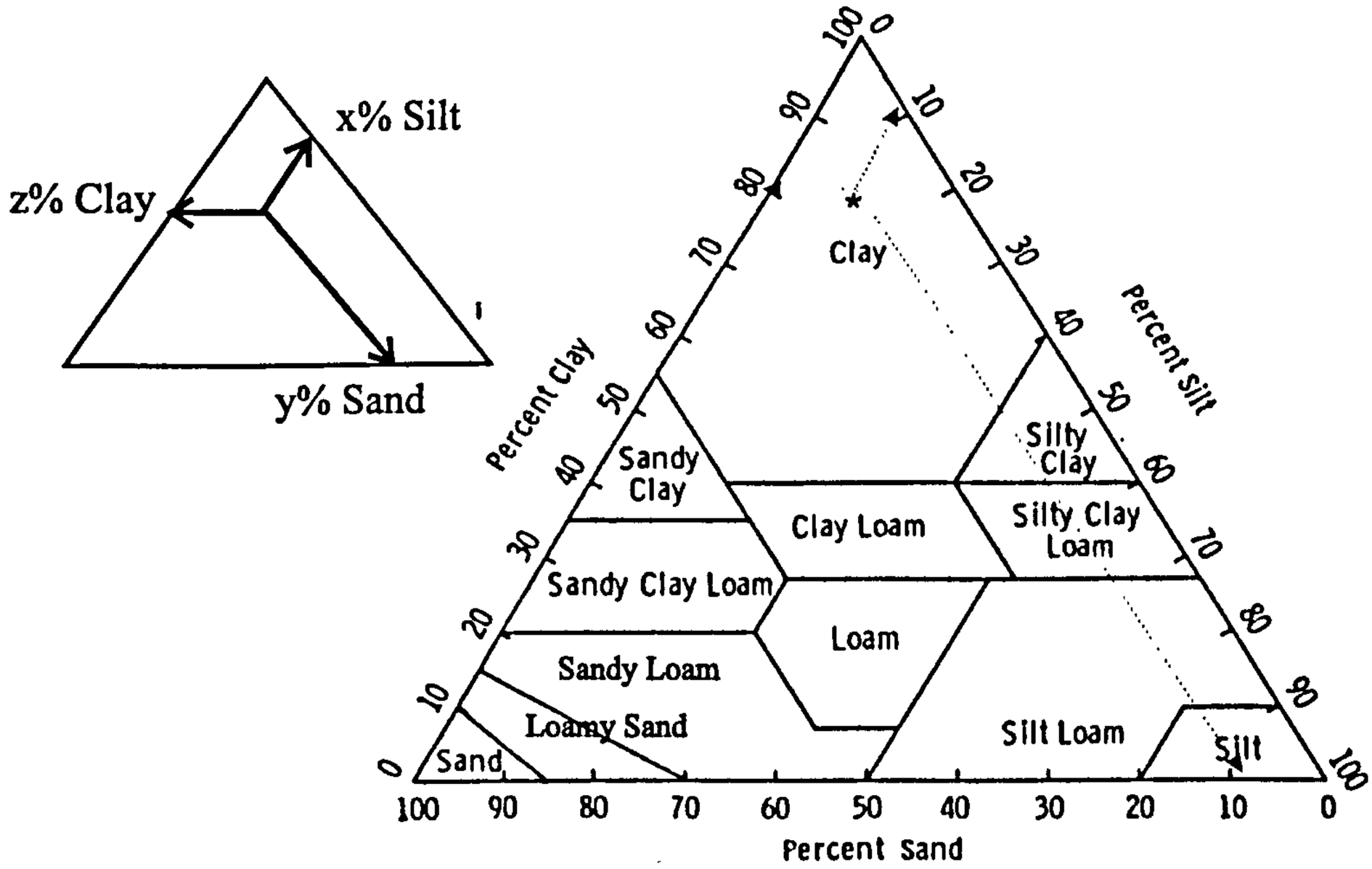

Figure 5.5 Soil textural classes (*from [2]*)

The dielectric constant of dry soil varies over the range between 2 and 4. And this is essentially independent of the frequency and temperature [2]. But wet soils exhibit dependence on frequency and temperature.

5.3.1. Moisture Dependence.

Generally the moisture content in soil is expressed in volumetric or gravimetric (by weight) scales. The volumetric moisture content is preferred much because the dielectric constant of the soil-water mixture is a function of the water volume-fraction in the mixture [2]. The moisture contents will affect the conductivity as well as the relaxation properties of the soil. Since bound water and the free water have different relaxation behaviours, textural compositions of soils also affect the dielectric losses.

5.3.2. Frequency Dependence

In an ideal situation, the dielectric properties of soil will remain constant at high and low frequencies, but it has a transition where the dielectric properties change quite significantly over a frequency range [10]. This region is known as the relaxation region. The relaxation phenomenon is due to the disturbance of the polar molecules by the impressed electric field such as the radar signals. The rotation of the individual

molecules due to the applied alternating field will be opposed by the thermodynamic forces and relaxation takes place at some specific frequencies. Since thermodynamic effects are involved, the losses depend on the temperature. Dielectric losses increase quit significantly in this region. This phenomenon can occur in the microwave band under wet soil conditions, causing significant losses. The relaxation frequency varies depending on the type of material. For example, water has a high relaxation frequency where as ice has a low relaxation frequency.

The dependence of soil properties on moisture content and frequency for some standard soil types are given in table 5.2. [2],

Soil Type	Volumetric Moisture	ε'_{soil}		ε''_{soil}	
		1.4GHz	5.0GHz	1.4GHz	5.0GHz
Sandy Loam (Sand 51.5%,Silt-35.0%, Clay 13.5%)	0.1	6	6	1	1
	0.3	17	18	3	3
	0.5	48	30	5	7.5
Loam (Sand 42.0%, Silt-49.5%, Clay 8.5%)	0.1	5.5	5.5	1	1
	0.3	17.5	16.5	3.2	3
	0.5	41	29	5.4	7.5
Silt Loam (Sand 30.6%, Silt-55.9% Clay 13.5%)	0.1	5	5	1	1
	0.3	16	16	3.4	3.0
	0.5	37.5	29	6	7.5
Silty Clay (Sand 5.0%, Silt-47.5%, Clay 47.5%)	0.1	4	3	1	0
	0.3	18	18	4	3
	0.5	31	27.5	9	7

Table 5.2 Dielectric properties of some standard soil types [2]

These values can be used to analyse the maximum noise limited penetrable depths of the PRSF-GPR under practical soil conditions.

Having formulated the various losses associated with the PRSF-GPR system it is appropriate to compare this analysis with more accurate theoretical predictions. Although comparisons with measurements are much more realistic, it is only possible for a limited soil conditions.

5.4. Comparisons with FDTD

The results calculated from the GPR model presented in section 3.3.2 were further used to calculate the power losses for each path involved in the system. The power loss can be calculated by comparing the power of transmitted and received signals at the required frequency. These losses are compared with the analytical predictions. Equations 5.1 to 5.23 shows that the losses associated with the system are more complex and involve various parameters. Hence it is appropriate to analyse these losses first in free space and then extend the analysis to more complex subsurface problems.

5.4.1. Object in Free Space

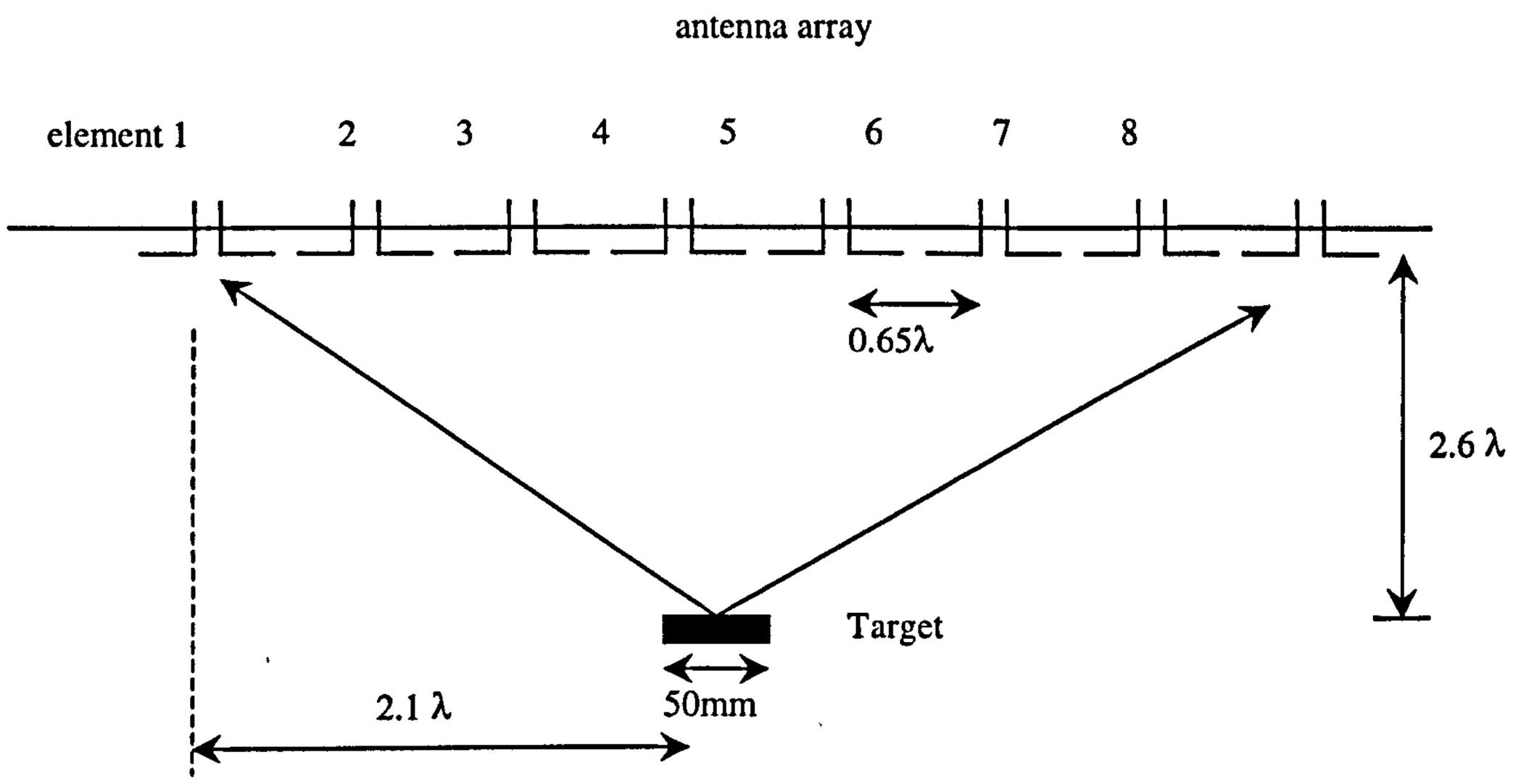

Figure 5.6 Metal plate in free space

FDTD calculations were performed in free space conditions with the same antenna array used in the GPR model for a metal plate of 50x50 mm as shown in figure 5.6.

The calculations were performed at 2.1GHz. The FDTD power estimations were performed by comparing the transmitted and received signal power. A fast Fourier transform was performed on the time domain signals and the total path loss was computed at 2.1GHz as shown below,

$$\text{The total path loss} = \frac{P_{received}}{P_{transmitted}} \tag{5.27}$$

The power losses for each path were estimated by calculating antenna losses: L_e, antenna mismatch losses: L_m, spreading losses: $L_{s(transmitter\text{-}target)}$ & $L_{s\text{-}element(target\text{-}receiver)}$ and target scattering loss: L_{sc}. A sample calculation when element 1 transmitting and element 6 receiving is given below,

Target offset from array = 332 mm

Target lateral displacement from the 1st element = 310 mm

Frequency of operation = 2.1GHz

Antenna gain (assuming 70^o and 100^o half power beamwidths in the principal planes) = 8.82 dB

Target size: square plate = $0.053 \times 0.053\ m^2$

Antenna efficiency L_e = 0 dB

Antenna mismatch L_m (for both antennas) = -0.5 dB

Spreading loss for forward path $L_{s(transmitter\text{-}target)}$ = 1.955 dB

Spreading loss for return path $L_{s\text{-}element(target\text{-}receiver)}$ = -22.2063 dB

Target scattering loss L_{sc} = -23.4878 dB

Total loss L = -44.2391 dB

The analytical predictions of power losses associated with each path are compared with the FDTD calculations in figure 5.7 and figure 5.8.

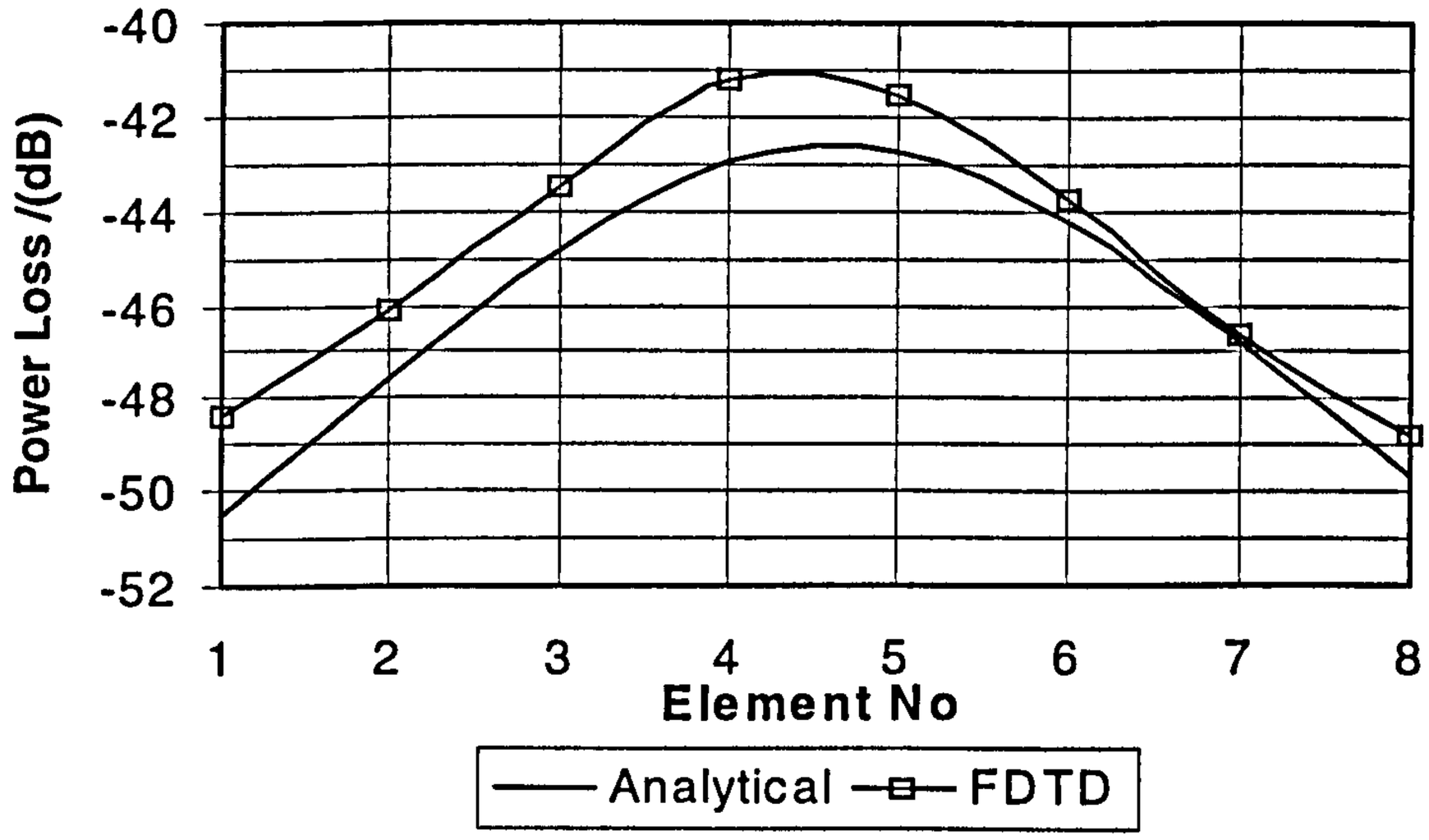

Figure 5.7 Power losses associated with each path when element 1 is transmitting

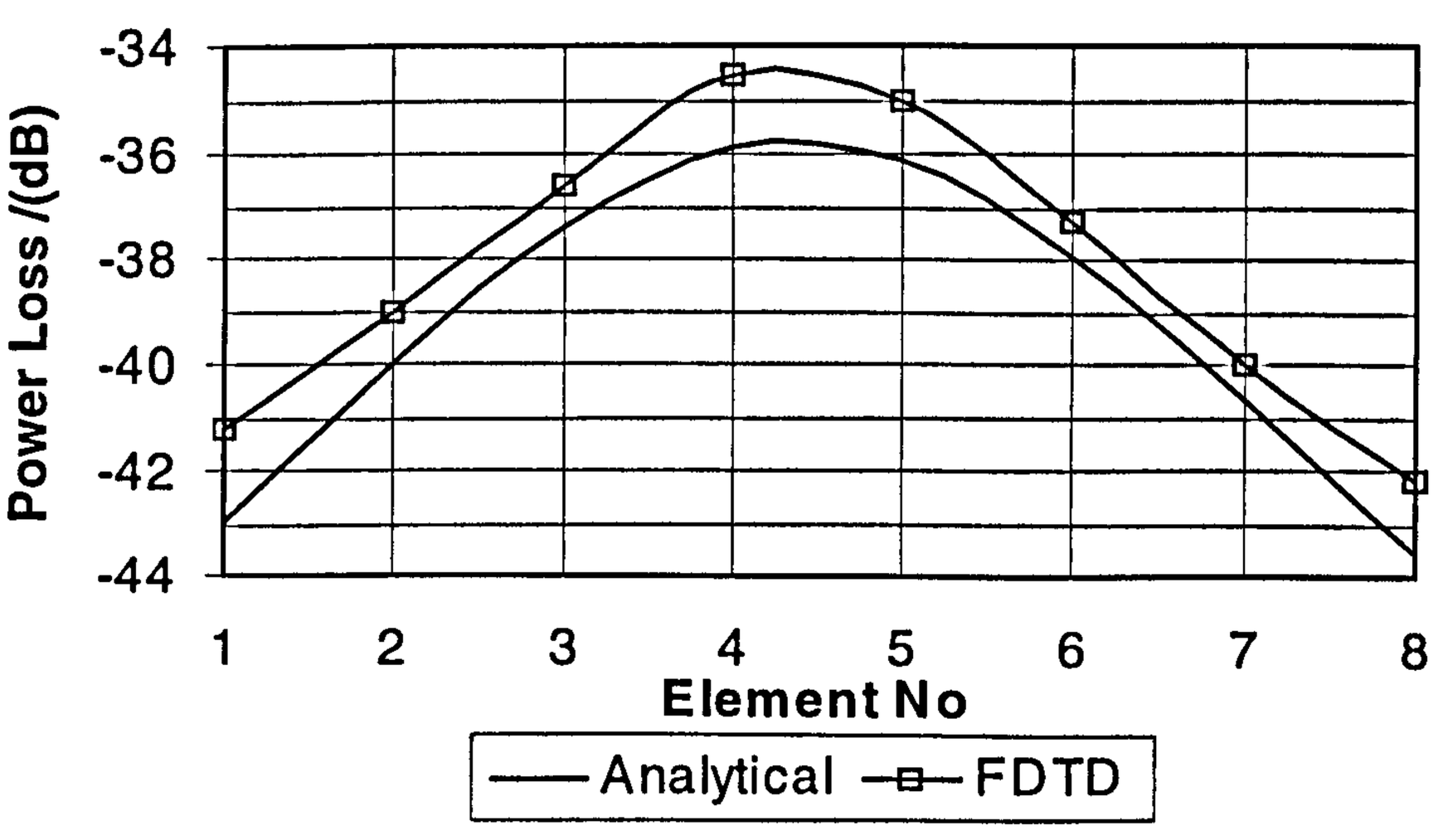

Figure 5.8 Power losses associated with each path when element 4 is transmitting

These results agree with a maximum error of 2.0dB and a mean error of 1.0dB. The mismatch seen between these losses are mainly due to the bi-static RCS estimations, which are generally appropriate for objects large compared to the wavelength. Furthermore, the approximate computations of solid angles would also introduced errors.

5.4.2. Buried Object

FDTD calculations were performed for objects buried in soil with various dielectric properties. Different depth and object sizes were employed to validate the analytical predictions. Figure 5.9 and figure 5.10 show the path losses for a metal plate of 30x30mm buried in soil with dielectric properties ε_r=6+j2 (i.e. ≈ 155 dB loss per meter at 2.1GHz) and also with ε_r=30. A sample calculation (when element 1 transmitting and element 3 receiving with ε_r=6+j2) is given below,

Target depth in soil	= 135 mm
Target lateral displacement from 1st element	= 310 mm
Frequency of operation	= 2.1GHz
Antenna soil separation	= 288 mm
Dielectric constant ε_r	= 6+j2
Antenna gain	= 8.8153 dB
Target size	= 0.03x0.03 m^2
Antenna efficiency L_e	= 0 dB
Antenna mismatch L_m (for both antennas)	= -0.5 dB
Transmission coupling loss L_{t1}	= -1.5645 dB
Retransmission coupling loss L_{t2}	= -1.0545 dB
Spreading loss for forward path $L_{s\ (transmitter\text{-}target)}$	= -0.038629 dB
Spreading loss for return path (single element)	
$L_{s\text{-}element\ (target\text{-}receiver)}$	= -31.5411 dB
Target scattering loss L_{sc}	= -26.0688 dB
Material attenuation loss L_a	= -42.7524 dB
Total loss L	= -103.52 dB

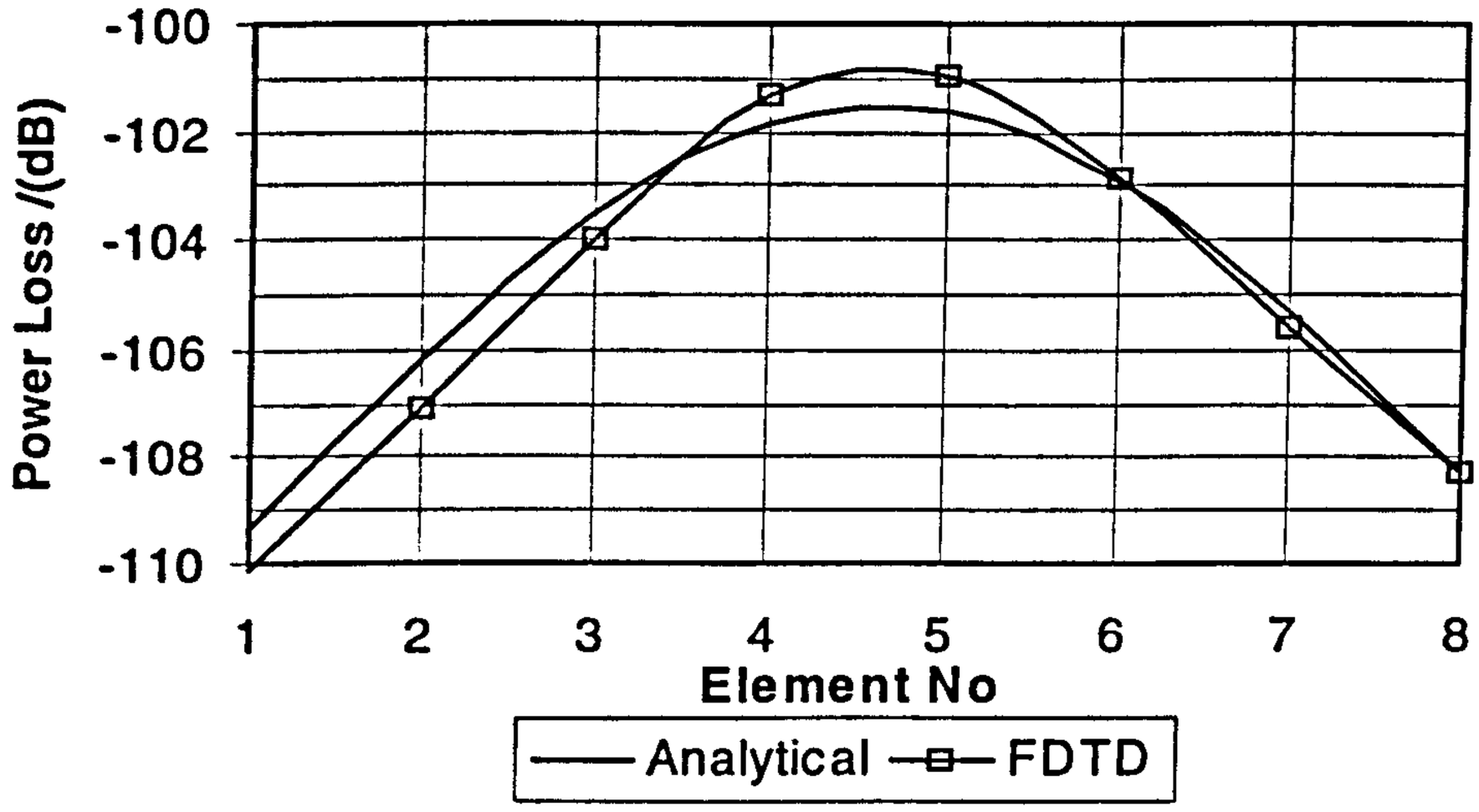

Figure 5.9 30x30 mm metal plate in a lossy soil with ε_r=6 and ε_{rr}=2

Figure 5.9 and figure 5.10 demonstrate the analytical predictions and FDTD calculations agree with a maximum error of 1.0 dB. As discussed in section 5.4.1, the mismatch seen between these losses are due to RCS estimations and the solid angle calculations.

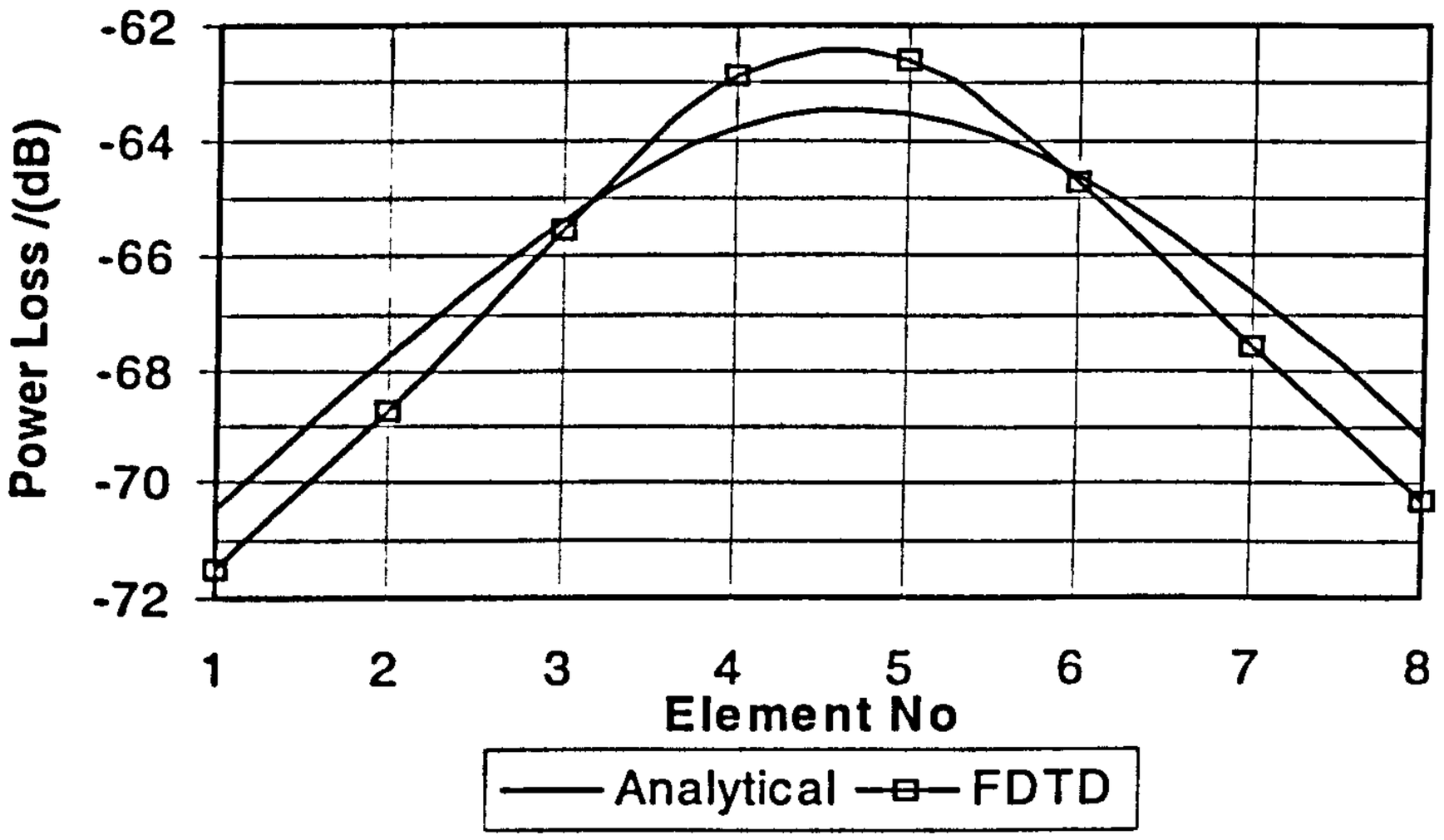

Figure 5.10 30x30 mm metal plate in lossless soil with ε_r=30

This analysis was extended to investigate the GPR model with the absorbing back plane. Figure 5.11 shows that the absorbing back plane introduces a further 2-3 dB loss. This extra loss is due to the conductivity used in the FDTD model, which would absorb some of the energy directed towards the reflector.

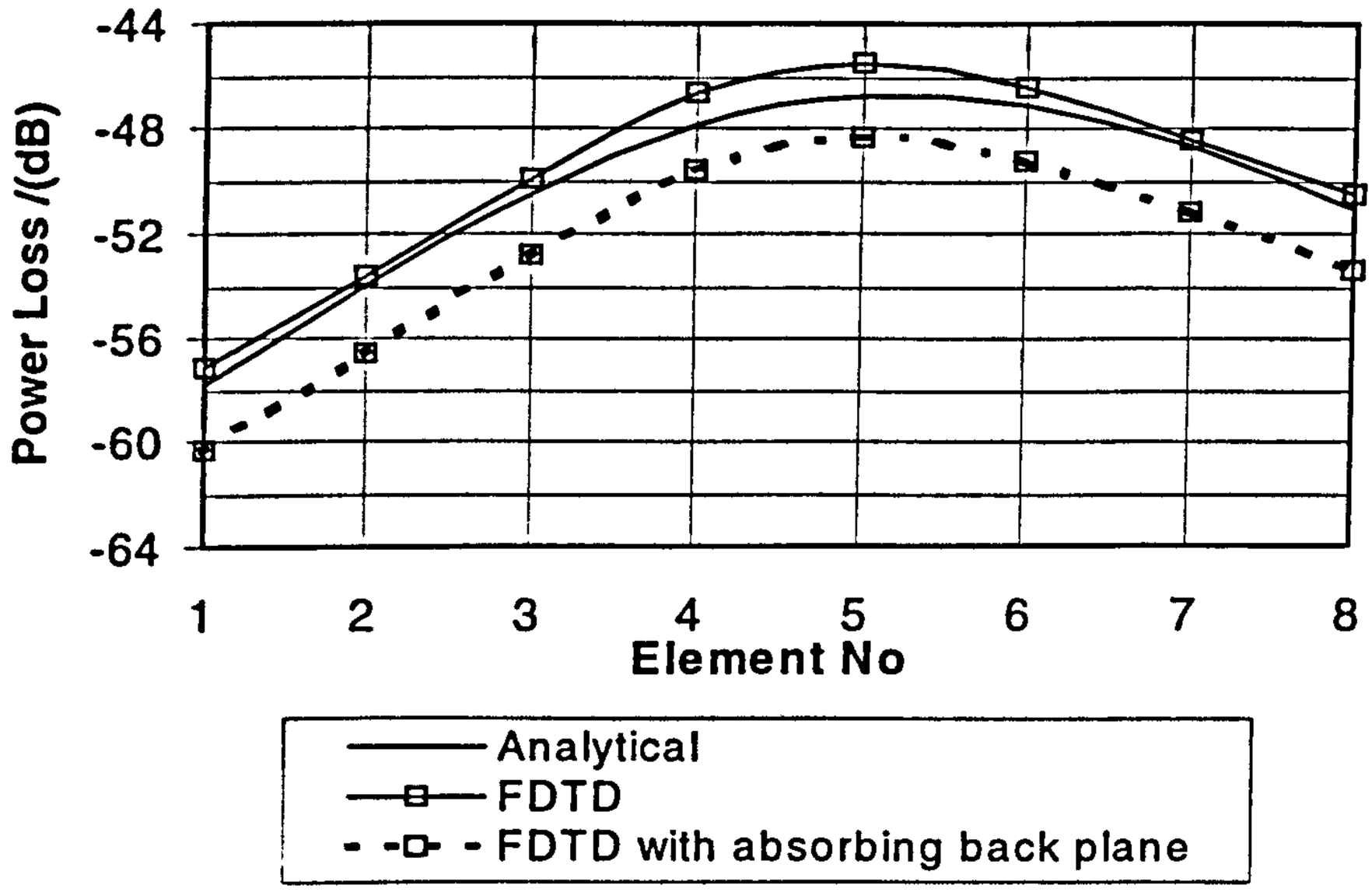

Figure 5.11 70x70 mm metal plate in a soil of ε_r=6

Although only a few scenarios have been considered, the comparison between the FDTD and the analytical method agree within ± 0.5 dB and have a maximum error of 1.0 dB. Hence this analytical method can be confidently employed with bigger problems involving the full array.

In this section, the received signal levels of individual elements have been analysed using the FDTD and an analytical technique. However the PRSF-SPR system makes use of an array to focus into the soil. Hence the coherently combined signal power will be the major factor to analyse the maximum detectable depth of the system. In a noise limited scenario, the target echoes from various paths will coherently add while the noise level remaining the same. The following section looks into the processing gain that can be achieved with this system.

5.5. Processing Gain of the PRSF System

The processing gain of the PRSF-GSPR system has been discussed in chapter 2 and it was verified for a simple case in chapter 3. The processing gain mainly depends on the number of elements that have the target in their field of view (based upon using the half power beamwidths) and the number of target resolution cells which contribute to

the return signal strength. Other factors include the clutter levels and the possibility of coherent combination. The number of antenna elements that have the target in their field of view as shown in figure 5.12 is a function of,

- Frequency of operation (or the inter element separation)
- Spacing between the antenna array and the soil-air interface.
- The target depth.
- The half power beamwidths.

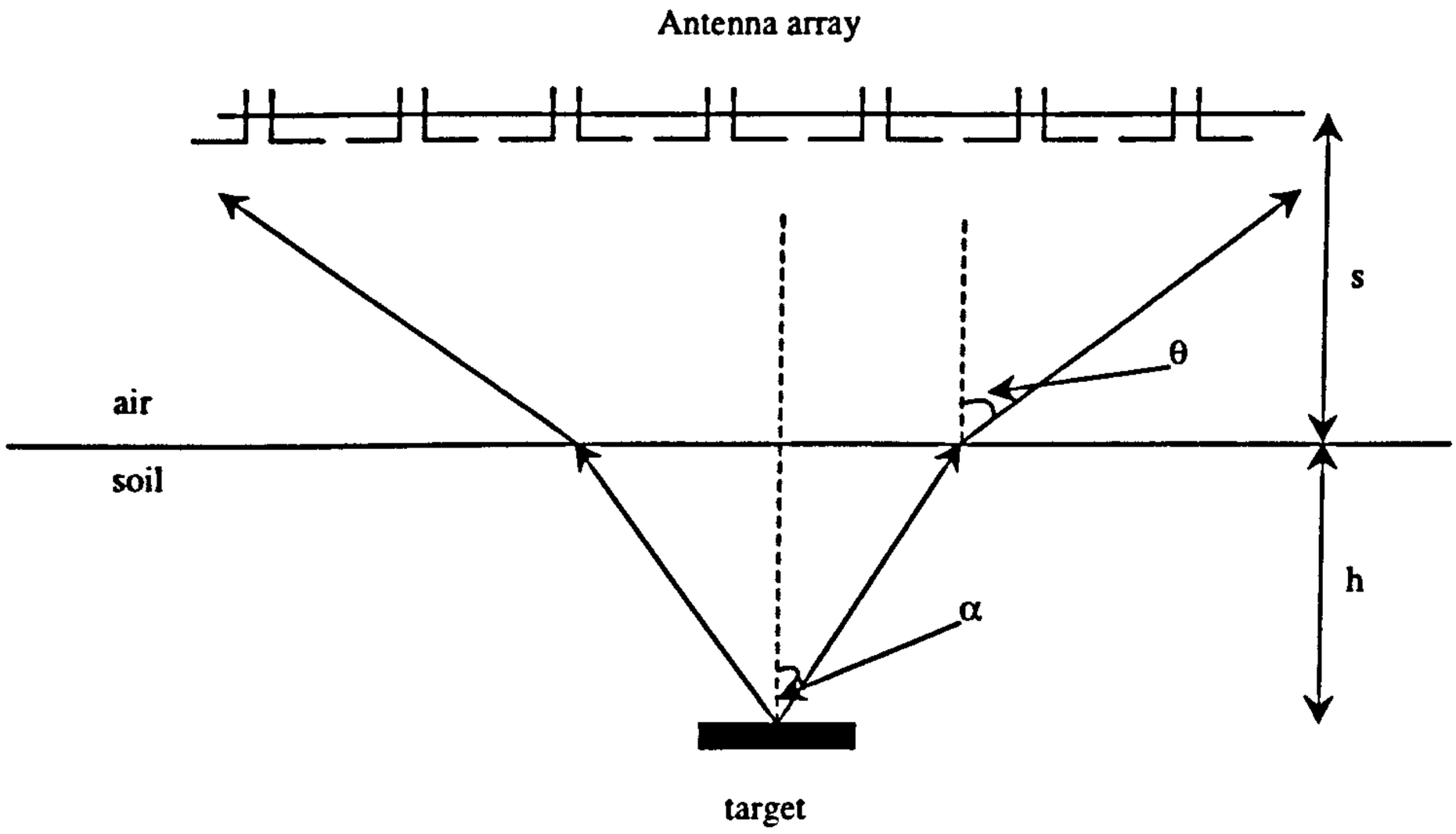

Figure 5. 12 Number of elements which can see the target

The number of elements, which can see the target can be analytically given by,

Useful array area illuminated by the back scattered signal

(considering the half power - beamwidths) $= \pi[h.\tan\alpha + S\tan\theta]^2$ (5.28)

Apperture area for each elements $= [k_o\lambda]^2$ (5.29)

Hence the number of elements $N = \pi\left[\dfrac{h.\tan\alpha + S\tan\theta}{k_o\lambda}\right]^2$ (5.30)

where,

h : Depth in soil.

S : Soil - Antenna separation.

θ : Half the beam width of the antenna element $\approx \pi/4$.

k_o : Normalised inter element spacing factor in the antenna array

Equation 5.30 shows that a higher number of elements will have deeper targets in their field of view, thus increasing the processing gain. But the physical array size (number of elements) will also restrict the achievable processing gain.

5.6. Noise Limits of the System

Noise will always be present in any practical systems due to antennas, cables, amplifiers, detectors etc. Generally in GPR systems, antenna and receiver noise is the primary deciding factor of the Minimum Detectable Signal level (MDS) when low clutter levels are present. The antenna noise temperature is ≈ 290K, for the beam looking into soil (solid angle corresponding to 70^0 and 100^0 half power beamwidths) [11]. The receiver noise power can be defined by its bandwidth and the temperature (290K). The minimum detectable signal due to system noise limits can be calculated from [11],

$$MDS = k(T_a + T_o(NF-1)).BW.SNR \tag{5.31}$$

Where,

k : Boltsman's Constant.

T_o : Ambient temperature in Kelvin.

T_a : Antenna noise temperature in Kelvin.

BW : Bandwidth of the system.

SNR : Signal to Noise Ratio

NF : Noise Figure of the Receiver given by,

$$NF = \frac{\text{noise at the actual receiver}}{\text{noise at the ideal receiver}} \tag{5.32}$$

For example, a system with 3GHz bandwidth, NF of 4dB [11] and a SNR of 10dB will give a MDS of -95 dB. Hence approximately a MDS of 100dB can be detected successfully.

The dynamic range of the system will need to be considered in the detection process and is defined as,

$$\text{Dynamic Range} = \frac{\text{Max Detectable Signal}}{\text{Min. Detectable Signal}} \tag{5.33}$$

The maximum possible signal would be the reflections from the air-soil interface or the coupling between transmitting and receiving antenna.

5.7. Maximum Detectable Depth of the PRSF-GPR System

The Maximum Detectable Depth (MDD) is a good measure to compare various parameters such as the frequency, array soil separations, array size and inter element spacing. Clutter levels will also affect the maximum detectable depth. The nature of clutter returns has been analysed in chapter 4, but the clutter levels that will limit the system capabilities needs a great deal of further analysis and it is outside the scope of this work. Zero clutter levels were assumed in these calculations. The array target configuration used in these calculations is shown in figure 5.13.

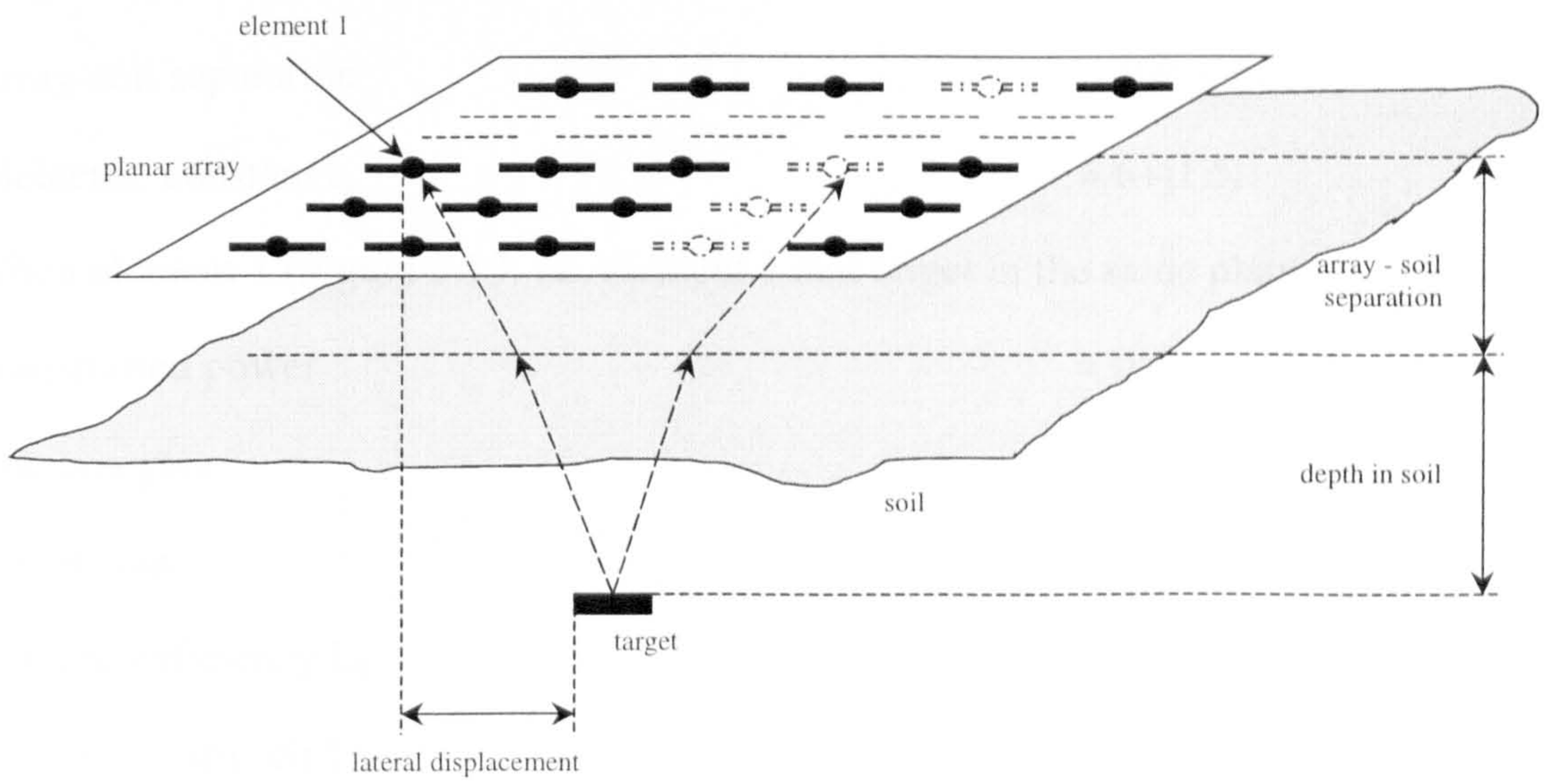

Figure 5.13 Array-target configuration for MDD estimation

A planar array, which is centrally located above the target as in figure 5.13, was considered in these calculations.

5.7.1. Variation of MDD with Frequency

Material attenuation losses in any GPR system will increase with frequency as in equation 5.23. But in the PRSF system, the high processing gain permits the use of higher frequencies. The MDD variation with frequency and the number of elements needed for detection at that depth when using a planar array is shown in figure 5.14. The transmitted power was assumed to be 1W [12] and these calculations were performed for a metal plate of 30x30mm in soil with dielectric properties, ε_r =6+j1.5 (soil attenuation of 55 dB/m/GHz) and ε_r =15+j3 (70 dB/m/GHz). The array-soil separation was maintained at 0.4m, while the inter-element spacing was 0.75 of wavelength. MDD was calculated by estimating the losses for a range of target depths and the maximum penetrable depth was estimated by interpolation (i.e. the depth which gives -100 dB total losses). A sample loss estimation at the MDD and the number of elements needed for detection for an operating frequency of 1GHz is given below,

Frequency of operation	= 1GHz
Lateral displacement of target from transmitting element	= 452 mm
Target depth in soil (MDD)	= 543 mm
Array-soil separation	= 400 mm
Dielectric constant ε_r	= 6+j1.5

When element 1 (Figure 5.13: i.e. element 1 and target in the same plane) transmitting,

Transmitted power	= 0 dB
Antenna gain	= 8.8153 dB
Target size	= 30x30mm
Antenna efficiency L_e	= 0 dB
Antenna mismatch L_m	= -0.75 dB
Transmission coupling loss L_{t1}	= -1.6185 dB
Retransmission coupling loss L_{t2}	= -0.89093 dB
Spreading loss for forward path $L_{s\ (transmitter\text{-}target)}$	= -4.899 dB

Spreading loss for return path (array) $L_{s\text{-element (target-receiver)}}$ = -17.1234 dB

Target scattering loss L_{sc} = -30.0911 dB

Material attenuation loss L_a = -61.2748 dB

Signal power received by the array (when element 1 is transmitting)

= -116.6477 dB

No of elements which have the target in their field of view = 17

Similarly considering all transmitting elements in a row above the target, the average signal power P_{ave} per element is calculated

Average signal Power P_{ave} = -121.3336 dB

Estimated processing gain G_{pros} = 21.3354 dB

Hence the expected total signal power when all possible elements transmitting

$= P_{ave} \times G_{pros}$

= -99.9982 dB

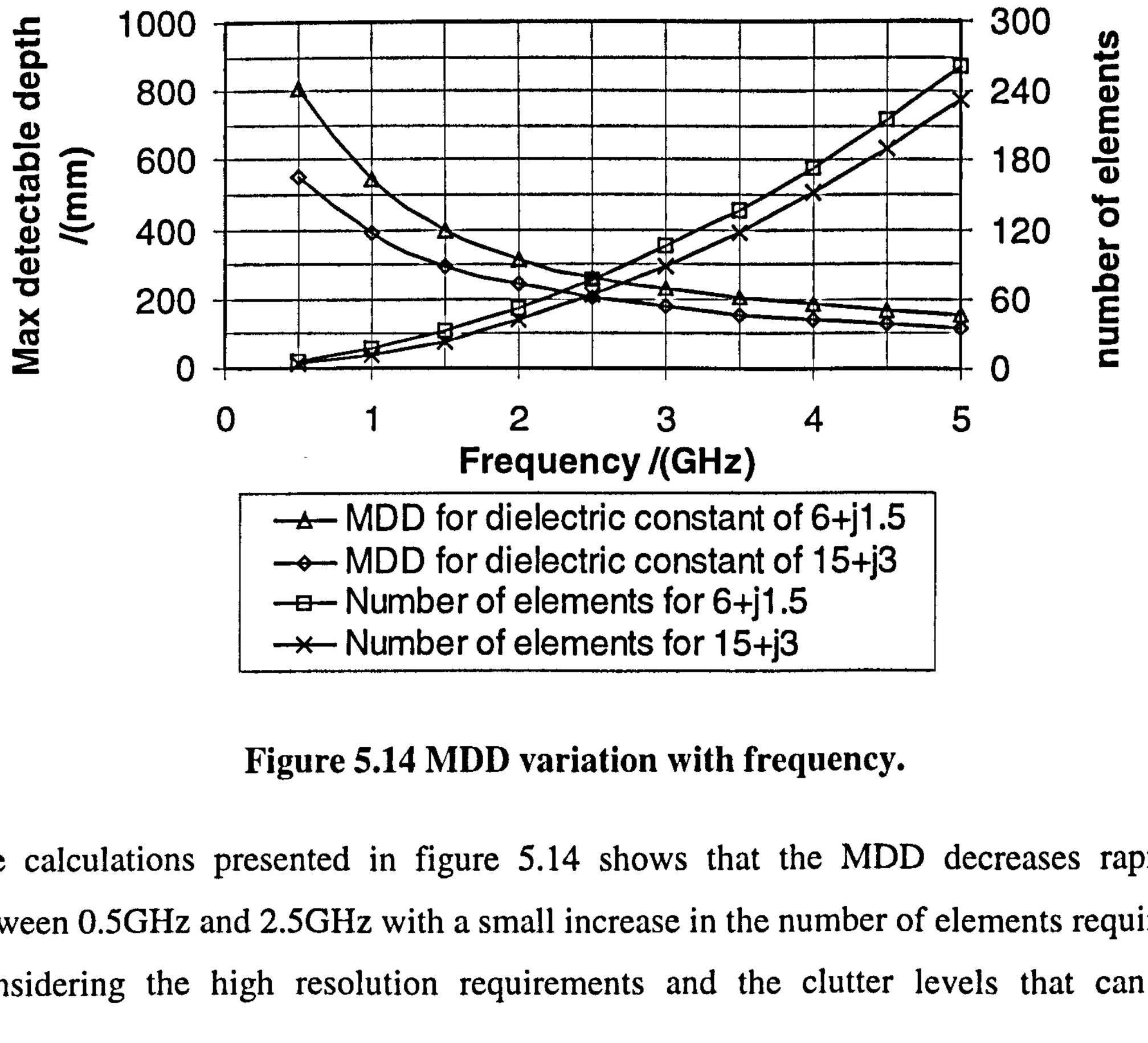

Figure 5.14 MDD variation with frequency.

The calculations presented in figure 5.14 shows that the MDD decreases rapidly between 0.5GHz and 2.5GHz with a small increase in the number of elements required. Considering the high resolution requirements and the clutter levels that can be

expected from high frequency systems it would be appropriate to have an operating frequency between 1.0 and 2.0GHz.

5.7.2. Variation of MDS with Array-Soil Separation

Spreading losses are another significant loss mechanism involved in GPR system. A larger array-soil separation will increase the spreading losses but it will also increase the processing gain as more elements can see the target resolution cell. A physically larger array will increase the hardware costs and restrict the mobility of the system. Figure 5.15 shows the variation of MDD with array soil separation for a frequency of 1.5GHz and inter-element spacing 0.75 of wavelength

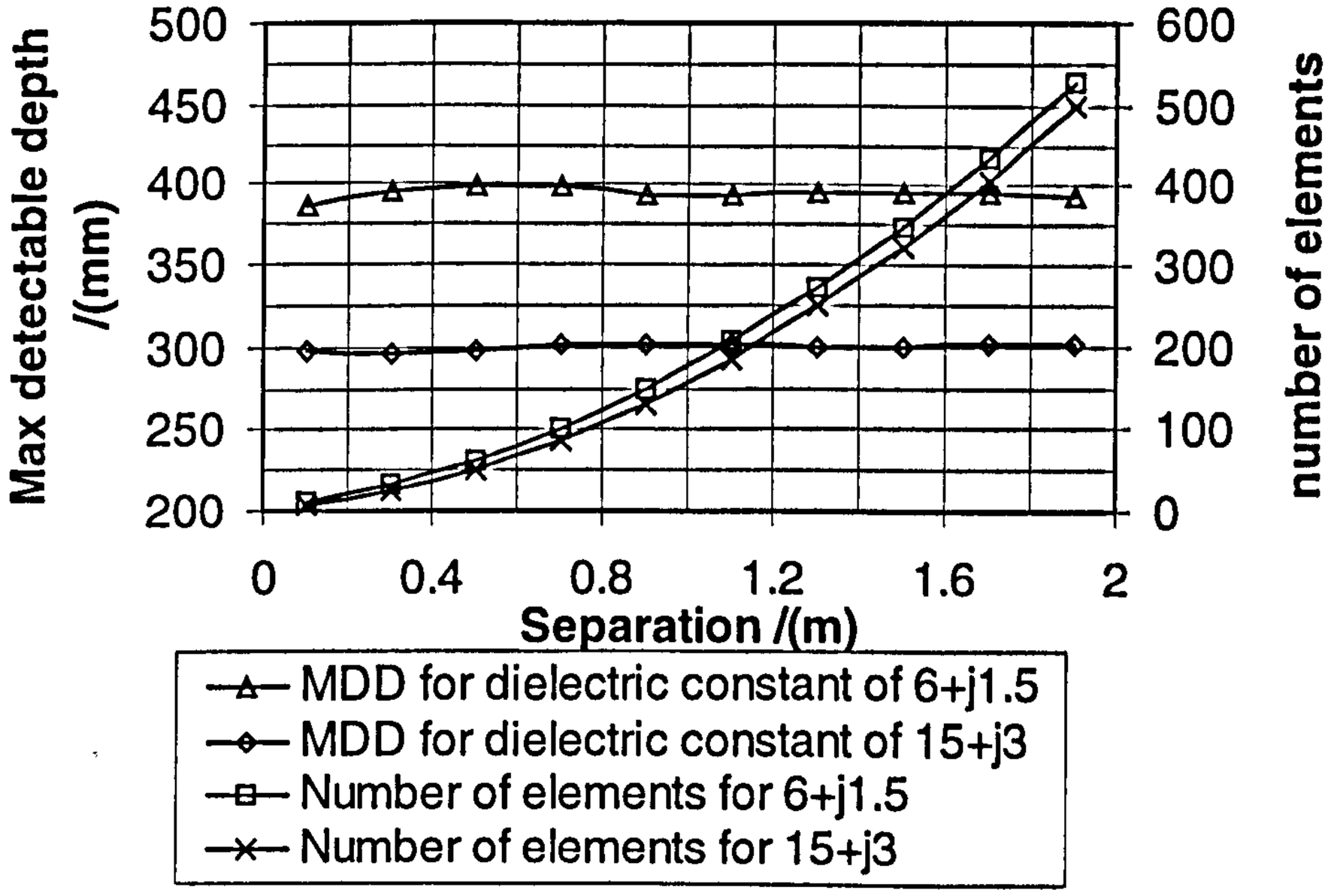

Figure 5.15 Variation of MDD with the array-soil separation

The calculated figures show that the number of elements required increases rapidly from 0.6m onwards and the MDD remains almost constant. Hence an array-soil separation of around 0.5m will give adequate separation and moderate the size of antenna array to around 60 elements.

5.7.3. MDD with Different Soil Types

Different soil conditions will also influence the target detecting capabilities of the system. As discussed in section 5.3.1, the moisture contents of soil will affect the

dielectric properties of soil. Table 5.3 gives the noise limited MDD under practical soil conditions listed in table 5.2. Calculations were performed for a metal plate of 30x30mm at 1.4GHz with an array-soil separation of 0.5m and 0.75 of wavelength inter-element spacing.

Soil Type	Maximum detectable depth for a 30x30mm metal plate		
	Volumetric moisture		
	0.1	0.3	0.5
Sandy Loam	600mm	300mm	250mm
Loam	600mm	300mm	200mm
Silt Loam	550mm	250mm	200mm
Silty Clay	500mm	250mm	150mm

Table 5.3 MDD in different soil conditions

Table 5.3 indicates that the MDD variation is relatively independent of the soil type, but depends on the moisture content. Hence for very wet soils the frequency of operation would have to be reduced for detection at deeper depths, though this would degrade the resolution.

5.8. Summary

This chapter has presented an analytical model that can be used to calculate the signal strengths in the full PRSF-GPR antenna array. The analytical model has been validated for free space and buried targets, with the more precise FDTD calculations. A maximum error of 2dB and a mean error of 0.5dB was observed. This model was further employed to calculate the noise limited maximum detectable depths of the system. The MDD has been used as a measure to analyse the operating frequency and array-soil separations associated with the PRSF-GPR system. From this analysis, it has been showed that an operating frequency in the range of 1 to 2GHz, array-soil separation of 0.5m with 0.75 of wavelength inter-element spacing is appropriate for a practical system with 60 elements. Such information is fundamental in the design of practical systems. Furthermore, the dielectric properties of soils have been discussed

and the noise limits are investigated for some soil types. The calculated MDDs for different soil types indicated that the system performance is almost independent of the soil type though is mainly a function of the moisture contents.

Having undertaken these analyses with theoretical calculations, it is appropriate to compare the necessary results with practical measurements. In order to facilitate the measurements, appropriate practical antenna designs are necessary. Although the simple printed dipole antenna was adequate for theoretical analysis, a wide band antenna is appropriate for practical purposes and this design is discussed in the following chapter.

References

[1] D.J.Daniels, *Surface Penetrating Radar* , IEE , UK 1988

[2] F.T.Ulaby, R.K.Moore and A.K.Fung, *Microwave Remote Sensing*, vol. 111, Artech House, 1986.

[3] R.Benjamin, Post Detection Synthetic Focusing in Near-field Radar, *Proceedings of EUREL/IEE International Conference on the Detection of Abandoned Land Mines*, IEE, Edinburgh, pp. 133-137, Oct 1996

[4] D.J.Daniels, Short Pulse Radar for Stratified Lossy Dielectric Layer Measurements, *Proceedings of the IEE*, vol. 127, pt F, No. 5, pp 384-388, 1980.

[5] M.J.B.Scanlan, *Modern Radar Techniques*, Collins, UK, Chapter 3.

[6] M.I.Skolnik, *Radar Handbook*, McGraw Hill, USA, Chapter 25, 1990

[7] R.E.Kell, On the Derivation of Bi-static RCS from Mono-static Measurements, *Proceedings of the IEEE*, vol. 53, pp. 983-988, 1965.

[8] S.Kingsley and S.Quagan, *Understanding Radar Systems*, Chapter 2, McGraw Hill, UK.

[9] R.A.Ross, Radar Cross Section of Rectangular Flat Plates as a Function of Aspect Angle, *IEEE Transactions on Antennas and Propagation*, vol. AP-14, no. 3, pp. 329-335, 1966.

[10] D.J.Daniels, Surface Penetrating Radar, *Electronics and Communications Engineering Journal*, pp. 165-182, 1996.

[11] M.I.Skolnik, *Introduction to Radar System*, McGraw-Hill, UK, 1962.

[12] E.M.Johanson and J.E.Mast, Three-dimensional Ground Penetrating Radar Imaging Using Synthetic Aperture Time-Domain Focusing, *SPIE Proceedings on Advanced Microwave and Millimeter Wave Detectors*, vol. 2275, July 1994.

6. Antenna Development for the PRSF-GPR

6.1. Introduction

Chapter 2 discussed the PRSF concept for ground penetrating radars and chapter 3 and 4 described the FDTD modelling of the PRSF-GPR system using a printed dipole. Analyses presented in the previous chapters also indicated the benefits of employing an antenna with a wide bandwidth. Chapters 6 and 7 now consider the development of a practical system for verification of the analysis and for demonstration of the concept in a more realistic situation.

Implementation of the PRSF-GPR system requires an antenna capable of providing both wide bandwidth and beamwidth characteristics. This antenna should also perform satisfactorily when soil is present. In the PRSF-GPR system, the antenna element would form part of a planar array. Although only one element transmits at a time, neighbouring elements will influence the performance of the transmitting element through mutual coupling and scattering.

Antenna development is presented in this chapter, with FDTD modelling employed to aid the analysis of the ground penetrating radar and hence its validation. Such complex analysis of the antenna in its operational environment can be easily accomplished with the FDTD method.

In the next section, a brief overview of existing antennas for conventional ground penetrating radar has been presented. For practical implementation of the PRSF-GPR system, a wide band printed bowtie antenna element was chosen for consideration. The antenna design (which utilises the FDTD techniques) is described giving attention to

its performance when soil is present. The effect of an absorbing antenna back plane (which was described in chapter 3) on the bowtie element properties are examined through practical measurements. Finally the bowtie element in an array configuration was analysed using FDTD and practical measurements.

6.2. Antennas for Surface Penetrating Radars

Design of antenna elements for GPR applications is challenging because of their operational environment. Antennas for in-contact mode operations have to be matched to the respective soil media, hence a design capable of operating in wide range of soil conditions needs to be considered. With the non-contact system developed here, the antenna should be matched to air though its characteristics will be altered by close proximity of the soil. With the exception of the CW holographic GPRs [1], most of the subsurface systems discussed in chapter 2 employ wide operating bandwidths (i.e.,0.1 – 1GHz, 0.5-3GHz) for fine resolutions. However, the upper end of the bandwidth often suffers from soil attenuation, and hence degradation of transmitted signals. Radiation characteristics of the antennas for subsurface operation often depend on the probing techniques. Synthetic aperture techniques generally require a wide beam pattern for higher resolutions and the conventional radars require a narrower beam pattern to reduce clutter effects. The conventional GPRs generally make use of a pair of antennas for transmission and reception (bi-static mode) placing fewer constraints over the physical dimensions. Different types of antennas such as travelling wave antennas, horns, spirals and dipoles can be used with the GPRs [2], and are described briefly below.

6.2.1. Travelling Wave Transmission Line Antennas

Travelling wave antennas used in subsurface operations are designed with transmission lines arranged in a "V" shape such that radiation propagates along its axis. The characteristic impedance of the transmission line varies from the feed impedance at one end to free space impedance at far end, thus enabling wide band characteristics through good impedance matching. In practice, the far end is terminated with resistive loads to avoid resonance and keep the antenna short [3]. These types of antennas are capable of producing $\pm 25^0$ half-power beamwidths [4]. Due to the V shape geometry,

different frequency signals travel through different paths and stretches sharp input pulses in the far field [5]. However, correction techniques are available to optimise pulse transmission [2]. As a results of their wide-band characteristics and simplicity, this form of travelling wave antenna is preferred in conventional GPRs and has been employed for dielectric layer measurements in a short pulse radar [6].

6.2.2. Horns

Horn antennas are widely used in many applications due to high directive gain, simple excitation and wide bandwidths. At higher frequencies the wider apertures may cause phase errors across the aperture and will degrade the directive gain. Phase errors can be minimised by employing phase correcting lens or having longer horns [7]. Therefore, for better performance the horns become larger and heavier. In subsurface applications the horns are employed in systems making use of a few antennas elements. Carin et al [8] used four resistively terminated horns for minefield detection in an ultra wide band synthetic aperture radar. Botros et al [9] used a single ridged horn to feed a parabolic reflector in a FM-CW system for detection of hidden objects in walls.

6.2.3. Spirals and other Frequency Independent Antennas

Another attractive choice for wide-band applications are frequency independent antennas. Frequency independent antennas are entirely defined by angles rather than linear dimensions as in other types of antennas hence giving a wide radiation characteristic. However, in practice, the physical dimensions of the antenna often limits the operating bandwidth. Spirals, bi-conical dipoles, Vivaldi antennas and log periodic structures fall in this category. Spirals are generally etched on copper-clad substrates and fed in the centre. These types of antennas are capable of producing circularly polarised waves and have half power beamwidths in the order of 75^0 [10]. The main disadvantage of these types of antennas is their dispersive nature. Since the high frequencies leave the antenna earlier than lower frequencies (radiation take place from a circular region one wavelength in circumference), transmission of sharp pulses are limited and result in a distorted transmitted signal. Hence techniques such as matched filtering must be employed to tackle this problem.

6.2.4. Dipole Elements

There are various dipole configurations such as cylindrical dipoles and crossed dipoles can be used in subsurface applications. Generally dipoles are characterised by linear polarisation, low directivity (wide beam patterns) and limited bandwidths compared to the other antennas discussed in this section.

Dipole elements are extensively used in subsurface operations because of their simple configuration. End loading techniques [11] has been used with dipole elements to reduce antenna ringing and transmit temporally short pulses without much distortion. But resistive loading always results in low efficiency. Because of its geometry the flat-plate resistively loaded dipole is a favourite choice in most geo-technical applications [12]. Another widely used dipole element is the resistively loaded crossed dipole [13]. Orthogonal arrangement of such dipoles gives excellent transmit-receiver isolation and is therefore very useful in systems using polarisation discrimination techniques.

6.2.5. Bi-Conical Antennas

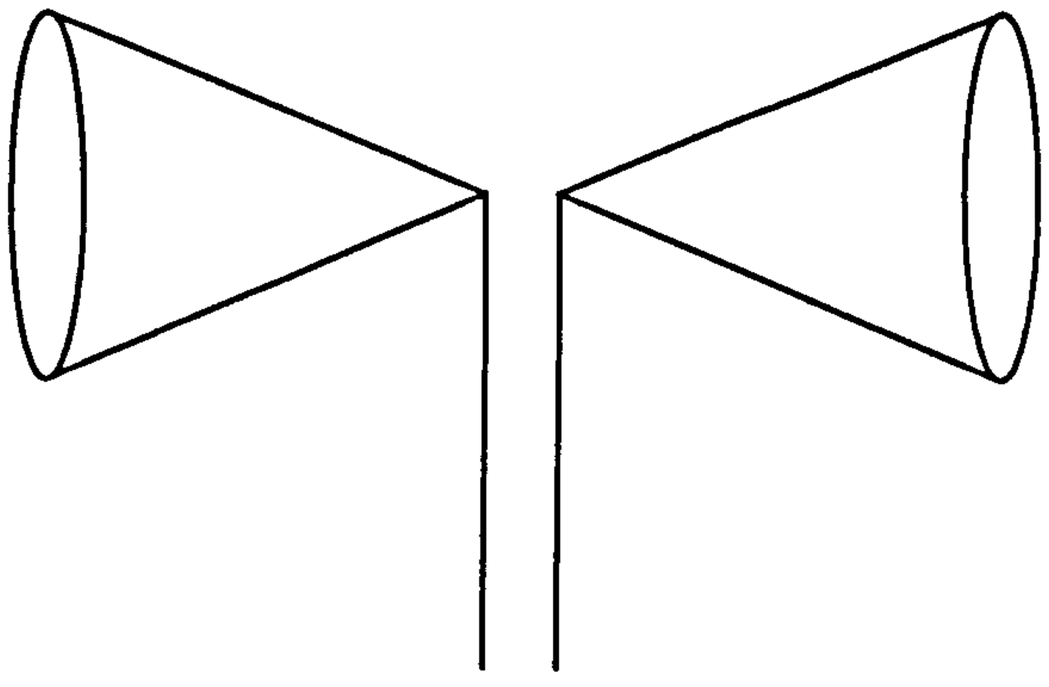

Figure 6.1 Bi-conical antenna

Bi-conical antennas are formed by placing two cones of 'infinite size' together. This kind of structure acts as guide for spherical waves in the same way that a uniform transmission line acts as a guide for plane waves [7]. The input impedance of an infinite bi-cone is dependent on cone angle and independent of its physical length-hence the antenna exhibits broad band characteristics. However in practical structures, figure 6.1, finite sizes determine a limited bandwidth compared to the infinite cone. Brown and Woodword provided a useful summary of measured input impedance of finite bi-conical antennas [14]. Shell or solid bi-conical structures are massive and

provide limitations in various practical applications. Hence various other simple practical designs appeared in the past. The flat triangular antenna (bowtie) [14] and the wire bi-conical antenna [15] are some of such simple structures. Smith et al [15] further showed that wire bi-conical antennas are band limited compared to the flat triangular and bi-conical antennas.

6.2.6. Bowtie Antennas

The flat triangular dipole or bowtie antenna is basically a simplified version of the bi-conical antenna. The first comprehensive analysis of its properties was conducted by Brown and Woodword [14]. They investigated the input and radiation characteristics through practical measurements. Bowties have gained considerable attention in subsurface applications because of their simplicity and relatively wide-band properties [16, 17].

The PRSF-GPR requirements as discussed in chapters 2, 3 and 4 can be mostly met by a bowtie antenna element and was therefore developed for this system.

6.3. Bowtie Antenna Design

A bowtie antenna element to operate at 1GHz was developed with the aid of FDTD techniques. The 1GHz frequency was selected to have good penetration depths and due to band limitations with test equipment (1.5GHz maximum frequency of a HP 54845A, Infinium digitising oscilloscope). The design process consisted of developing (with the aid of FDTD techniques) a wide-band single bowtie element fed by a co-planar strip line and subsequent integration of a coaxial cable to feed the strip line through a quarter wavelength balun by practical means. Suitable impedance matching between the antenna and feed was achieved by tapering the strip line feed. Finally the complete antenna structure was modelled with FDTD and compared with the practical measurements. The comparison between the FDTD antenna model and practical measurements is essential to verify the design and for the comparison of the complete three-dimensional GPR model

6.3.1. Antenna Configuration.

The antenna element was fed by the balanced co-planar strip line, which passed through a rectangular hole in the aluminium reflector (ground) plane. The co-planar strip line was fed from a coaxial cable via a $\lambda/4$ balun with the strip line being tapered to obtain suitable impedance matching. The complete antenna structure used in the FDTD modelling is shown in figure 6.2.

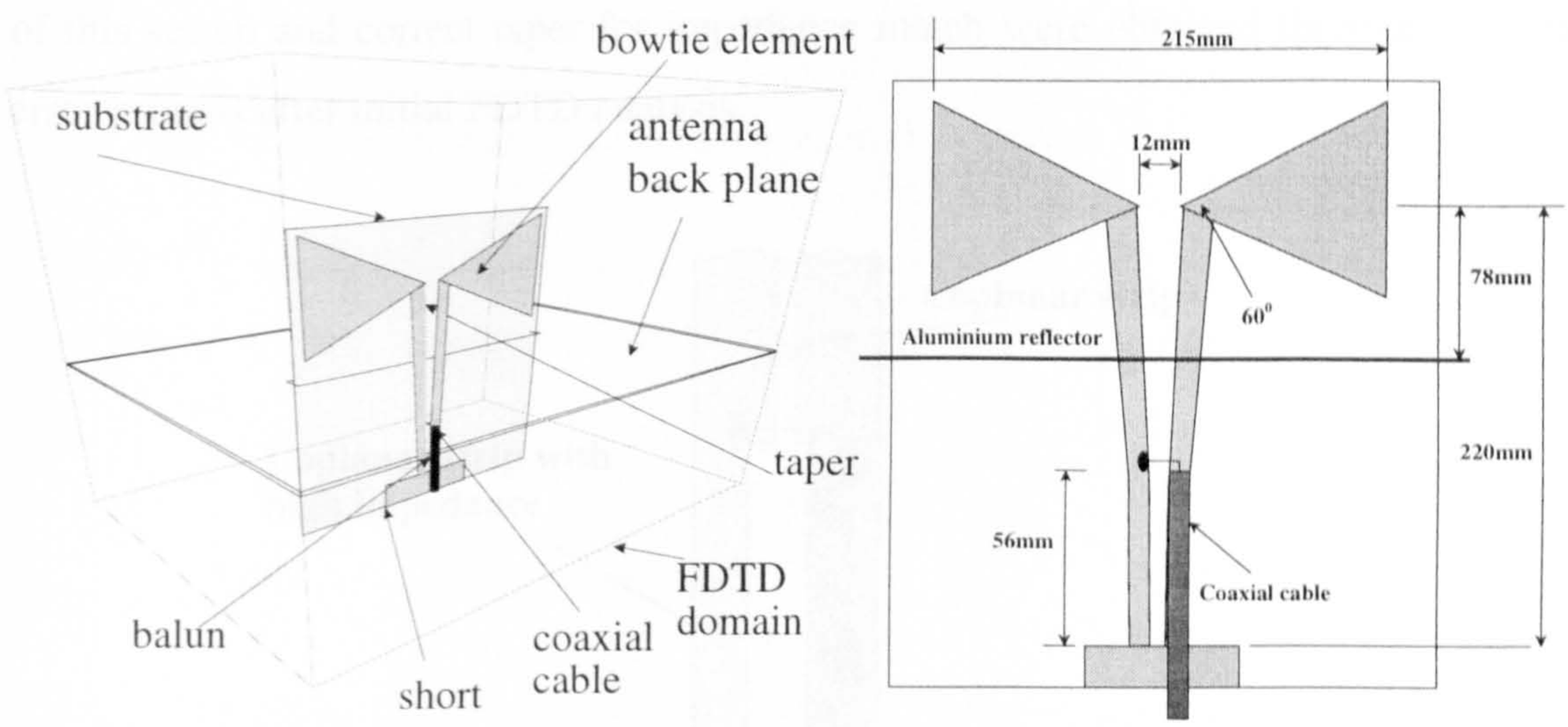

Figure 6.2 The complete FDTD antenna model

6.3.2. Unbalanced to Balanced Line Transitions (Balun)

Printed bowtie dipoles have to be fed by balanced feeding arrangements, as unbalanced current distributions tend to disturb the radiation patterns. Unbalanced transmission lines are defined as one in which the two conductors are at different potentials with respect to ground. The capacitance with respect to ground of individual elements are different and hence unequal currents flow in the conductors. On the other hand balanced transmission lines have the same (but opposite) currents. A device that permits connection between balanced and unbalanced systems, which supports equal currents in the balanced section are known as *bal*anced to *un*balanced converters or *baluns*. Generally baluns are analysed by considering the balanced and unbalanced mode currents separately. Most baluns short circuit the unbalanced currents and permit the balanced currents to flow into the balanced section. A practical system used with the bowtie dipole is shown in figure 6.3.

In figure 6.3 the shorted stripline section (≈λ/4 at centre frequency) offers high impedance (almost open circuit) for the balanced mode currents and forces currents to flow into the balanced section. For unbalanced mode currents this shorted section acts as a short circuit preventing any unbalanced currents. Generally the shorted section of the strip line has narrow band characteristics unless high characteristic impedance values are used [18]. The balanced section of the strip line was tapered in the section leading to the dipole to achieve impedance matching. The actual physical dimensions of this set-up and correct taper for impedance match were obtained through trial and error process after initial FDTD analysis.

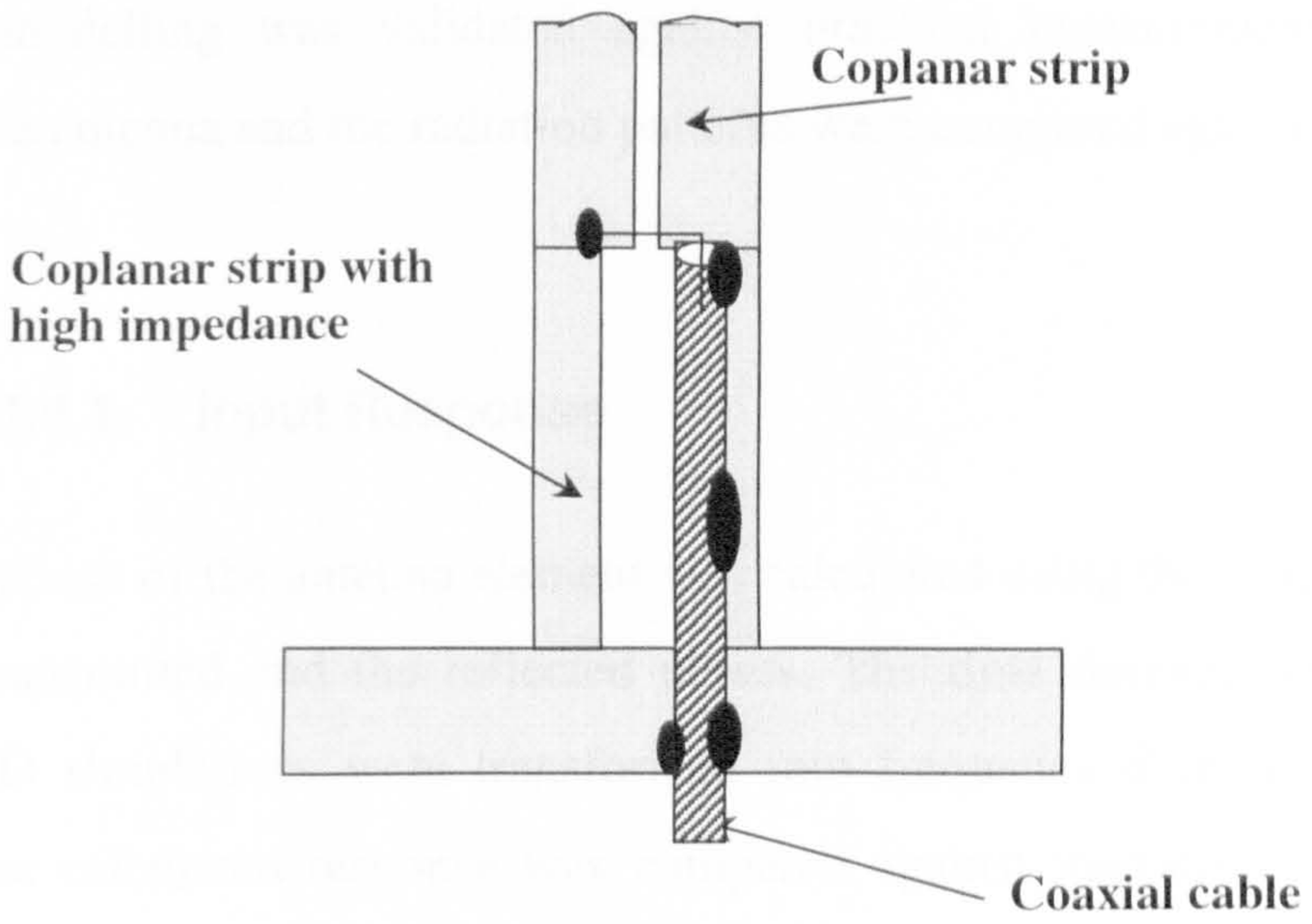

Figure 6.3 The balun structure

Coplanar strips consist of two strips running parallel on the same surface of a dielectric slab. These lines are very useful in feeding printed balanced structures like printed bowties. Quasi-static and full-wave analyses of the characteristics of these lines are possible [19].

A suitable coplanar stripline (approximately 50 Ω) was designed using FDTD methods for transition from 50 Ω coaxial cable to striplines. The shorted section of the stripline in figure 6.3 with higher characteristic impedance was designed to give a better antenna-feed match and without unwanted radiation from this section of the stripline.

6.3.3. FDTD Modelling

The complete printed bowtie dipole structure was represented by the FDTD model shown in figure 6.2. The antenna element 210mm in length and the feed were modelled on a substrate of dielectric constant 2.2 (RT/DUROID 5880). The model space was limited using absorbing boundary conditions [20]. For wideband excitation, a single Gaussian pulse of 250 ps width was employed in the simulation process as described in chapter 3.

6.3.4. Comparisons with Measurements

The FDTD modelling was validated against practical measurements. The input response of the antenna and the radiation patterns were compared against the measured results.

6.3.4.1. Input Response

The input response of the antenna element was calculated using the frequency domain data of the transmitted and the reflected pulses. The time domain results achieved through FDTD simulations were transformed into frequency domain using Fourier transform. The calculated response was compared against measurements performed using a HP 8510 network analyser and shown in figure 6.4.

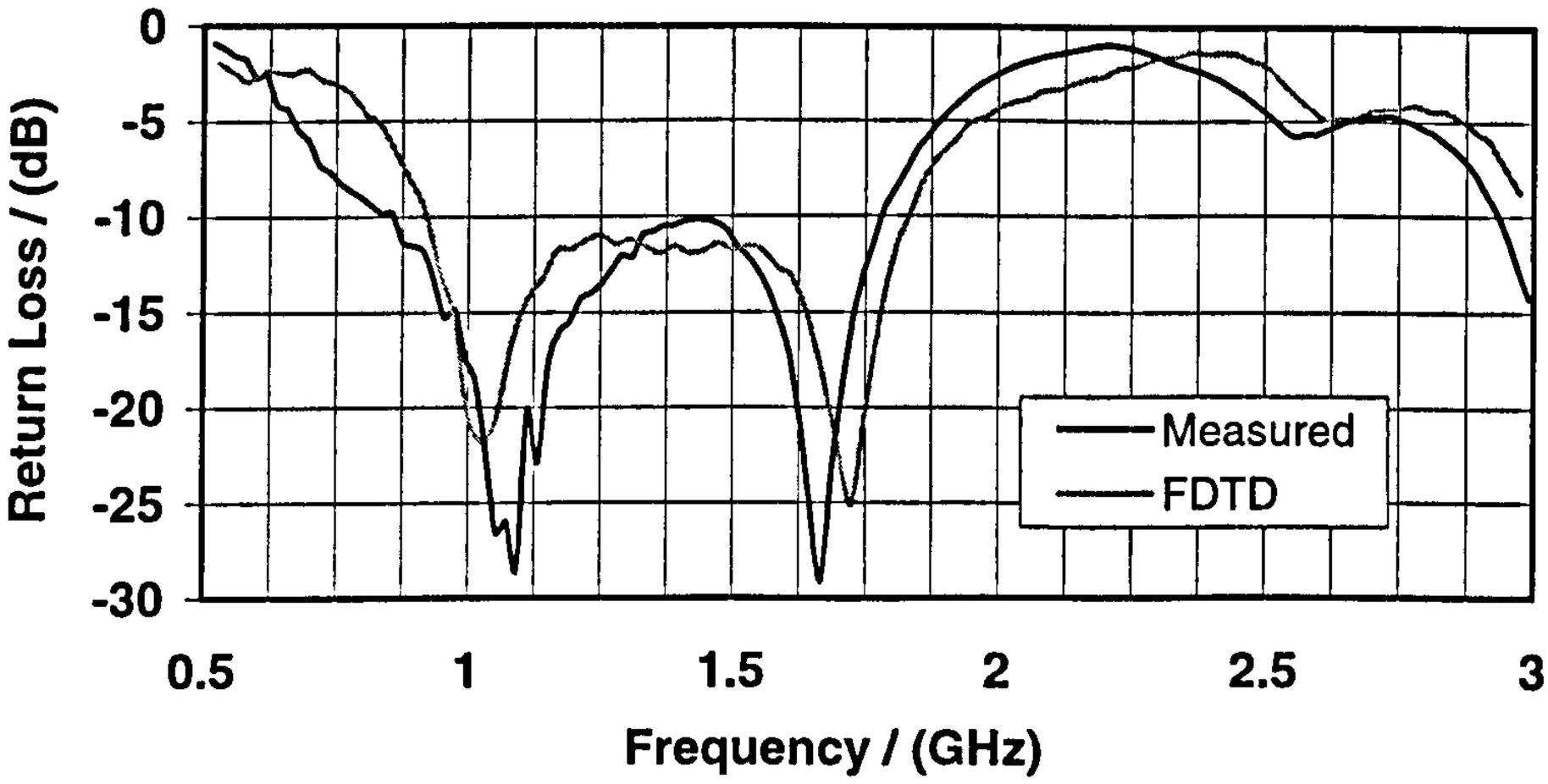

Figure 6.4 Input response of the bowtie element

These results show a very good correlation between measured and calculated results. It can be seen that the antenna has a -10 dB antenna-feed match from 0.8GHz to 1.8GHz. This wide band characteristic is very useful for the transmission of temporally narrow pulses and shows a large improvement compared to the printed dipole antenna described in section 3.3.1. This had only a 35% bandwidth.

6.3.4.2. Radiation Patterns

It is important to analyse the radiation patterns over the frequency range of interest to verify whether the antenna is acting as a useful radiating element. FDTD analyses were carried out to calculate the radiation patterns over this frequency band and compared with practical measurements performed in an anachoic chamber. The FDTD calculations were obtained through near-far transform at 0.8GHz and 1.2GHz as described in section 3.3.1.3. The comparisons of the co-polar patterns are shown in figures 6.5 and 6.6. Although not shown, the cross-polar levels were all 15 dB lower than the co-polar levels.

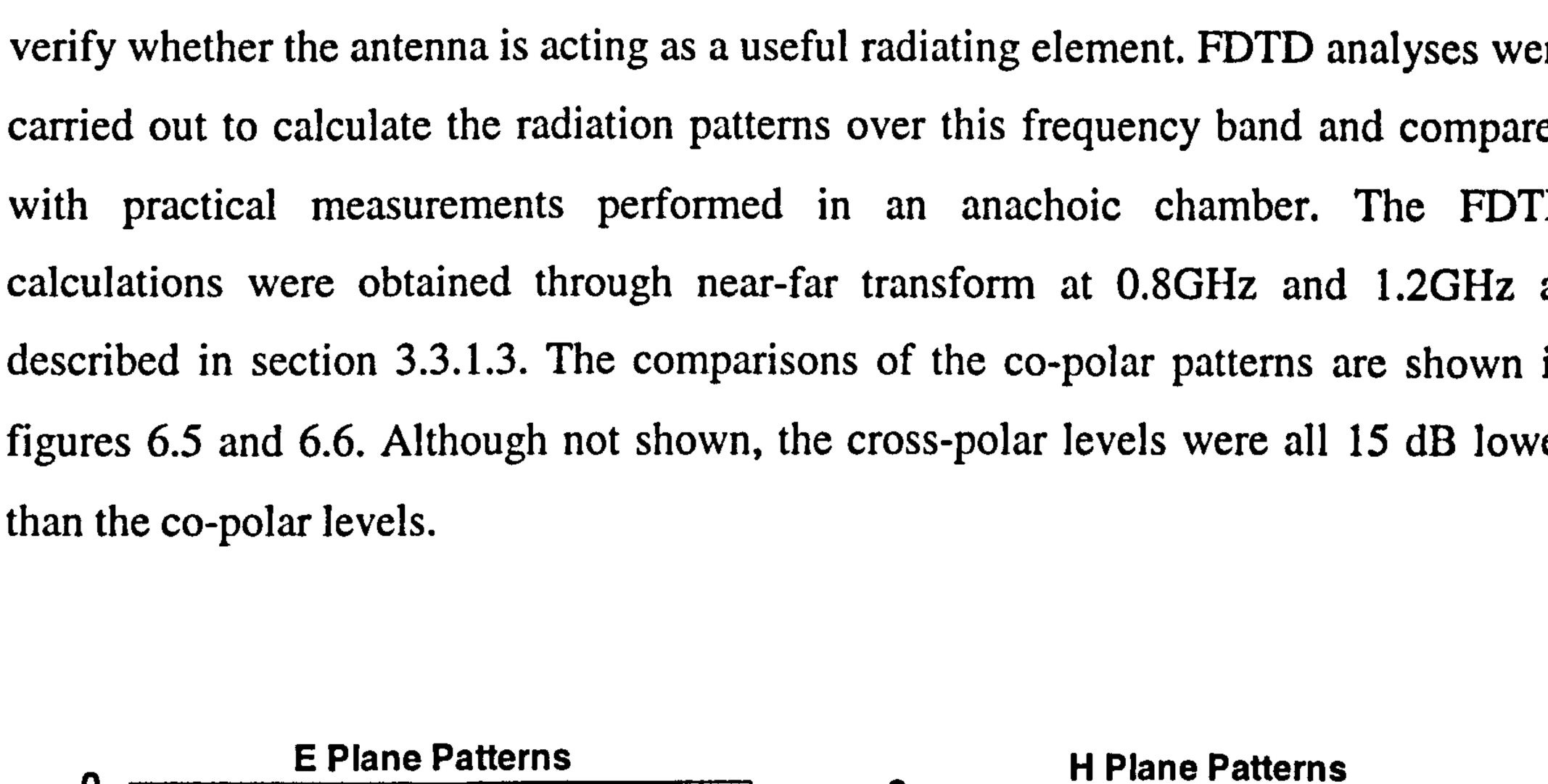

Figure 6.5 Radiation patterns at 0.8GHz

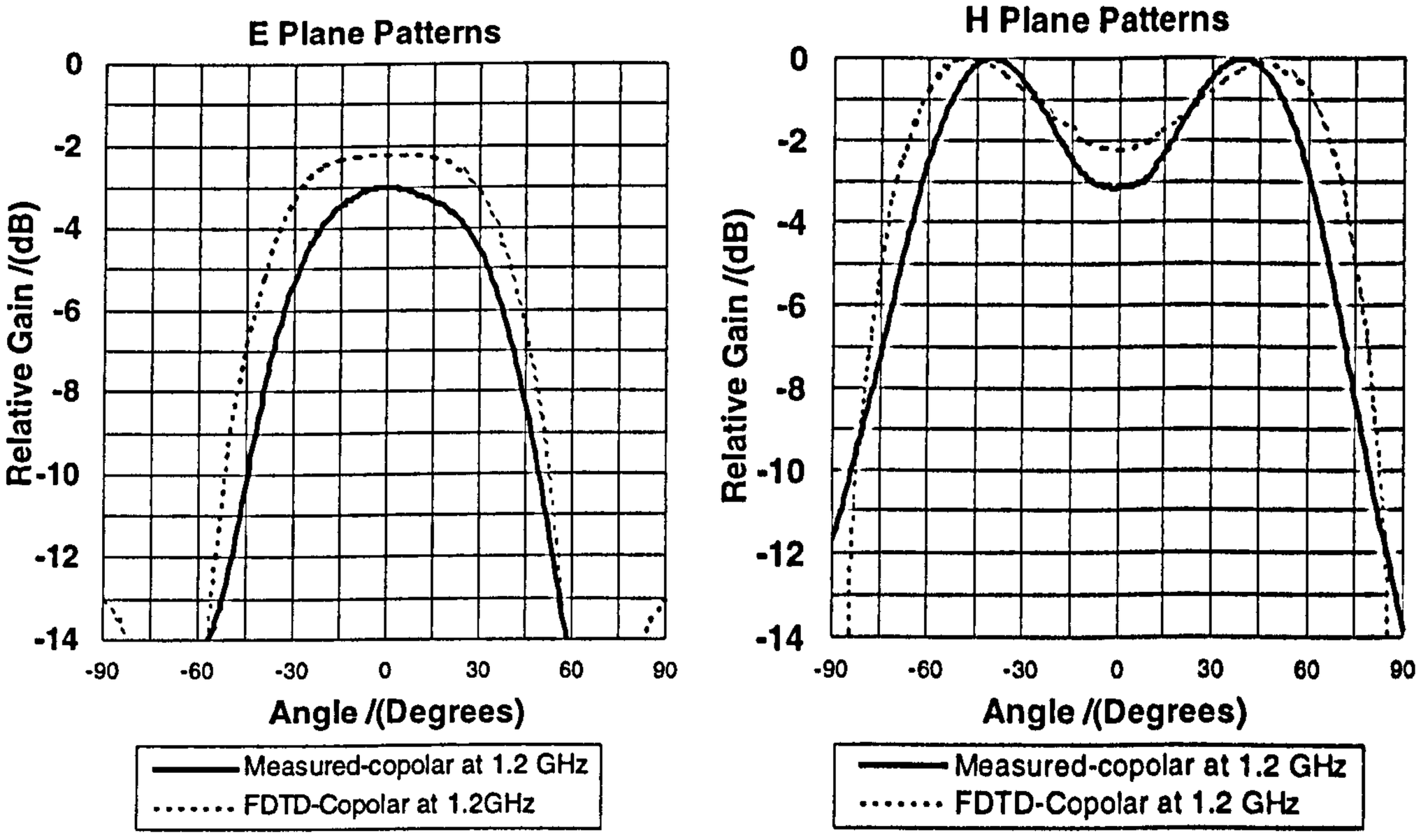

Figure 6.6 Radiation patterns at 1.2GHz

The measured H-plane co-polar response is broad, with -3 dB beamwidths of $\pm 50^0$ at 0.8GHz and $\pm 55^0$ at 1.2GHz. The E-plane co-polar response is narrower than the H-plane response, having -3dB beamwidths of $\pm 30^0$ at 0.8GHz and 1.2GHz.

It should be noted that in the FDTD model, the tapered strip line and the bowtie are staircase approximated to fit the actual dimensions. The connector, the dielectric substrate losses and the finite size of the antenna ground plane were also not incorporated in the FDTD model and it was these effects that were the most likely causes of the small differences seen in FDTD model and practical measurements. The radiation pattern measurements and model results deviate mainly due to the finite size of the ground plane and diffraction at metal edges.

Although a better than –10dB antenna-feed match was obtained from 0.8 to 1.8GHz, due to the formation of a null at 0^0 in the H plane pattern, the antenna could only usefully be operated from 0.8 to about 1.2GHz. The null formation is due to bowtie-ground plane spacing, which corresponds to $\lambda/4$ at 1GHz. This null deepens above 1.2GHz as the cancellation by the reflected signals become more significant.

6.4. Bowtie in a Ground Penetrating Radar

Although satisfactory performances were observed in chapter 3 when the simple printed dipoles were closer to soil, it is important to analyse this particular bowtie

antenna in its operating environment before implementing it in a practical system. The input and radiation characteristics were therefore analysed when soil was in the vicinity of the antenna element. Accurate practical measurements of the radiation pattern in subsurface is difficult due to the complexities involved in such measurement, hence the numerical FDTD techniques were employed to calculate the radiation characteristics in the subsurface.

6.4.1. FDTD Modelling

The input and radiation characteristics were analysed incorporating soil in the FDTD model discussed in section 6.3.3. Homogenous soil was modelled with a dielectric constant of 4 (equivalent to sandy loam), which was placed 2 wavelengths (at 1GHz: 600mm) from the antenna element, figure 6.7. Probes were placed in the model to measure the field levels.

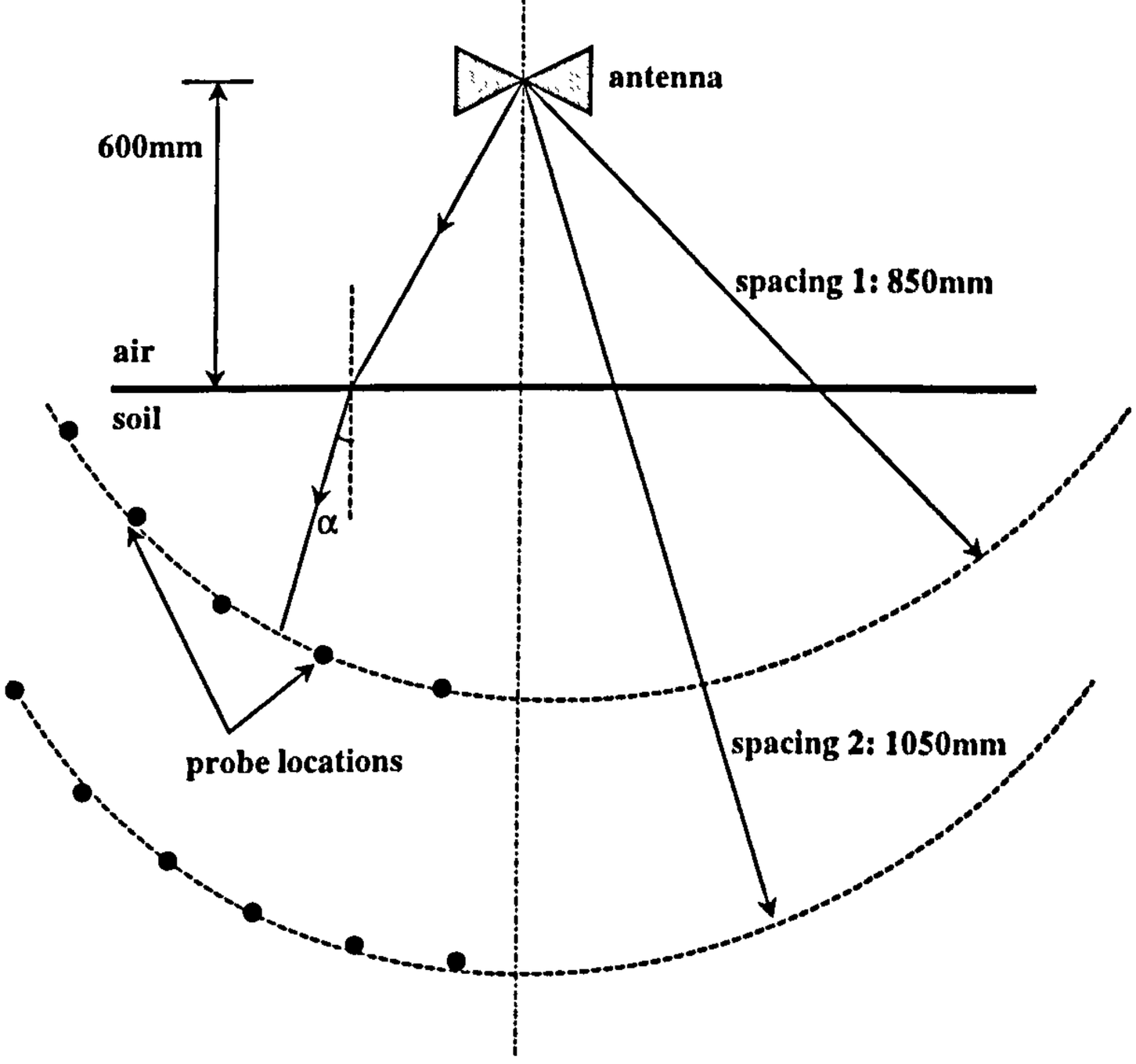

Figure 6.7 FDTD model for near-field calculations

6.4.2. Numerical Results and Measurements.

The measured input response and the calculated input response were barely distinguishable from that in figure 6.4 as the 2 lambda spacing between antenna and soil producing minimal effects on the input response. The calculated in-soil radiation patterns (against convergent angle α) are shown in figure 6.8. In these calculations the refraction at the air-soil interface was taken into account and the patterns were calculated using the probes as shown. The refraction effects are important since the converging angle is the primary concern of the PRSF technique. Two sets of calculations were performed to verify these analysis by calculating the patterns at two different constant spacing (850mm and 1050mm) from the antenna. The constant spacing was maintained in order to have approximately equal spreading losses. Only the E plane patterns were calculated in this method as the wide H plane patterns need very large computational space.

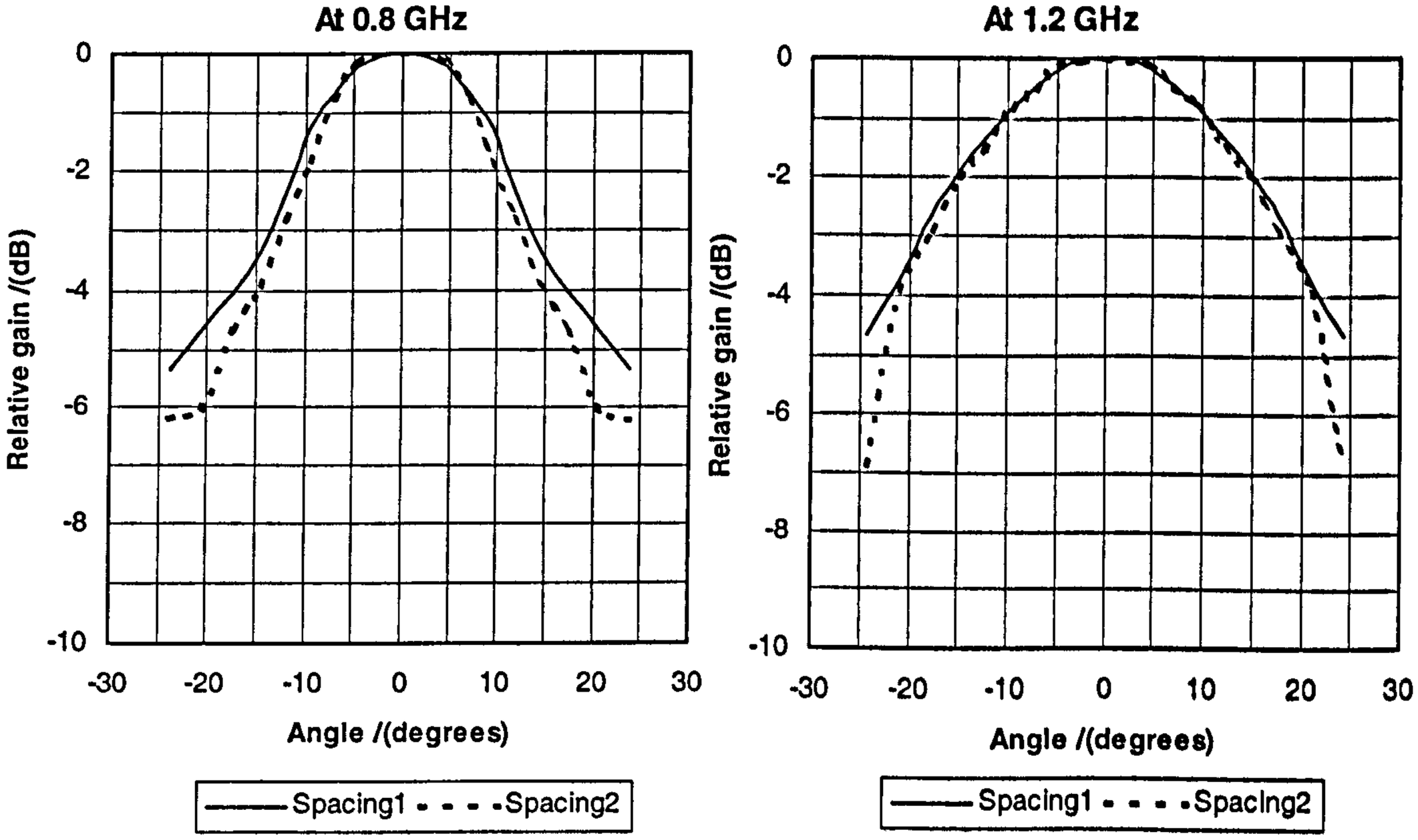

Figure 6.8 Calculated in-soil radiation pattern on the E plane

The calculated radiation patterns in figure 6.8 are similar to figure 6.5 in shape with reduced in-soil half power beam widths. This reduction in beamwidth is due to refraction of the electromagnetic waves at the air-soil interface.

6.5. Bowtie Antenna Design with Absorbing Back Plane

Having performed the initial bowtie antenna design it was necessary to investigate the antenna behaviour when the absorbing back plane was present because the bowtie antenna has different physical shape and characteristics from that of a simple printed dipole.

The vertically placed bowtie element was designed with a metallic back plane to screen the system from possible interference and to enhance the gain of the element. The metallic back plane was placed at $\lambda/4$ from the Bowtie dipole. Analysis in chapter 3 showed that the metallic back plane introduces reverberations and an absorbing back plane was a possible solution to this problem, though obviously reduced the gain of the system.

6.5.1. Absorbing Back Plane

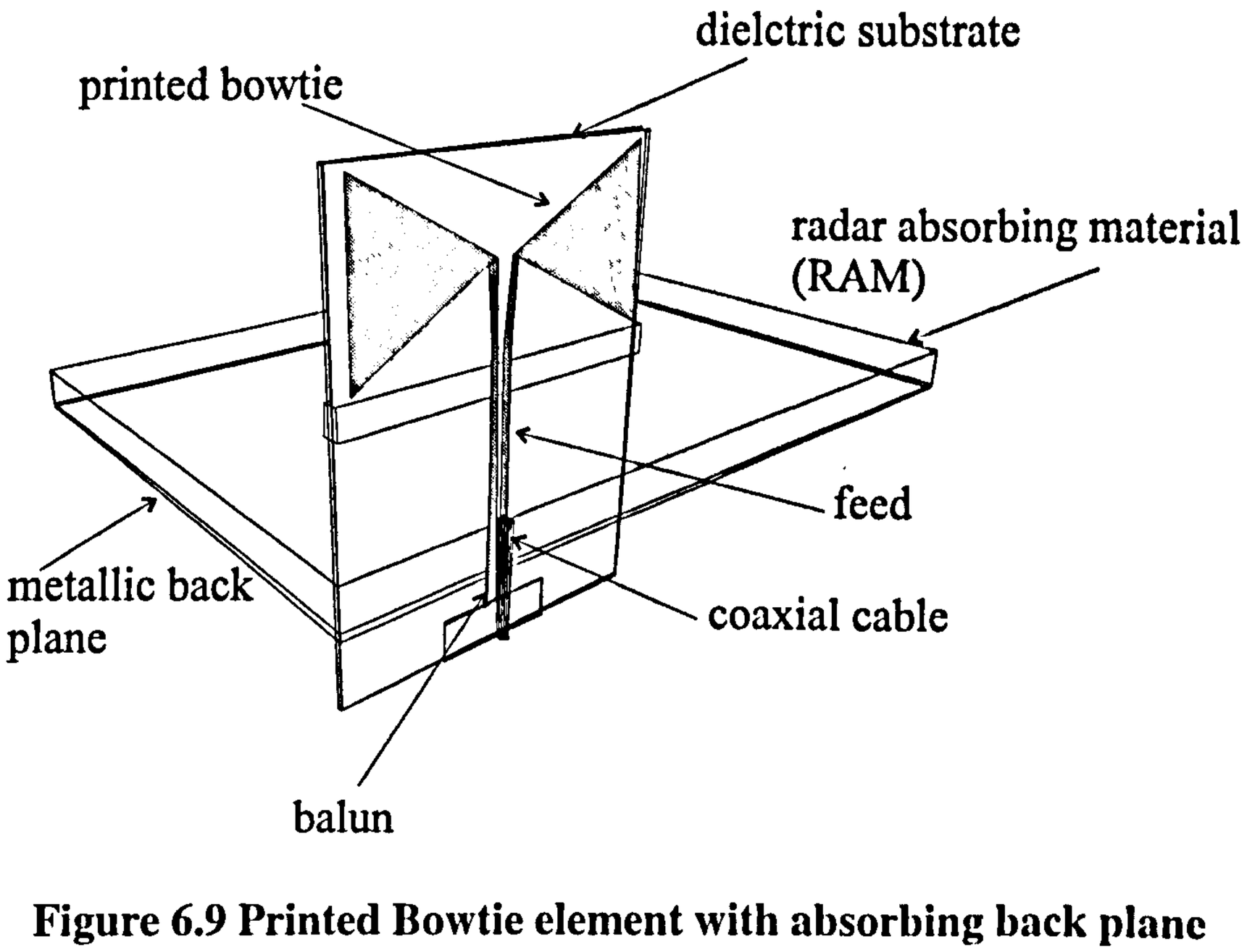

Figure 6.9 Printed Bowtie element with absorbing back plane

Radar Absorbing Material (RAM)- carbon loaded foam, was introduced between the bowtie element and the metallic antenna back plane as in figure 6.9. The RAM was 40mm thick (sufficient thickness to absorb the reverberating signals) and glued to the metallic back plane. Adequate spacing was allowed between feed and the absorbing layer.

Inclusion of an absorber to the bowtie element would partly absorb the transmitting energy and will have some effects on the radiation patterns. Generally, the energy, which reflects from a metallic back plane, placed at λ/4 from the element will enhance the radiated energy. However, for the wide band antenna element considered here such a λ/4 effect is of little use, since this separation would only apply to a narrow frequency band.

6.5.2. Antenna Performance with Absorber

The input response and far-field radiation patterns of the antenna element with absorbing back plane were measured. The measured return loss shown in figure 6.10 is almost similar to figure 6.4 as the metallic back plane partly eliminates the reflections.

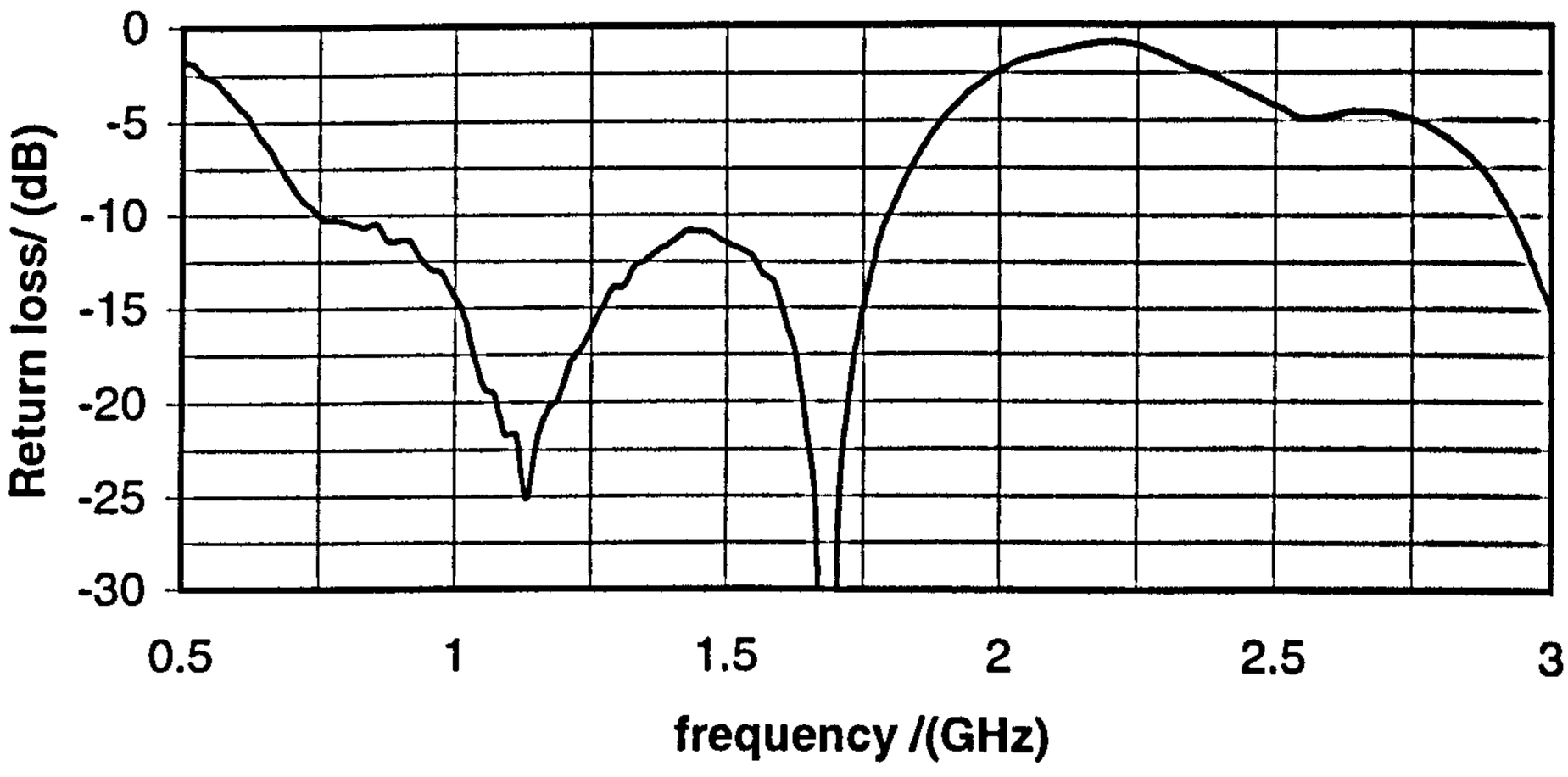

Figure 6.10 Input response of bowtie with absorbing back plane

The measured far-field radiation patterns shown in figure 6.11 and figure 6.12 indicate a good improvement as the λ/4 effect is partly eliminated. These patterns shows that the incorporation of an absorber gives a wider pattern over a larger frequency band. Only the –10dB impedance match of element-feed (1.3GHz ± 0.5GHz ≅ 80%), realistically limits the operating bandwidth. Hence the requirements of the system to transmit narrow band pulses can be met with the inclusion of the absorbing back plane.

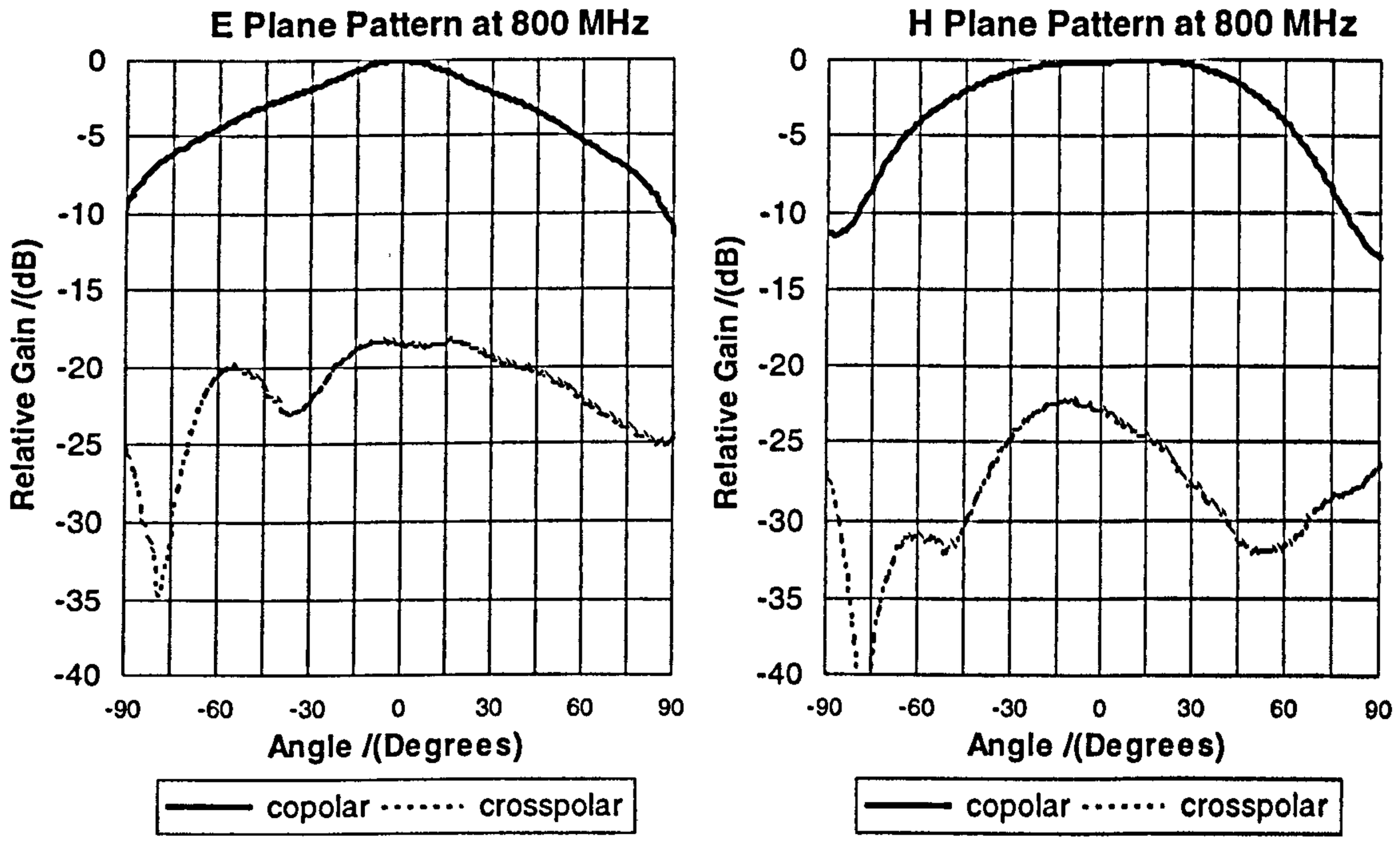

Figure 6.11 Measured far-field radiation patterns at 0.8GHz

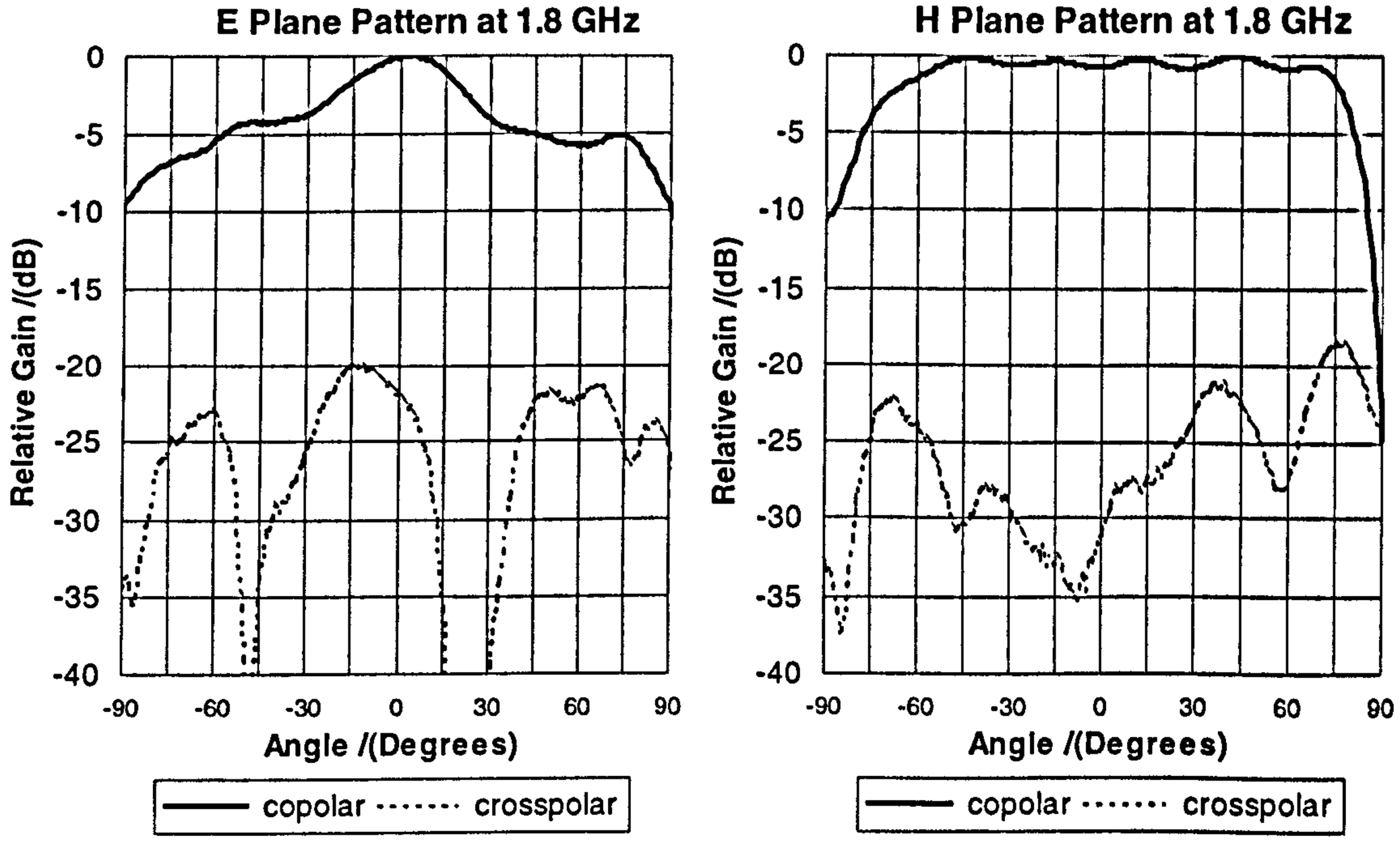

Figure 6.12 Measured far-field radiation patterns at 1.8GHz

The relative on axis (0^0) radiated power levels were also measured during these measurements and the power levels with and without the back plane are given in table 6.1.

	Maximum signal level/(dB) (relative to 0.8GHz)		
Frequency/ (GHz)	0.8	1.2	1.8
Without absorbing back plane	0	-0.04	-
With absorbing back plane	-3.2	-1.8	-5.0

Table 6.1 Maximum radiated signal levels

The measured maximum signal levels show that the power degradation is about 3.2dB at 0.8GHz and 1.8 dB at 1.2GHz. This degradation is because of beam widening and partial absorption of the reflected signals.

These analyses show that the bowtie element with an absorbing back plane has a better characteristic than the previously employed printed dipole antenna element. For the PRSF-GPR system considered in this thesis, the bowtie element should also function in an array and hence the next section considers the bowtie in an array set-up.

6.6. Antenna Array

Analysis with FDTD simulations indicated that the mutual couplings between collinear elements are high compared to equally spaced broadside elements. Hence a staggered arrangement as in figure 6.13 was considered and found to give almost equal mutual couplings between neighbouring elements.

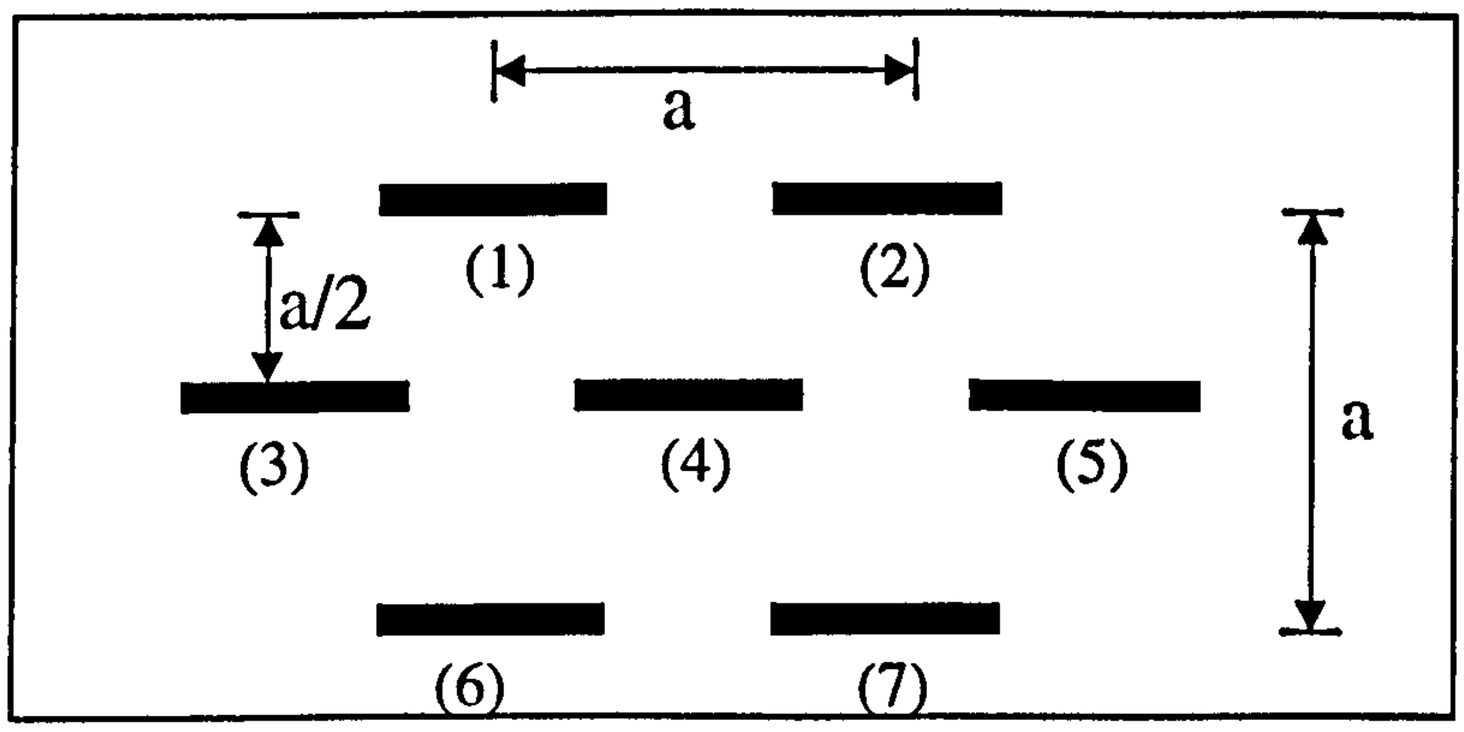

Figure 6.13 Array configuration

In the PRSF-GPR system one element will transmit at a time and all other relevant elements will receive the scattered signals. Hence the *active element pattern* (i.e. while

one transmitting other elements in the array are terminated with matched loads) is important since degradation of the beam patterns will effect the resolutions of the system. Although the FDTD analysis in chapter 3 agreed with the predicted resolutions, only broad side elements were employed in that analysis.

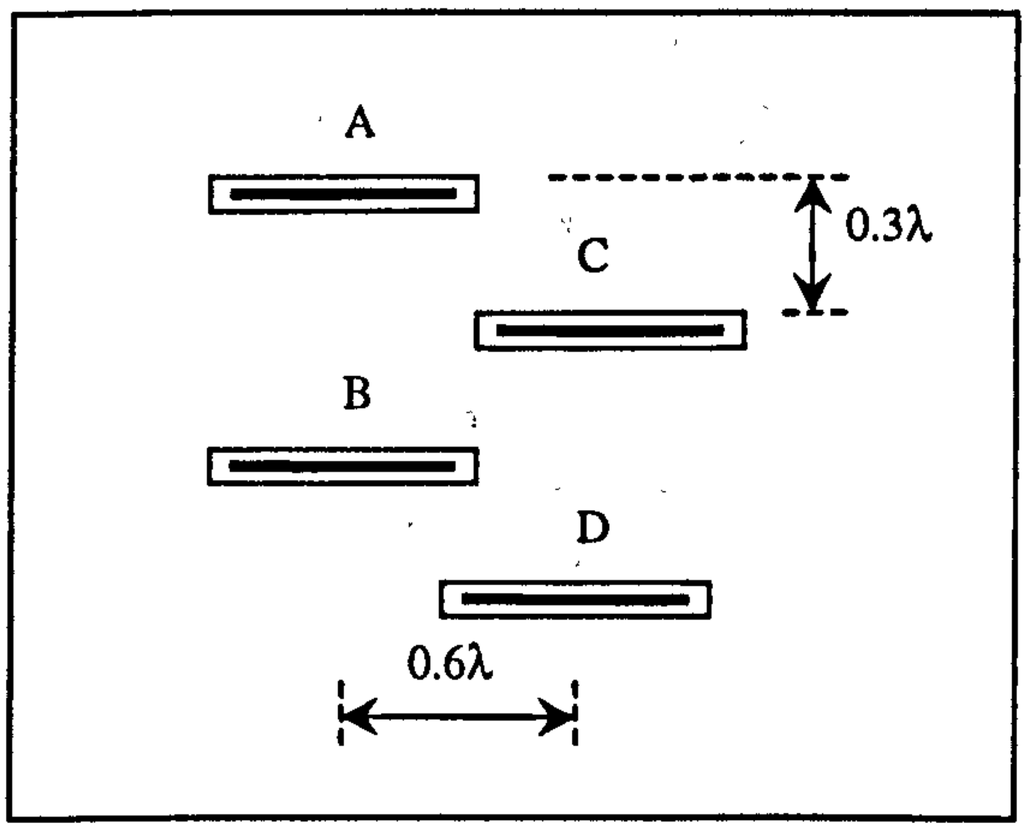

Figure 6.14 Array configuration used in the measurements

In order to get a better understanding of the coupling in an array, the mutual couplings and active element radiation patterns were measured for a 2x2 element antenna array with 0.6λ spacing. The array employed in this measurement is shown in figure 6.14.

Measurements from an array with a=0.6λ spacing gave less than -15 dB mutual coupling between the neighbouring elements in the frequency range of interest. A selection of measured mutual couplings are shown in figure 6.15.

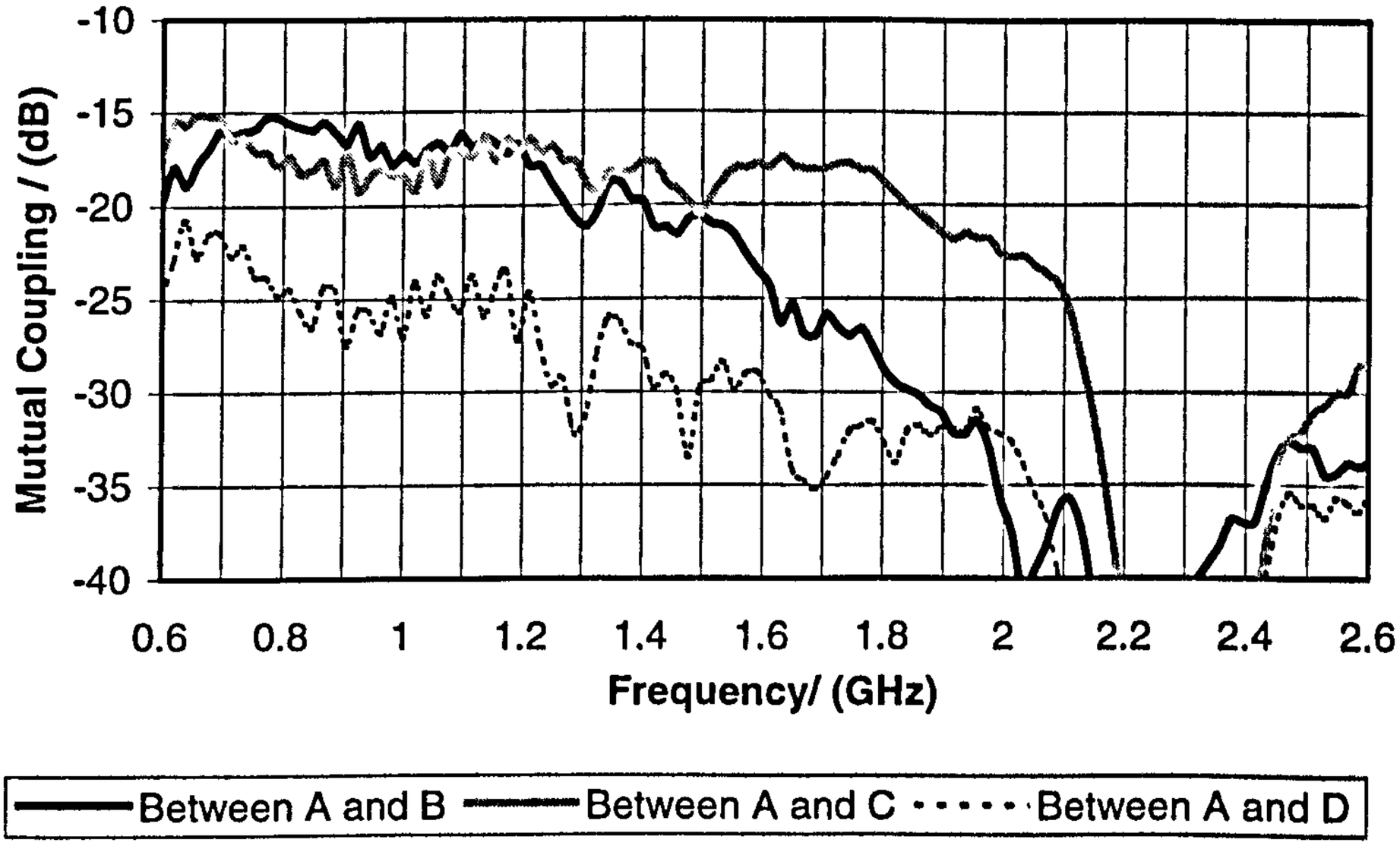

Figure 6.15 Mutual Coupling between elements

The active element pattern of element C was measured on the principal planes at 1GHz. The measured radiation patterns are shown in figure 6.16.

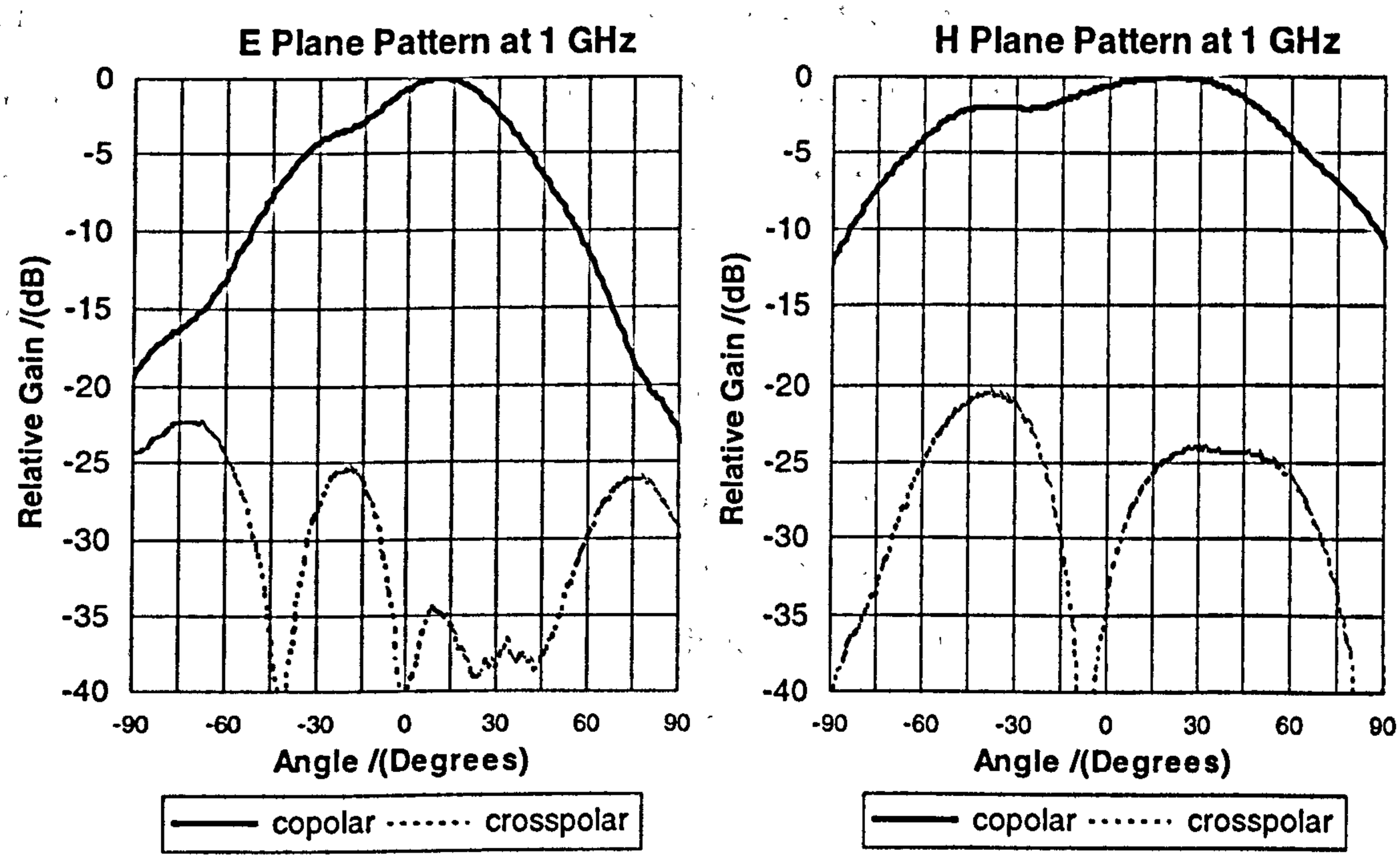

Figure 6.16 Radiation pattern of a four element array at 1GHz

As expected, the measured radiation patterns shows beam squinting and some degradation compared to the isolated antenna patterns, though these are also considered to be acceptable, since there are no formation of nulls in the range of $\pm 45^0$. The mutual coupling between elements and the non-symmetrical nature of the array configuration are the main factors, which contributed to this behaviour. Measurements at higher frequencies also displayed similar degradations. The mutual coupling effects can be minimised by increasing inter element spacing though this will also effect the processing gain of the system. The optimum separation would need further investigations and is outside the scope of this work.

6.7. Conclusions

This chapter presented an antenna element design for the PRSF-GPR system and has included details of balun and impedance matching. The FDTD techniques have been successfully employed for the design, and the final design has been compared with practical measurements. The bowtie element had -10dB return loss bandwidth from

0.8GHz to 1.8GHz (80%). However the useful radiation patterns were limited to about 40% because of a null formation around 0^0 (boresight). Analysis indicated that this null formation was due to the $\lambda/4$ separation between the element and the metallic back plane in which λ corresponded to 1GHz. The measured H-plane co-polar response was broad, with a -3 dB beamwidth of $\pm 50^0$ at 0.8GHz and $\pm 55^0$ at 1.2GHz. The E-plane co-polar response was narrower than the H-plane response, having a -3dB beamwidth of $\pm 30^0$ at 0.8GHz and 1.2GHz.The in-soil radiation patterns have also been computed with the FDTD techniques and showed satisfactory performance in soil.

Furthermore, the effects of the absorbing back plane on the bowtie element have been analysed with practical measurements. The measured input response displayed negligible differences to the element without the absorber. However, the radiation patterns showed remarkable improvements with the elimination of the null at 0^0 giving useful radiation patterns from 0.8GHz to 1.8GHz. The only drawback was that the maximum radiated signal strength was reduced because of beam widening and partial absorption of the reflected signals.

Finally the bowtie antenna element in an array configuration has been analysed with practical and numerical methods and showed expected beam squinting but not to an unacceptable level. The optimum spacing between elements and techniques to reduce mutual couplings need further investigations and it is outside the scope of this thesis.

References

[1] R.P.Dooley, X-band Holography, *Proceedings of the IEEE*, vol. 53, pp. 1733-735, 1965.

[2] D.J.Daniels, *Surface Penetrating Radar*, IEE, 1996.

[3] C Balanis, *Antenna Theory Analysis and Design*, John Willey & sons, NewYork, 1982

[4] D.J.Daniels, D.J.Gunton and H.F.Scott, Introduction to Subsurface Radar, *Proceedings of the IEE*, vol. 135, Pt. F, no. 4, pp. 278-320, 1988.

[5] E.A.Theodorou, M.R.Gorman, P.R.Rigg and F.N.Kong, Broadband Pulse Optimised Antenna, *Proceedings of the IEE*, vol. 128, Pt. H, no. 3, pp. 124-130, 1981.

[6] D.J.Daniels, Short Pulse Radar for Stratified Lossy Dielectric Layer Measurements, *Proceedings of the IEE*, vol. 127, Pt. F, no 5, 1980.

[7] J.D.Kraus, *Antennas*, McGraw-Hill, London, 1950.

[8] L.Carin, N.Geng, M.McClure, J.Sichina and L.Nguyen, Ultra Widwband Synthetic Aperture Radar for Mine Field Detection, *IEEE Antennas and Propagation Magazine*, vol. 41, no. 1, pp. 18-33, 1999.

[9] A.Z.Botros, A.D.Olver, L.G.Cuthbert and G.Farmer, Microwave Detection of Hidden Objects in Walls, *Electronics Letters*, vol. 20, no. 9, pp. 379-380, 1984.

[10] T.E.Morgan, Spiral Antennas for ESM, *Proceedings of the IEE*, vol. 132, Pt. F, no. 4, pp. 245-251, 1985.

[11] J.G.Maloney and G.S.Smith, A study of Transient Radiation from the Wu-King Resistive Monopole – FDTD Analysis and Experimental Measurements, *IEEE Transactions on Antennas and Propagation*, vol. AP-41, no.5, pp.668-675, 1993.

[12] T.L.By, F.Kong and H.Westerdahl, Geo-Radar Development at the Norwegian Geo-technical Institute, *Proceedings of the 4th International Conference on Ground Penetrating Radar*, pp. 21-28, 1992.

[13] L.Peters, J.J.Daniels and J.D.Young, Ground Penetrating Radar as a Subsurface Environmental Sensing Tool, *Proceedings of the IEEE*, vol. 82, no. 12, pp. 1802-1822, 1994.

[14] G.H.Brown and O.M.Woodword Jr, Experimentally Determined Radiation Characteristics of Conical and Triangular Antennas, *RCA Review*, vol. 13, pp. 425-452, 1952.

[15] C.E.Smith, C.M.Butlare and K.R.Umashankar, Characteristics of Wire Biconical Antenna, *Microwave Journal*, pp. 37-40, Sep 1979

[16] G.S.Smith and W.R.Scott, A Scale Model for Studying Ground Penetrating Radar, *IEEE Transactions on Geoscience and Remote Sensing*, vol. GE-27, no. 4, pp. 358-363, 1989.

[17] Z.Junrong, L.Fengyu, W.Hongqi, C.Meng and H.Yan, The Development of Subsurface Impulse Imaging Radar and its Applications, *Proceedings of the 4th International Conference on Ground Penetrating Radar*, pp. 71-77, 1992.

[18] G.Oltman, The Compensated Balun, *IEEE Transactions on Microwave Theory and Techniques*, vol. MTT-14, no. 3, pp. 112-119, 1966.

[19] K.C.Kupta, R.Garg and I.J.Bahl, *Microstrip Lines and Slotlines*, Artech House, 1979.

[20] G.Mur, Absorbing Boundary Conditions for the Finite Difference Approximation of the Time Domain Electromagnetic Field Equations, *IEEE Transactions on Electromagnetic Compatibility*, vol. EMC-23, no. 4, 1981, pp. 377-382

7. Analysis and Comparisons of PRSF-GPR with Practical Measurements

7.1. Introduction

The PRSF-GPR has been theoretically analysed in chapters 2,3,4 and 5. This chapter analyses and compares the predictions with practical measurements. The antenna element developed in chapter 6 is used for the construction of an 8 element linear array. Since the bandwidth of the test equipment allowed measurements up to 1.5GHz, all measurements and comparisons were performed at 1GHz. These measurements have been conducted at the GPR measuring facility at the University of Bristol (see Appendix D) with different array configurations (number of elements, inter element spacing) as the construction of the measuring facility was progressively developed.

The FDTD model presented in chapter 3 was modified to incorporate the bowtie elements (Chapter 6) at 1GHz and this model is used for all the analyses in this chapter. The comparisons include the time domain signals, resolutions, signal power and the clutter returns, which have been analysed in the previous chapters. This chapter also considers a method to measure the dielectric properties of soil and the improvements with processing methods such as adaptive techniques and the use of the later part of signal for near surface detection.

7.2. Dielectric measurements

In the past, several techniques have been employed to measure the average dielectric properties of soil such as,

- The wave guide transmission technique [1].
- Free-space transmission technique (employing two antennas) [2].
- Single probe method [3, 4].
- Time domain reflection method [5], dielectric probes.

Dielectric properties measured using these techniques are available in the published literature and some were described in chapter 5. Most of these techniques use a soil sample for the measurements rather than measurements in the field (except the single probe method). Placing the sample in these devices requires extra care to avoid unwanted reflections, which will modify the measured results, hence a different technique is employed in this section to give accurate measurements in the field.

The complex dielectric constant of soil, which is used with comparisons (slightly wet loamy soil), was measured using ground probes, figure 7.1. The ground probes were matched to the soil at 1GHz to perform the measurements at the operating frequency of the PRSF system. Although it is matched at this frequency, matching is not critical for this type of measurement technique.

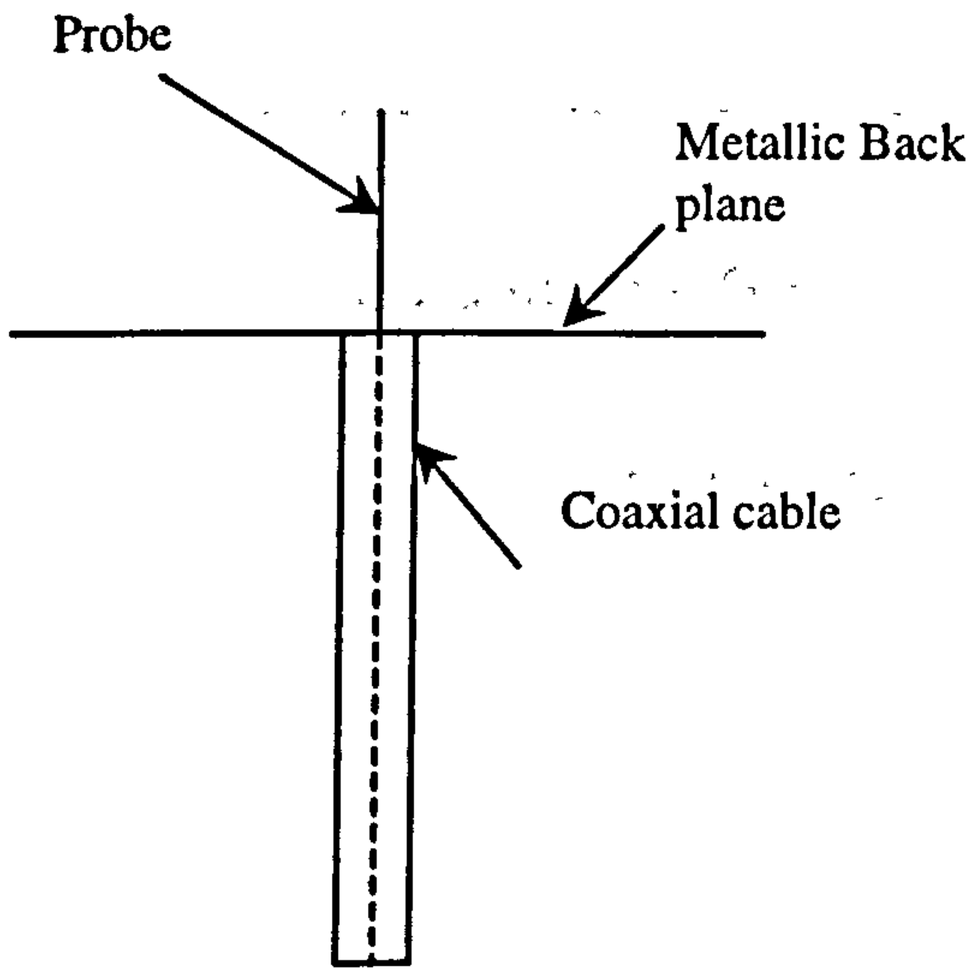

Figure 7.1 The ground probe

The ground probes employed in these measurements were monopoles with a metallic back plane, and were inserted in the ground with the back plane on the soil-air interface. The back plane was sufficiently large to ensure the measured dielectric properties do not significantly incorporate the free space characteristics.

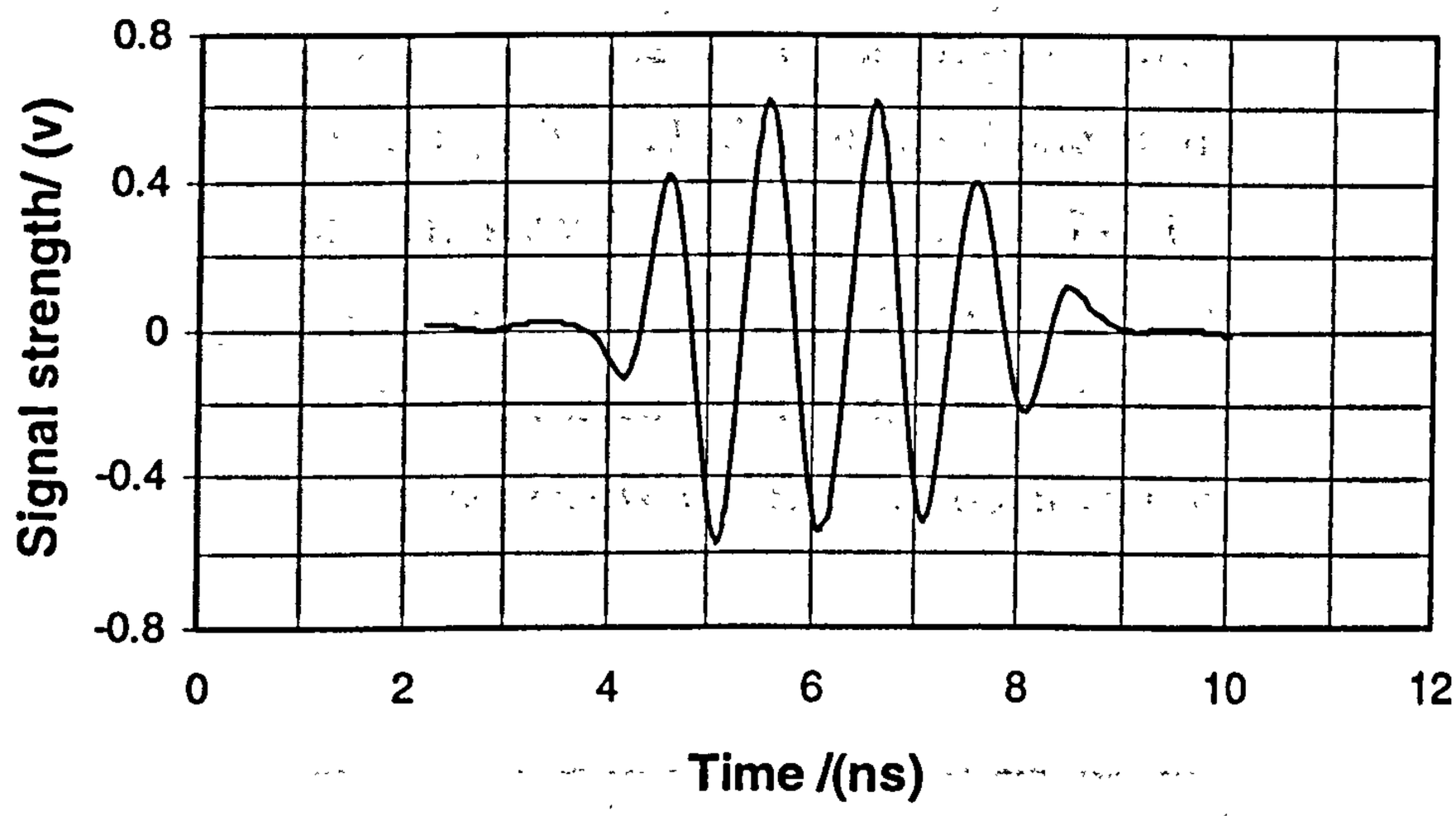

Figure 7.2 Transmitted signal

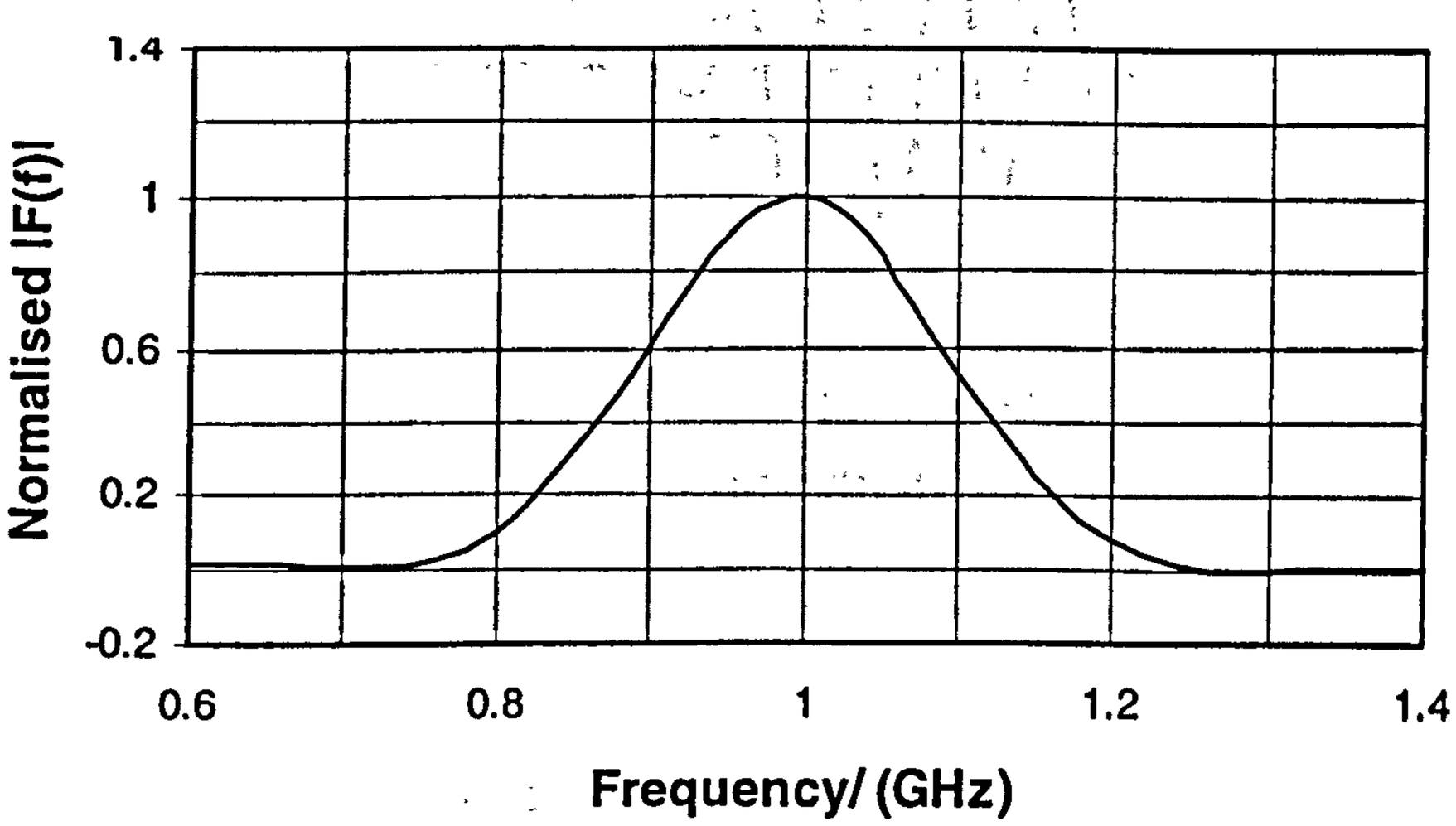

Figure 7.3 Spectrum of the transmitted signal

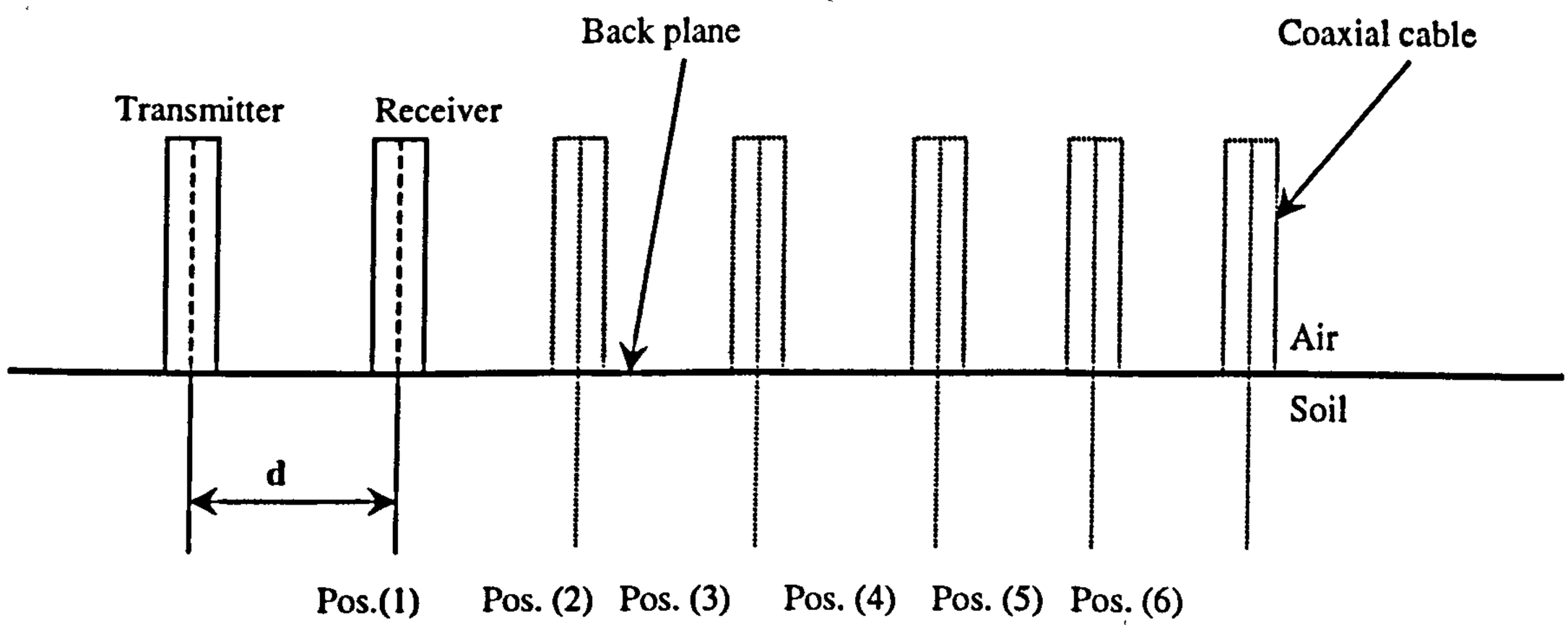

Figure 7.4 Experimental set up for dielectric measurement

A four-cycle pulse at 1GHz (Figure 7.2 and Figure 7.3) was transmitted into the soil using a transmitting ground probe and observations were made at eight different receiving locations using the second probe as in figure 7.4. Figure 7.5 shows the received signal at probe position 6. A four-cycle pulse was employed since it was used with the other practical GPR measurements and theoretical analyses These recorded data were used to calculate the relative dielectric constant and the loss factor of the soil.

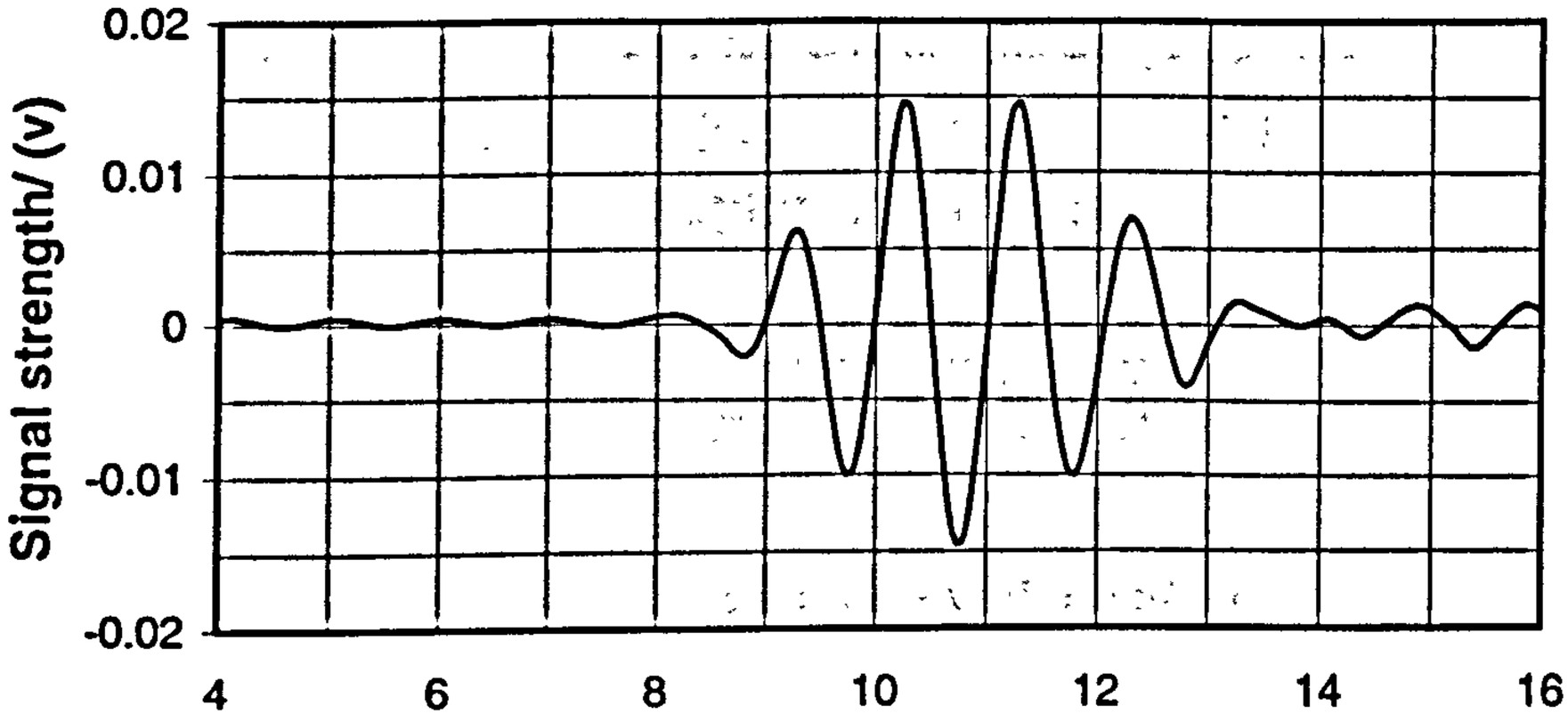

Figure 7.5 Received signal at probe position 6

7.2.1. Relative Dielectric Constant

The average relative dielectric constant of soil can be calculated using the time delay and the displacement relation ship as shown below,

$$d = c_{soil}\, t \tag{7.1}$$

where,

c_{soil} : velocity in soil

d : displacement from transmitter

t : time delay

$$t = \frac{\sqrt{\varepsilon_r}}{3x10^8} d \tag{7.2}$$

$$\varepsilon_r = 9x10^{16} \left(\frac{t}{d}\right)^2 \tag{7.3}$$

Equation 7.3 can be used to calculate the dielectric constant of soil. The time delays of the first cycle, associated with the displacements are shown in figure 7.6.

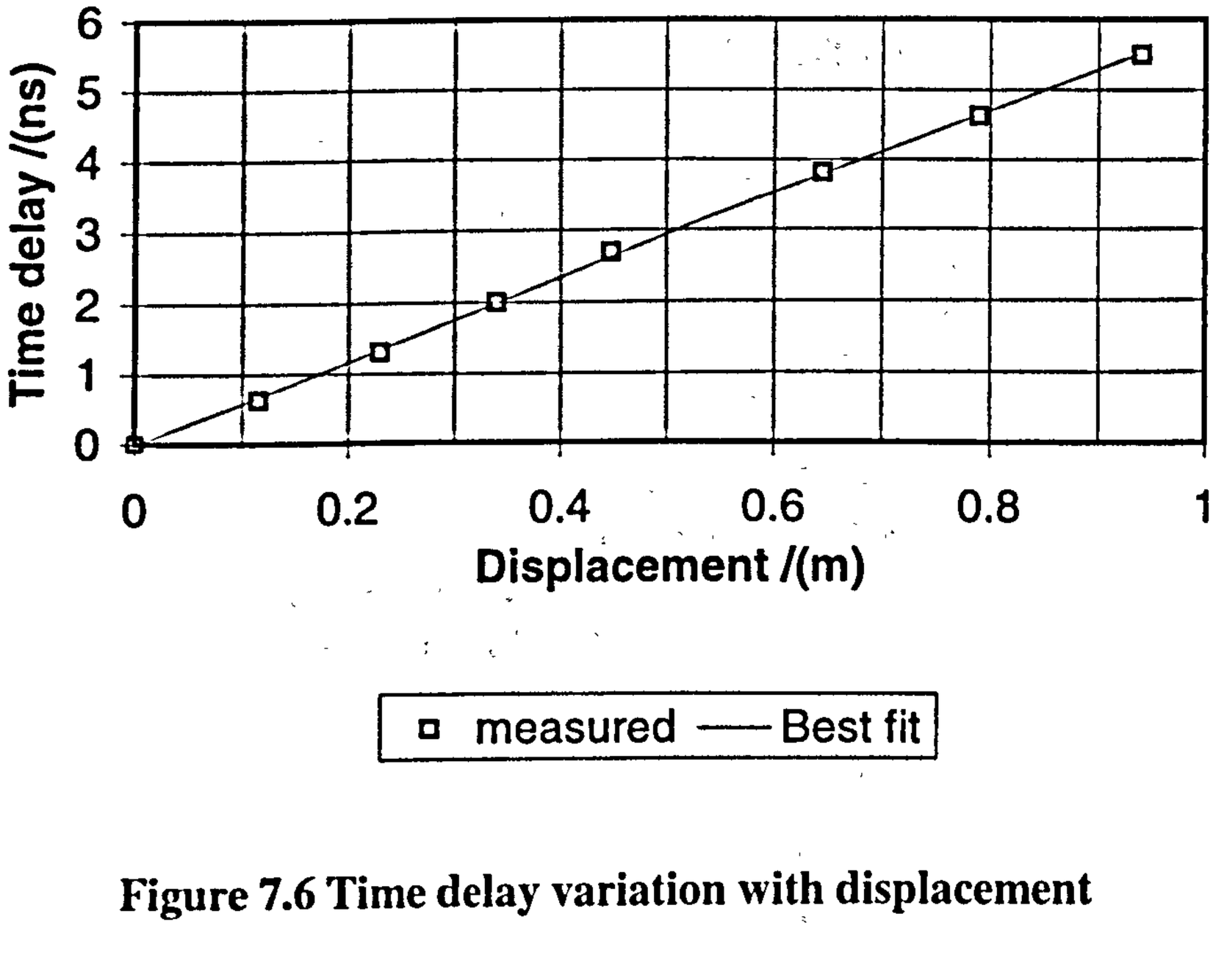

Figure 7.6 Time delay variation with displacement

The gradient of the curve in figure 7.6 was used with equation 7.3 to calculate the dielectric constant of soil.

7.2.2. Loss Factor

The combined conductive and dipolar losses can be calculated from the measured signal power levels at different locations. The formulation of this method is given below. The ratio between the transmitted power and the received power can be given by [6, 7],

$$\frac{P_r}{P_t}=\left[\frac{\lambda_{soil}}{4\pi d}\right]^2 \times e^{2\alpha} \times G \qquad (7.4)$$

where

P_r :Received power

P_t :Transmitted power

α :Soil attenuation coefficient.

d :distance between transmitter and the receiver.

G :Transmitter receiver gain.

$$\alpha = 2\pi df\sqrt{\frac{\mu_o\mu\varepsilon_o\varepsilon_r\left[\sqrt{\left(1+\tan^2\delta\right)}-1\right]}{2}} \tag{7.5}$$

$$\tan\delta = \frac{\varepsilon_r^{"}}{\varepsilon_r}$$

So equation 7.4 becomes :

$$P_r = \frac{K}{d^2}e^{2\alpha_1 d} \tag{7.6}$$

where,

$$K = \left[\frac{\lambda_{soil}}{4\pi}\right]^2 \times G \times P_t$$

$$\alpha_1 = 2\pi f\sqrt{\frac{k_1\left[\sqrt{\left(1+\tan^2\delta\right)}-1\right]}{2}}$$

$$k_1 = \mu_o\mu\varepsilon_o\varepsilon_r$$

In log format,

$$\log\left(P_r.d^2\right) = 2\alpha_1 d + \log(K)$$

This relationship can be expressed in $y = mx + c$ format, hence

$$\varepsilon_r^{"} = \varepsilon_r.\sqrt{\left(\left\{\frac{2}{k_1}\left[\frac{\alpha_1}{2\pi f}\right]^2+1\right\}^2-1\right)} \tag{7.7}$$

The received signal powers at different probe locations were estimated through Fourier transformation of the received signal at 1GHz. Signal strength variation with displacement is shown in figure 7.7.

The gradient of the curve in figure 7.7 was used with equation 7.7 to estimate the complex dielectric constant of soil. In figure 7.6 the measured values closely follow the best-fit curve while in figure 7.7 the measured values deviate slightly from the average. The sensitive nature of equation 7.7 requires precise measurements and probe mismatch (at different locations) and reflections from the sandbox and metallic ground plane edges would have contributed to these errors.

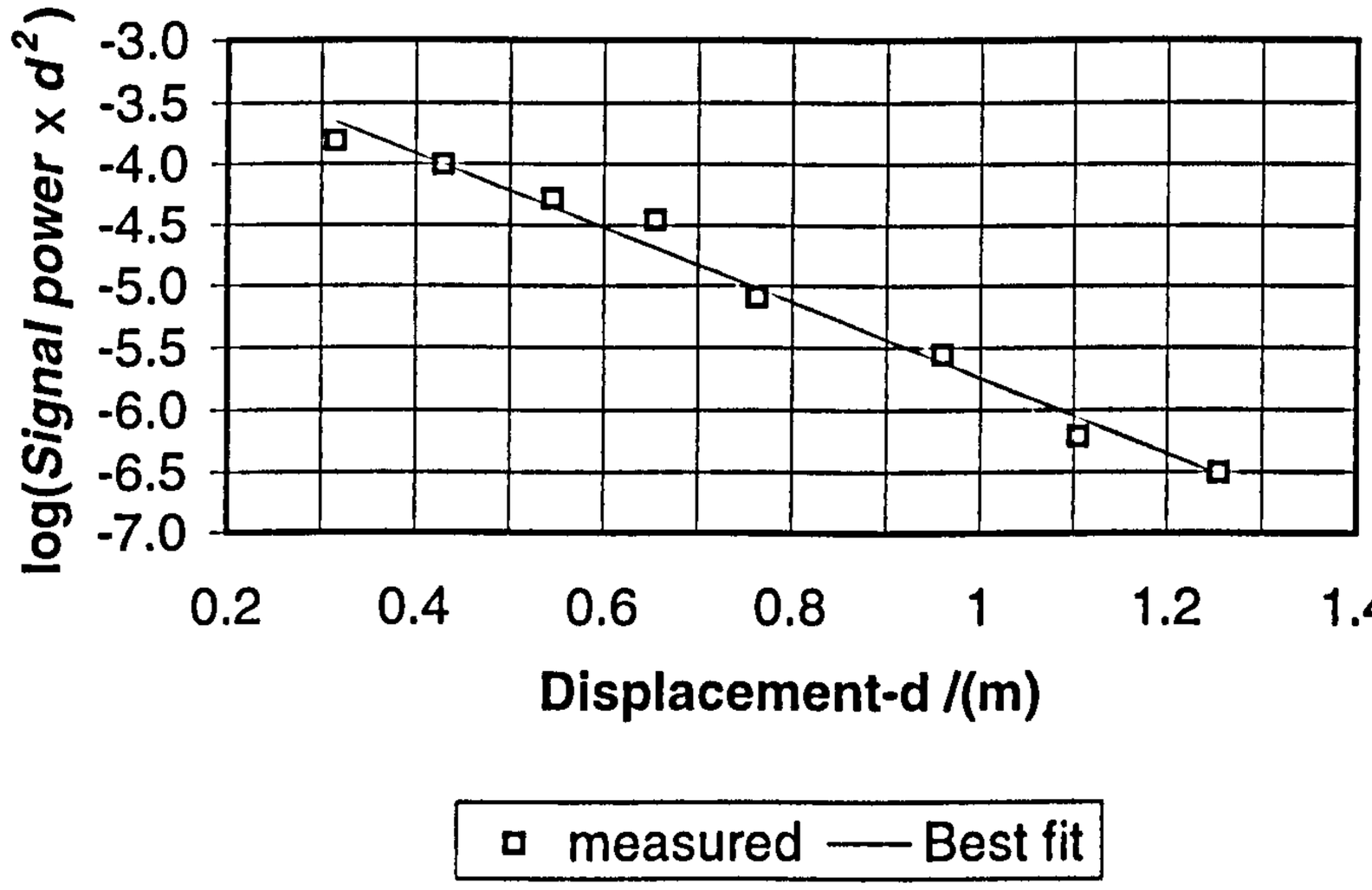

Figure 7.7 Variation of signal strength at 1GHz with displacement

These estimated values were further compared with measurements on soil samples performed using a commercial dielectric probe (HP85070B). This dielectric probe measures the reflection coefficient from a soil sample and the parameters are calculated using some calibrations performed in free space and pure water. The calculated values using the method described in this section and the dielectric probe measurements at 1GHz are tabulated in table 7.1.

Method	ε_r	ε''_r
Ground probes	3.17±0.065	0.26±0.014
Dielectric probe	2.95±0.15	0.21±0.011

Table 7.1 Measured dielectric properties of soil at 1GHz

Differences in the dielectric constant are generally small and would relate to target position error of the order of < 4 mm for a target buried at 200mm. The dielectric probe measurements vary when more pressure is applied on the probe tip, which is normally immersed in the soil sample while performing measurements. Air trapped closer to the probe tip and the sample size will also introduce errors in these

measurements. Hence the values measured using the ground probes method was used in all comparisons performed in this chapter.

7.3. Bowtie FDTD Model and Comparisons

The analytical and practical analyses were compared with the results from a bowtie GPR model. The GPR model presented in chapter 3 was modified to incorporate 8 bowtie elements with the soil modelled with the dielectric properties given in section 7.2. A metal target of 10cmx10cm was positioned at 780mm offset from the first element and 200mm depth in soil. Two wavelengths spacing at 1GHz was maintained between the antenna array and the air-soil interface. The GPR model employed in these analyses is shown in figure 7.8 and this closely resembles the experimental set up shown in figure 7.9.

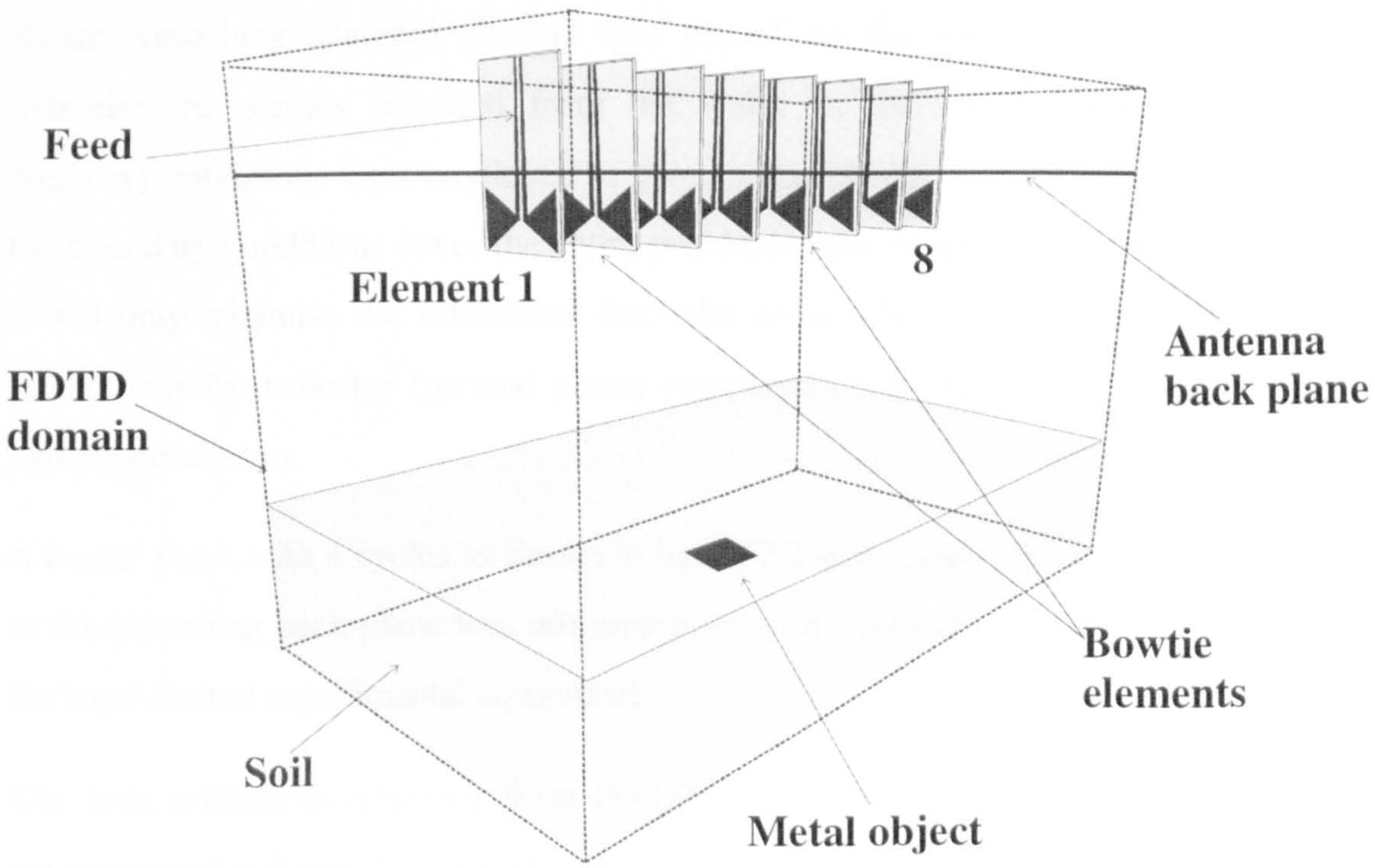

Figure 7.8 The bowtie GPR model (FDTD)

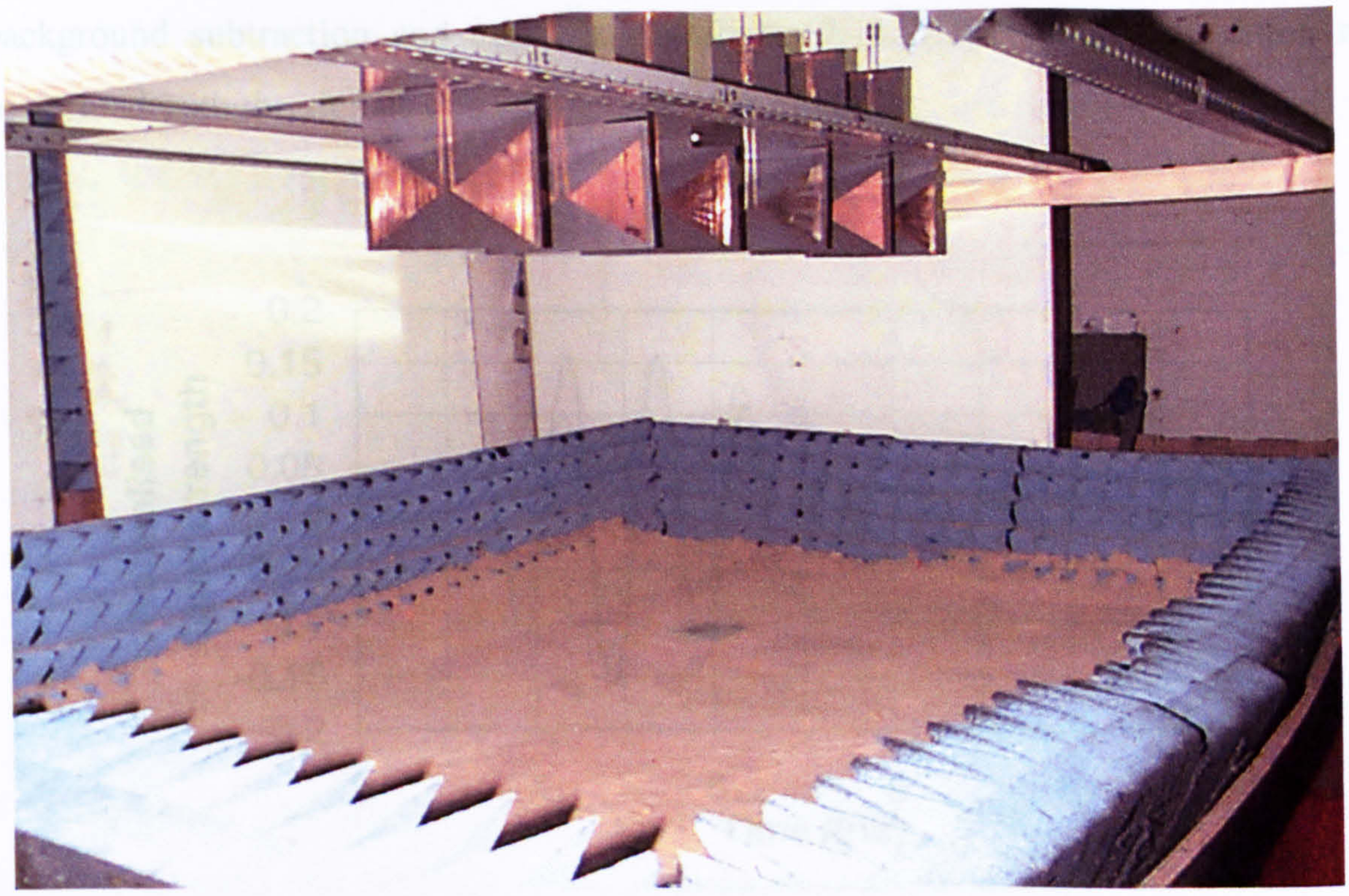

Figure 7.9 The experimental set-up

Radar Absorbing Material (RAM) was placed on the walls of the sandbox to minimise the signals reflected from the walls, in the FDTD model, absorbing boundary conditions were employed to give similar effects. Here in the FDTD model the boundary conditions cover the entire problem space while in the measuring set-up it will only minimise the reflections from the walls. The FDTD model also had an infinite metallic reflector (ground plane) compared to the finite ground plane of the experimental array.

A longer pulse with 4 cycles as shown in figure 7.2 was employed to excite the model as the absorbing back plane was not incorporated in this particular model and due to the band limited experimental equipment.

The total reflections obtained from FDTD simulations and practical measurements are compared in figure 7.10 for element 1 transmitting and element 2 receiving. These signals were normalised with the transmitted signal strength to compare the magnitudes. Although great care was taken to use exactly the same pulse for the excitation of the FDTD model and the measurement system, some minor differences were present. Reflections from a metal plate buried in soil was calculated through

background subtraction and compared in figure 7.11. Background subtraction was performed with the signals obtained without the target.

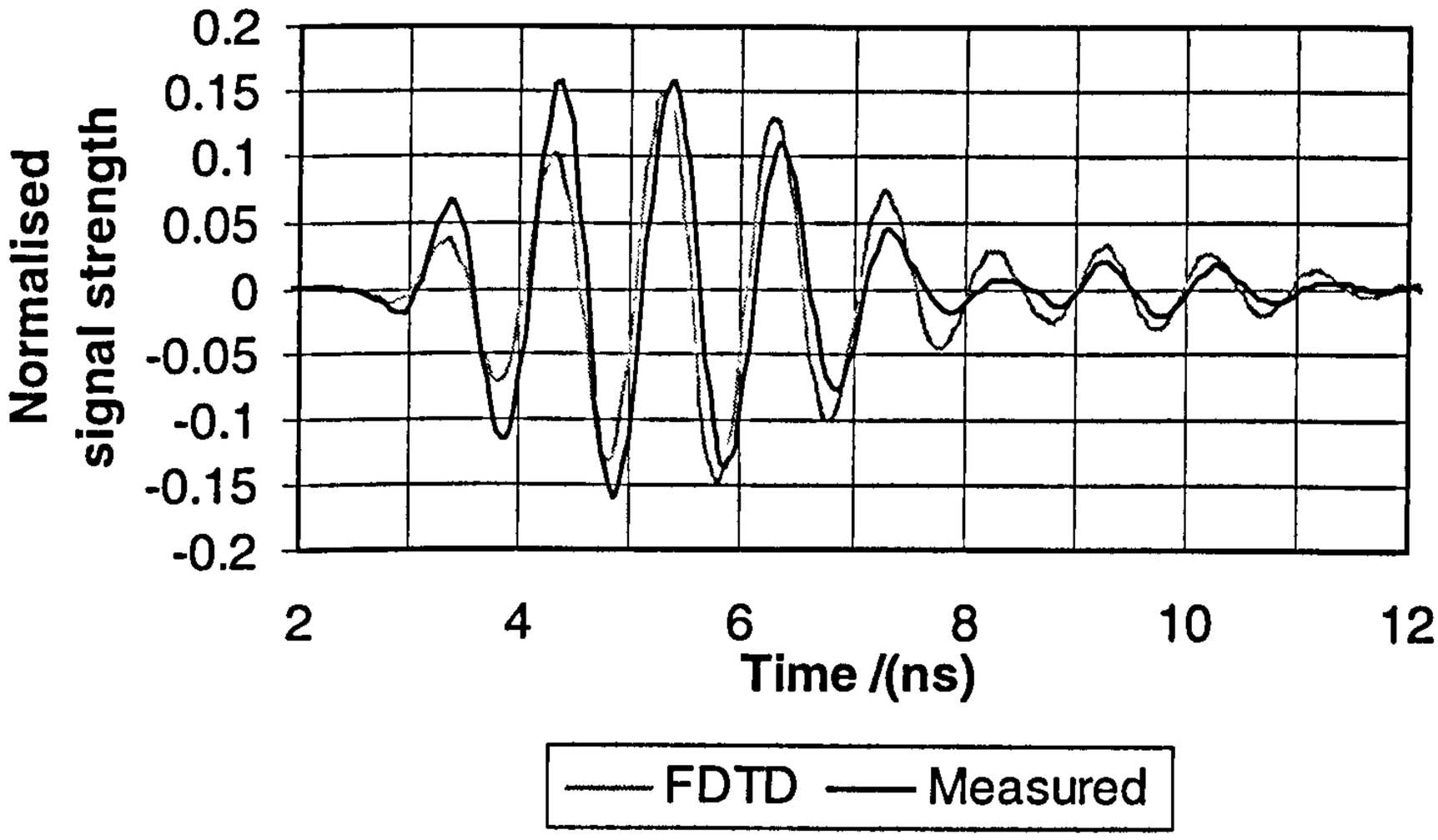

Figure 7.10 Received signal for element 1 transmitting and element 2 receiving (shown in figure 7.8)

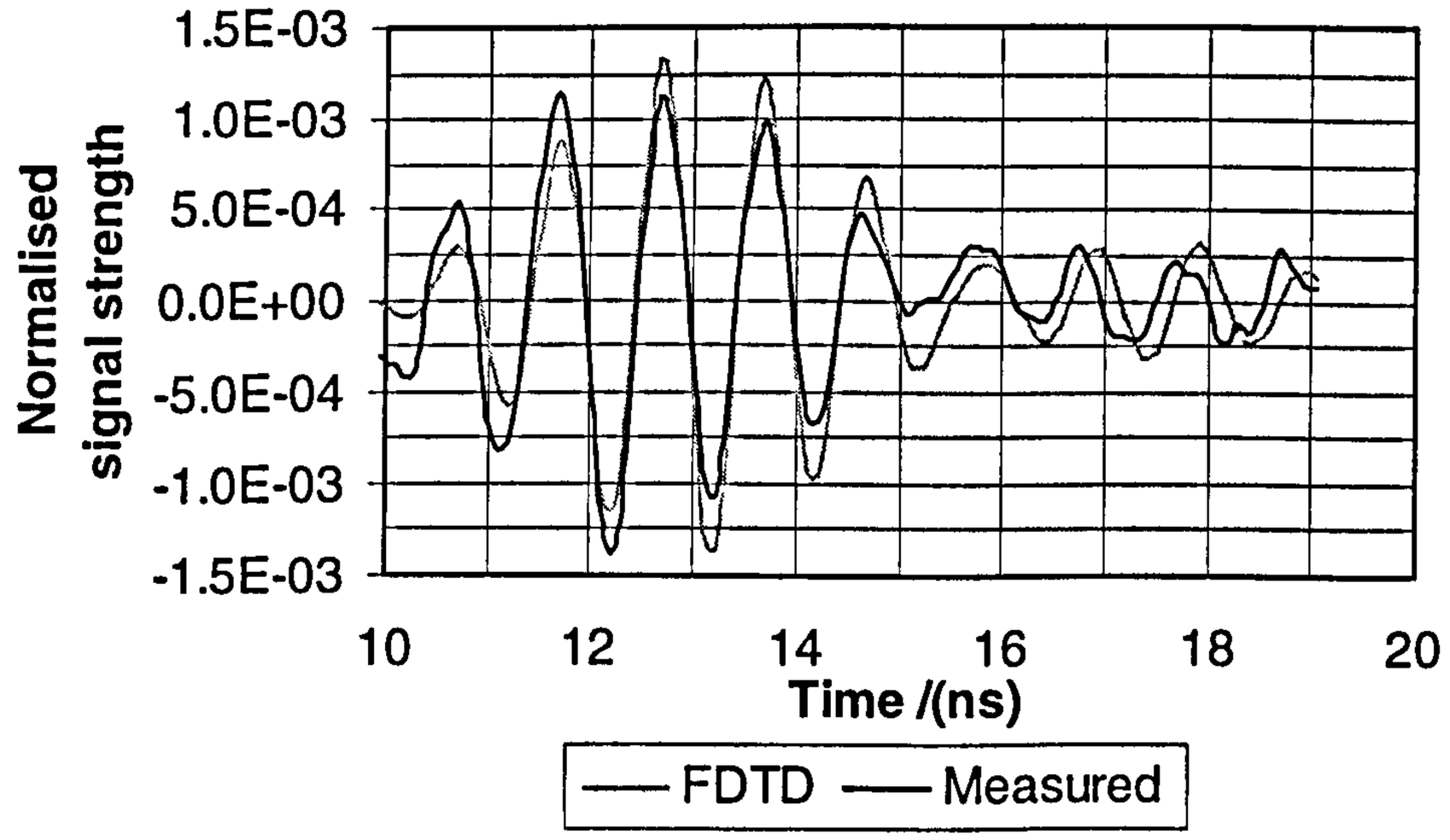

Figure 7.11 Reflections from the buried object

Figure 7.11 shows a very good agreement between the FDTD and the measured results in terms of time delay and amplitude. Although the background subtraction works well with the FDTD results it is not perfect with the measured results. This can be due to several factors such as thermal noise, disturbance in soil and triggering problems with the oscilloscope, which was being used at its limits of operation.

Having compared the calculated time domain signals with the measured signals it is now appropriate to extend the analysis to compare the resolutions associated with the PRSF-GPR system.

7.3.1. Synthetic Focusing and Resolutions

The calculated and measured results from the previous sections were synthetically focussed laterally and vertically to compare the resolutions in these directions. Signals from 14 paths when element 1 and 8 transmitting, were employed in this analysis so as to cover the full convergent angle and to minimise computations with the FDTD. The laterally and vertically focussed signals are shown in figure 7.12 and figure 7.13 respectively.

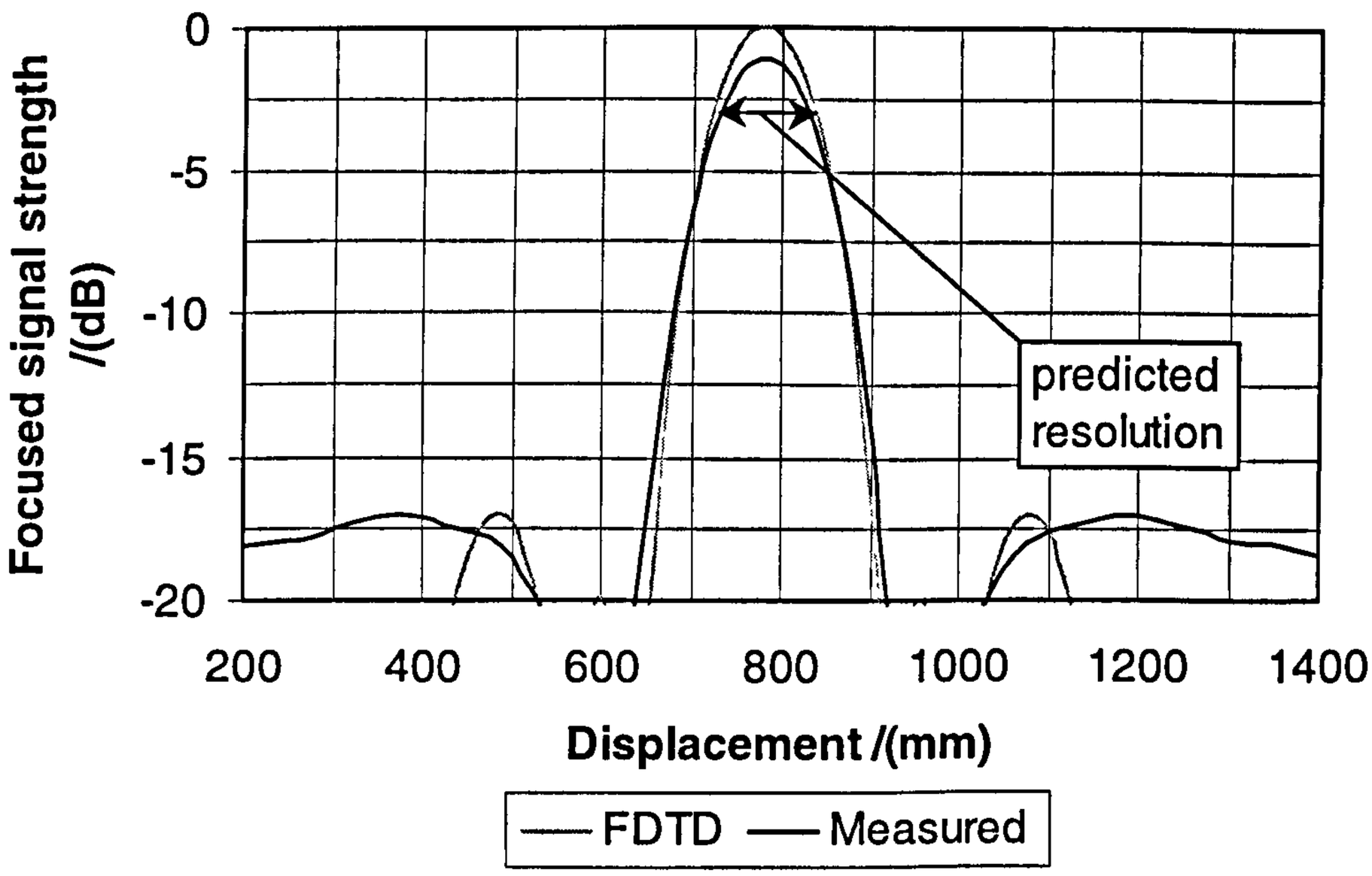

Figure 7.12 Lateral focusing through the target locations of 200mm in soil

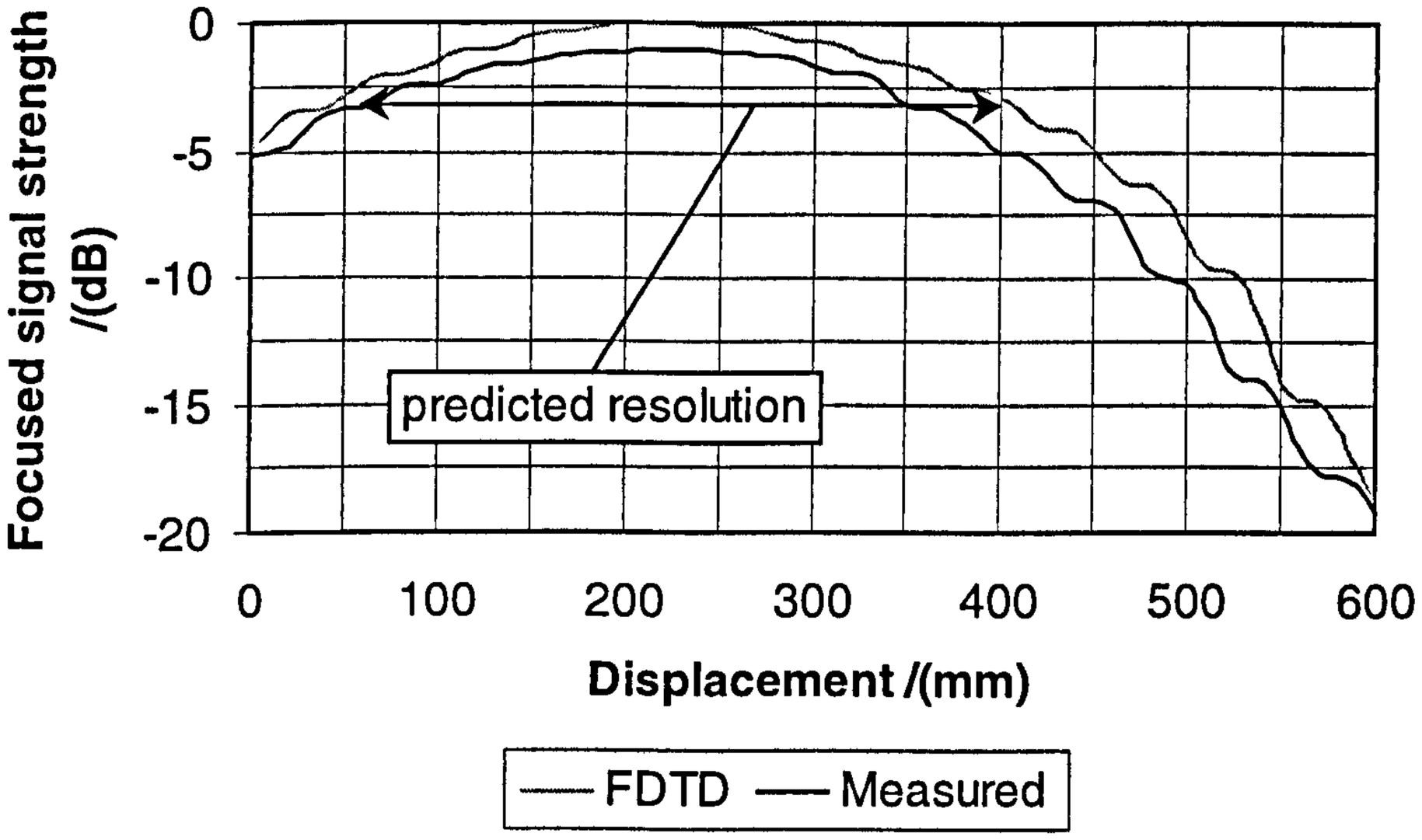

Figure 7.13 Vertical focusing through target location

Figure 7.12 and figure 7.13 show the target at its correct location of 780mm offset and 200mm deep with a lateral resolution of ≈100mm and a vertical resolution of 350mm. These resolutions also agree with the analytical predictions of $\lambda_{air}/(2\theta_{air})$≈90mm and $2\lambda_{soil}$≈340mm, specified in [8]. The focussed signal strengths were normalised with the maximum FDTD levels to compare half power points of the focused signals. Figure 7.12 shows that there are some minor differences between the FDTD and the measured results. Analysis of these differences indicated that the aligning errors in synthetic focusing is the main factor. These aligning errors can be due to,

- Minor errors with the estimated dielectric constant
- Assumption of a homogenous media
- Analytical errors with the path length calculations (antenna positions etc)
- Assumption of flat air-soil interface

These errors can be minimised by aligning the signals adaptively to give maximum signal strength at the target location and to use the same aligning procedure at other resolution cells.

7.3.1.1. Local Adaptive Optimisation

In order to implement a practical adaptive scheme, the adaptive technique must be employed after the target locations are approximately established. This optimisation will minimise the signal spillage into other resolution cells. Most aligning errors described in section 7.3.1 will vary with the path length, longer in-soil paths will have larger aligning errors compared to shorter path lengths. Hence these correcting aligning factors at the target location must be further modified when using at different locations. A simple scheme was employed with the results obtained with a deeply buried metal plate (150mmx150mm) at 300mm depth and 780mm offset.

Unlike the results presented in figure 7.12, the deeply buried targets had more aligning problems due to the in homogeneous nature of soil (The soil was damper at deeper locations). The correction factors (time offsets) for alignment at the target location were scaled with the path lengths to correct errors due to path length variation at other locations as shown in equation 7.8.

$$CF_i = \frac{CF_{target}}{l_{target}} \times l_i \tag{7.8}$$

where,

CF_i :correction factor for location i

CF_{target} :correction factor at target location

l_{target} :path length associated with the target

l_i :path length associated with location i

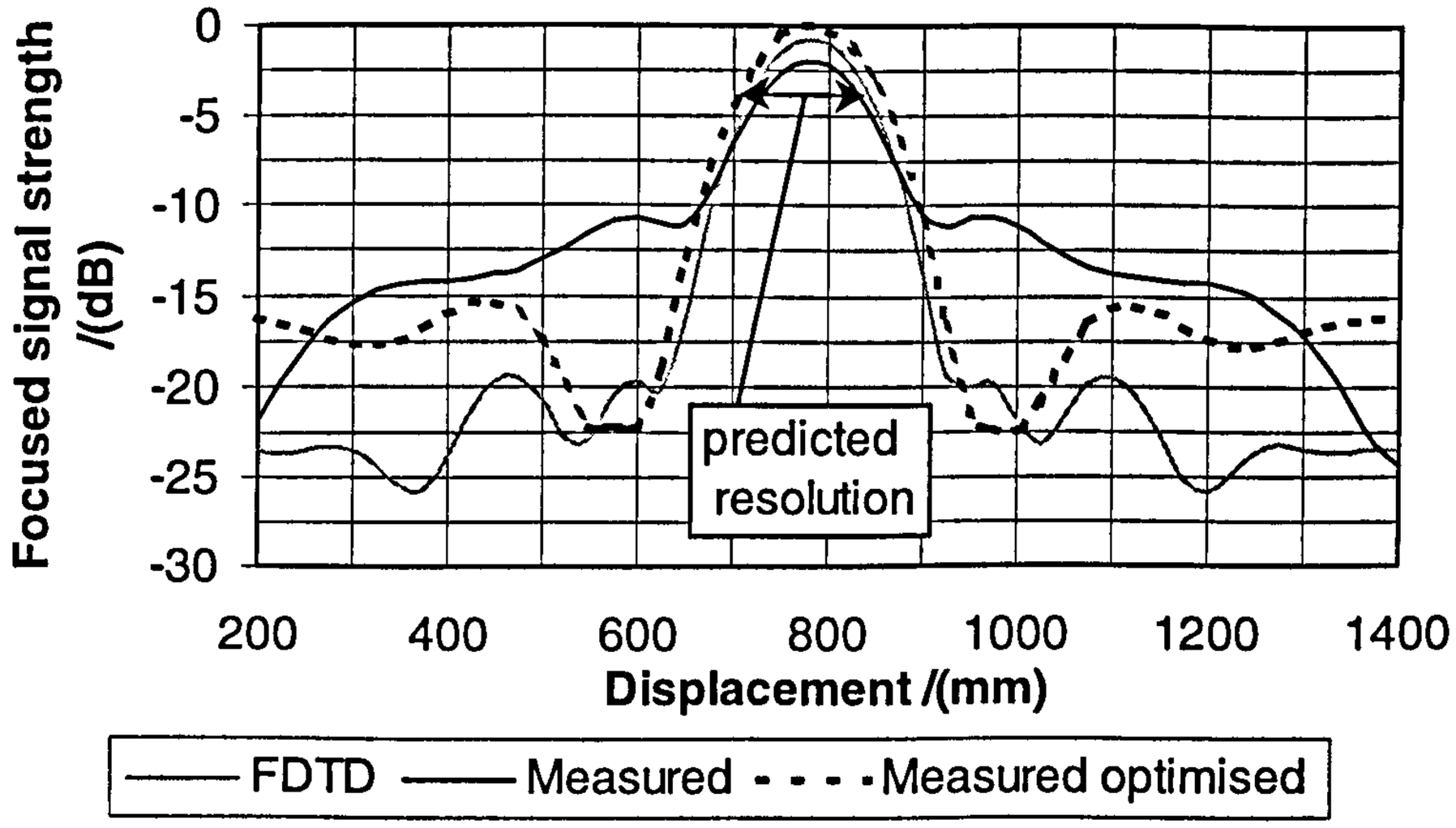

Figure 7.14 Lateral focusing with optimisation at 300 mm in soil

Figure 7.14 shows the improvements with this local optimisation procedure. The experiments were conducted with fairly homogeneous soil, hence in more challenging soil conditions optimisation techniques are essential for the successful target detection.

7.3.2. Power Estimations

The above sections compared the signals in time domain and the resolutions associated with the PRSF-GPR system. Analysis presented in chapter 5 compared analytical power loss estimations with the FDTD simulations. In this section the comparisons are performed with the measured and FDTD results at 1GHz. The signals measured from metal targets of size 100mmx100mm and 150mmx150mm buried at 200mm and 300mm depths were employed in these estimations. The power losses were calculated as described in chapter 5 for element 1 transmitting and others receiving.

Figure 7.15 and figure 7.16 shows the comparison between the analytical, FDTD and the measured results. Although good agreement with a maximum error of ≈1.3 dB and a mean error of ≈0.7 dB is seen between analytical and FDTD analyses, the measured results show fluctuations at some receivers, these errors are possibly due to practical errors such as target orientations. Since the target size used in these analyses falls into the resonance RCS region ($< \lambda$) the orientation of the target scatter centres with respect to the transmitting and receiving element is critical for RCS predictions.

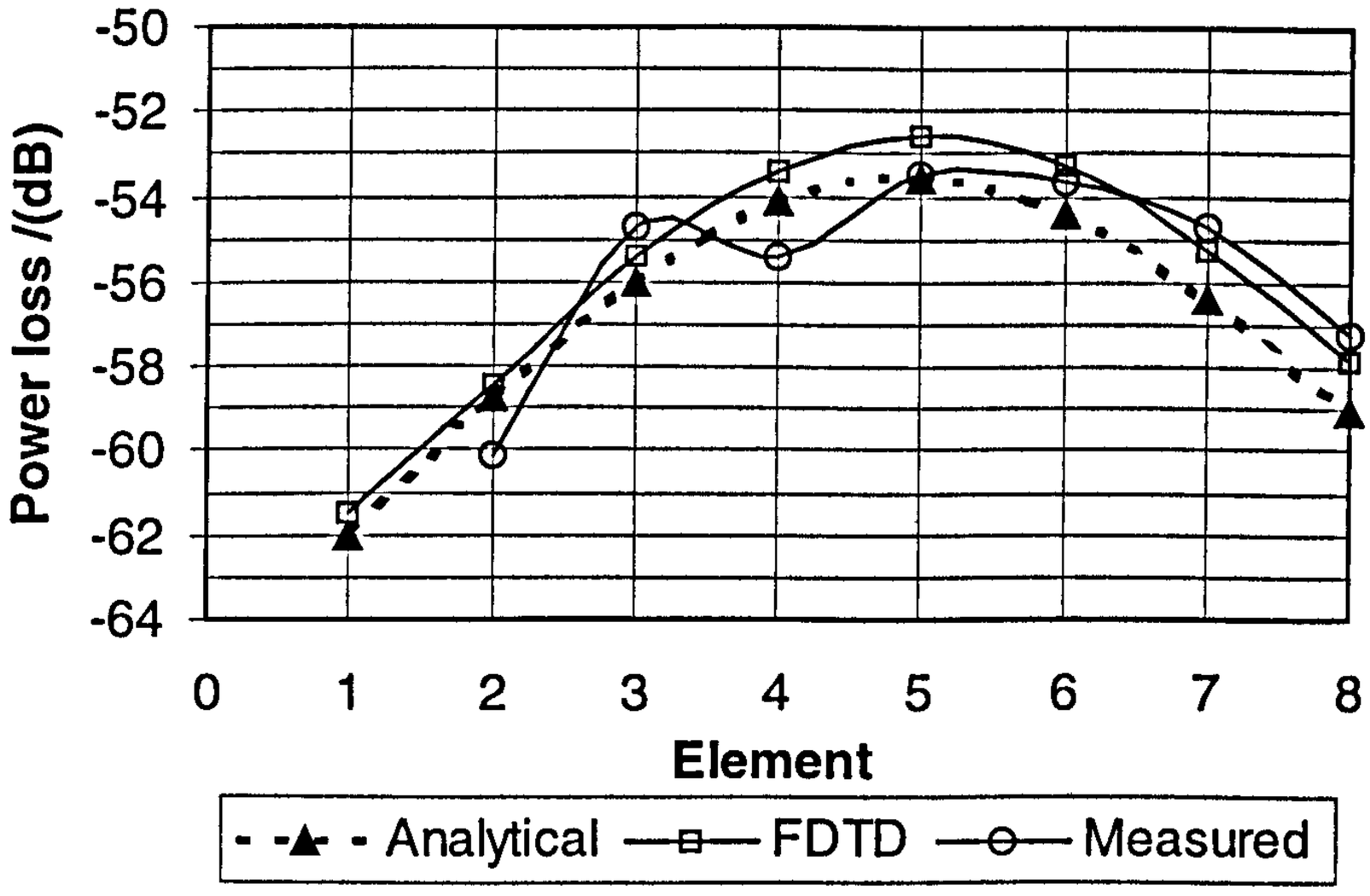

Figure 7.15 10cmx10cm metal plate at 200mm depth in soil

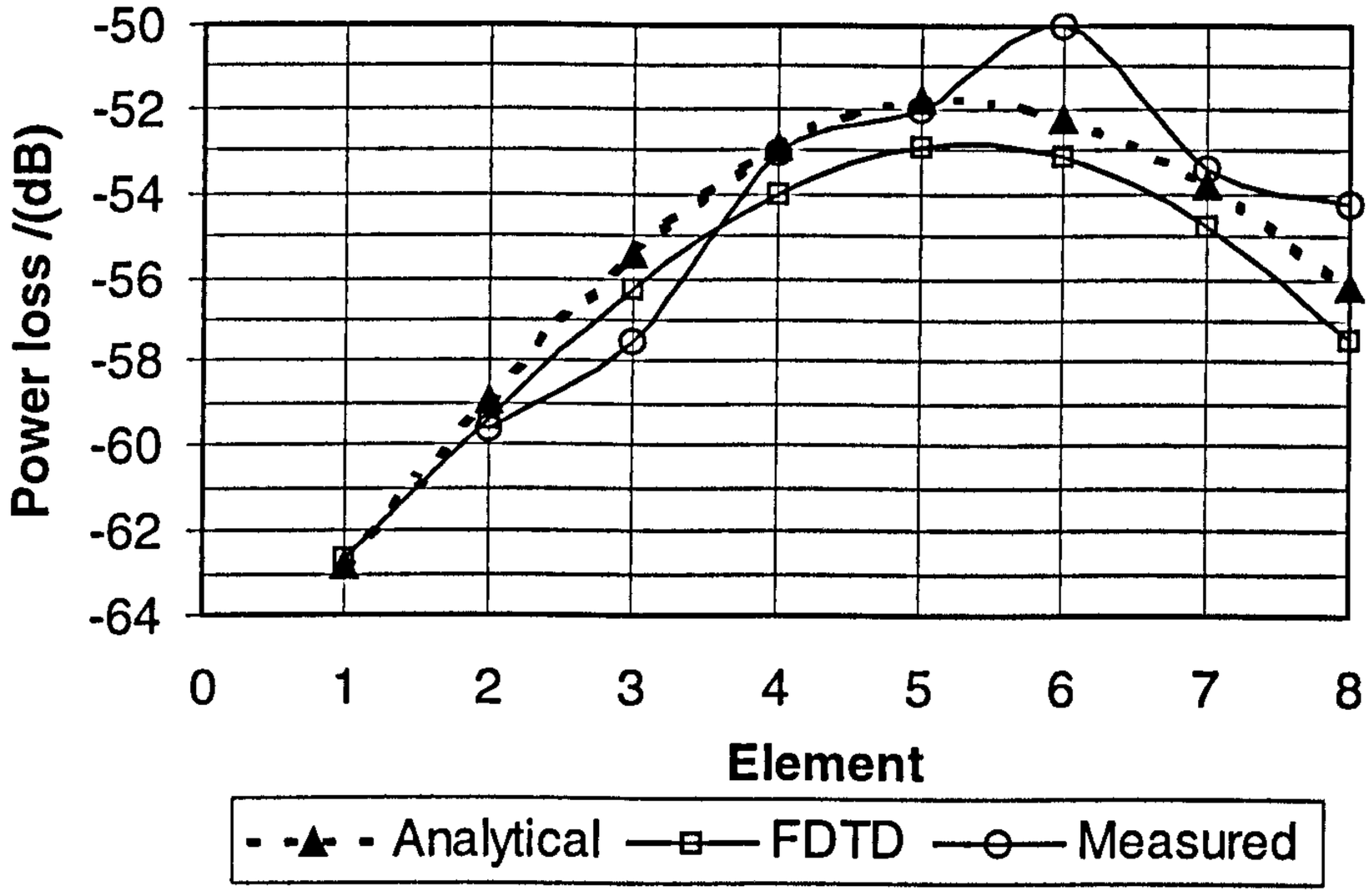

Figure 7.16 15cmx15cm metal plate at 300mm depth in soil

7.4. Clutter Estimations

The clutter returns analysed in chapter 4 (section 4.3.3) were compared with the practical measurements using small metal plates randomly distributed in soil. A line array of 7 bowtie elements with one wavelength spacing were employed in these measurements with elements 2,4 and 6 as transmitters (Figure 7.9). An absorbing back plane was used for this array to prevent the multiple bounces, as these reverberations will affect the comparisons at deeper depths. A different clutter distribution to that presented in chapter 4 with 76 small metal plates (30mmx30mm) in a soil volume of 1.4mx0.65mx0.35m: 239pebbles/m^3 was employed in order to extend this analysis to different scenarios.

Figure 7.17 shows the comparisons between analytical, FDTD and the measured clutter returns, where the results are normalised with respective maximum values. Although these show a similar pattern, the measured clutter power is shifted towards the air-soil interface. The imperfect background subtraction process with the measured results would have caused non-coherent combination of the signals from the air-soil interface contributing to the shift. The FDTD analysis also have errors due to reflections from the absorbing boundaries, this is evident around 350mm to 450mm which is closer to the absorbing boundary, which was at 550mm.

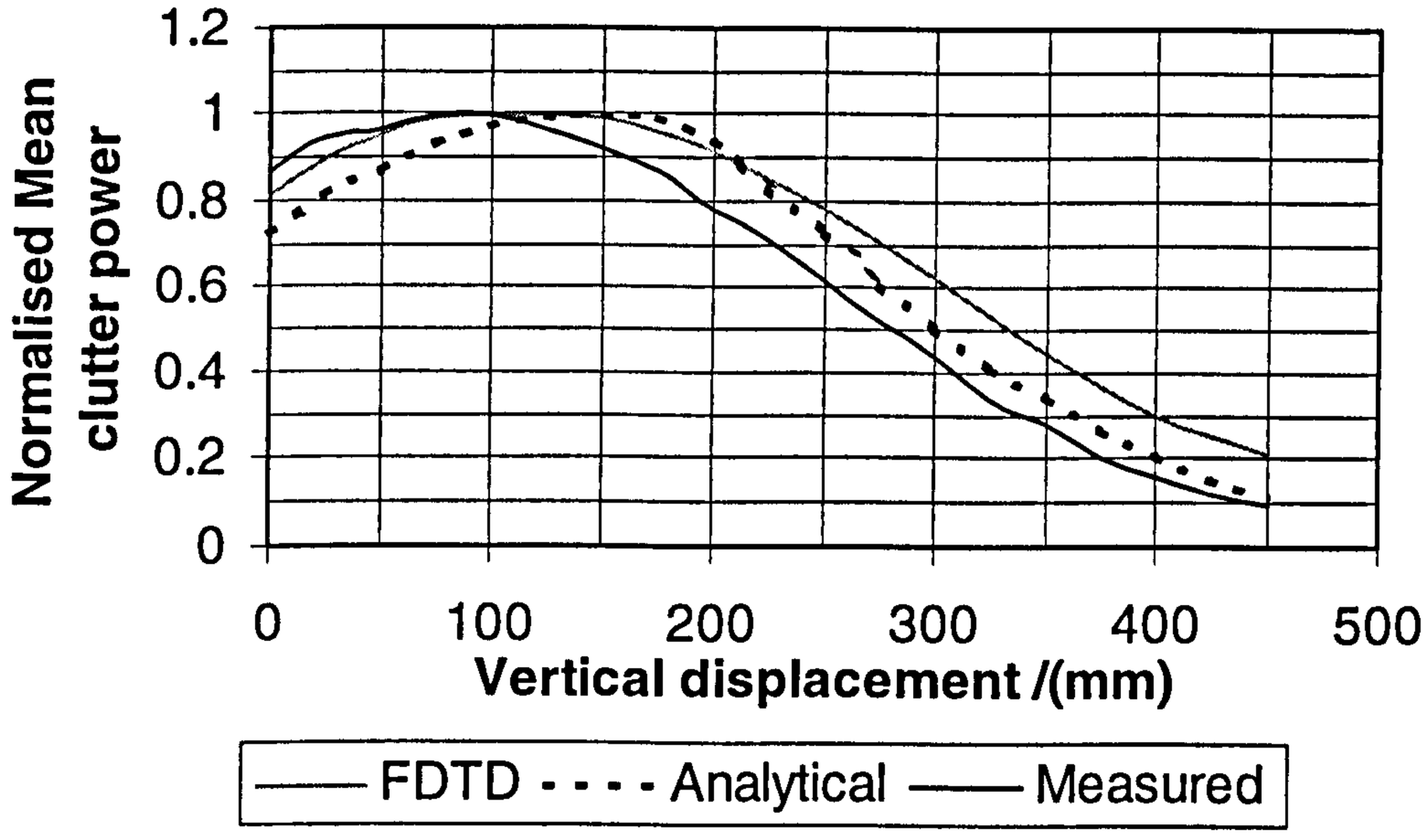

Figure 7.17 Comparison of mean clutter power

7.5. Focusing with Part of the Signal

The near surface detection analysis presented in chapter 4, section 4.2 was applied to measured results using longer (4 cycle) pulses. For a four-cycle pulse length, the strong specular reflections will interfere approximately up to a depth of 300mm, hence the focusing procedure with the total reflected signals will give results that are dominated by the surface reflections and hence masking target signals.

A line array of 7 elements with lambda spacing and absorbing back plane was utilised for these measurements with all possible transmitters giving 21 distinct paths. In this experiment, five metal plates of different sizes were buried at locations specified in table 7.2. The four-cycle pulse at 1GHz shown in figure 7.2 was employed in this analysis.

Measured results from 21 paths were synthetically focussed at appropriate depths. Focusing with the full-transmitted signal and with the later part of the signal is compared in figures 7.18 and 7.19. The pulse lengths for the improved focusing near

surface were varied from very short (0.5 cycles) at 50mm depth to long (2cycles) at 250mm. For depths, which are not effected by the specular reflection, the full-transmitted signal can be employed.

Metal Object	Size (mm^2)	Vertical displacement h/(mm)	Lateral displacement x/(mm)	Lateral displacement y/(mm)
1	10x10	50	810	0
2	7x7	100	540	0
3	6x6	150	1090	0
4	10x10	200	270	0
5	10x10	250	1260	0

Table 7.2 Target locations

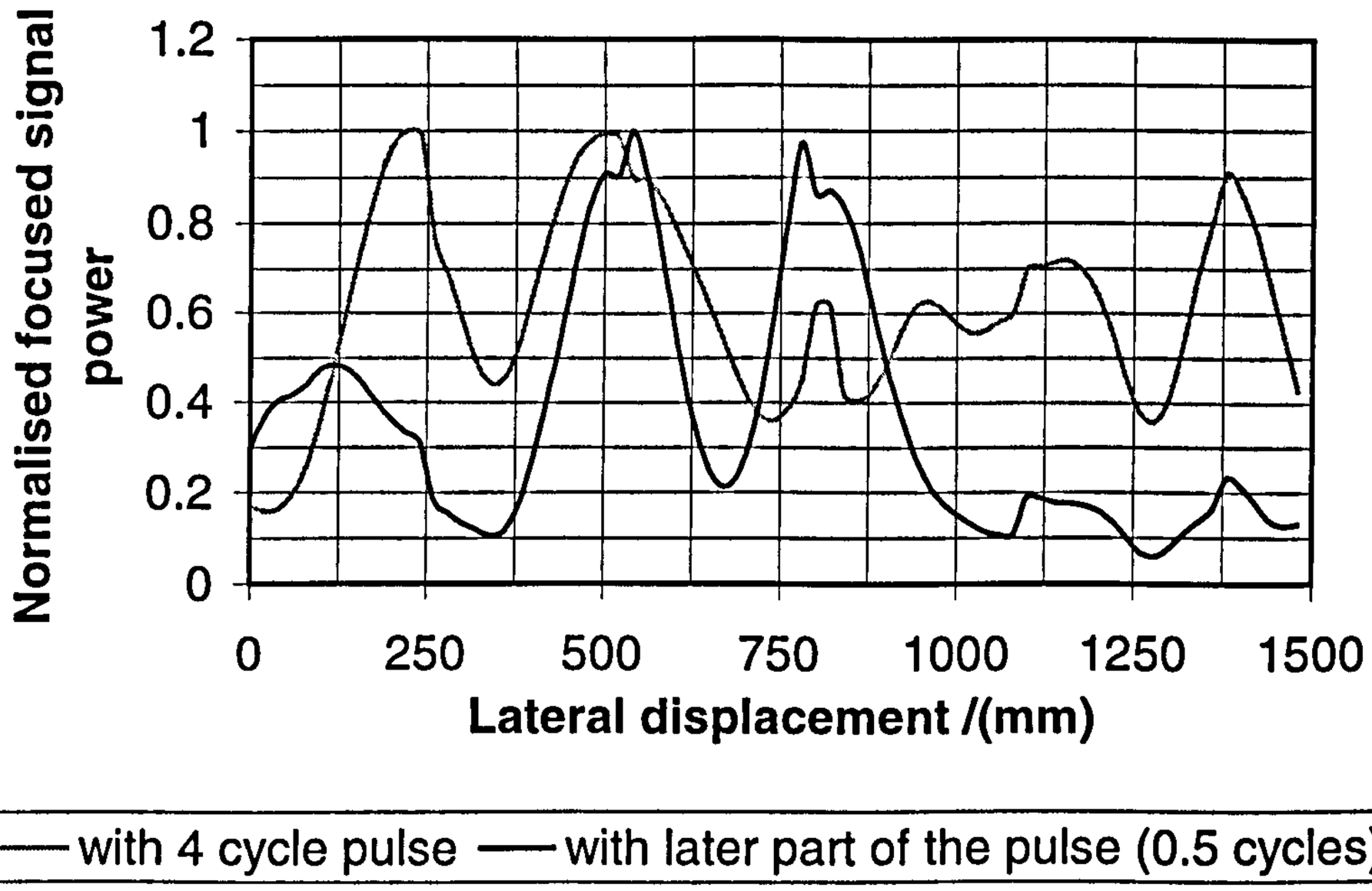

Figure 7.18 Lateral focusing at 50mm depth

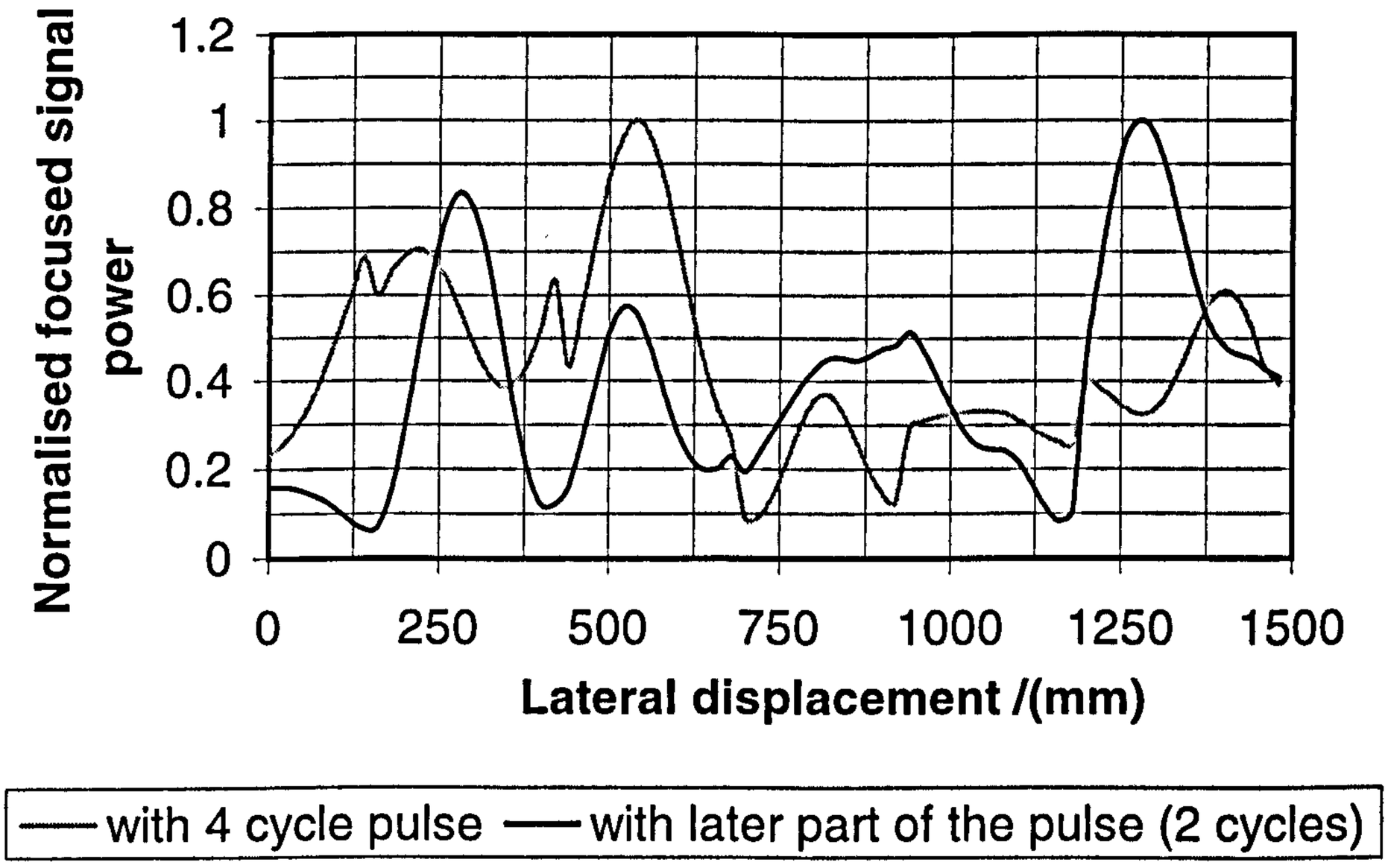

Figure 7.19 Lateral focusing at 250mm depth

These figures clearly identify the targets at their buried locations with different signal levels. The focussed target signal levels will vary depending on the shape of the transmitted pulse as the later part of the signals have a lower amplitude than the middle part as shown in Figure 7.2. Deeper and shallower targets are also visible in these figures which are focussed at different depths, as the vertical resolution of the system is ≈350mm in soil.

This analysis demonstrates the ability of this technique for near surface detection with longer pulses. It can be seen that the detection of shallow targets are enhanced with technique.

7.6. Summary

A ground probe technique to measure the complex dielectric properties of soil in practical environments has been described. Dielectric measurements were also carried out with a commercial dielectric probe (HP85070B) in order to verify the measured properties and produced similar values. Employing the measured dielectric properties, the analyses presented in this thesis using FDTD techniques and analytical methods have been successfully compared with practical measurements. The practical

measurements were performed in the GPR measuring facilities at University of Bristol using a linear array of Bowtie elements. The time domain comparisons presented in section 7.3 shows a good agreement in terms of amplitude and time delays and demonstrate the capabilities of the FDTD techniques to analyse complex problems of this nature. Synthetic focusing of the measured results also demonstrated a lateral resolution of ≈100mm and a vertical resolution of 350mm for a 1GHz system with bowtie elements, which agrees with the FDTD and analytical predictions. It has also been shown that the measured power losses associated with each path agree with the FDTD and analytical predictions, which have a maximum error of 1.3dB and a mean error of 0.7dB. Furthermore the nature of clutter returns from pebble-like objects has been compared with the measured results. In addition to these comparisons, techniques such as the adaptive focusing and the use of the part of transmitted signal for near surface focusing have been shown to enhance the detection process.

References

[1] W.R.Scott and G.S.Smith, Measured Electrical Constitutive Parameters of Soil as Function of Frequency and Moisture Content, *IEEE Transactions on Geoscience and Remote Sensing*, vol. 30, no. 3, pp. 621-623, 1992.

[2] M.T.Hallikainen, F.T.Ulaby, M.C.Dobson, M.A.El-Rayes and L.Wu, Microwave Dielectric Behaviour of Wet Soil- Part 1 Empirical Models and Experimental Observations, *IEEE Transactions on Geoscience and Remote Sensing*, vol. GE-23, no. 1, pp. 25-33, 1985.

[3] P.K.Hayes, A single Probe on-Site Method of Measuring the Dielectric Constant and Conductivity of Soft Earth Media over a 1GHz Bandwidth, *IEEE Transactions on Geoscience and Remote Sensing*, vol. GE-20, no. 4, pp. 504-509, 1982.

[4] E.M.Nassar, R.Lee, and J.D.Young, A Probe Antenna for In Situ Measurements of the Complex Dielectric Constant of Materials. *IEEE Transactions on Antennas and Propagation*, vol. 47, no. 6, pp. 1085-1093, 1999

[5] P.Hoekstra and A.Delaney, Dielectric Properties of Soil at UHF and Microwave Frequencies, *Journal of Geophysics*, vol.79, no. 11, pp. 1699-1708, 1974.

[6] J.Griffiths, *Radio Wave Propagation and Antennas*, Prentice-Hall, UK, 1987.

[7] D.J.Daniels, *Surface Penetrating Radars*, IEE, UK, 1996.

[8] R.Benjamin, Near-field Spot Focused Microwave Sensing for the Detection of Buried Land-Mines, *Proceedings of EUREL/IEE International Conference on the Detection of Abandoned Land Mines*, IEE, Edinburgh, pp. 128-132, Oct 1996

8. Conclusions and Future Work

8.1. Summary

Subsurface probing is important in a variety of diverse fields and the search for suitable tools to accomplish this task has given birth to new techniques and ideas. A wide range of probing techniques such as seismic, electrical-resistivity, gravitational methods and electromagnetic methods are being employed. Ground Penetrating Radar (GPR) has been found to be an attractive option for subsurface probing. In a GPR, an electromagnetic signal is transmitted into the soil and the reflected signals from the object buried in soil are collected using receiver antennas. Various techniques such as non-contact operation, pulsed techniques, filtering methods, image recognition methods and synthetic aperture techniques have been incorporated to enhance basic GPR performance. However the conventional GPR systems have limitations regards to depth of penetration, false alarm rate, operation in clutter environment and operating speed [1, 2, 3].

The Post Reception Synthetic Focusing (PRSF) technique [4] in GPR problems is an attractive solution to improve performance. The PRSF-GPR employs a planar array to transmit and receive signals for near-field focusing. In this method, one element transmits at a time and the subsequent reflected signals are recorded at all the elements that have the resolution cell in their 'field of view'. Off-line near-field focusing is achieved by applying appropriate two-way timing corrections. High-resolutions, low power, high search rate and better performance in clutter environment are possible with this technique. The work presented in this thesis has theoretically and practically

analysed this technique for subsurface probing and investigated methods that will enhance the detection process.

The FDTD method has been identified as a useful technique in analysing the GPR problem and has been employed in this thesis to investigate the PRSF-GPR problem. This theoretical investigation has been utilised to identify limitations, investigate possible enhancements and aid practical designs. The Microwave and Mathematical Modelling Group, within the Centre for Communications research (University of Bristol) have been developing the FDTD techniques since 1987 and have applied it to a wide range of electromagnetic problems. The code developed at University of Bristol has been used in this thesis to analyse the GPR problem.

A practical system with a line array (bowtie elements) has been utilised to verify the theoretical investigations and to practically analyse the GPR problem. All practical measurements have been conducted at 1GHz due to the maximum frequency of the digitising oscilloscope of 1.5GHz. The GPR measuring facility at University of Bristol (described in Appendix D) has been employed in these measurements.

In chapter 1, the existing surface probing techniques have been described with the main emphasis on the GPR that is a suitable technique that can meet the present day requirements. The surface probing techniques that have been discussed include resistivity method, gravity method, magnetic methods, thermal method, nuclear method, seismic methods and electromagnetic methods. Furthermore, various analytical and numerical techniques that can be used to analyse complex electromagnetic problems have been presented, and the FDTD method has been identified as the analysing tool to investigate GPR problem.

Chapter 2 considered the GPR methods in detail and provided background information on the existing methods. The employment of the GPR in various fields and the basic operations have been described. The signal types and identification methods that are being used with present day GPRs have been outlined. The pulse modulated carrier and the impulse or base band signals are widely employed because of their simplicity. Among the identification and processing techniques that have been discussed, the PRSF technique is capable of minimising the limitations suffered by most conventional GPRs. The PRSF technique, which has been the main consideration of this thesis, has

been described in detail with more emphasis on frequency, resolutions, operation in clutter environment and limitations due to surface features.

Chapter 3 gave a brief introduction to the numerical FDTD method that was employed to analyse most of the complex problems associated with the PRSF-GPR method. A numerical FDTD model for the PRSF-GPR has been developed and used to demonstrate the basic properties of this method. Initially a dipole antenna element was analysed separately and then incorporated into the GPR model. The PRSF-GPR FDTD model consists of a dipole antenna array, feed lines, soil and the buried object. The concept of post reception synthetic focusing and its basic properties have been demonstrated with the FDTD results. In this analysis, it has been shown that the lateral resolution of the system is 65mm for a 2.1GHz system, which is $\approx\lambda/(2\theta)$ as predicted through analytical estimations (see Appendix A). The lateral resolution was tested for a variety of soil permitivities and has been shown to be independent of the soil. The vertical resolution, defined by the pulse length of the transmitted signal, has also been estimated through FDTD and is in good agreement with the analytically predicted value. Furthermore, a technique to reduce the reverberations in this system by employing absorbing antenna back plane has been investigated and was found to reduce the effects due to multiple bounces which can lead to possible false identification of buried targets.

In Chapter 4, the PRSF-GPR FDTD model has been further modified and employed to analyse the PRSF operation in various soil conditions including: near field detection and operations in clutter media, non-flat ground and stratified media. Analysis in volume clutter environment looked into the nature of clutter returns from pebble-like objects and an analytical technique has been employed to estimate these effects. These estimates were also employed to demonstrate clutter reduction techniques. Detection in a sloping ground condition has been analysed with soil dielectric constants of 3,8 and 16 for a 10^0 sloping ground and indicated that the target can be identified with a lateral error of $\approx$ 20-35mm and a vertical error of $\approx$5-10mm. These errors were almost independent of the soil dielectric property since the converging cone (see figure 4.14 in section 4.4.1) becomes narrower with high dielectric constants and hence giving small variations in path lengths.

Techniques that can enhance the detection process in challenging environments have also been described and investigated with the FDTD calculations. Detection in near surface and stratified media can be improved when employing part of the signal for focusing, and this method has been successfully investigated with FDTD results. Furthermore analysis in stratified media indicated that high impedance ratios (>2) interfered with the synthetic focusing process and hence require additional processing such as background subtraction (i.e., subtracting signals without the target obtained through measurements or calculations).

Noise limits of the PRSF-GPR system and the system parameters to aid practical designs have been discussed in chapter 5 with practical soil dielectric properties and their classifications. An analytical model has also been formulated to compute the return signal strengths from individual paths and this was verified against the FDTD calculations with a maximum error of 2dB and a mean error of 1dB for a number of scenarios. This model is useful in analysing the full GPR system and for optimising the system parameters against noise. Furthermore, the noise limited maximum detectable depths under various practical soil conditions have also been investigated. It has been showed from this analysis that an operating frequency in the range of 1 to 2GHz, array-soil separation of 0.5m with 0.75 of wavelength inter-element spacing is appropriate for a practical system with 60 elements

In chapter 6, the development of a wide band printed bowtie antenna element that can be employed in a practical PRSF-GPR system has been discussed. Therefore this chapter included a summary of existing GPR antennas. FDTD methods were employed to design the antenna and the design was verified against practical measurements.

The bowtie element with an absorbing back plane had a -10dB bandwidth from 0.8GHz to 1.8GHz and suitable radiation patterns over the frequency band. The far-field patterns (centred on broadside), at 0.8GHz and 1.8GHz produced a wider beam ($\approx 50^0$) in the H plane and a narrower beam ($\approx 30^0$) in the E plane. Furthermore, the active element radiation pattern of the bowtie element in a 2x2 array has been analysed with practical measurements at 1GHz. As expected, the far-field radiation patterns indicated beam squinting and some degradation due the non-symmetrical nature of the array configuration and the mutual coupling between elements. The optimum spacing

between elements and techniques to reduce mutual couplings were not considered in this thesis and need further investigation.

Most theoretical analyses presented in this thesis have been validated against practical measurements and described in chapter 7. These measurements and comparisons have been conducted at the GPR measuring facility at University of Bristol with different array configurations (number of elements, inter element spacing) as the construction of the measuring facility progressed through different stages. Furthermore a dielectric measuring technique has been introduced and employed to measure the complex dielectric properties of the soil. Dielectric measurements were also carried out with a commercial dielectric probe (HP85070B) in order to verify the measured properties and produced similar values. An antenna array of 8 bowtie elements (described in chapter 6) with 0.6λ spacing at 1GHz was employed to compare the time domain signals, PRSF process, lateral and horizontal resolution and the signal strengths from each paths. The time domain signals agreed with the FDTD calculations performed at 1GHz in magnitude and time. The resolutions also produced similar values (lateral resolution of ≈100mm and vertical resolution of 350mm) with minor errors due to aligning errors in the synthetic focusing process. An adaptive technique to reduce such aligning errors has also been tested, but this technique needs further enhancements to operate in much complex scenarios. The analytical model formulated in chapter 5 to estimate the signal strengths from each individual paths agreed with the practical measurements and the FDTD calculations with a maximum error of 1.3dB and a mean error of 0.7dB with the FDTD. Furthermore, detection near the air-soil interface and the nature of clutter returns from pebble-like targets presented in chapter 4 have also been demonstrated and compared with practical measurements from a 7 element array with a wavelength inter element spacing. Clutter returns from pebble like targets agreed with the FDTD and the analytical estimations with minor errors due to the absorbing boundary in the FDTD model and the background subtraction process with practical measurements.

In this thesis, theoretical and practical analyses have been carried out in order to, analyse the system properties in practical environments, improve understanding, identify limitations, verify the possible solutions before implementing expensive systems, aid practical designs and test enhancing techniques. System properties such as

target detection, resolutions, processing gain and operation in clutter environment have been analysed and compared with practical measurements. Limitations due to reverberation, detection near air-soil interface, non-flat ground, stratified soil, clutter from pebble like objects and system noise limits have been identified. Employment of absorbing antenna back plane, focusing with part of signal to improve detection near air-soil interface and stratified ground, analysing of clutter reduction techniques and adaptive focusing technique to improve alignment errors have also been analysed in order to overcome the limitations. Furthermore, development of a practical wide band antenna element, analyses of system parameters under noise conditions and a dielectric measuring method have been successfully considered.

8.2. Future Work

Having analysed the PRSF-GPR using FDTD and practical methods, a number of opportunities now exist for future research.

8.2.1. FDTD Model

Analyses of the PRSF-GPR indicated that this method is a useful technique to enhance the detection process and the FDTD method is an efficient tool in analysing these types of problems. The PRSF-GPR FDTD model can be further improved to incorporate,

- Dispersive soil characteristics to analyse wide band operation [5]
- Sub-griding techniques to reduce the memory requirements and run time [6]
- Inhomogeneous soil properties to analyse more practical soil conditions [7]
- Dielectric targets such as plastic mines to investigate their RCS in different soil media.
- Rough surface features to analyse its effects on the focusing techniques

8.2.2. Clutter Analysis and System Parameters

Generally noise and clutter effects will limit the GPR detection capabilities. In chapter 5 the noise limits of the PRSF-GPR system have been considered. The nature of clutter returns from pebble like targets has been analysed in chapter 4, but the clutter

levels that will limit the system capabilities and the influence of system parameters on clutter needs a great deal of further analysis.

Development of an analytical model in line with FDTD modelling will help to achieve this task. The analytical model presented in chapter 5 can be further improved to model the clutter returns from pebble like targets and stratified media interfaces. Although it is difficult to estimate the RCS of very small targets, FDTD analysis can be used in these estimations to find a suitable value. Clutter returns from media interfaces can be estimated from half power beam intersections ("petals") on the interface. A survey of practical subsurface clutter returns is also necessary for a realistic analysis.

Since clutter is a major obstacle in subsurface detection, clutter reduction techniques are important. In chapter 4, the merits of using clutter reduction techniques have been demonstrated with FDTD results. But application of such techniques in more practical scenarios needs further investigations and improvements. There is much scope for further research in this direction.

8.2.3. Processing

Time alignment of the received signals in focusing requires the knowledge of the dielectric constant of the soil hence focusing in inhomogeneous soil conditions would lead to defocusing conditions. A possible solution to this problem is to employ adaptive techniques to align the received signals. A simple adaptive technique has been described and demonstrated in chapter 7. Employing adaptive techniques needs careful considerations in high clutter environments since clutter signals can be mistaken for target returns. Further investigations in the following fields are required for this technique to be successful:

- Discrimination between target returns and clutter
- Estimation of an average dielectric constant of soil
- Estimation of approximate target location
- Dependence of alignment errors with path lengths

8.3. Concluding Remarks

This thesis has made contributions to the numerical modelling of radar systems and in particular to the study of ground penetrating radars. A useful technique to enhance the GPR method has been successfully analysed in order to identify limitations, improve understanding, analyse enhancing techniques and aid practical design. The important subjects such as resolutions of the radar system, signal strength estimations, operation in complex soil conditions, nature of clutter returns from pebble like targets and development of a wide band antenna element have been effectively considered.

References

[1] R.Benjamin, Near-field Spot Focused Microwave Sensing for the Detection of Buried Land-Mines, *Proceedings of EUREL/IEE International Conference on the Detection of Abandoned Land Mines, IEE*, Edinburgh, pp. 128-132, Oct 1996

[2] D.J.Daniels, Surface Penetrating Radar, *Electronics and Communications Engineering Journal*, pp. 165-182, Aug. 1996.

[3] D.J.Daniels, Surface Penetrating Radar for Industrial and Security Applications, *Microwave Journal*, vol. 37, no. 12, pp. 68-82, 1994.

[4] R.Benjamin, Post Detection Synthetic Focusing in Near-field Radar, *Proceedings of EUREL/IEE International Conference on the Detection of Abandoned Land Mines*, IEE, Edinburgh, pp. 133-137, Oct 1996

[5] R.Luebbers, F.P.Hunsberger, K.S.Kunz, R.B.Standler and M.Schneider, A Frequency Dependent Finite Difference Time Domain Formulation for Dispersive Materials, *IEEE Transaction on Electromagnetic Compatibility*, vol. EMC-32, no.3, pp. 222 - 227, 1990.

[6] K.M.Krishnaiah and C.J.Railton, A Stable Subgridding Algorithm: An application to Eigenvalue Problems, *Telsiks–97 Conference Proceedings*, University of Nis, pp. 112-115, 1997.

[7] F. L. Teixeira, W. C. Chew, M. Straka, M. L.Oristaglio and T. Wang, Finite-Difference Time-Domain Simulation of Ground Penetrating Radar on Dispersive, Inhomogeneous, and Conductive Soils, *IEEE Trans. Geoscience and Remote Sensing*, vol.36, no.6, pp. 1928-1937, 1998

Appendix A

Analytical Calculation of Lateral and Vertical Resolution

This appendix presents the derivation of the lateral and vertical resolution of a synthetic aperture system [1].

A.1 Lateral Resolution

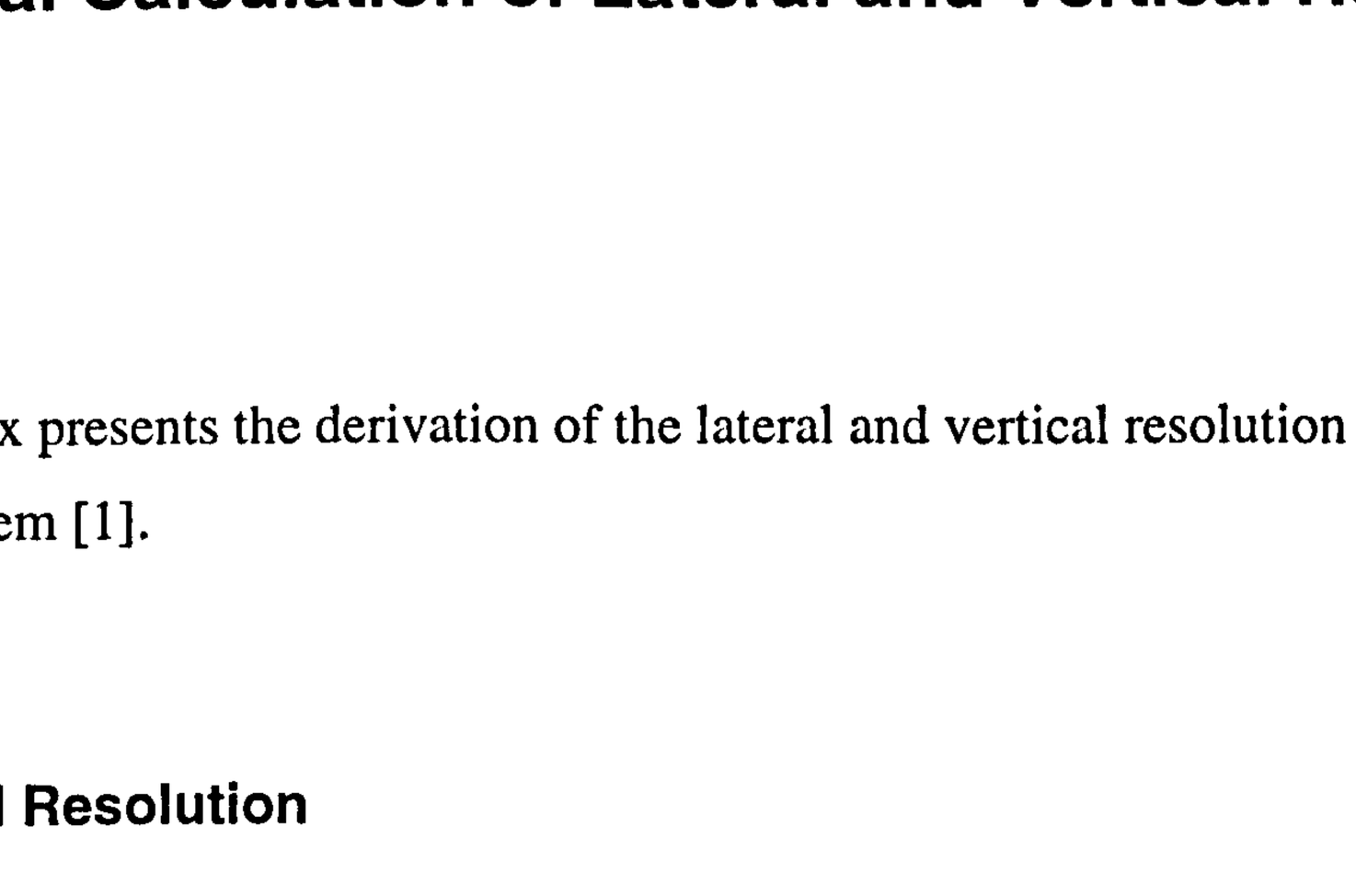

Figure A.1 Path length variation in lateral direction

An along-track displacement from the focal point P by r/2 to the right to P', as shown in figure A.1, would change the path to the left-hand end of the array from L to L' (and would change that to the right-hand end from R to R'). L and L' are long and although their far ends coincide, they are essentially parallel. L' is lengthened (at its bottom end) by (r/2).sin (θ/2), compared to L. Similarly R' is shortened by (r/2) sin (θ/2), relative to R.

Thus the two-way paths from P to the aperture suffer a progressive phase error from end to end of the array, relative to its focused condition, of $\pm\frac{2\pi}{\lambda}r.\sin\frac{\theta}{2}$.

For coherent addition the limits are given by,

$$\pm\frac{2\pi}{\lambda}\mathrm{r}.sin\frac{\theta}{2} = \pm\frac{\pi}{2} \qquad \text{(A.1)}$$

$$\mathrm{r}.sin\frac{\theta}{2} = \frac{\lambda}{4} \qquad \text{(A.2)}$$

The same applies for displacement -(r/2). Thus for small θ,

$$\text{Lateral resolution } \mathrm{r} = \frac{\lambda}{2\theta} \qquad \text{(A.3)}$$

A.2 Vertical Resolution

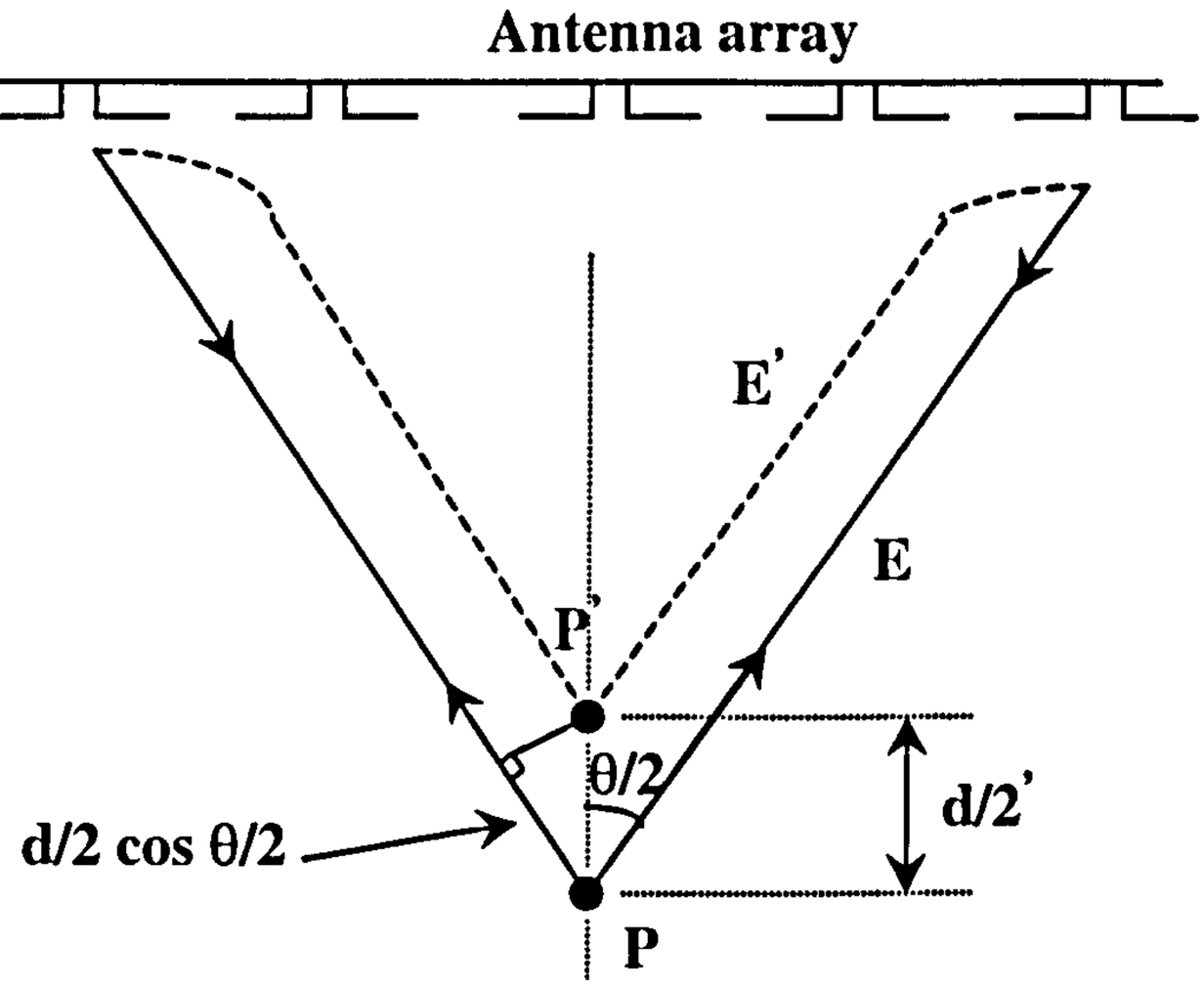

Figure A.2 Path length variation in vertical direction

An across-track displacement from the focal point P by +δ/2 towards the aperture P', as shown in figure A.2, would shorten the path to the centre of the array by +δ/2. However, E_r, the old path length to the right-hand end of the array, and E_r' its new equivalent, are long and although their far ends coincide, they are essentially parallel (and similarly for E_l and E_l' on the left).

E_r is shortened by (δ/2) cos (θ/2), compared to E_r. The variation of the two-way path lengths to the aperture relative to that for its focused condition causes a symmetric progressive phase error from the centre of the array to the two ends of

$$\frac{2\pi}{\lambda}\delta\left(1-cos\frac{\delta}{2}\right) \qquad =\frac{2\pi}{\lambda}\delta\frac{\theta^2}{8} \tag{A.4}$$

The limits for coherent addition is given by (considering the full aperture)

$$\frac{4\pi}{\lambda}\delta\frac{\theta^2}{8} \qquad =\pi \tag{A.5}$$

$$\text{Hence the vertical resolution } \delta \qquad =\frac{2\lambda}{\theta^2} \tag{A.6}$$

References

[1] R.Benjamin, Synthetic Aperture Antennas, *Microwave Journal*, pp. 68-81, 1995.

Appendix B

Derivation of Inflection Point between Air and Ground

This appendix presents the derivation of the inflection point between air and ground.

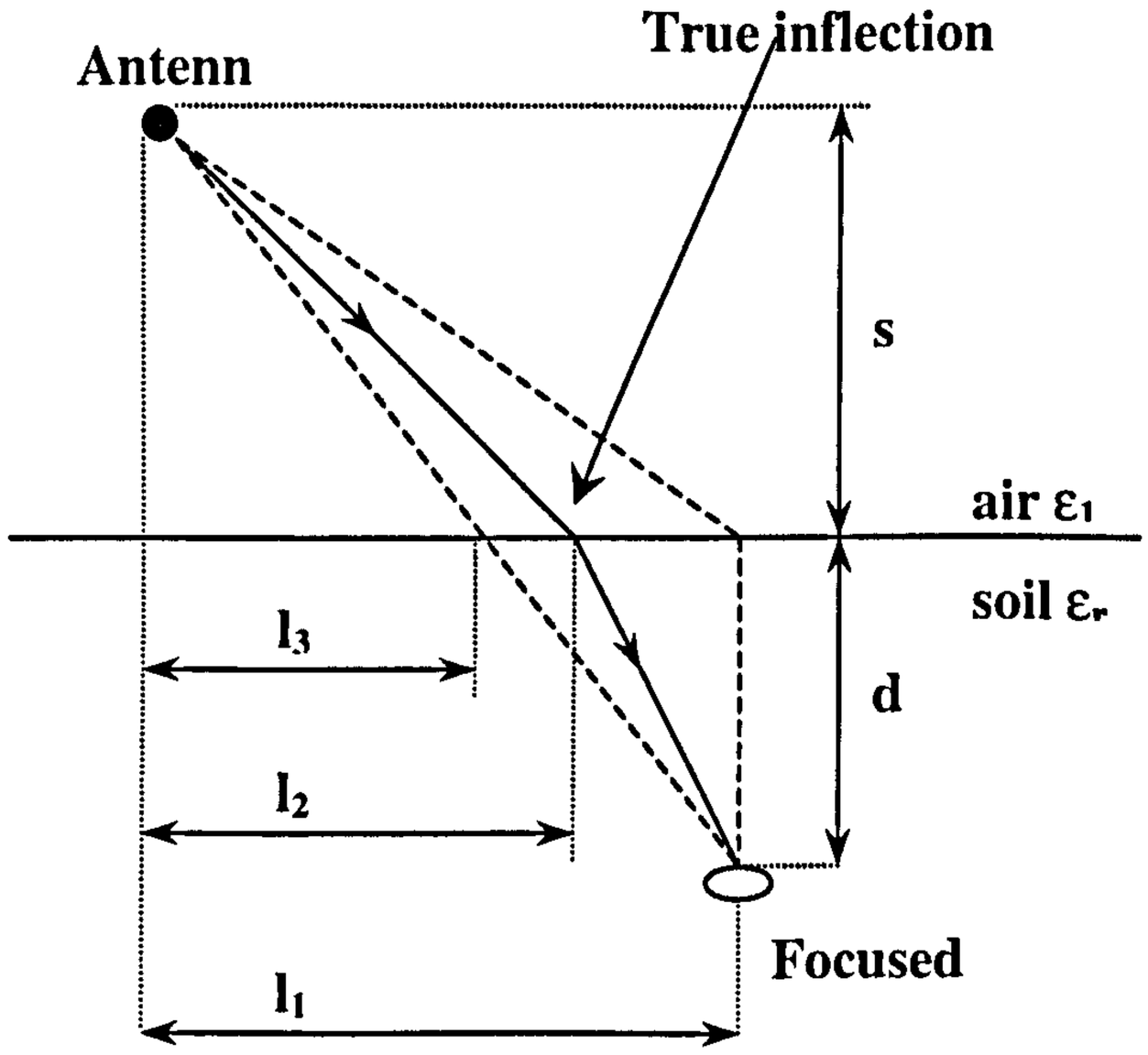

Figure B.1 Point of inflection between air and ground

Solving for the inflection point is not a trivial problem and cannot be done in closed form. Hence approximate methods are followed to find the true inflection point.

If $\varepsilon_1 = \varepsilon_r$ then the ray takes the straight path which penetrates the boundary at $L=l_3$

If $\varepsilon_1 << \varepsilon_r$ then the ray takes the path which penetrates the boundary at $L=l_1$

These two cases are extreme cases and the true inflection point will be between l_1 and l_3.

Hence a better approximation for the true inflection point will be,

$$l_2 = l_1 + \sqrt{\frac{\varepsilon_1}{\varepsilon_r}}(l_3 - l_1) \tag{B.1}$$

For more precise values, l_2 can be further improved by checking Snell's law at this point and adjusting it for better values.

Appendix C

Clutter Reduction Technique

This appendix presents the clutter reduction technique proposed for the PRSF system [1].

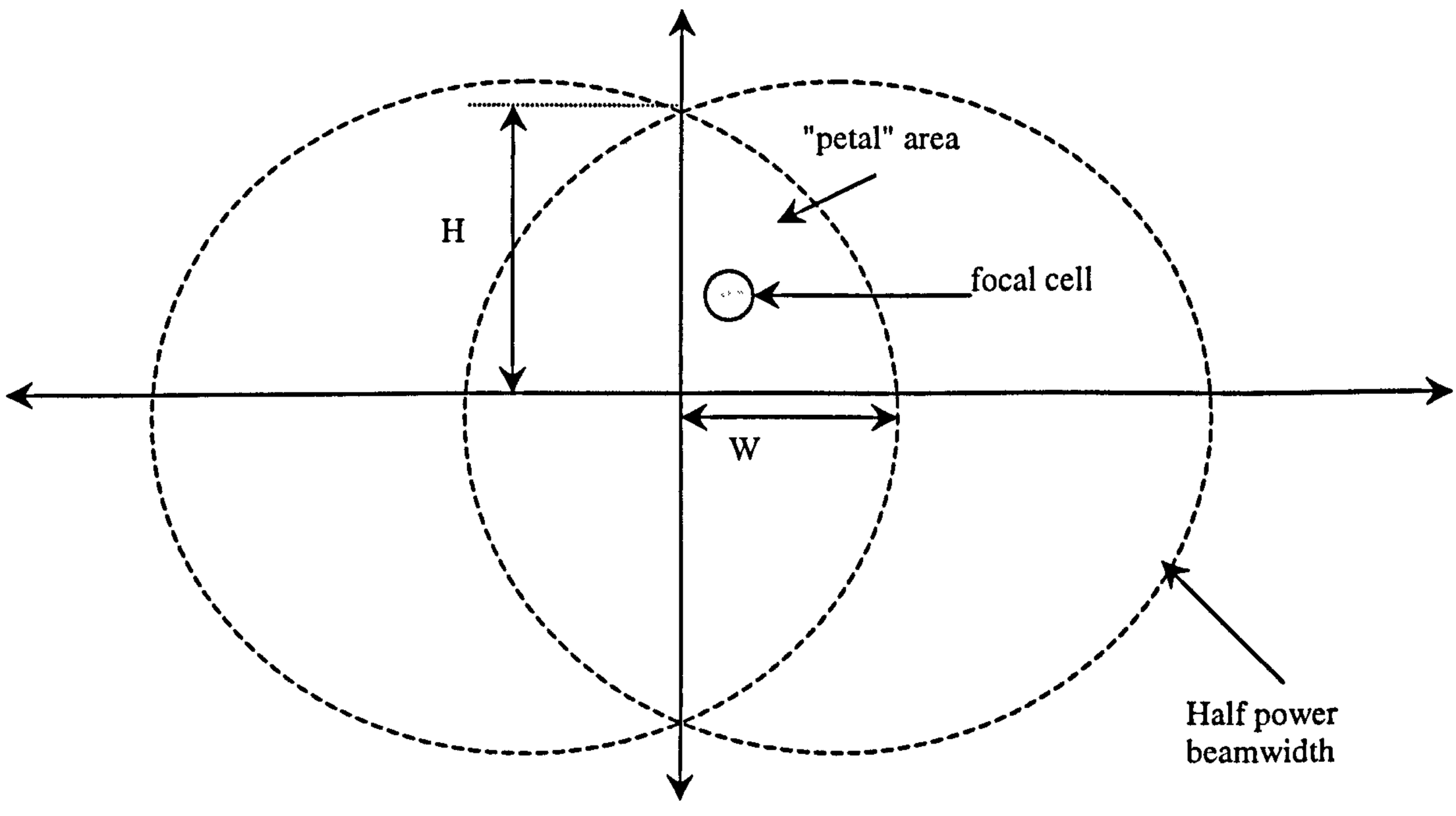

Figure C.1 Petal area

For a specific path, *the common-delay common-view clutte*r signals will emerge from the petal area shown in figure C.1.

Approximate Petal area A_c $= 2Hx2W$

$= 4\ HW$

Hence to minimise the effects of non-coherent volume clutter on the reconstructed image, each path should be weighted inversely to this *common-delay common-view clutter area.* This weighting is particularly important when a few paths are associated with much stronger clutter than the reminder.

Hence in post reception synthetic focusing, the focused signal is given by,

$$V = \sum_{i=1}^{n} \frac{1}{A_{c_i}} U(t - T_i) \tag{C.1}$$

where,

V	:Synthetically focused signal.
$U(t)$	:Signal received from path i at time t.
n	:Number of paths which are associated with the resolution cell.
T_i	:Path delay from the transmitting element to the receiving element via the resolution cell.
A_{c_i}	: Petal area for path i.

References

[1] R.Benjamin, Clutter and Related Effects in Post-Reception Synthetically-Focused Ground-Penetrating Radar, *Report for DERA on Microwave Detection of Subsurface Objects*, UK, Nov 1998

Appendix D

Experimental Set-up

This appendix presents the GPR experimental set-up at the Centre for Communications Research (CCR), University of Bristol, that was used in all GPR practical measurements.

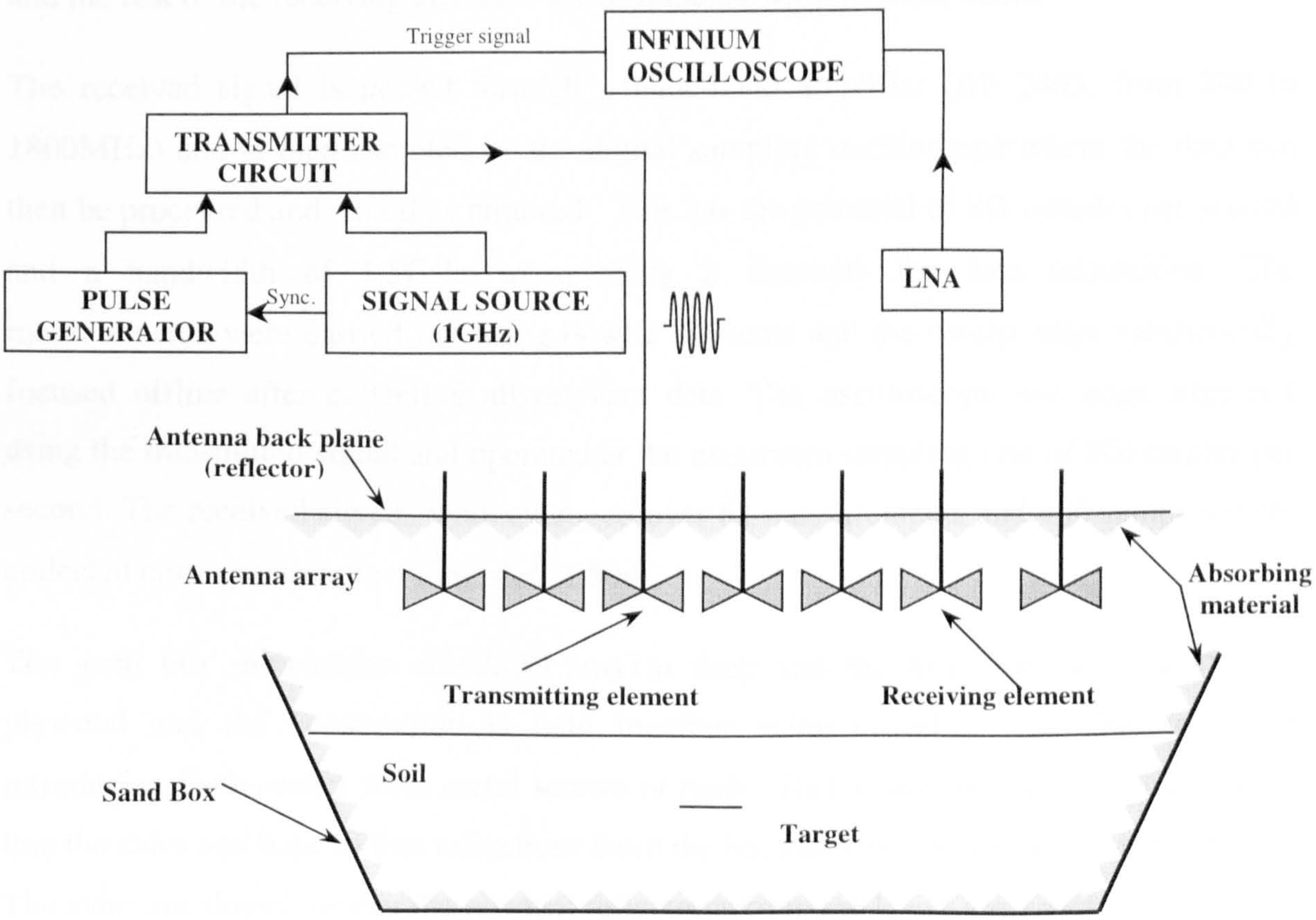

Figure D.1 Experimental Set-up

The experimental set-up consists of a RF pulse generator, digitising oscilloscope (Infinium, HP 54845A), a Low Noise Amplifier (LNA), bowtie antenna elements and a sandbox lined with Radar Absorbing Material (RAM).

The RF pulse generator is capable of producing a 4ns pulse modulated by a 1GHz sinusoid using widely available off-the-shelf circuits and test equipments. The pulse repetition rate is set at around 100KHz and the transmitted pulse, without any amplification, is around 10dBm.

The bowtie elements are fed through coaxial cables and have an operating bandwidth of 80% (0.8GHz to 1.8GHz) and a beamwidth of $\approx \pm 35^0$ in the E-plane and $\approx \pm 55^0$ in the H-plane at 1GHz. The antenna array is implemented by securing wooden and metal beams above the sandbox and the antenna elements are suspended by their metallic back planes. During measurements, a single receiving element is connected to the digital oscilloscope and the rest of the receiving elements are terminated with matched loads.

The received signal is passed through a wide-band amplifier (RF 2403, from 200 to 1800MHz) and is then sampled by the digital sampling oscilloscope where the data can then be processed and stored as required. This has the potential of 8G samples per second and a bandwidth of 1.5GHz when using 2 channels for data acquisition. The measurements were carried out using bowtie elements and the results were synthetically focused offline after collecting all relevant data. The oscilloscope was edge triggered using the transmitted signal and operated at the maximum sampling rate of 8Gsamples per second. The received signals were averaged over 64 measurements and 400 samples were collected corresponding to a time slot of 50ns.

The sand box dimensions are 2mx1.3mx1m deep and the box sides are made from plywood and the construction is held together using doweling and glue to avoid introducing back-scatter from metal screws or nails. Radar absorbent material is used to line the sides and base so that reflections from the boundary of the workspace are reduced. The sides are sloped, so that the residual reflections from the RAM are directed away from the relevant antenna element. The box is filled with 1.12tons of builders sand which has a permittivity of around 3.2 at 1GHz. The main advantages of using a sandbox to replicate

the ground for the system measurements is that the climate is fixed, unlike outdoor field measurements where the measuring workspace is subject to the prevailing weather conditions. This means that important factors, such as humidity, temperature, ground moisture content and permittivity, can be tightly controlled making results repeatable.